TRABAJO DE FIN DE MASTER

Análisis y modelización de la dispersión de olores producidos en una estación depuradora de aguas residuales en Oliva (Valencia)

Presentado por

Andreas Luckert

Para la obtención del

Master en Ingeniería de Caminos, Canales y Puertos

Curso: 2018/2019

Fecha: 30/08/2019

Tutor: García Bartual, Rafael Luis

Cotutor: Aguado García, Daniel

Tutor externo: Norbert Frank de la Universidad de Heidelberg, Alemania

Declaration on oath

I, the undersigned, hereby confirm that I have written the accompanying thesis by myself, without contributions from any sources other than those cited in the text and acknowledgments. This applies also to all graphics, drawings, maps and images included in the thesis.

Place and date:
Heidelberg, 30 August 2019

Signature:

Foreword

First and foremost, I would like to thank all my supervisors I have had during the accomplishment of this one-year thesis.
To begin with, I thank my two supervisors from the UPV Prof. Dr. Rafael García Bartual and Dr. Daniel García Aguado who have always supported me both subject-related and also mentally throughout the entire research project.
The same applies to my German supervisors from the University of Heidelberg Prof. Dr. Norbert Frank and Dr. Martina Schmidt who were able to pay attention to my concerns even from the distance.
In addition, I would like to thank the company Global Omnium S.L. and all its staff involved with this project; in particular Carlos Lafita Lopez, Fernando Andrés Tomas, Mauro Orts Zamorano and Oscar Hernándis Martínez. Without their continuous will to support me in getting the project done and giving me access to the measuring sites and the associated data, it would not have been possible to carry out this thesis.
Also, I would like to mention Sergi Segura i Llópez, in his role as data administrator of the non-commercial meteorological association AVAMET, who kindly provided me multiple times with the meteorological data related to Platja de Pego and Oliva Poble, whose extraction was sometimes a quite laborious task. Additionally, it would like to give my special thanks to Clint R. Tillerson in his profession as physical scientist with the U.S. EPA/OAQPS/AQAD Air Quality Modeling Group, who gave me during the last month of my work a lot of helpful advice related to error and warning messages of AERMET and AERMOD.
By and large, I would like to thank again all of the aforementioned people along with my parents who helped me make this possible in the first place. Concerning mental and also content-based support, my special thanks goes to Melanie Pardo Espinoza.
Apart from all of the above-mentioned, I am also grateful for having received the ERASMUS Placement scholarship funding for the period when I lived in Valencia, Spain. The assistants Sarah Fatemi and Anna Feldbein from the ERASMUS-Konsortium KOOR/BEST in Karlsruhe did a great job in helping me along with the paperwork and resolving any other doubts.
Concerning the writing conventions used throughout this document, the style will be American English, such as "odor", "organized", "favorable", "labeled", "modeled", etc.
As for the tools employed in this thesis, the main code was developed in python 3.7, the document written with LaTeX typesetting and the overall operating system was Linux Ubuntu. The AERMOD model is written in FORTRAN and in order to combine all preprocessors of AERMOD with own python scripts for data importation and manipulation, other python and also Bash scripts were created.
Furthermore, as a general advice for the reader, I would like to suggest the use of an PDF reader with a functionality like "go back to the last visited page" (which is not necessarily the directly previous page). This will be especially useful when clicking on hyperlinks within this PDF, which bring you directly to a figure or table, a bibliography source, an equation, an other (sub)section etc., and then you would like to go back. In the case of Linux users, the Okular PDF reader is a good choice.

Abstract

Data analysis and dispersion modeling of the odor emissions from a wastewater treatment plant in Oliva (Valencian Community, Spain):

Wastewater treatment plants (WWTPs) play a fundamental role in the protection of the aquatic environment. These facilities prevent organic matter, nutrients and other pollutants from reaching natural aquatic ecosystems. However, when located in the proximity of residential areas, they can produce odor and noise nuisance. This is the case of the WWTP Camping San Fernando in Oliva, Spain, which led to complaints. As for the odors, in the context of sewage treatment they usually originate from the anaerobic decomposition of organic compounds, which in presence of sulfate results in hydrogen sulfide (H_2S). Due to the low solubility of H_2S in wastewater, it is released into the atmosphere, producing a strong unpleasant smell. In this study, the main goal is to resolve through scientific methods whether or not perceptible H_2S concentrations can occur in the residential area in question by the odorant emissions of the mentioned WWTP. In order to tackle the problem, two measurement campaigns were carried out covering around 220 days in total. By means of a thorough data analysis of the essential variables involved, such as wind speed, wind direction and the H_2S concentrations in its role as the central pollutant, it could be shown via contrasting annual, monthly and daily patterns, that the probability to be affected for these residential areas is the highest from June to August between 7 p.m. and 7 a.m., i.e. from evening until morning. Moreover, the daily concentration patterns also fit to this conclusion. In order to substantiate it, dynamic olfactometry measurements were conducted by two expert panelists in addition to the employment of the AERMOD model. With this conservative Gaussian dispersion model, it was possible to determine under which conditions H_2S concentrations above the perception threshold of 0.00047 parts per million (ppm) can occur at the residential dwellings. The most realistic scenario suggests that no perceptible concentrations occurred during any of the studied periods. However, the worst case scenario, which assumed constantly high volume outflows of the WWTP, showed that it is indeed possible to perceive odors at the dwellings. With the on-site olfactometry measurements, it could be confirmed that the wind direction is the deciding factor whether or not an odor can be noticed at a specific place. Different locations of interest on the WWTP site and at the boundary to the dwellings yielded no perceptible odors during the olfactometry measurement times. Finally, concerning the modeling results, all the scenarios tested confirmed that the concentrations remain significantly below values hazardous to health at all places of interest, both for the WWTP staff and the local residents. The recommended 15-minute average exposure limit for H_2S is 10 ppm, whereas the maxima from the model output next to the emission source remained below 1 ppm.

Análisis y modelización de la dispersión de olores producidos en una estación depuradora de aguas residuales en Oliva (Valencia):

Las estaciones depuradoras de aguas residuales (EDARs) juegan un papel fundamental en la protección del medio ambiente acuático. Estas instalaciones evitan que la materia orgánica, los nutrientes y otros contaminantes lleguen a los ecosistemas del agua natural. Sin embargo, cuando se encuentran cerca de viviendas, pueden producir olores y ruidos molestos, siendo el caso de la EDAR Camping San Fernando en Oliva, España. En cuanto a los olores, en el contexto del tratamiento de aguas residuales, generalmente originan a partir de la descomposición anaeróbica de compuestos que, en presencia de sulfato, resultan en sulfuro de hidrógeno (H2S), debido a la baja solubilidad del H2S en las aguas residuales, se libera a la atmósfera, produciendo un fuerte olor desagradable. En este estudio, el objetivo principal es abordar de una forma sistemática la modelación de la distribución de las concentraciones de olor perceptibles en las proximidades del punto generador de olor causadas por H2S de la EDAR mencionada. Más concretamente, determinar la posibilidad de afecciones en el área residencial próxima a la depuradora citada. Para abordar el problema, se llevaron a cabo dos campañas de medición intensivas, cubriendo alrededor de 220 días en total. Mediante un análisis de las variables esenciales involucradas, como la velocidad del viento, la dirección del viento y las concentraciones de H2S en su papel de contaminante central, se pudo demostrar a través de contraste de patrones anuales, mensuales y diarios, que la probabilidad de que estas áreas residenciales se vean afectadas es la más alta desde junio a agosto entre las 7 p.m. y 7 a.m., es decir, desde la tarde hasta la mañana. Además, los patrones diarios de concentración también se ajustan a esta conclusión. Para justificarlo, se realizaron mediciones de olfatometría dinámica por dos expertos, además del empleo del modelo matemático AERMOD. Con este modelo gaussiano conservador de dispersión, fue posible determinar en qué condiciones las concentraciones de H2S pueden tener lugar por encima del umbral de percepción [0.00047 ppm] cerca de dichas viviendas residenciales. El escenario más realista sugiere que no hay concentraciones perceptibles durante cualquiera de los períodos estudiados. Sin embargo, en el escenario *worst-case*, que asumió salidas constantes de flujo de la EDAR con un alto volumen, mostró que realmente es posible percibir olores en las viviendas. Con las mediciones de olfatometría *in situ*, se pudo verificar que la dirección del viento es el factor decisivo para detectar o no un olor en un lugar específico. Diferentes lugares de interés tanto en el recinto de la EDAR como en el límite de las viviendas no dieron lugar a percepción alguna de olores durante los tiempos de medición de olfatometría. Finalmente, con respecto a los resultados de la modelización, todos los escenarios probados confirmaron que las concentraciones permanecen significativamente por debajo de los valores peligrosos para salud en todos los lugares de interés, tanto para el personal de la EDAR como para los residentes locales. El límite recomendado de exposición promedio de 15 minutos para H2S es de 10 ppm, mientras que los máximos de la salida del modelo junto a la fuente de emisión permanecieron por debajo de 1 ppm.

Anàlisi de dades i modelització de la dispersió de les emissions d'olor d'una planta de tractament d'aigües residuals a Oliva (València):

Les estacions depuradores d'aigües residuals (EDARs) juguen un paper fonamental en la protecció del medi ambient aquàtic. Aquestes instal · lacions eviten que la matèria orgànica, els nutrients i uns altres contaminants arriben als ecosistemes de l'aigua natural. No obstant això, quan es troben prop d'habitatges, poden produir olors i sorolls molestos, sent el cas de la EDAR Càmping Sant Ferran a Oliva, Espanya. Quant a les olors, en el context del tractament d'aigües residuals, generalment originen a partir de la descomposició anaeròbica de compostos que, en presència de sulfat, resulten en sulfur d'hidrogen (H2S), a causa de la baixa solubilitat de l'H2S en les aigües residuals, s'allibera a l'atmosfera, produint una forta olor desagradable. En aquest estudi, l'objectiu principal és resoldre a través de mètodes científics, si o no concentracions d'olor perceptibles, causades per H2S de la EDAR esmentada, poden ocórrer en l'àrea residencial en qüestió. Per a abordar el problema, es van dur a terme dues campanyes de mesurament cobrint al voltant de 220 dies en total. Mitjançant una anàlisi exhaustiva de les dades de les variables essencials involucrades, com la velocitat del vent, la direcció del vent i les concentracions d'H2S en el seu paper de contaminant central, es va poder demostrar a través de contrastar patrons anuals, mensuals i diaris, que la probabilitat que aquestes àrees residencials es vegen afectades és la més alta des de juny a agost entre les 7 p. m. i 7 a. m., és a dir, des de la vesprada fins al matí. A més, els patrons diaris de concentració també s'ajusten a aquesta conclusió. Per a justificar-ho, mesuraments d'olfactometria dinàmica van ser realitzades per dues panelistas experts, a més de l'ús del model AERMOD. Amb aquest model gaussià conservador de dispersió, va ser possible determinar en quines condicions les concentracions d'H2S poden ocórrer per damunt del llindar de percepció de 0.00047 parts per milió (ppm) prop d'aquests habitatges residencials. L'escenari més realista suggereix que no hi ha concentracions perceptibles durant qualsevol dels períodes estudiats. No obstant això, en l'escenari *worst-case*, que va assumir que constants eixides de flux de la EDAR amb un alt volum, va mostrar que realment és possible percebre olors en els habitatges. Amb els mesuraments d'olfactometria *in situ*, es va poder verificar que l'adreça del vent és el factor decisiu per a detectar o no una olor en un lloc específic. Diferents llocs d'interés tant en el recinte de la EDAR com en el límit dels habitatges no van donar lloc a cap percepció d'olors durant els temps de mesurament d'olfactometria. Finalment, respecte als resultats de la modelització, tots els escenaris provats van confirmar que les concentracions romanen significativament per davall dels valors perillosos per a salut en tots els llocs d'interés, tant per al personal de la EDAR com per als residents locals. El límit recomanat d'exposició faig una mitjana de de 15 minuts per a H2S és de 10 ppm, mentre que els màxims de l'eixida del model al costat de la font d'emissió van romandre per davall d'1 ppm.

Contents

1 Introduction

The reader will be introduced to the topic in this first section which illustrates the background, scope and an outline of the thesis. Another intention is to create an awareness for the relevance of the research topic. In the fourth subsection, a short introduction of the wastewater treatment plant (WWTP) site "Camping San Fernando" will be given, which includes primarily geographic data and photographs of the facilities. For further information about the particular processes, the reader is referred to the theory section 2.

1.1 Background

To start with, the idea for this thesis emerged out of the public pressure brought about by various resident complaints regarding odor nuisance in the immediate vicinity of the wastewater treatment plant (WWTP) Camping San Fernando. As far as the location of this WWTP is concerned, it is situated in the tourist region Oliva which lies at the seashore about 70 kilometers in the South of Valencia in Spain (see details under 1.4.3) with a distance of a little more than 300 meters from the beach (see figure 1). Unfortunately, it lies in the heart of a residential area wherefore avoiding disturbance of the local people is an important concern.
In order to help the interested reader understand the pressing relevance of this issue, a commonplace example shall be given hereinafter:
Suppose that you walk through a city and all of the sudden you smell the well-known odor of sewage leaking from a gully or drain nearby. Now, imagine you take a seat outside of a restaurant, order your favorite meal and again, suddenly the above-mentioned smell appears with a quite offensive intensity. Given that the bad smell does not vanish in an instant, you might get up and leave. Both of these just made-up scenarios could very well happen to everyone of us, but fortunately we are not bound to stay in the place where the odor nuisance occurs. We can leave.
By contrast, the people afflicted by sewage odors in their homes, cannot just go away. They live there. As a consequence, their daily life could be substantially affected, from sitting outside in their gardens, terraces and balconies via having their meals either outside or inside while the windows are opened through to impairing their sleep at night.

1.2 Scope

The main research question of this thesis is whether or not the immediate residents of the WWTP Camping San Fernando in Oliva (Valencian Community, Spain) can objectively experience odor nuisance particularly caused by the odorants $\mathrm{H_2S}$ and $\mathrm{NH_3}$ emitted from the WWTP.
If so, which meteorological conditions and situations related to the WWTP processes make the disturbance either possible at all or facilitate its occurrence?
Given that human perception thresholds are exceeded, is this also true for limit concentrations hazardous to health? If this is the case, to what extent are these limits exceeded, how often does this happen on average and which measures could finally be taken to mitigate or even solve the problem?
Following on from this, granted that odorant emissions transcending the aforementioned threshold concentrations reach the residential buildings on a regular basis, would it be possible to model these situations in conjunction with local weather and terrain data and draw conclusions on extreme situations and worst case scenarios?
Moreover, can a reliable correlation be found between the chemical concentrations of odorants and the perceived offensiveness by people with the aid of conducting selective occasional olfactometry

measurements? If not, why?

1.3 Outline

To start with, some general information regarding the WWTP site, the operator Global Omnium S.L. and the complaints lodged by affected residents are going to be presented in the following subsection. Afterwards, general theoretical concepts will be illustrated in order to give the reader a good grounding necessary to understand the subsequent sections. Following to the theory part, the method section explains the investigation instruments and models employed to carry out the project. Then, the results attained through applying these methods are going to be analyzed thoroughly in connection with an ensuing discussion aiming at putting the results into context and interpret their meanings. Finally, conclusions on the findings will be drawn and recommendations for further research projects will be given.

1.4 Information on WWTP Camping San Fernando

1.4.1 General aspects

Top view of WWTP site and surroundings

In the following screenshot taken from Google Maps 1 the position of the WWTP site is indicated along with its beeline distance to the seashore with the aim to put the WWTP's position in a geographical context: flat and residential area, and moreover directly next to the Mediterranean Sea. In addition, it is embedded within the residential area which gives rise to possible conflicts with the local people.

Figure 1: Labeled top view extracted from Google Maps in satellite view of the WWTP Camping San Fernando in Oliva, Comunidad Valenciana, Spain.

Project partner Global Omnium S.L.
The company's official web page is [Glo]. Part of their wide range of services is water management which they provide in many parts of the Autonomous Valencian Community. These services include, inter alia, water supply to towns, sewerage, sanitation, drainage and sewage treatment and laboratory tests.

Contact persons
The main reference person throughout the project was Carlos Lafita López, working in the research and investigation division in Valencia. The principal contact on-site was Mauro Orts Zamorano being an executive responsible for several WWTPs in the region of Oliva. He needed to be present in almost any occasion for giving access to the facilities. For security reasons there should always be an employee present supervising the works on-site.
Carlos is responsible for carrying out the olfactometry measurements (see subsection 3.1), sometimes accompanied by his colleague Fernando Andrés Tomas. They are both schooled and the measuring instrument is calibrated to them (see fig. 37 and 35).
As far as the management of this particular WWTP is concerned, the person in charge of this job is Oscar Hernándis Martínez.

1.4.2 Close-up labeled top view and facility scheme

In the figures 1, 2 and 4 different top views of the WWTP site and its immediate vicinity are depicted. To this end, screenshots extracted from Google Maps in satellite mode were used. Additionally, in

order to put these screenshots into a geographical context, the Google Maps compass symbol has been embedded into each of the top views.

Figure 2: Closer top view screenshot from Google Maps of the WWTP site including labels in green of each part of the entire facility, such as the canalization entrance, the nearby Pumping Station 2, the bioreactor, the decanter and the affected residential area.

Apart from that, the labeled screenshot from Google Maps is illustrated in another way by the following basic scheme 3 labeled with all important parts of the facilities.

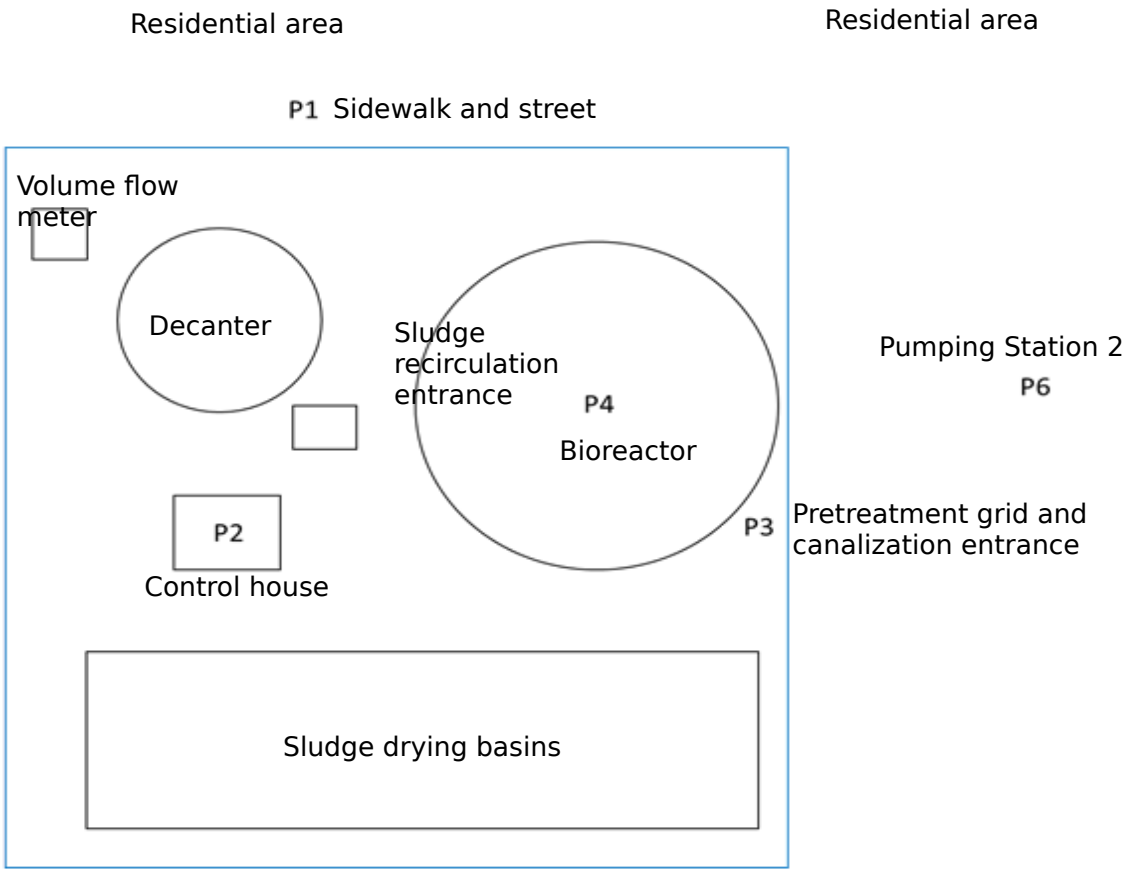

Figure 3: Schematical site plan of the WWTP area with labeled facilities.

Concerning the dimensions of the scheme, some metric data regarding a selection of the WWTP elements will be given in the following list:

Area of sludge drying basis: 11 m x 5 m

Diameter of the bioreactor: 22 m

Diameter of the decanter: 12 m

1.4.3 GPS and elevation data

Apart from the details mentioned previously, for certain applications, especially the modeling, the information about the exact GPS location and the elevation above average sea level is paramount. The following data were extracted on 2 October 2018 from the Google Maps-coordinate finder [Goo], which includes additional information such as elevation above sea level.

Latitude: 38.88882981

Longitude: -0.0467303

Altitude above sealevel: 4m

1.4.4 Details on complaints due to odor nuisance

In particular, the labeled screenshot 4 includes the measurement locations for both the olfactometry and gas measurements along with the origin of the complaints due to odor nuisance. Although the entire project idea stems from complaints occurred before the first measurement campaign was launched on 16 July 2018, even during this very campaign another oral complaint due to odor nuisance was received on 1 August 2019 from the residential area marked in yellow in the screenshot 4. As for the specific place from where the complaint came from, the building east (left when looking from the street separating the hotel and the WWTP site) of the hotel on the other side of the street with respect to the WWTP premises. It should also be mentioned, that among all the WWTPs in the area the WWTP in question "Camping San Fernando" is the only one which had been subject to complaints concerning odor nuisance (status August 2018). Exact location and time data on these complaints do not exist, only the date and the general part of the residential area. The general area where all complaints stem from is marked in yellow within the labeled figure 4.

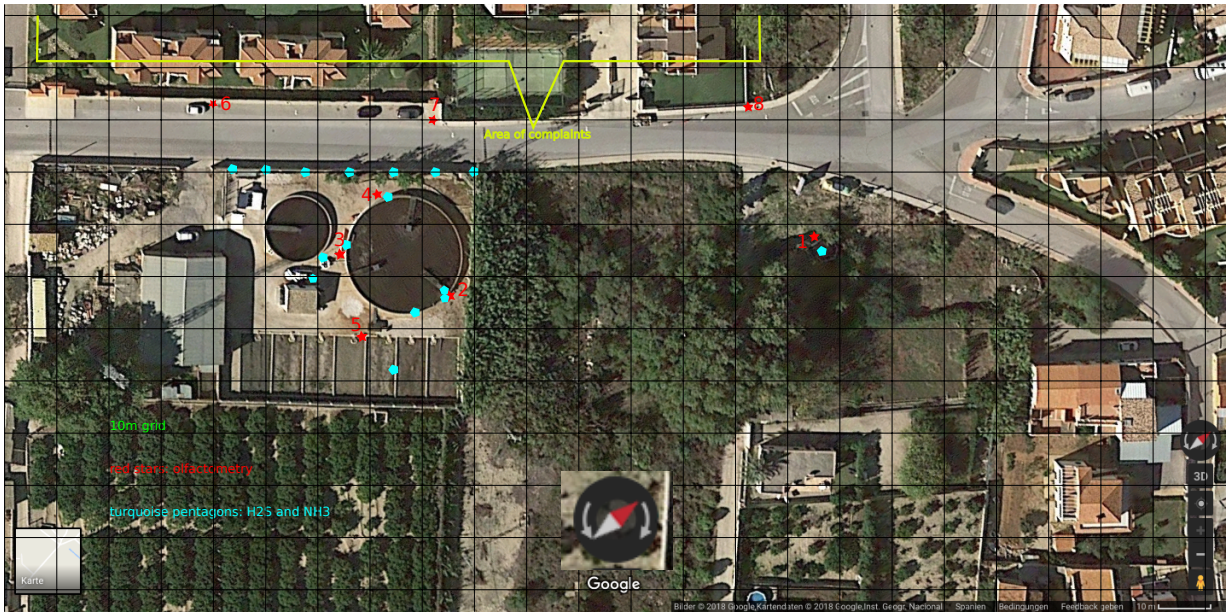

Figure 4: Labeled top view extracted from Google Maps showing all gas measuring points in turquoise pentagons, where the instruments (see 3.1.1) were installed. Apart from that, the olfactometry points are displayed in red stars. They stand for the locations where the panelists measured with the Nasal Ranger olfactometer (compare subsection 3.1.2). Moreover, the residential area, where the complaints were made, is highlighted in yellow.

1.4.5 Detailed illustrations of the WWTP's facilities

In this subsection, the elements of which the WWTP Camping San Fernando consists (see scheme 3 or labeled screenshot 2) are going to be described in further detail and depicted with photographs.

Bioreactor

First, the wastewater arrives directly from the canalization into the bioreactor (see picture 5), after having been pumped from either Pump Station 1 or 2. As for this project, only Pump Station 2 was of concern as it lies merely 70 meters from the canalization entrance (compare scheme 3 or 2).

Figure 5: General side view of the bioreactor on the WWTP site Camping San Fernando in Oliva, Spain.

Then, in the bioreactor microorganisms are cultivated which decompose the organic material under aerobic conditions. In order to meet the associated chemical oxygen demand (COD), the water body is constantly mixed with surrounding air. This will be characterized further in the forthcoming paragraph 1.4.5 which is going to provide facts on the aeration system of the bioreactor.
In comparison with anaerobic conditions, aerobic decomposition causes generally less bad odors since aerated conditions allows microorganisms to inhibit production of odorants and moreover generate much less CO_2 and CH_4 emissions. Thus, the main source for bad smells originates from the canalization outflow into the bioreactor due the accumulated sewer gases, the local lack of oxygen and the turbulence caused by the waterfall when flowing from the inlet pipe into the open-air bioreactor pool (see figure 6).

Figure 6: Photo of the bioreactor entrance during the first measuring campaign 2018 showing the active part of the pumping cycle (compare fig. 55 and 56) with a turbulent squirting waterfall, which was caused by the coarse grate installed directly underneath the pipe outlet.

Figure 7: Closeup of the bioreactor entrance during the second measuring campaign 2019. As of spring 2019, it comprises of a new subterranean canalization entrance into the bioreactor with previous filtering via rotation sieves.

Aeration system of the bioreactor

Before 3 August 2018, this task was solely accomplished by three turbines installed at the water surface producing a lot of noise (compare figure 8), which as a consequence had led to complaints. As a result, on 3 August 2018 the old system was replaced by a Venturi submarine system which is able to suck in air by means of a tube into the deeper water layers providing the system with oxygen likewise, but with a significant decrease in noise generation.

The open-air WWTP site disposes of a bioreactor (figure 5) with its three turbines (figure 8) meeting the chemical oxygen demand (COD) of the system. In the beginning of August, the bioreactor's ventilating system was exchanged in favor of a three Venturi machines below the water surface (see figure 9) in order to decrease the generated noise due to mixing the waste water with air.

Nevertheless, the old aeration system has been employed afterwards, for example on the launching day 3 April 2019 of the second measurement campaign as indicated in figure 10.

Figure 8: Photograph of the previous water surface turbines providing the oxygen supply of the bioreactor system with the aim to maintain it in an aerobic working state.

Figure 9: View of the new Venturi aeration system in action (shot taken on 5 September 2018).

Figure 10: Snapshot of the old turbine aeration system in the bioreactor functioning during the visit of the WWTP Camping San Fernando when launching the second measurement campaign as of 3 April 2019.

The exchange of the aeration was undertaken as a reaction to other complaints regarding noise pollution, which is beyond the scope of this project and was thus not examined. The replacement was mentioned as it could have had an effect on the odor generation of the bioreactor. However, according to the data analysis (see results and discussion section 4) it is clear that the only relevant emission source is represented by the canalization entrance.

Decanter

Further on, the site has a decanter which can be seen in figure 11. The decanter is connected to the bioreactor and the next step in the treatment process. In order to maintain a proper concentration of microorganisms, both the surface and bottom sludge of the decanter are extracted on a regular basis. The extracted wastewater sludge is being partially recirculated into the bioreactor in order to maintain an appropriate biomass and thus microorganism level. Generally, the further sedimentation and separation of building sludge takes place in the decanter. The water leaving the decanter is almost ready for being led back into the environment, which is done after being disinfected by chlorine. As opposed to the standard scheme of a WWTP, the project WWTP Camping San Fernando does not comprise of a primary decanter, where the wastewater enters coming from the canalization previously to flowing into the bioreactor. By contrast, in this particular open-air WWTP, the sewage water is directly fed into the bioreactor, and afterwards in a secondary decanter before it is finally disinfected

by chlorine and released.

From time to time, the continuously formed surface sludge needs to removed from the decanter. The difference of before and after can be better imagined when comparing picture 11 with 12.

Figure 11: Photograph of the decanter next to the bioreactor within the WWTP site on 20 June 2018. The process of surface sludge building can be observed when comparing this picture to photograph 12 taken more than one month later on 27 July 2018.

Figure 12: Another photograph of the decanter more than one month later than picture 11 showing the difference in surface sludge building. For this reason, the surface sludge is pumped off just like the thicker bottom sludge of the decanter.

Sludge drying basins

Next to the bioreactor and behind the control house, as seen from the street, the sludge drying basins (fig. 13) are situated.

Figure 13: Side view of the sludge drying basins within the WWTP site.

It is important to note that it is not permitted to operate the sludge drying basins inside the WWTP terrain between June 15 and September 15 due to enhanced production and volatility of odorants during the hottest season (see 2.3.5). As a consequence, the liquid sludge recently extracted from the decanter is transported to another place during this time.

Pump stations

Moreover, the canalization outflow into the bioreactor is fed by two pumps, one of which is situated close by in just about 65 meters linear distance, called Pump Station 2 (or in Spanish "estación de bombeo de aguas residuales 2" (EBAR 2)). This very pump station is illustrated in the following pictures in different states. First, in figure 14 the state before the grate was removed in favor of a metal plate for sealing the pump well on 5 August 2018. As for the details of Pumping Station 2, it is accessible via a public parking lot through a small fenced area about 60 meters linear distance toward the beach from the WWTP Camping San Fernando. The pumping station is now sealed by metal plates since 7 August 2018 (see fig. 16). Before, it was closed a pervious grid as can be seen in figure 14. What is more, the gas measuring tubes for H_2S and NH_3 are visible in the very middle of the well shaft. Before the sealing was accomplished, photographs of the well's interior could be taken which demonstrate the canalization in- and outflow. The small waterfall, visible in figure 15, gives rise to turbulent gas outflow into the air. Luckily, the main odorant H_2S is denser than air and thus hardly ascends and escapes the well in high quantities (for more information, see the results section 4). In the figure 15 a small waterfall can be seen due to the overfilled filtering grid. Apart from that, the well was close to a regular cleaning event. This routine aims to remove the accumulated odorous material inside the well. Another reason for this, besides generated odors, is preventing overflow during heavy rainfalls. Finally, the new pump well surface after sealing can be inspected in photo 16. This measure was undertaken in order to prevent odor leakage from the well. Odors are especially generated by the filled grid and accumulated odorous material at the well bottom, which as a consequence has to be cleaned on a regular basis. Moreover, the turbulence created by the small waterfall of the filled

grid favors even more odor generation (see fig. 15).

Figure 14: Top view of the well grid belonging to Pumping Station 2 around 60 meters beeline from the WWTP site, which can be confirmed via the labeled satellite figure 2.

Figure 15: View inside the well of Pumping Station 2.

1.4.6 Other facts about the WWTP Camping San Fernando

Furthermore, it was mentioned that this particular WWTP is not under the influence of groundwater level rising and thus there is no input of salt water from the Mediterranean Sea. This is an important fact for the pH- and other water-related values both within the canalization and the process basins and pipes belonging directly to the WWTP site.

Figure 16: Pumping station 2 after sealing with metal plates on 7 August 2018.

2 Theory section

In this section of the thesis, the reader will be introduced further in important concepts concerning odor perception, generation, control, measurement and dispersion modeling. To start with, generic information about the wastewater treatment plants are going to be provided in what follows.

2.1 General information about wastewater treatment plants (WWTP)

According to [Wat09, p.2 et seq.], wastewater typically averages 99.94% water by weight. Only a small 0.06% is actually waste material that is either dissolved or suspended in the water. Aside from human waste, other water pollutants include food particles, paper products, dirt, oil and grease, proteins, organic materials such as sugars, inorganic materials such as salts, personal care products, pharmaceuticals, cleaning chemicals, among others.
Treatment plants are designed to accomplish a stream of clean water that is safe to return to the environment. What happens in a wastewater treatment plant is essentially the same process that occurs naturally in a stream or lake. A treatment plant simply helps speed up water's natural process. In a typical stream or lake, bacteria and other small organisms living in the water body feed on waste. While consuming this food, the organisms eliminate waste and produce new bacterial cells, carbon dioxide, and other products in a natural cycle. However, as the bacteria consume the wastewater, they also consume oxygen. In order to support aquatic life, a water body must maintain a certain level of dissolved oxygen, which is typically absorbed from the air and aquatic plants. If only a small amount of untreated wastewater enters a stream, bacteria can consume the waste along with the necessary oxygen, and then the water body will naturally replenish its lost oxygen. Trouble begins if the amount of wastewater discharged into a stream is so great that bacteria consuming the waste deplete the available supply of dissolved oxygen that fish and other aquatic organisms need for survival. Growing human populations can cause the volume of wastewater to increase beyond a level that the natural process can absorb and purify by itself. To help maintain an effective balance, wastewater treatment facilities are employed to supplement nature's work. In a wastewater treatment plant, bacteria and other organisms are also used to consume waste, but in a much more controlled process.
Occasionally, wastewater can also contain substances that cannot be completely removed by microorganisms in wastewater treatment, e.g. pesticides, heavy metals, nutrients, and pharmaceuticals. Because these substances may have adverse health or environmental effects on downstream water supplies, wastewater treatment plants must go above and beyond the natural process and use complex, auxiliary treatment processes to remove what the bacteria cannot consume. Additionally, some wastewater could contain potentially harmful bacteria, viruses, and other microorganisms, which are different from the beneficial bacteria feeding on the waste. Therefore an important process after treatment is the removal of disease-producing pathogenic bacteria and organisms through disinfection before the water is discharged.
Most private homes, businesses, and institutions throughout the modern world are connected to a network of below-ground pipes that carry their wastewater to a treatment plant. Sanitary sewer systems carry only domestic and industrial wastewater, while a combined sewer also carries storm water runoff. Wastewater in these systems either flows by gravity or is pumped into the treatment plant, and in some cases a combination of both methods is used. Once it arrives at the plant, wastewater is typically treated through a series of five major steps:
preliminary treatment, primary treatment, secondary treatment, tertiary treatment, and disinfection, along with processes to reuse or to dispose of the remaining products.

2.1.1 Preliminary treatment

Following [Wat09, p.6], this step helps remove many of the solids that could clog pipes and disable treatment plant pumps down the line. Screening removes large objects, such as sticks, rags, leaves, plastics, sanitary products, rocks, toys, or trash. In the examined WWTP located in Oliva (Comunidad Valenciana, Spain) this work was being accomplished by metal grids installed directly at the outflow of the sewer (s. fig. 17).

Figure 17: Picture of the coarse grate which was installed formerly at the outlet of the sewage system preventing chunky material from entering the primary biological reactor of the WWTP Camping San Fernando.

During the winter season 2018/19, the old canalization entrance was replaced by a new system containing an automatic rotating sieve and a submerged inlet. The difference before and after can be seen when comparing the two on-site photographs 6 and 7.
Treatment plant screens are built to withstand the flow of untreated wastewater for years at a time and are typically made of steel or iron bars set in parallel about one-half inch apart. Some treatment plants use devices that combine the function of a screen with that of a grinder to further reduce the impact of large solids on downstream processes.
The sand, grit, and gravel that make it through the screens are picked up in the next stage of pretreatment - the grit chamber. Grit chambers are large tanks designed to slow down wastewater just long enough for the grit to drop to the bottom. Sometimes the grit is washed after its removal from the chamber and disposed of, which could mean being buried in a landfill or incinerated.

2.1.2 Primary treatment

In the report [Wat09, p.7] it is mentioned that primary treatment involves a more sophisticated settling tank, also called a sedimentation tank or clarifier. In this phase, a series of operations removes most of the solids that will float or settle, a process that can remove up to $50\,\%$ of pollutants.

With respect to the object of examination, i.e. the WWTP Camping San Fernando in Oliva, Comunidad Valenciana, the primary treatment is already included into the secondary treatment with the biological reactor and successive decantation system (s. fig. 11 and 8).

Sedimentation removes the solids that are too light to fall out in the grit chamber. These tanks are designed to hold wastewater for several hours. During that time, floating material, such as oil and grease, can be skimmed off the top, and suspended solids can drift to the bottom of the tank, where they are collected by mechanical scrapers and pumped out of the bottom of the tank. The solids removed at this point are called primary solids, and they are usually pumped along for further treatment or solids thickening. The floatable substances collected are either sent on with the primary solids for treatment, disposed of, or incinerated.
This is the end of the primary stage of treatment. Most of the solids in the stream that can be removed by the purely physical processes of screening, skimming, and settling have been collected, and secondary treatment using biological or chemical processes is next in line.

2.1.3 Secondary treatment

According to [Wat09, p.7 et seq.], wastewater flowing out of primary treatment still contains solid materials, either floating on the surface, dissolved in the water, or both. In a natural stream, these substances would be a source of food for protozoa, fungi, algae, and hundreds of varieties of bacteria and microorganisms. This is also the case in wastewater treatment plants, and particularly in the WWTP Camping San Fernando this job is accomplished by the bioreactor (see figure 5). The secondary treatment process is a highly controlled artificial environment where the ideal conditions are created for microscopic organisms to work as fast and efficiently as they can. Care is taken to create an environment with the appropriate temperature, oxygen level, and contact time to support rapid and complete consumption of dissolved wastes. Feeding on waste just as they would in nature, the microorganisms biologically convert the dissolved solids in the wastewater into suspended solids, which can then physically settle out. The final products are carbon dioxide, cleaner water and more microorganisms.

2.1.4 Activated sludge process

There are several methods available to help treatment plants control microorganisms in order to filter or settle out the resulting solids. However, one of the most common forms of secondary treatment is the activated sludge process. In this method, incoming wastewater and microorganisms are mixed in a large tank using constant aeration and agitation for a period from a couple of hours to an entire day. The microorganisms are essentially "activated" by bubbling oxygen through the mixture. This process is also applied in the bioreactor of the WWTP Camping San Fernando, as can be seen in figure 5 and 8.
Activated sludge is a continuous process, meaning a portion of the settled solids containing active microorganisms, also known as return activated sludge, is circulated back to the beginning of the process to continue working. The portion that does not go back into circulation is called waste activated sludge, and it is piped on for further treatment.
The mixture of water and microorganisms flows on to a sedimentation tank, similar to the one used in primary treatment, where the microorganisms and other solids settle to the bottom.

2.1.5 Aerated basins and lagoons

Returning to [Wat09, p.8], some communities, also the WWTP Camping San Fernando to be analyzed, use aerated basins or lagoons for secondary treatment as well (s. fig. 8). The primary biological

reactor together with its neighboring decantation basin can be seen in figure 2.

This form of treatment relies heavily on the interaction of sunlight, algae and oxygen, and since these interactions are relatively slow, the wastewater is artificially aerated to speed up the process. As with membrane bioreactors, this process usually operates without the use of a sedimentation tank. Suspended solids settle to the bottom of the lagoon where they remain or are removed every couple of years. Generally speaking, lagoons are simpler to operate than other forms of secondary treatment, but can be less efficient on the other hand.

After the first step of aerated biological treatment in the WWTP Camping San Fernando, a decantation basin removes the suspended organic material from the remaining wastewater, as it can be reviewed in figure 11.

At the end of most secondary treatment processes, $85-90\,\%$ of the waste has been removed from the water.

2.1.6 Disinfection

Following [Wat09, p.9], disinfection is the final stop in the treatment process in many plants before the water is released back into the environment. Disinfection significantly reduces any remaining bacteria and viruses and helps protect the public from exposure to potentially pathogenic microorganisms. Although for years many plants relied on methods involving chlorination to do the job, alternative methods, such as ultraviolet and ozone disinfection, are becoming more widespread.

In the traditional process of chlorination, which is also used in the WWTP Camping San Fernando after the wastewater has passed through the bioreactor and the decanter, a chlorine solution is added to wastewater to disinfect or kill present pathogens. However, since chlorine gas can be hazardous to human health, many plants are moving to sodium hypochlorite solutions, which are similar to the chlorine found in swimming pools, or bleach. Because chlorine can remain in the water after the disinfection process is completed, it can also be carried into the stream. Some sensitive water bodies require the removal of this remaining chlorine, because it can be toxic to the aquatic organisms living in the stream. The removal process, called dechlorination, is usually performed by adding sulfur compounds (sulfur dioxide) to absorb the chlorine.

Once the water has been properly disinfected it can be safely sent on its way back to the oceans, rivers, lakes, or streams in the communities or on for other uses. Following [Hal12, p.1], it can also be used for groundwater recharge or agricultural purposes, if it is sufficiently clean.

2.1.7 Solids processing and handling

Following [Wat09, p.10], wastewater treatment processes not only create clean water, but also leave behind solids which need to be treated as well, and handling these solids can often be more expensive and complex than the actual process of purifying the water.

Untreated solids are often referred to as sludge, and treated solids are known as biosolids. However, these mixtures of solids and wastewater are not that thick and molasses-like. In fact, they are slurries of water and solids that are roughly 100 times more concentrated than the wastewater that first enters a plant, which is still only about $3-6\,\%$ solids. Because these mixtures contain so much water, and more mass equates to higher processing and handling costs, it is logical for plants to try to dispose of or recycle as much liquid as possible. Solids-handling processes are designed to help make that happen. The spectrum of handling techniques is divided into processes that condition, thicken, stabilize, and dewater solids.

Dewatering is typically accomplished by mechanical means. Filters, centrifuges and sludge presses remove even more water from the biosolids. Other techniques such as drying beds (used in the WWTP

Camping San Fernando, s. fig. 13) can also be used to dewater, producing up to $50\,\%$ solids which equals roughly the consistency of dry soil. At the end of the process, the concentrated solids can be beneficially used through land application, composted for use as a soil conditioner, incinerated for thermal or energy recovery, or placed in landfills.

2.2 Odor perception

In the work [Car+14, p.3 et seq.] it is stated that odor response is a very subjective and difficult to predict issue since it depends on the detection response for each person. The main problem is that the odor is a result of many different odorants substances and their interaction. This odorants' interaction, whose principles are still unclear, influences the odor perception (Gostelow and Parsons 2000). It is necessary, though, to distinguish between *odorants and odors*.

The odorant is the responsible compound that actually generates an odor. On the other hand,

the odor is the perceived effect when the odorant has been detected and interpreted by a sensory system.

This interaction between the odorant properties and the odor generated is not very clear due to the lack of theoretical knowledge of the human olfactory system (Gostelow et al.2001). Lebrero et al. (2011) presented an exhausted odor assessment and management review where a number of studies about odor analysis, classified in sensory, chemical, and online analysis, are evaluated. Many attempts have been made in order to establish a correlation between the odor concentration, expressed as odor units ($\mathrm{OU_E\,m^{-3}}$) or odor intensity, with the actual chemical concentration for several nuisance compounds (Gostelow et al. 2001; Hobbset al. 2002; Lacey et al. 2004; van Thriel et al. 2006; Tsaietal. 2008; Lehtinen and Veijanen 2011). Volatile organic (sulfur) compounds (VO(S)Cs), hydrogen sulfide and ammonia have been the focus of the studies due to their known unpleasant odor and irritation character. It has been demonstrated that the relationship between odor units and chemical concentration follows an exponential function and may be expressed by Steven's law as follows (Ferreira2012):

$$c_{\mathrm{OU}_i} = \mathsf{k}_i * c_i^{\mathsf{n}} \tag{1}$$

where

$c_{\mathbf{OU}_i}$ is the odor concentration of species i in $\mathrm{OU_E/m^{-3}}$,

$\mathbf{k}_i$ is the proportional parameter of species i in $\mathrm{OU_E/ppm}$,

n is the dimensionless exponential parameter of species i, and

c_i is the chemical concentration of species i in ppm.

Steven's law (1) establishes an exponential relationship between the chemical hydrogen sulfide concentration and the odor intensity or concentration. Both the proportional and exponential parameters must be carefully calibrated in each case. This expression works well and it is meaningful for a range outside of 0.4 - 0.6 ratios for binary mixtures because inside this range it overestimates the actual values (Ferreira2012).
Steven's law has shown good results for odor estimation in sewage and wastewater treatment plants using hydrogen sulfide chemical concentration as an indicator (Gostelow et al. 2001; McGinley and Sensory 2008; Lehtinen and Veijanen2011).

Conclusion on Stephen's Law from [Car+14, p.3 et seq.]
Even though equation (1) works quite well for hydrogen sulfide, an important drawback of this expression is that this relationship cannot be used for other indicator compounds since the prediction accuracy decreases compared to the H_2S-case. For instance, ammonia does not present an apparent relation as a consequence that it preferentially occupied sensor receptor cell sites more than other odorants, producing a constant stimulus and leading to alter the olfactory acuity (Tsaiet al. 2008). Furthermore, there are no conclusive results about the performance and interaction, within the emissions from WWTP facilities, for other odorant compounds such as reduced sulfur.

2.2.1 Official statutes and definitions concerning odor nuisance and pollution

After a general introduction into human odor perception, the official limit definitions are going to be explained regarding what is actually considered a nuisance or pollution. Hereinafter, the emphasis will be put on the national Spanish and regional Valencian law since these are the relevant and authoritative values to consider in the context of this project.

I) Spanish National Institute of Occupational Health and Safety (INSST)
The official statute "Exposure Limits for Chemical Agents at Work in Spain 2019" [Ins19] published by the National Institute of Occupational Health and Safety (INSST), belonging to the Ministry of Labor, Migration and Social Security - Government of Spain of the Ministry of Labor, provides regulatory limit values for both target chemical compounds of this project, i.e. $\mathrm{NH_3}$ and $\mathrm{H_2S}$.

General terminology
The terms described in the following originate from the document [Ins19] which is written in Spanish Language as it was emitted by the Spanish Government. Therefore, the acronyms are going to remain according to their meaning in Spanish even though the entire words are going to be put in English for the reader.

Daily Exhibition (ED):
According to the passage [Ins19, p.15f], it is the average concentration of the chemical agent in the worker's breathing zone measured or calculated in a weighted form with respect to the real working time of a day, i.e. it is assumed a standard labor day of eight daily hours. The average concentration to the aforementioned standard day involves considering the set of different exposures of the worker in (fractions of) hours throughout the actual working day, each one with its corresponding duration, as equivalent to a single eight-hour uniform exposure: $ED = (\sum_{n=1}^{n} c_i * t_i)/8$
Of course, the 8 hours can be replaced by any different daily working duration. Moreover, the sum over all times of exposure should equal the entire working day duration.

Short Duration Exhibition (EC):
This value works in the same way as the aforementioned with the main difference of the mean duration for which the sum is weighted (here 15 minutes) and also that those 15 minutes should be recorded end-to-end (see [Ins19, p.16f]): $EC = (\sum_{n=1}^{n} c_i * t_i)/15$

Environmental Limit Value - Daily Exposure (VLA-ED):
The VLA-ED is the reference value for the Daily Exhibition (ED), as it has been defined above. In this way, the VLA-ED represents conditions to which it is created, based on the current knowledge that most of the workers can be exposed 8 hours a day and 40 weekly hours throughout working life without suffering adverse effects for their health.

Environmental Limit Value - Short Exposure Duration (VLA-EC):

The threshold stands for the reference value of the Short Exposure Duration (EC), as it has been defined before. The VLA-EC must not be exceeded by any EC throughout the workday. For those chemical agents that have effects recognized as acute effects, but whose main toxic effects are of a chronic nature, the VLA-EC constitutes a complement to the VLA-ED and therefore, both limits have to be assessed when dealing with these chemical agents. By contrast, chemical agents of mainly acute effects, as for example irritating gases, a VLA-EC is sufficient for its evaluation.

Valores límite indicativos europeos (VLI):

European limit value index

II) Valencian Ministry of Agriculture, Environment, Climate Change and Rural Development

Whereas the previous definitions originate from the national regulations of Spain, the following definitions of atmospheric emissions levels of certain pollutants include proper values, particularly regarding hydrogen sulfide ($\mathrm{H_2S}$) on the regional scale of the Autonomous Valencian Community (see more details under [Dia18, p.24] and in the extracted table 20).

Furthermore, it is stated, according to [Dia18, p.24], that if there is no specific regulation that determines the emission levels of a certain activity, the limits set in the corresponding authorization may be established based on the values given in table 20, as long as there are techniques available that safeguard their compliance.

Moreover, the results of the emission measurements should refer to normal operating conditions of the installation without prior dilution, unless there is a specific legislation or authorization indicating a deviant reference.

III) Alternative international statutes and parameters

The following odor measurement parameters obtained from [Hal12, p.6 et seq.] refer to different odor concentration limits:

Perception Threshold (ATC: Absolute Threshold Concentration):

Defined as the minimum concentration that can be detected by $100\,\%$ (in some cases by $50\,\%$ as in [Hal12, p.18 et seq.]) of the persons involved with an olfactory analysis. In some cases the geometric mean of the measurements of the single members is used.

Odor Number (TON: Threshold Odor Number):

Represents the number of dilutions needed to reduce the concentration of the sample to the ATC.

Maximum Exposure Concentration (TLV: Threshold Limit Value):

Stands for the maximum concentration at which persons can be exposed for a period of 8 hours a day, 6 days a week and 50 weeks a year (weighted average over 8 hours), for a work life of 40 years.

Maximum Allowable Concentration (MAC: Maximum Allowable Concentration):

Maximum concentration which should never be exceeded.

Dilution-to-Threshold (D/T) ratio:

At first, the definition given by one of the olfactometry panelists involved in the field campaigns

will be illustrated. According to his statement, the unit "40 PPTV BUTANOL" employed in the collected data stands for "40 parts per trillion volume mixing ratio", or in short "40 ppt". The measuring instrument must have been calibrated to each individual nose of the panelists and the reference unit in this context was 40 ppt(v) butanol. This unit refers to the degree of dilution achieved by a neutral gas without odor; in this case butanol. With this gas, the external odor is obscured initially with the highest degree of dilution and the panelist will diminish the dilution from maximum to zero until reaching a point where the dilution is not sufficient anymore to mask the external odor. At exactly this point, the "Dilution-to-Threshold (D/T) ratio" will be noted down in order to express the intensity of the external odor.

Apart from the aforementioned definition, according to [Hal12, p.18 et seq.], a (dynamic) olfactometer directly measures and quantifies odor strength in the ambient air using the operating principle of mixing odorous ambient air with odor-free filtered air in discrete volume ratios. The discrete volume ratios are called "Dilution-to-Threshold" (D/T) ratios (see eq. (2)).

$$\frac{\text{D}}{\text{T}} = \frac{\text{Volume of Carbon-Filtered Air}}{\text{Volume of Odorous Air}} \tag{2}$$

To measure intensity, the olfactometer introduces an odorous gas as a baseline against which other odors are compared. The instrument "Nasal Ranger Olfactometer" used in [Hal12, p.18 et seq.] has an accuracy of $\pm 10\%$ and a response time of 2 seconds. The categories of the D/T ratios are:
>=2 Noticeable, >=7 Objectionable, >=15 Nuisance, >=31 Nauseating

Stephen's Law:

In subsection 2.2 "Steven's law" was mentioned (1) which establishes an exponential relationship between the chemical hydrogen sulfide concentration and the odor intensity/concentration according to [Car+14, p.3 et seq.]. Steven's law has shown good results for odor estimation in sewage and wastewater treatment plants using hydrogen sulfide chemical concentration as an indicator (Gostelow et al. 2001; McGinley and Sensory 2008; Lehtinen and Veijanen2011). For further details see the aforementioned subsection 2.2.

2.2.2 Threshold concentrations of ammonia ($\mathbf{NH_3}$)

Concerning the ammonia limit values, only those from the national level were taken into account and are explained in the following paragraph.

Spanish National Institute of Occupational Health and Safety (INSST)

In the accordance with the above-mentioned official statute "Exposure Limits for Chemical Agents at Work in Spain 2019" the ammonia limit values are depicted in the subsequent table 18 extracted from [Ins19, p.38].

Nº CE	Nº CAS	AGENTE QUÍMICO (año de incorporación o de actualización)	VALORES LÍMITE				NOTAS	INDICACIONES DE PELIGRO (H)
			VLA-ED® ppm	VLA-ED® mg/m³	VLA-EC® ppm	VLA-EC® mg/m³		
	12172-73-5	Amianto:Amosita	0,1 fibras/cm³				**C1A**, t, r	**350-372**
	77536-67-5	Amianto:Antofilita	0,1 fibras/cm³				**C1A**, t, r	**350-372**
	12001-29-5	Amianto:Crisotilo	0,1 fibras/cm³				**C1A**, t, r	**350-372**
	12001-28-4	Amianto:Crocidolita	0,1 fibras/cm³				**C1A**, t, r	**350-372**
	77536-68-6	Amianto:Tremolita	0,1 fibras/cm³				**C1A**, t, r	**350-372**
205-483-3	141-43-5	2-Aminoetanol (2008)	1	2,5	3	7,5	vía dérmica, VLI	**332-312-302-314**
		Aminometano	véase Metilamina					
207-988-4	504-29-0	2-Aminopiridina	0,5	1,9				
200-521-5	61-82-5	3-Amino-1,2,4-triazol		0,2			ae, VLI	**361d-373**-411
		Amitrol	véase 3-Amino-1,2,4-triazol					
231-635-3	7664-41-7	Amoníaco	20	14	50	36	VLI	221-**331-314**-400
203-564-8	108-24-7	Anhídrido acético	5	21				226-**332-302-314**
201-607-5	85-44-9	Anhídrido ftálico	1	6			Sen	**302-335-315 318-334-317**
201-604-9	85-42-7	Anhídrido hexahidroftálico (2007)				0,005	FIV, Sen	**318-334-317**

Figure 18: Extract from the regulation of the environmental limit values of daily and short exposure (see [Ins19, p.38]) associated with ammonia (or NH_3), here called "Amoníaco" in Spanish. Together with the limit concentrations provided both in mg/m^3 and ppm (assuming standard conditions and gas state of the pollutant, derived from mg/m^3 employing the conversion written under [Ins19, p.19]), the H-Phrases explained in the list 2.2.2 are included as well.

Apart from that, the H-phrases associated with ammonia were extracted and translated from the same document [Ins19, p.170ff] and are mentioned in the info table 18 under the term "Amoníaco". Following, their corresponding definitions are outlined:

H221: Flammable gas

H314: Causes severe skin burns and eye damage

H331: Toxic if inhaled

H400: Very toxic to aquatic life

2.2.3 Threshold concentrations of hydrogen sulfide (H_2S)

As for the hydrogen sulfide limit values, apart from the national Spanish level regulations those from the regional scale of the Valencian Community were also considered.

I) Spanish National Institute of Occupational Health and Safety (INSST)
In conformity with the aforementioned official statute "Exposure Limits for Chemical Agents at Work in Spain 2019" the hydrogen sulfide thresholds are displayed in the following table 19 taken from [Ins19, p.105].

Nº CE	Nº CAS	AGENTE QUÍMICO (año de incorporación o de actualización)	VALORES LÍMITE				NOTAS	INDICACIONES DE PELIGRO (H)
			VLA-ED®		VLA-EC®			
			ppm	mg/m³	ppm	mg/m³		
201-058-1	77-78-1	Sulfato de dimetilo	0,05	0,26			**C1B**,vía dérmica, Sen,r	**350-341-330-301 314-317**
232-104-9	7786-81-4	Sulfato de níquel, como Ni		0,1			**C1A**,Sen,r,TR1B	**350i-341-360D 372-332-302-315 334-317**-400-410
222-995-2	3689-24-5	Sulfotep		0,1			vía dérmica, VLBa, VLI, s, FIV	**310-300** 400-410
200-846-2	75-18-3	Sulfuro de dimetilo	10					
215-147-8	1306-23-6	Sulfuro de cadmio, como Cd. Fracción inhalable		0,01			**C1B**,VLB®,r	**350-341-361fd 372-302**-413
215-147-8	1306-23-6	Sulfuro de cadmio, como Cd. Fracción respirable		0,002			**C1B**,VLB®,r,d	**350-341-361fd 372-302**-413
231-977-3	7783-06-4	Sulfuro de hidrógeno (2012)	5	7	10	14	VLI	220-**330**-400
252-545-0	35400-43-2	Sulprofós (2013)	0,008	0,1			VLBa, s, FIV	
202-273-3	93-76-5	2,4,5-T		10			vía dérmica	**302-319-335 315**-400-410
238-877-9	14807-96-6	Talco (sin fibras de amianto) Fracción respirable		2			d, e	

Figure 19: Extract of the definitions of the environmental limit values of daily and short exposure (see [Ins19, p.105]) related to hydrogen sulfide (H_2S), here called "Sulfuro de hidrógeno (2012)" in Spanish. Along with the limit concentrations given both in mg/m^3 and ppm (assuming standard conditions and gas state of the pollutant, derived from mg/m^3 employing the conversion provided under [Ins19, p.19]), the H-Phrases explained in the list 2.2.3 are mentioned.

In the same way as proceeded with ammonia, the H-phrases related to hydrogen sulfide were taken and translated from the same document [Ins19, p.170ff] and are stated in the table 19) under the naming "Sulfuro de hidrógeno (2012)". Henceforth, the definitions of these H-phrases are explained:

H220: Extremely flammable gas

H330: Fatal if inhaled

H400: Very toxic to aquatic life

II) Valencian Ministry of Agriculture, Environment, Climate Change and Rural Development

The decree 228/2018 of 14 December [Dia18] published by the Valencian Council, which is in charge of the emission control caused by activities potentially polluting the atmosphere, falls in line with the above-mentioned environmental short time exposure limit of 10 ppm (compare 19 with 20). This equals approximately 7.17 ppm considering a molecular weight of H_2S of 34.1 g/mol following the standard conversion procedure to be found on the web page [Can19] as well as in the document emitted by the Spanish Government [Ins19, p.19].

Contaminantes	*Unidades*	*Niveles de emisión*
Partículas	mg/m^3	30
HCl y cloruros (expresado como HCl)	mg/m^3	10
HF y fluoruros (expresado como HF)	mg/m^3	5
H_2S	mg/m^3	10
SO_2	mg/m^3	350
NO_x (expresado como NO_2)	mg/m^3	450
CO	mg/m^3	100

Figure 20: Hydrogen sulfide (H_2S) limit value of 10 mg/m^3 extracted from [Dia18, p.24] in the decree 228/2018 of 14 December published by the Valencian Council, which is a regional institution belonging to the Autonomous Valencian Community in Spain.

III) Other international sources

The abbreviations needed in the forthcoming pollutant limit definitions are listed in the following:

OSHA: The Occupational Safety and Health Administration is responsible for protecting worker health and safety in the United States.

NIOSH: The National Institute for Occupational Safety and Health, a US Federal agency responsible for conducting research and making recommendations for the prevention of work-related disease and injury.

IDLH: Immediately dangerous to life and health (level that interferes with the ability to escape) (NIOSH)

PEL: Permissible exposure limit (enforceable) (OSHA) ppm: parts per million

REL: Recommended exposure limit (NIOSH)

In the following table 1 threshold concentrations of various chemical compounds are listed; also those of the measured gaseous pollutants ammonia and hydrogen sulfide. It should be noted that the the threshold concentrations differ a lot from one odorant to another. As for the meaning of ATC, TLV and MAC, please see the aforementioned list 2.2.1.

Table 1: Threshold concentrations in ppm of a selection of bad odor precursors extracted from [Hal12, p.7].

Compounds	ATC (ppm)	TLV (ppm)	MAC (ppm)	Olfactory sensation
Hydrogen sulfide	0.00047	10	50 (USA), 20 (UK)	Rotten eggs
Ammonia	46.8	25	37.5 (UK)	Pungent
Methyl mercaptan	0.0021	10		Rotting cabbage
Carbon disulfide	0.21	20		Sweet/pungent
Biphenyl sulfide	0.0047			Burned rubber
Dimethyl sulfide	0.001			Rotting vegetables

International definitions concerning hydrogen sulfide

The Worker Exposure Limits extracted from [OSH] are listed with explained abbreviations below.

NIOSH REL (10-min ceiling): 10 ppm (15 mg/m3)

OSHA PELs:

General Industry Ceiling Limit: 20 ppm

General Industry Peak Limit: 50 ppm (up to 10 minutes if no other exposure during shift)

Construction 8-hour Limit: 10 ppm

Shipyard 8-hour limit: 10 ppm

NIOSH IDLH: 100 ppm

International definitions concerning ammonia

In table 1, a great difference can be seen between ammonia and other common gases associated with bad odors, such as hydrogen sulfide. According to the related source [Hal12], ammonia has a higher perception threshold than the TLV (and partially even the MAC), whereas concerning the other gases it is just the other way round. Those gases can be perceived already before dangerous concentrations are reached.
Following [Age04], OSHA has set an 8-hour exposure limit of 25 ppm and a short-term (15-minute) exposure limit of 35 ppm for ammonia in the workplace. NIOSH recommends that the level in workroom air should be limited to 50 ppm for 5 minutes of exposure.
Furthermore, other ceiling concentrations for ammonia can be found in a study of [Sme+07] in which odor and lateralization (irritation) thresholds (LTs) for ammonia vapor were measured using static and dynamic olfactometry. The purpose of the study was to explore the test–retest reliability and comparability of dynamic olfactometry methodology, generally used to determine odor thresholds following the European Committee for Standardization guidelines in the context of odor regulations to outside emissions, with static olfactometry. Within a 2-week period, odor and LTs for ammonia were obtained twice for each method for 24 females. No significant differences between methods were found: mean odor detection thresholds (ODTs) were 2.6 parts per million (ppm) for either method ($P = 0.96$), and mean LTs were 31.7 and 60.9 ppm for the static and dynamic method, respectively ($P = 0.07$).
In addition, the Centers for Disease Control and Prevention ([CDC94]) stated the following values:

NIOSH REL: 25 ppm (18 mg/m3) TWA (Time-Weighted Average) concentration, 35 ppm (27 mg/m3) STEL (Short Term Exposure Limit)

Current OSHA PEL: 50 ppm (35 mg/m3) TWA concentration

1989 OSHA PEL: 35 ppm (27 mg/m3) STEL

1993-1994 ACGIH TLV: 25 ppm (17 mg/m3) TWA concentration, 35 ppm (24 mg/m3) STEL

Description of substance: Colorless gas with a pungent, suffocating odor

LEL: 15% (10% LEL, 15,000 ppm)

Original (SCP) IDLH: 500 ppm

Basis for original (SCP) IDLH: The chosen IDLH is based on the statement by AIHA [1971] that 300 to 500 ppm for 30 to 60 minutes have been reported as a maximum short exposure tolerance [Henderson and Haggard 1943]. AIHA [1971] also stated that 5000 to 10000 ppm are said to be fatal [Mulder and Van der Zahm 1967] and exposures for 30 minutes to 2500 to 6000 ppm are considered dangerous to life [Smyth 1956].

Additionally, following the definitions of acute exposure guideline levels (AEGLs) in the guideline of the Committee on Acute Exposure Guideline Levels, Committee on Toxicology, National Research Council ([Lev08]), AEGL-1 is the airborne concentration (expressed as parts per million (ppm) or milligrams per cubic meter (mg/m^3)) of a substance above which it is predicted that the general population, including susceptible individuals, could experience notable discomfort, irritation, or certain asymptomatic non-sensory effects. However, the effects are not disabling and are transient and reversible upon cessation of exposure.
The AEGL-1 value was based on a study in which 2 out of 6 human subjects experienced faint irritation after exposure to ammonia at 30 ppm for 10 min (MacEwen et al. 1970).

- The odor of ammonia can be detected by humans at concentrations $>$5 ppm,
- the odor is highly penetrating at 50 ppm (10 min).
- Human volunteers exposed to ammonia showed slight irritation at 30 ppm (10 min),
- moderate irritation to the eyes, nose, throat, and chest at 50 ppm (10 min to 2 h),
- moderate to highly intense irritation at 80 ppm (30 min to 2 h),
- highly intense irritation at 110 ppm (30 min to 2 h),
- unbearable irritation at 140 ppm (30 min to 2 h) and
- excessive lacrimation and irritation at 500 ppm.
- Reflex glottis closure, a protective response to inhaling irritant vapors, occurred at 570 ppm for 21- to 30-year-old subjects, 1,000 ppm for 60-year-old subjects, and 1,790 ppm for 86- to 90-year-old subjects.

Finally, according to the Hazardous Substance Fact Sheet about ammonia published by the New Jersey Department of Health ([Hea07]), the odor threshold is 5 ppm. They state that odor thresholds vary greatly and generally one should not rely on odor alone to determine potentially hazardous exposures.

2.3 Odor generation

According to [SS05, p.29], odor can be defined as a stimulus of olfactory cells in the presence of specific compounds including VOCs and VICs, which are treated in more detail in subsection 2.3.2.

2.3.1 Odor causing mechanisms

Corresponding to [Cen17, 23 et seq.], the processes generating odor in a typical Indian municipal solid waste (MSW) landfill site are listed below. These can be generalized to the processes occurring in sewage systems and WWTPs.

Volatilization
: is the most important mechanism for odor emissions and occurs when odorants of a dissolved or pure substance skip to an adjacent gas layer for waste at this surface, this action results in immediate transport into the atmosphere.

Biodegradation
: is the disintegration of organic material by bacteria, fungi or other biological means. Biodegradable matter being organic based serves as a nutrient for microorganisms, the decomposition of biodegradable substances may proceed through both aerobic and anaerobic process. Anaerobic processes generate more odorous compounds.

Photo-decomposition
: such as photo dissociation, photolysis, or photo-decomposition are chemical reactions induced by physical energy in which a chemical compound is broken down by photons. Enormous solar flux which accelerates the rate of biodegradation and volatilization thereby increases odor nuisance.

Hydrolysis
: Municipal solid waste (MSW) generally have high moisture content. Hydrolysis is the reverse of a condensation reaction wherein two molecules combine into a larger one and eject a water molecule. Thus hydrolysis adds water to break down, whereas condensation builds up by removing water. The odorants soluble in water pass to leachate which in turn gives rise to odor emission through volatilization.

Combustion
: is a chemical reaction that occurs between a fuel and an oxidizing agent that produces energy, usually in the form of heat and light. In a MSW landfill site self-ignition may also occur due to production of methane and the heat generated at the dump site triggering the ignition automatically, which produces obnoxious odorous gases.

2.3.2 Odor generators

Following [Hal12, p.6 et seq.] and [Car+14, p.1 et seq.], odorous compounds originate from the microbial decomposition of compounds with a high molecular weight, especially proteins and mainly when anaerobic conditions are reached. Anaerobic fermentation, more specifically hydrolysis and acidogenesis, is an important precursor to the other anaerobic processes involving the transformation of large, complex organic molecules into smaller, simpler molecules that can be directly utilized by other microorganisms as a substrate. The organic products of anaerobic hydrolysis generally do not contribute directly to odor emissions from sewers, with the exception of the hydrolysis of organic sulfur-containing compounds by bacteria resulting in the production of hydrogen sulfide, organic sulfides and disulfides. In regards to the chemical nature of the odors, most of unpleasant environmental odors

are related with sulfide-derived compounds. According to [Che+15, ch.5] and [Car+14, p.2] methane and carbon dioxide are the main gaseous products of anaerobic digestion and along with hydrogen sulfide (see subsection 2.3.5) the main atmospheric emissions from WWTP. Nevertheless, depending on the nature of the incoming precursors, pH and redox potential, different odor-related substances may be biologically formed in anaerobic reactors.

Mixture of odorants According to [SS05, p.29], the most common odor problems are generally caused by mixtures of highly volatile compounds with very low threshold detection limits that are in low concentration in air. Several authors identified VOCs (see subsection 2.3.2) together with H_2S (see subsection 2.3.2) as being the major odor stimuli in sewer pipes and aerobic wastewater treatment plants (Smet and van Langenhove 1998).
In the work of [Car+14, p.2] it is stated that control odor strategies depend on the knowledge of the interactions between its chemical components and their dilution in the atmosphere after being emitted. Hydrogen sulfide is a common compound in the atmospheric emissions from wastewater treatment plants (WWTP) but, if other odor species, such as volatile organic sulfur compounds (VOSCs), are also emitted, the final odor effect will be modified by the synergetic action of these organic volatile substances, changing the typical odor of rotten egg to another one more or less unpleasant odor (Laing et al. 1994). For this reason, it is quite complicated to predict the odor characteristics of gas mixtures even though their exact chemical composition could be determined. From the beginning of the 20th century, plenty of research has been done in regard to the effects of several different odor constituents. However, there is little research related with odor mixtures of more than two substances (Laing et al. 1994).

Volatile organic compounds (VOCs) According to the VOC and odor definition on [SS05, p.29], VOCs are emitted as gases from certain solids or liquids. Furthermore, it is stated that the generic term "VOC" includes a variety of chemical compounds, some of which may have short- and long-term adverse health effects. Moreover, they have been identified as a major contributor to smog, which can cause respiratory problems such as eye irritation, headache, haze, and damage to plant and animal life. As also mentioned in [SS05, p.29], Title I of the Clean Air Amendment (CAA) defines a VOC as any compound containing carbon, excluding carbon monoxide, carbon dioxide, carbonic acid, metallic carbides or carbonates, and ammonium carbonate, which participates in atmospheric photochemical reactions. Following [SS05, p.29], a more clear definition is provided by the United States Environmental Protection Agency (US EPA), and typically regards VOCs as organic compounds having vapor pressure exceeding 0.1 millimeters of mercury (mmHg) at standard conditions ($20°$C and 760mmHg).

Furthermore, in accordance with [Hal12, p.6], organic compounds containing nitrogen or sulfur atoms (often VOCs) are associated with bad odors, which also fits the statement of [Car+14, p.2].

Following [Cen17], [Hal12, p.6], [Car+14, p.1 et seq.], [SS05, p.29] and [Che+15, ch.5], VOC-odorants identified within WWTPs and landfills are: Reduced amino-compounds, reduced sulfur-compounds, aldehydes and ketones, indole and skatole, aromatics, terpenes and organic acids.

Following, in table 2 a summary of sulfur and nitrogen containing odorous compounds in the influent wastewater at WWTPs is presented. The average concentrations are given in micrograms per liter, which is equivalent to to milligrams per cubic meter.

Table 2: Average concentrations in micrograms per liter of sulfur- and nitrogen-containing odorous compounds in the influent wastewater at a treatment plant (Hwang et al. 1995), extracted from [Hvi+02, p.6].

Compound	Average concentration ($\mu\mathsf{g}\,\mathsf{l}^{-1}$)	Range of concentrations ($\mu\mathsf{g}\,\mathsf{l}^{-1}$)
Hydrogen sulfide	23.9	15 - 38
Carbon disulfide	0.8	0.2 – 1.7
Methyl mercaptan	148	11 - 322
Dimethyl sulfide	10.6	3 - 27
Dimethyl disulfide	52.9	30 - 79
Dimethylamine	210	-
Trimethylamine	78	-
n-propylamine	33	-
Indole	570	-
Skatole	700	-

Now, when converting the average H_2S concentration of 23.9 $\mathsf{mg/m^3}$ provided by table 2 via the according dimensionless Henry Coefficient of 0.92 from table 3 by utilizing Henry's law (3), one obtains an average H_2S concentration in the gas phase of around 22 $\mathsf{mg/m^3}$. This values lies significantly above the perception threshold of approximately 0.0007 $\mathsf{mg/m^3}$. The latter value was converted from the value of 0.00047 ppm (see table 1) assuming standard temperature and pressure, similarly to the Henry coefficients given in table 3.

Volatility of odorous gases

According to [SS05, p.30], the gas-liquid phase equilibrium of the pollutant can be described by Henry's law (3)

$$C_{\mathsf{g}_i} = \mathsf{H}_i \cdot C_{\mathsf{l}_i} \tag{3}$$

where C_{g_i} is the concentration of pollutant i in the gas phase, H_i is the Henry's coefficient, and C_{l_i} is the concentration of i in the liquid phase. Henry's coefficient is found in the literature in different units. Using a non-dimensional Henry's coefficient ($\mathsf{mg\,gas\,l^{-1}\,/\,mg\,liquid\,l^{-1}}$), substances with values over 0.01 are considered volatile, and the higher the value, the less soluble the substance is in water. In table 3, a selection of Henry's Coefficient of common odorous compounds is displayed.

Table 3: Henry's dimensionless coefficient for some common odor-generating compounds in water at standard temperature of $25°\mathsf{C}$, quoted from [SS05, p.30].

Compound	Henry's coefficient (non-dimensional)
Hexane	30.9
Oxygen	29.1
Hydrogen sulfide	0.92
Toluene	0.25
Benzene	0.22
MIBK (methyl iso-butyl ketone)	0.016
Ethanol	0.0012
Ammonia	0.0005

Moreover, Henry's Coefficient depends on temperature and the chemical potential of the liquid phase. More details on these dependencies for various chemical compounds can be found in the works of [SR01].

Volatile inorganic compounds (VICs)

Following [Hal12, p.6], apart from the predominating VOCs, other odorants can be identified. According to [SS05, p.29], the inorganic gases are called volatile inorganic compounds (VICs) and include hydrogen sulfide (H_2S) and ammonia (NH_3), which are considered to be the main causes of odor when the sewage comes mainly from households [Hal12, p.6]. Those gases are also the odorants of interest in this project.

Hydrogen sulfide: H_2S due to its relative importance as the usual main odorant in sewage systems and WWTPs (more details can be found within its own subsection 2.3.5)

Ammonia: NH_3 (profound measurement and mitigation measures can be found in the review [Raj+18])

Inorganic/mineral acids: According to [Wike], they form hydrogen ions and the conjugate base when dissolved in water. Commonly used mineral acids are sulfuric acid, hydrochloric acid and nitric acid.

Concerning hydrogen sulfide, table 4 displays concentration ranges and thresholds with associated effects of odors and corrosion within a sewer system.

Table 4: Levels of total hydrogen sulfide concentrations in the wastewater of a sewer system with an associated scaling of severity in terms of bad odors and corrosion (see [Hvi+02, p.8]). The concentrations are given in grams sulfur per cubic meter.

H_2S concentration level ($gS\,m^{-3}$)	Identified problems
<0.5	minor
0.5 - 3	medium
>3	considerable

Moreover, table 21 gives an outline of the typical components of sewer air under anaerobic conditions.

Figure 21: Typical composition of sewer air reported by Thistlethwayte and Goleb (1972), extracted from [Hvi+02, p.7]. The compositions correspond to dry weather and anaerobic conditions in the sewer. The right hand column lists the concentration ranges by volume from top to bottom in descending order.

Group no. and components	Order of concentration range b volume
1. Carbon dioxide, CO_2	0.2-1.2%
2. Hydrocarbons and chlorinated hydrocarbons	
a. Hydrocarbons, mainly aliphatics C6-C14 and mostly C8-C12 (petrol)	up to 500 ppm
b. Chlorinated hydrocarbons, mostly trichlorethylene with ethylene dichloride and some carbon tetrachloride	10-100 ppm
3. Hydrogen sulfide, H_2S	0.2-10 ppm
4. Odorous gases and vapors	
a. Sulfides (mostly methyl mercaptan and dimethyl sulfide; some ethyl mercaptan)	10-50 ppb
b. Amines (mostly trimethylamine and dimethylamine; some diethylamine)	10-50 ppb
c. Aldehydes (mostly butyraldehyde)	10-100 ppb

Following [Hvi+02, p.7], these results from the table in fig. 21 reported by Thistlethwayte and Goleb (1972) indicate that the concentrations of the constituents of groups 3 and 4 tend to be related. That is to say the constituents of group 4 (a, b and c) tend to vary according to the levels of the H_2S concentrations roughly in the ratio of 1:50 to 1:100. They conclude that this observation suggests that although the H_2S concentration alone may not be a sufficient measure of potential sewer air odor levels, H_2S concentration measurements probably are sufficient for most studies of sewer gases. Other authors, primarily dealing with odors related to WWTPs, have also observed that H_2S can be considered a relevant indicator for an odor level (Gostelow and Parsons 2000).

Conclusion on hydrogen sulfide
According to [Hvi+02, p.8], from an engineering point of view, hydrogen sulfide is therefore especially relevant to deal with. In conclusion (see [Hvi+02, p.11]) it seems both acceptable and appropriate to use the concentration of sulfide in wastewater as an indicator of potential odor problems related to the collection of wastewater. [Hvi+02, p.9]

The sampling methodologies for the analysis of some of the odorants listed above, e.g. by gas chromatography, mass spectrometry and others, can be read in detail from [Cen17, p.63 et seq.].

2.3.3 Types of odor sources

The source type which applies to this project is the point source as the stack vent is sufficiently small. The outflow pipe comprises a diameter of around 0.2 meters. Other source types, such as line, area and volumes sources are not applicable to the WWTP Camping San Fernando. In particular, according to [Pra+18] and [Car+14], a point source can be defined as follows:
Discharges from a small openings such as stack or vent. A point source of pollution is a single identifiable source of air, water, thermal, noise or light pollution. In addition, it usually makes negligible

or smaller contribution, distinguishing it from other pollution source geometries. The sources are called point sources because in mathematical modeling, they can be approximated as a mathematical point to simplify analysis.

2.3.4 Odor source locations

There are a number of sources for odors within wastewater treatment and solids management facilities [Hal12]. The process steps of a general treatment plant with focus on the current object of investigation were mentioned in section 2.1. Significant potential sources at treatment facilities include:
Headworks area, primary clarifiers, solids holding and thickening tanks, aerobic digesters, dewatering systems, solids loading areas.
In the case of the WWTP Camping San Fernando, the only relevant odor generator is the canalization entrance into the open-air bioreactor basin, which could be compared to headworks, screens or primary clarifier.

According to [Car+14], the main stages of the whole process in which the odor generation has been identified are wastewater collection, transfer, and treatment, establishing that during the wastewater transfer from the collection systems to the treatment plant, significant amount of unpleasant odor substances can be emitted from manholes, joints, and terminations, specially if anoxic conditions are developed (Gostelow and Parsons 2000; Gostelow et al.2001; Dincer and Muezzinoglu 2007).
The main odor sources in the wastewater process may be located at the plant entrance, if the water contains septic conditions, and/or during the sludge treatment where anaerobic conditions generate new odorants as an inherent part of the bioprocess (Hobson 1995). Also, other process units as the primary settlers can stimulate the emission of substances previously generated in the plant entrance because of their calm flow conditions. Moreover, if the sludge purge is not sufficient to remove anaerobic activity, new odorants substances could be formed. From Capelli et al. (2009) it is conceivable that the main odor sources are the primary and sludge treatment stage. They point out that the collecting system has more influence in odor formation than treatment stages. In the graphic 22 the estimated distribution of odor sources is depicted.

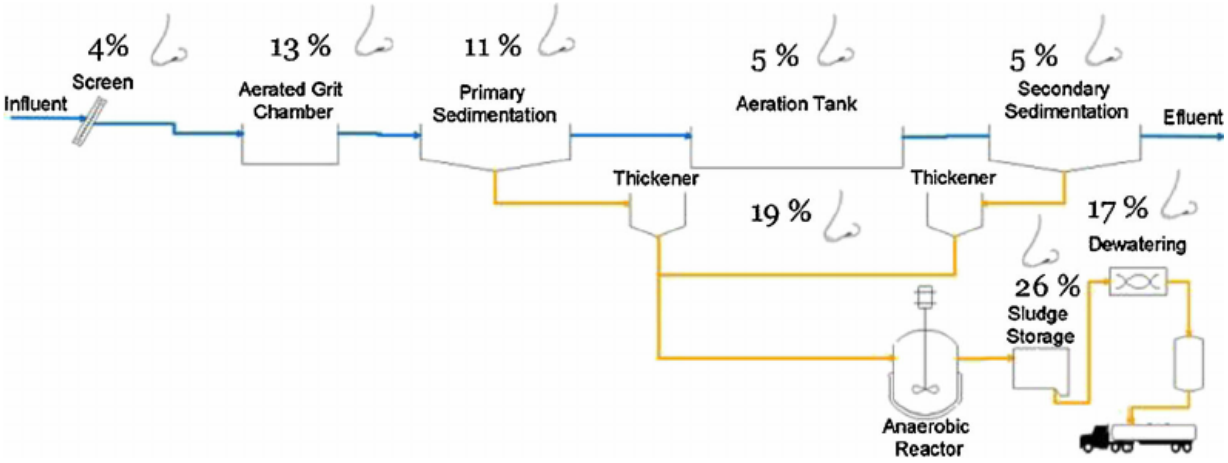

Figure 22: Flow chart of a typical WWTP labeled with odor sources and their contribution to odor emissions. This diagram is based on data from WWTP facilities located in France and Germany, adapted from Stuetz and Frechen (2001), extracted from [Car+14].

According to [Che+15], hydrogen sulfide (more details in subsection 2.3.5), resulting from the de-assimilative reduction of sulfates or thiosulfates, is the most common compound associated with

the sewage odors, but other sulfur compounds may also contribute (van Langenhove and de Heyder 2001). In the sewer networks and interceptor sewers, most of the generated sulfide occurs in the biofilm layer fixed on the walls of pipes or sludge deposits at the bottom of the pipes (WEF 2004). This can be understood from fig. 23.

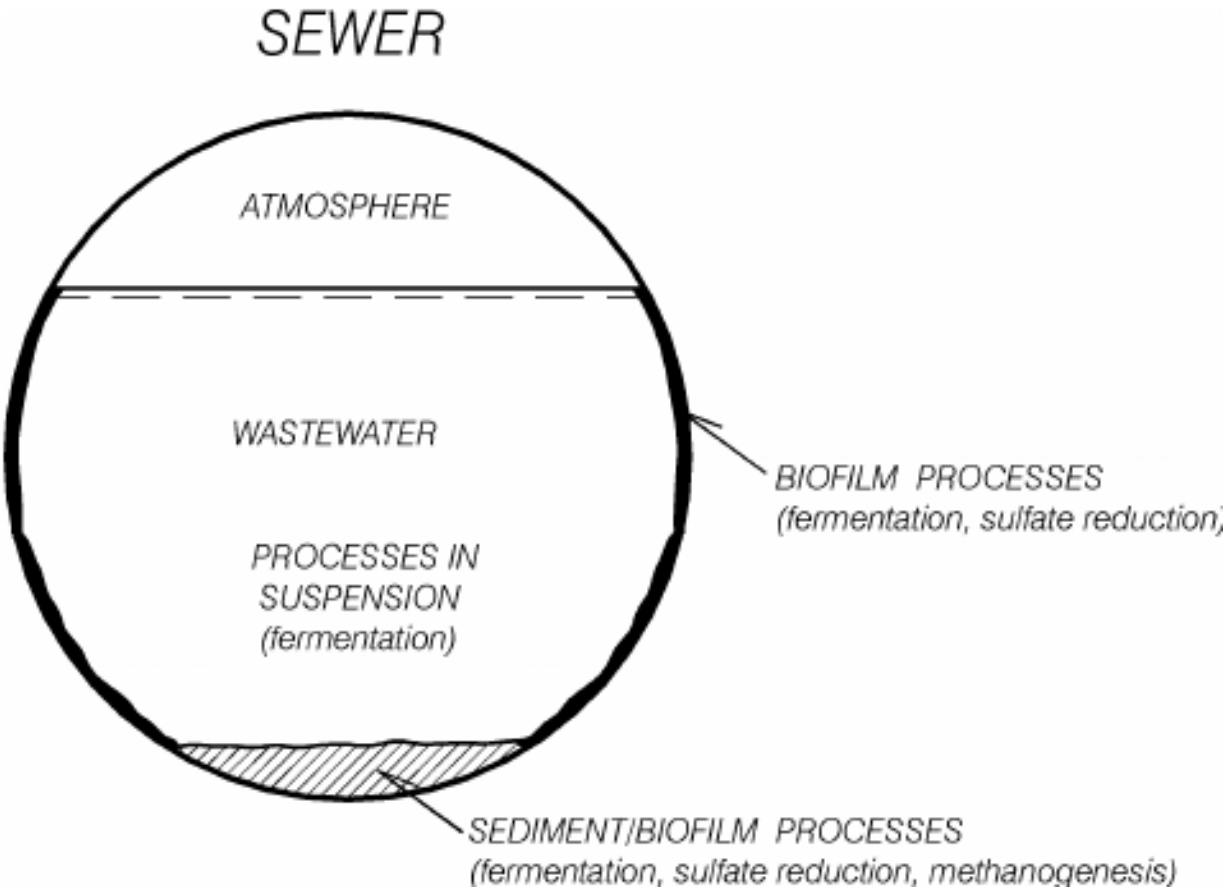

Figure 23: Schematic cross section of a gravity sewer pipe subject to anaerobic conditions. It illustrates the details of its subsystems and the occurrence of microbial processes (adopted from [Hvi+02]).

The monitoring studies of a WWTP mentioned in [Hal12, p.51] indicate that the hot-spots were located near the headworks building (screens, screenings conveyors, washers, grit basins, grit classifiers, residuals containers, etc.), filter press and activated sludge tanks. According to [Hal12, p.17], researchers have identified that friction drag on the sewer headspace by the flowing water moves air downstream in a sewer. This airflow is dependent upon the wastewater velocity, the diameter/size of the sewer and the area of the available headspace, but the air in a sewer is all moving downstream and enters the headworks with the flow. This odorous volume of air is forced into the wet well/influent works where it slightly pressurizes the receiving airspace.
In the paper of [Fis+18a] more details on the source locations of H_2S and methyl mercaptan (MeSH) production and its assessment can be found.

2.3.5 Hydrogen sulfide as main odorant

According to [RD], hydrogen sulfide is a flammable, colorless gas that smells like rotten eggs. People usually can smell hydrogen sulfide at low concentrations in air ranging from 0.0005 to 0.3 parts per million (ppm). Hydrogen sulfide occurs naturally in crude petroleum, natural gas, volcanic gases, and hot springs. It can also result from bacterial breakdown of organic matter, which applies to the context of this investigation. Apart from wastewater treatment plants, other industrial sources of hydrogen sulfide include petroleum refineries, natural gas plants, petrochemical plants, coke oven plants, food processing plants, and tanneries.
H_2S has a low threshold odor value around 0.5-1 ppb that is in the same order of magnitude as several VOCs produced by fermentation [Hvi+02]. It is a component with a relatively high Henry's law constant (see eq. 3 and table 3), i.e. it is a substance with a relatively high tendency to be emitted from the wastewater phase and occurs as a malodorous substance.
In the work of [God+18] more profound details on the adverse effects on human health and measuring methods can be found.
Additionally the works of [Mat+18] offers information about the complex sulfur cycle in sewage systems and the consequences of the products involved, mainly the assessment of sulfide production in a full scale wastewater sludge rising main. Particularly it is stated a model for sulfide generation with cross-references to other models and their authors. Also, in accordance with [Hvi+02], sulfide is directly related to corrosion of sewer networks and also to serious human health problems.

Production
Sulfate-reducing (resp. sulfur-reducing) bacteria (abbreviated with "SRB") generate usable energy under low-oxygen conditions by using sulfates (resp. elemental sulfur) to oxidize organic compounds or hydrogen; this produces hydrogen sulfide as a waste product.
According to [Car+14, p.7 et seq.], the main mechanisms of hydrogen sulfide formation correspond to two degradation routes: sulfate-reducing bacteria action and amino acids transformation.
Sulfate reducing bacteria use both the sulfate contained in the media and the VFA as substrates for growth. Thus, sulfate reducing bacteria can compete with methanogenic archaeas for carbon source (VFA) and electron donor, such as hydrogen sulfide, which may lead to the inhibition of the methanogenic stage (Kalyuzhnyi et al. 1998; Chen et al. 2008; Chou et al.2008). This mechanism is important when treating salty waste waters or with high level of soap waste. The protein degradation path is more important in the treatment of livestock wastewater (Peu et al. 2012). Methionine has been reported as the main precursor amino acid in hydrogen sulfide generation (Derbali et al. 1998; Du and Parker2012). There are several kinetic expressions for this process in literature, for which some authors have used first-order rate (Du and Parker 2012) whereas others consider Monod kinetic (Mu et al. 2008; Ramirez et al. 2009). Many authors have used hydrogen sulfide as a tracer compound to predict the odor intensity estimated from its chemical concentration, for instance using Steven's law (Gostelow et al. 2001; Stuetz and Frechen 2001; Hvitved-Jacobsen et al. 2002; Peu et al.2012).
According to the conclusions in [Hvi+02, p.11], the negative effects of anaerobic conditions in the wastewater of sewer networks are associated to a great extent with the emission of volatile substances. Theoretical considerations and also results from practice support the use of sulfide as an indicator of such problems including unpleasant odors:

- Unpleasant odors are related to both fermentation and sulfate respiration, both types of processes occurring simultaneously in wastewater of sewer networks under anaerobic conditions.
- Fermentable substrate and fermentation products are potential substrates for the sulfate reducing biomass. An indirect link between the formation of malodorous VOCs and sulfide therefore

exists.

Sewer process models could include oxidation and precipitation of sulfide in the water phase, emission into the sewer atmosphere, adsorption on the sewer walls, the following oxidation and finally ventilation and emission into the city atmosphere.
Since infiltration and inflow inversely affect the H_2S concentration, the average daily temperature (positive correlation, facilitates the growth of microbes) along with daily precipitation (negative correlation) was used in the works of [Hal12, p.17] to gain a better insight. On [Hal12, p.17] it is stated that the negative correlation with precipitation is owing to the infiltration and inflow problems which increase the volume of wastewater to be treated by the facility and thus does not provide sufficient detention time or the anaerobic conditions required by the bacteria to produce the sulfides. Moreover, in accordance to [Hal12, p.9], hydrogen sulfide generation is inversely related to the flow rate, so that waste streams with low flow rates are more likely to possess high levels of hydrogen sulfide. The rate of sulfide production depends upon the environmental conditions in the slime layer. The following wastewater conditions are the most critical parameters which impact the rate of sulfide production:

Concentration of organic material and nutrients:
These materials diffuse into the slime layer and are consumed by the SRB.

Sulfate concentration:
Sulfate and organic matter will be used by the SRB in the ratio of approximately 2:1, depending upon the relative concentrations of each.

Dissolved oxygen:
DO is critical in determining whether anaerobic or aerobic bacteria will dominate the breakdown of organic material in the wastewater. If the DO concentration is in excess of 1.0 mg/L, aerobic bacteria will likely dominate the activity, particularly on the outer layers of an attached biofilm. Consequently, increased DO will reduce the production of sulfide by limiting the food reaching the anaerobic bacteria.

pH: The pH determines the proportions of HS- and H_2S found in the wastewater and it directly influences the amount of hydrogen sulfide gas available for release into the atmosphere.

Temperature:
Each degree Celsius increase in temperature represents a 7 percent increase in the biological activity of the SRB (up to 30° C).

Wastewater velocity:
Velocity of the wastewater in the sewer influences the thickness of the slime layer and deposition rates for organic material.

Surface area:
The flow depth influences the free water surface and determines the submerged pipe surface in which the slime layer may form.

Detention time:
This factor is particularly important in force mains, submerged sewers, and sewers with little DO present. As the detention time increases, more oxygen is consumed, oxidation- reduction potential (ORP) decreases, and organic material becomes more solubilized, a condition that favors the SRB.

These bacteria use oxygen in the most readily available form: first from elemental oxygen, then nitrate oxygen, followed by sulfate oxygen. As nitrate is usually not available in wastewater, bacteria will consume sulfate oxygen after depleting elemental oxygen, leaving bisulfide ions to combine with hydrogen to form aqueous H_2S. At pH 7, the bi-sulfide ion and aqueous H_2S in solution are equally proportionate. PH, Henry's law, and the turbulence of the waste stream govern the rate at which aqueous H_2S is converted to atmospheric H_2S. A lower pH produces more aqueous H_2S and increases the rate of H_2S transfer to the gas phase.
Turbulent wastewater also facilitates the release of H_2S to the atmosphere.
With respect to Henry's Law (3) and the above-mentioned selection of Henry's Coefficients 3, the gas-liquid phase equilibrium, in particular of H_2S, can be affected if the compound reacts in the liquid (s. [SS05, p.30]). H_2S dissociation depends on pH and, as can be seen in the following reactions (Card 1998), when pH is under 5, practically all the sulfide is as H_2S and in physical equilibrium with the gas phase. At pH 10, sulfides are mainly as HS-, which is a very soluble compound, and the apparent Henry Coefficient can be three orders of magnitude lower than at pH 5.

$$H_2S_{(g)} \leftrightarrow H_2S_{(l)} \tag{4}$$

$$H_2S_{(l)} \leftrightarrow HS^- + H^+, \quad Ka_1 = 1 \cdot 10^{-7}, \quad pK_a = 7.0 \tag{5}$$

$$HS^- \leftrightarrow S^{-2} + H^+, \quad Ka_2 = 1.3 \cdot 10^{-13}, \quad pK_a = 12.9 \tag{6}$$

2.4 Odor control

Following the content of [SS05, ch. 3.2] "Methods of Odor and VOC Control", it is important to consider the physical, thermodynamic and reaction properties to select a sound method. The difference in the properties of the target compounds and the conditions of the stream determine the control method. According to [Che+15, ch. 5], the selection criteria for the most proper alternative depends on two main criteria: Gas flow and odorous gases concentration.
Regarding odor control in anaerobic reactors, several other criteria should be considered, such as odorous gases biodegradability, local characteristics (including human resources), source and exact locations of emissions and design aspects related to gas capture and conveyance, the relative concentration of H_2S in the biogas, energy recovery plans and treatment goals (Burgess et al. 2001; Kennes et al. 2001). In a qualitative analysis of the main features of each method for the treatment of odorous emissions from sewage treatment plants, Chernicharo et al. (2010) indicate that direct combustion, biochemical methods, and particularly biofilters offer the best perspectives for the treatment of waste gases.
Corresponding to [SS05, ch. 3.2], table 5 lists the relevant properties that are commonly used to characterize VOCs and to select a control method.

Table 5: Selection of essential properties of odor-generating environments when assessing which method to employ in order to mitigate the problem (quoted from [SS05, p.32 et seq.]).

Property	Description
Phase	Gases or liquids
Compounds with covalent or polar bonds	Covalent chemical bonds produce compounds that have a uniform electric charge throughout the compound. On the other hand, the polar compounds show an electric charge.
Ionization	Ionization is a rapid reaction. All acids, bases and salts produce ions in solutions.
Vapor pressure	The pressure exerted by the vapor under conditions of equilibrium with its liquid, under a particular temperature.
Solubility in water	The actual quantity of a gas that can be present in solution is determined by the solubility of the gas as defined by Henry's law (3).
Reactivity	Ability of a compound to react with itself or another compound. It is quantified by a reaction rate. The ability of microbes to transform a compound is called biodegradation.

Furthermore, a classification of common technologies applied for VOC, H_2S and odor control is shown in fig. 24.

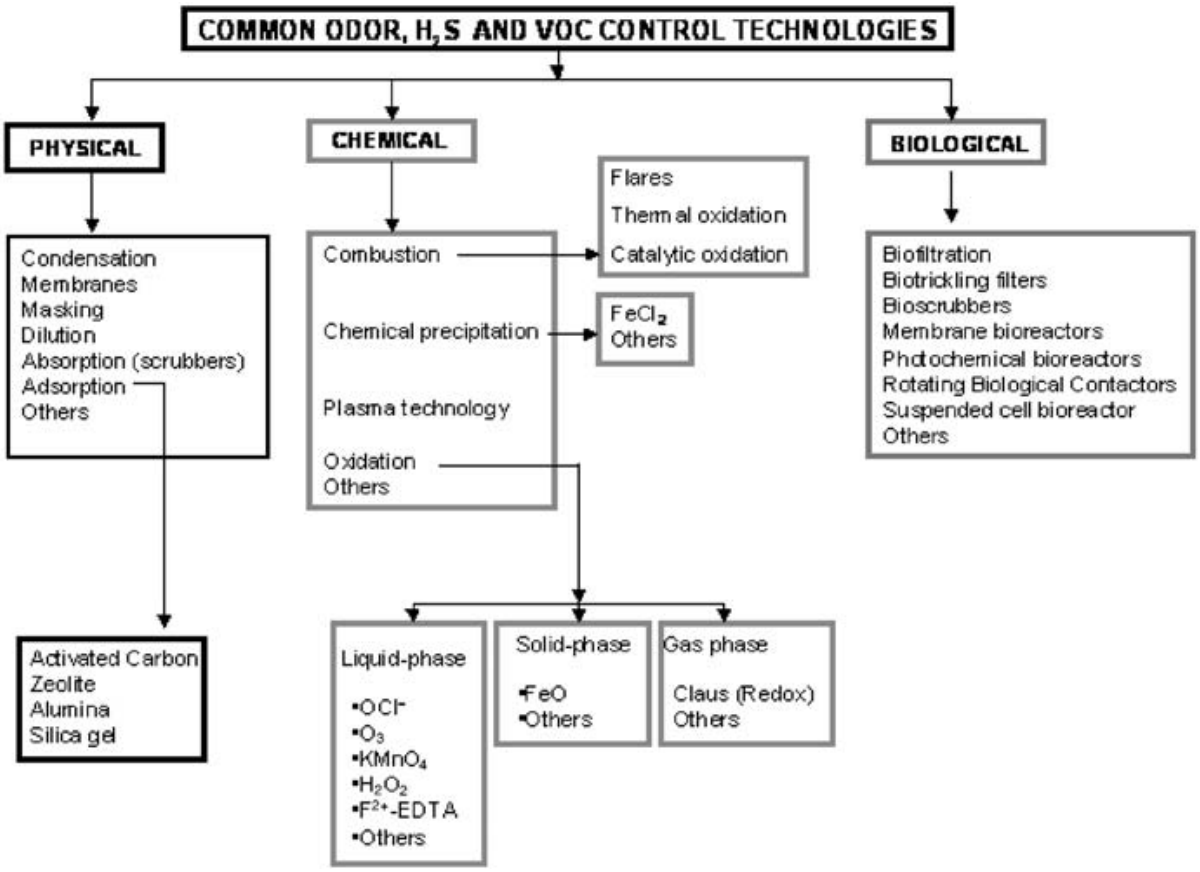

Figure 24: Classification of common technologies to control or prevent the emission of volatile organic compounds (VOCs) and other typical odorants (extracted from [SS05, p.31]).

The classification is based on the nature of each control technology, physical, chemical or biological. Generally, the physical processes are applied for waste gas streams where the flow and pollutant concentration are high. Important parameters for biological treatment are the solubility and the biodegradability of the compounds. The most important advantage of biological treatment methods over physical and chemical technologies is that the biological processes can be conducted at normal temperatures ($10-40\,^{\circ}\mathrm{C}$) and atmospheric pressure. Biological methods are inexpensive, simple to operate, and ecologically clean as compared with the physicochemical treatments.
However, to accomplish a good selection of a treatment method, it is recommended to take into account flow rate and pollutant concentration (s. fig. 25) as well as the category of the compound that is considered to be removed.

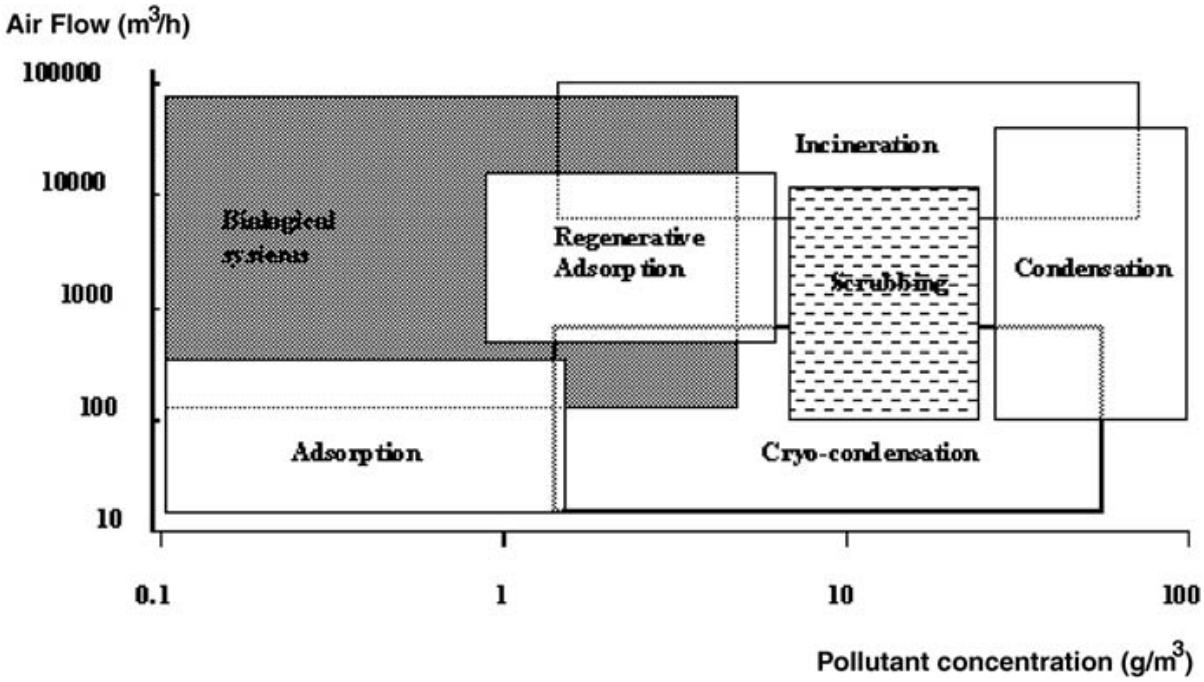

Figure 25: Applicability of various air pollution control technologies based on airflow rates in cubic meters per hour and pollutant concentrations in grams per cubic meter (quoted from [SS05, p.35]).

There are other important factors that determine the selection, such as temperature, oxygen content of waste gas, stream composition, solubility, operating schedule, utility and maintenance requirements. The investment and maintenance costs and the possible secondary environmental impacts must be evaluated, too.

Long-term monitoring

It is good practice to design and develop an effective real-time feedback to the operational personnel to identify and rectify problems associated with odor emissions [Hal12, p.52]. As a result, an innovative Real-time Odor Monitoring and Management System [RTOMMS] can be developed by employing the following techniques:

1. Collecting continuous data on odor levels and on-site meteorological conditions using modern commercial devices that are capable of transmitting data to a receiver and then to a server.
2. Developing a software application integrating ambient air quality data (odor levels), meteorological data, and dispersion modeling techniques to assess the strenghts of various sources in real-time to rank sources with high nuisance (with the help of the industry partner).
3. Suggesting strategies to increase capture and control efficiency to alleviate odor nuisance.

The approach has high scalability because all urban areas have WWTPs with odor nuisance. Investment in monitoring, assessing and controlling pollution helps to avoid outcomes to human health and also the surrounding ecosystems that are usually in the end more costly than preventive action.

Perceived odor mitigation through sight protection in the WWTP Camping San Fernando
In the particular case of this WWTP, the operators built a visual protection fence on top of the old and low wall enclosing the site (see figure 26).

Figure 26: Picture of the sight protection fence built on top of the old low wall surrounding the WWTP-site (shot on 3 April 2019).

This very fence is adorned with an opaque coverage of artificial green leaves, which gives the site as seen from outside, apart from the mere visual protection, an even pleasant appearance in comparison to before, when you could either see an old wall or even the facilities inside. As a matter of fact, apart from the objectively measurable odorant concentrations, it is also paramount to take into account the psychological tolerance of the local people. Thus, every visual improvement or coverage, such as also the aforementioned sealing of the pumping well, is already a great contribution to the betterment of the coexistence of residents and a WWTP amid the residential area.

2.5 Odor measurement

Within subsection 2.2 odor perception is explained as highly subjective for each person. In the following, various odor measurement approaches are shown.

2.5.1 Odor estimation

The odor estimation [Car+14, p.5 et seq.] is necessary to predict the emission rate to the atmosphere of a number of odor substances by using activity parameters of the entire plant or process unit (fuel consumption, raw material rate, etc.). Several governmental guides provide procedures to estimate emission values applied to wastewater treatment plants (USEPA 1997; AUEPA1999; NSWEPA2001). Particularly, National Pollutant Inventory of AUEPA (1999) describes different methods, from the most to the least accurate as follows:

1. **Sampling or direct measure:** quantifies the associated unit emission, with high cost
2. **Mass balance:** identifies the input and output amount of the odor substance referred to a control volume
3. **Fuel analysis and other engineering calculations:** empirical equations based on mass transfer and liquid-gas equilibrium. Its complexity increases as more unit processes are involved.
4. **Emissions factors (EFs):** selecting the adequate EFs, emissions rates from activity process parameters are calculated. Generally, EFs are collected from a large database with similar emissions-processes. EFs should be used when either no other information is available or when it is demonstrated that the generated emissions are negligible.

2.5.2 Difficulties in odor measurement

As a foreword to this subsection, it shall be mentioned that the project-specific difficulties are going to be mentioned in the final conclusion section 5.

Olfactometry:
According to [Hal12, p.53], it is recommended to have a "panel-of noses" trained to get a better understanding of the odor levels and thus to get more accurate results, since the (dynamic) olfactometer reading is very sensitive and specific to individuals.

Precision and accuracy:
It is essential that the measurement devices provide a sufficient precision and accuracy (up to ppb) to be able to measure the chemical concentrations or odors in a useful manner [Hal12, p.50 et seq.].

Weather influence:
To understand the movement of the plume from the various odor generating sources, it is important to take into account meteorological parameters as well. This helps establishing the concentration variation with wind speed and direction, which in turn facilitates to predict the location where one may find hot spots and a suitable location to set up the monitoring equipment [Hal12, p.50].

Mixtures of odorants and their relation to chemical concentrations:
In the work of [Cap+13], especially in the conclusion chapter 6, lots of experimental and model approaches are summarized. It is of major concern to distinguish between ideal situations of a sole odorous substance emitted and the real case of a mixture of at least two, wherefore a pure chemical concentration measurement of the involved compounds does not account for the actual odor concentration. Following [Cap+13, p.735], the presence of odors in the environment may be evaluated based on chemical measurements, which are easier to carry out compared to

direct odor measurements, even though results are not typically comparable, i.e. one cannot conclude from a chemical concentration of a substance, or a mixture of several to a final odor concentration.
On the other hand, a study of [Guo+17] about MSW landfills and incineration in Eastern China proved that the Pearson correlation coefficients between chemical concentration and olfactory odor concentrations of those MSW facilities showed a better positive linear correlation on all the data (transfer station + incineration plant + landfill) with $R^2 = 0.918$ ($n = 15$, $P < 0.01$). This means that 91.8% of the variance in olfactory odor concentration could be explained by the chemical concentrations of VCs, which was here significantly higher than the results in other studies.
More details on the topic can be found in subsection 2.5.2.

Correlation of concentration and odor activity As already mentioned above, the chemical identification of odorous compounds is not directly correlated to the determination of odor properties according to [Cap+13, p.735]. In accordance with [Wikc], measurements by gas chromatography give information about volatile organic compounds, but the correlation between analytical results and actual odor perception is not direct due to potential interactions between several odorous components. Following [Cap+13, p.736], for the purpose of obtaining significant information about odors based on the results of chemical analyses in the field, thus trying to relate the chemical composition of an odorous mixture to its odor concentration, it is important to account for the odor potential of the identified compounds (which depends on their odor detection threshold concentration) and to calculate the so called Odor Activity Value (OAV), which represents the sum of the concentrations of the odorous compounds weighted with their Odor Threshold (OT) (Kubícková and Grosch, 1998; Nuzzi et al., 2008):

$$\mathrm{OAV} = \sum_{i=1}^{n} \frac{C_i}{\mathrm{OT}_i} \tag{7}$$

where

OAV is the Odor Activity Value in $\mathrm{OU_E/m^3}$,

C_i is the concentration of the chemical compound i in $\mathrm{mg/m^3}$, and

OT stands for the Odor Threshold of compound i in $\mathrm{mg/\,OU_E}$.

Still, the odor concentration calculation based on the OAV in (7) entails strong imprecision. One reason for this imprecision might be the difficulty of finding reliable OT values, given that the values that can be found in literature for a single odorous compound often differ by several orders of magnitude (Capelli et al., 2008a). Moreover, if synergetic effects of odorous compounds are present, such a calculation will underestimate the odor concentration of the odorous mixture.
A study by Capelli et al. (2012b) reports the attempt of correlating the odor concentration c_{od} measured in correspondence of several odor sources of a complex industrial area including steel industry, different chemical industries for the production of polypropylene, its products and other activities mainly for the treatment of waste waters and solid waste both with the total Volatile Organic Compound (VOC) concentration and with the OAV.
Fig. 27 and 28 show the correlation between total VOC concentration and odor concentration and the correlation between OAV and odor concentration, respectively.

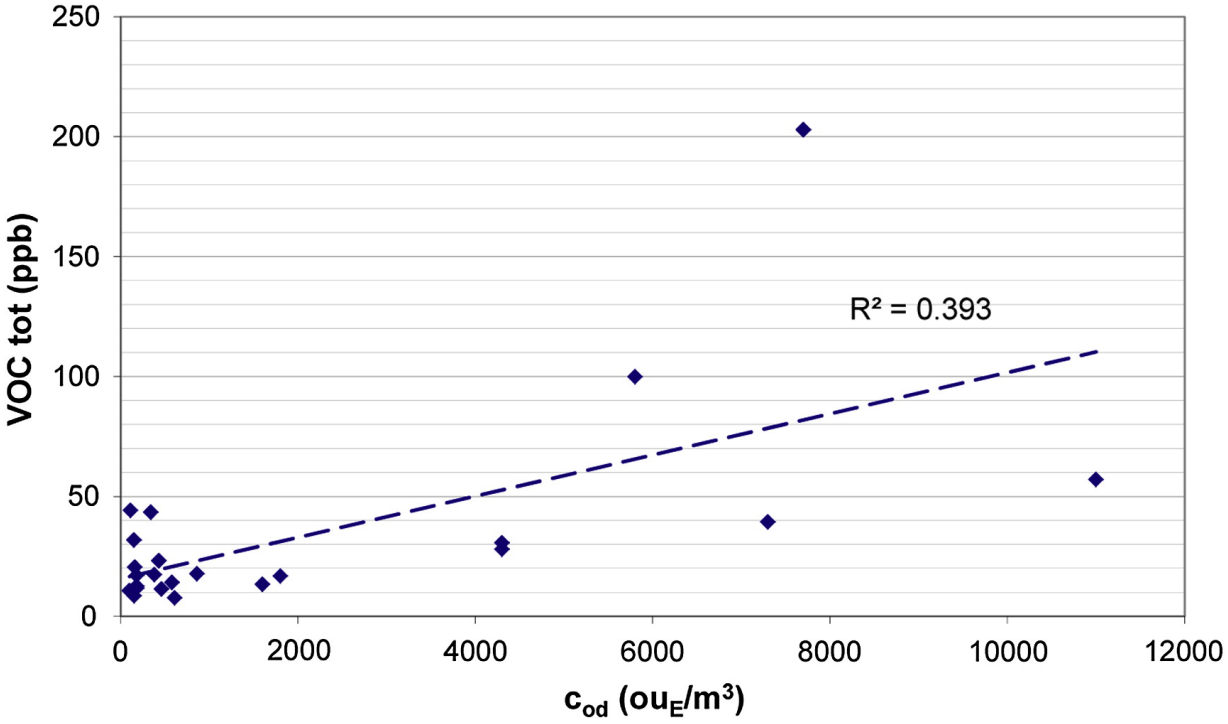

Figure 27: Correlation between total VOC concentrations in parts per billion (ppb) and odor concentrations in European Odor Units (OU_E) per cubic meter (quoted from [Cap+13]).

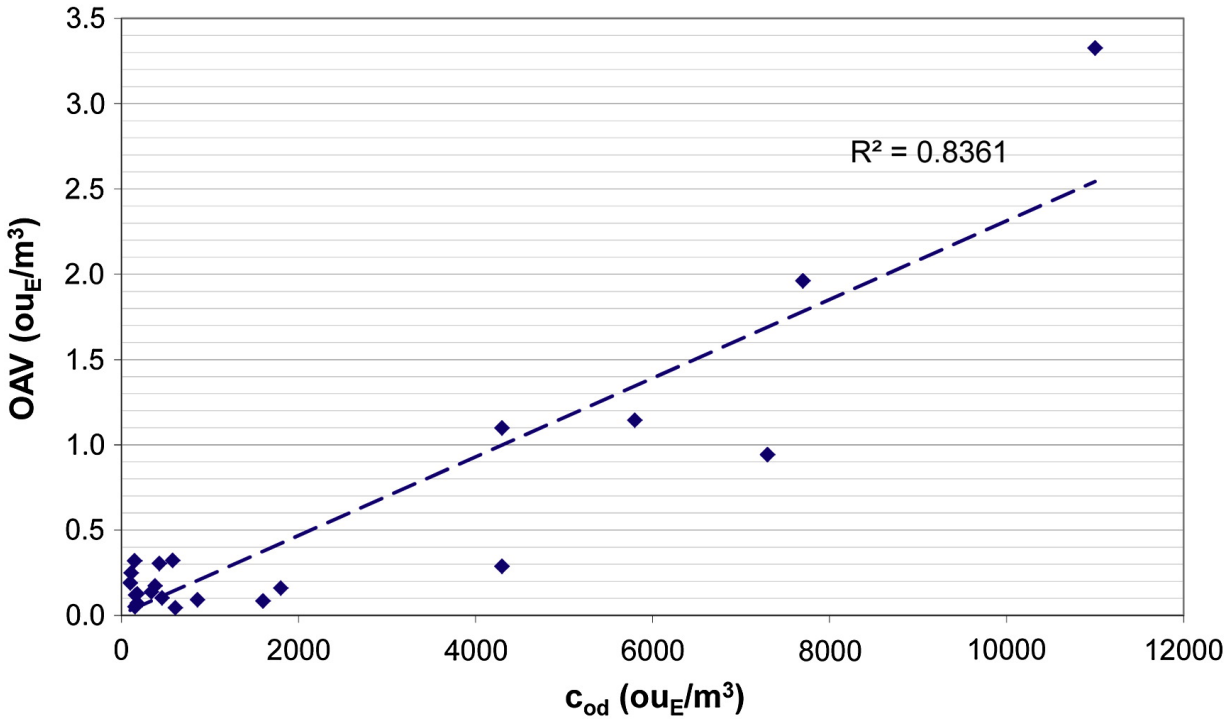

Figure 28: Correlation between total OAV and odor concentrations both in European Odor Units (OU_E) per cubic meter (quoted from [Cap+13]).

It can be observed that the OAVs are about two orders of magnitude lower than the corresponding measured odor concentration values. This difference may be due to the already mentioned difficulty of finding reliable OT values.
Another important observation concerns the fact that the correlation between OAV and cod ($R^2 = 0.836$) effectively turned out to be significantly better than the correlation between total VOC concentration and the cod ($R^2 = 0.393$). This result proves that the OAV, being a sort of total concentration weighted by the odor thresholds of the single compounds contained in an odorous mixture, does account for the different relative contribution of each compound to the mixture total odor concentration, and therefore is most suited to describe the odor properties of an odorous mixture than just the total VOC concentration, which, on the contrary, does in no way account for the odor properties of the mixture components.
More details on the topic can be found in subsection 2.5.3.

2.5.3 Direct odor measuring methods

Dynamic olfactometry
According to [Hal12, p.18 et seq.], an odor is caused by one or more volatilized chemical compounds, that is perceived by the sense of olfaction. The measurement of odor concentration is the most widespread method to quantify odors. An olfactometer is used to detect and measure ambient odor dilution.
The method is based on dilution of an odor sample to the odor threshold (the point at which the odor is only just detectable to $50\,\%$ of the test panel (trained jury of "noses"). The numerical value of the odor concentration is equal to the dilution factor that is necessary to reach the odor threshold.
The Nasal Ranger Olfactometer was used in [Hal12, p.18 et seq.] for odor detecting and measuring device. The instrument directly measures and quantifies odor strength in the ambient air using the operating principle of mixing odorous ambient air with odor-free filtered air in discrete volume ratios. The discrete volume ratios are called "Dilution-to-Threshold" ratios (D/T ratios) according to (2). The user's nose is placed firmly inside the nasal mask and inhales at a comfortable breathing rate while standing at rest. The nasal mask has an outlet for exhaled air to exhaust downward. Therefore, the user inhales through the Nasal Ranger and exhales downward through the outlet check valve. To measure intensity, the olfactometer introduces an odorous gas as a baseline against which other odors are compared. The instrument has an accuracy of $\pm 10\,\%$ and a response time of 2 seconds. The categories of the D/T ratios are:
$>=$2 Noticeable, $>=$7 Objectionable, $>=$15 Nuisance, $>=$31 Nauseating
Here, it shall be mentioned that in this project, the Nasal Ranger was also deployed by the two field panelists of Global Omnium S.L. on-site at the WWTP. More information on the device regarding its technical data sheet, measuring accuracies etc., please see subsection 3.1.2.

Odor wheels:
Corresponding to [Fis+18b, p.222, ch. "4. Conclusions"], odor wheels are a useful method of combining both olfactory and chemical data in order to link nuisance emissions from biosolids processing to process conditions.

Field Investigations Methodology (with human panel):
With regard to different application settings the discrepancies between external observers and affected residents are discussed in terms of different information processing strategies, namely stimulus-based (bottom-up) for the panel and memory-based and, thus, subject to cognitive bias for the residents (top-down).
More information on this method can be found under [Cap+13, ch. 4 "Sensorial measurements"].

Population investigation method:

Due to the fact that this topic would go beyond the scope of this thesis, the reader is kindly referred to the following literature for further information: please see [Cap+13, ch. 4 "Sensorial measurements"] and the psychological aspects of the approach as mentioned within "Field Investigations Methodology" [Suc+08].

Electronic noses:

In [Cap+13, ch. 5 "Electronic Nose"] it is described as another means for measuring odors in the field and determining odor exposure directly at receptors called "electronic noses". The instruments should be suitable for the continuous analysis of the ambient air at receptors, thereby detecting the presence of odors, and possibly classifying and/or quantifying them, as well.
Moreover, this technology is able to carry out multiple odors detection and recognition, which stands for a dynamic odor change from no odor to a single odor and multiple odors (see fig. 29), which is the most common situation in a real-world environment [KRH11, p.464]. Therefore, it is necessary to sense and recognize techniques for dynamic odor changes. To recognize multiple odors, the proposed method must include odor data acquisition using a smell sensor array, odor detection using entropy, feature extraction using Principal Component Analysis (PCA), recognition candidate selection using Tree Search, and recognition using Euclidean Distance of Odor Vectors. These are calculated from a data base compared to the measured vector components, the entire process is schematically displayed in fig. 30.

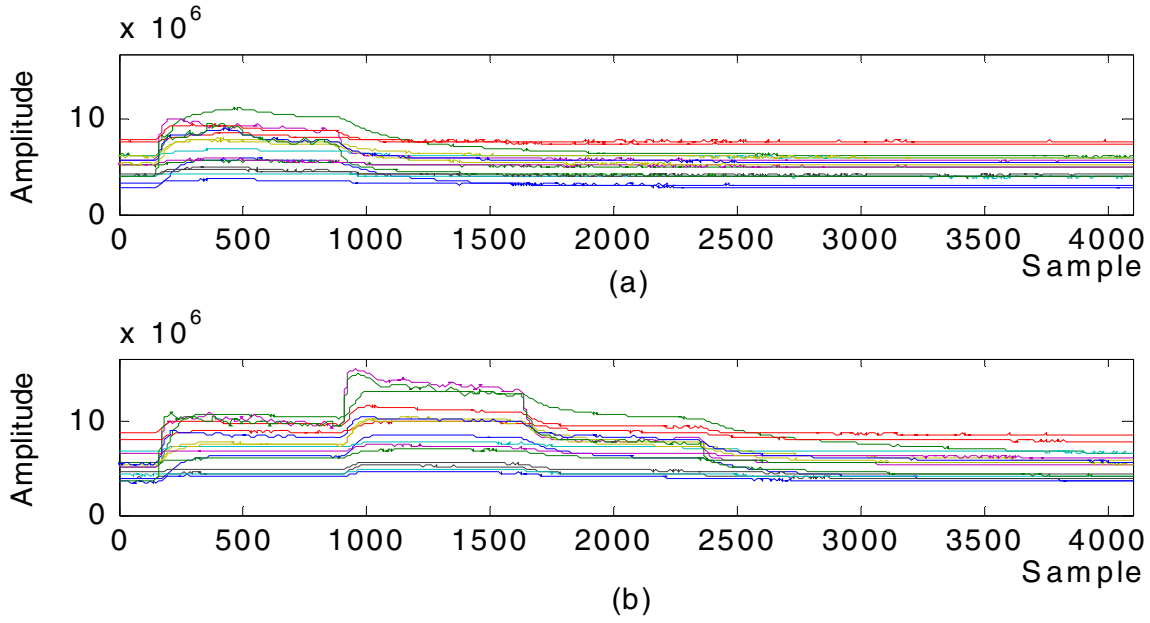

Figure 29: Single (a) and multiple (b) odor patterns visualized by plotting amplitudes against samples (quoted from [KRH11, p.466]).

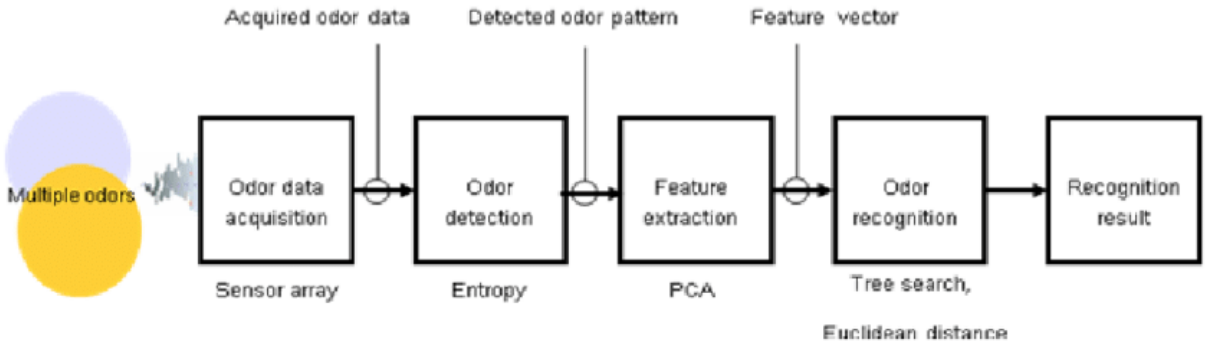

Figure 30: Odor recognition system block-diagram from [KRH11, p.467]

As for the working principle, the electronic nose is a complex system with a human-nose-like structure (Pearce, 1997; Sankaran et al., 2012), which can be defined as "an instrument which comprises an array of electronic chemical sensors with partial specificity and an appropriate pattern recognition (PR) system, capable of recognizing simple or complex odors" (Gardner and Bartlett, 1994). The electronic nose does not perform a chemical analysis of the analyzed mixture, but the partially selective sensor array produces a kind of "olfactory pattern", which can be subsequently classified based on a reference database acquired by the instrument in a previous training phase (Capelli et al., 2008b; Ampuero and Bosset, 2003).

Conclusions on dynamic olfactometry

According to [Hal12, p.19], the olfactometer however, was not found to be a very accurate means to measure and quantify odors since the olfaction varied from person to person and was extremely subjective. The olfactometry analyses of ambient air in the field are not recommended because of frequent variations of odor concentrations in ambient air and the low resolution of these methods.
Despite the advantages of the classic analytical methods (accuracy, reproducibility, etc.), olfactometry remains the best available approach to measure odors directly, in order to objectively quantify the perception of odors [Hal12, p.46]. Given the readings, one cannot really derive any conclusive results. Perhaps, a better understanding would be obtained if the experiment is repeated. Inter-panel variability also exists which could cause discrepancies.
According to [Kim16, p.116 et seq.] the predictive data of hazardous pollutants acquired based on dynamic olfactory method appears to leave many questions regarding the actual reliability of such approach. To date, the extent of odor pollution is generally described with the aid of either indirect means such as quantitative analysis based on instrumental detection or by the use of direct (sensory or olfactometry) methods (Kim and Park, 2008; Kim and Kim, 2014; Jo et al., 2015). According to the bad odor prevention law in Korea (KMOE, 2008), the use of the human sensory method like the air dilution sensory (ADS) test is recommended as a primary means to assess the level of odor pollution via the assessment of dilution to threshold (D/T) ratios (2) (ASTM, 1991; Nicell, 2003). However, for the actual control of odor pollution from emission sources, it is a critical step to gain quantitative data for each of all different offensive odorous compounds that contribute effectively to odor pollution. It should be noted that the method of Palmiotto et al. (2014) for diagnosing odor pollution due to landfill sources is based solely on direct olfactory technique. As such, the interpretation of the resulting odorant dispersion model with the input of olfactory data alone is apt to restrict the full assessment of odorant mitigation in various aspects. Most noticeably, the lack of information concerning the chemical speciation of odorants or their relative contribution should be a critical limiting factor for proper evaluation of odor propagation or dispersion as well as their impacts. Thus, to gain the balanced

information of odor pollution due to strong sources like landfill activity, it is desirable to simultaneously apply both direct and indirect approaches. Consequently, one may be able to atone for the limitations of each other and to evaluate the effect of such strong sources for the establishment of proper control tactics.
For further information on the olfactometry method see [Cap+13, ch. "4. Sensorial measurements"], and also the approach of "Odor Wheels" combining olfactory and chemical methods in one single device [Fis+18b, p.222, ch. "4. Conclusions"]).

2.5.4 Indirect odor measuring methods

Activity chart and sampling plan The "Activity chart for odor and odorant monitoring in existing MSW landfill sites" on [Cen17, p.47] gives an overview of the steps to be taken. From there, useful tips for WWTPs can be derived. For on-site monitoring instructions and a field data sheet proposal see [Cen17, p.50 et. seq.]. To begin with, the objectives of the study ought to be clearly documented which may range from complying with regulatory requirements, to identify long and short term trends, to detect accidental releases, or to develop a data base or inventory of pollutant levels.

Upwind and downwind sampling method In the upwind-downwind method [Cen17], have minimum points to ascertain concentration at upwind direction of the pollution source and several concentrations at several points selected on the basis of prevalent wind direction are obtained in downwind directions. The difference between the upwind and downwind concentrations is considered to be the contribution of the source. Wind speed, wind direction and other meteorological variables are monitored during the sampling procedures. Methods for sampling for this method are obtained from the USEPA (USEPA, 1993). The downwind part should be investigated more thoroughly since the variation of odor concentration can be significant. Since the upwind part is considered to be clean, less measurement points are sufficient.
Using a dispersion model and available meteorological information, the net concentration is used to solve for the emission rate. Air dispersion models such as AUSPLUME, AERMOD and CALPUFF may be used to estimate emissions from volume and area sources in this manner to obtain downwind concentrations for this method. More details on modeling are to be obtained in section 2.6.

Ambient and source monitoring, hot-spot and perimeter analysis As suggested in the Master's thesis [Hal12], various gas analyzing equipment for monitoring can be used for different requirements which depend on the area of application. By saying this, it refers to the question which odorant is measured and which concentration ranges are expected, and following up on this also where it shall be measured. For instance, measuring at the headworks or canalization outflow, higher concentrations can be expected than during a perimeter analysis around the WWTP-site. Moreover, every odorant has a distinct associated perception threshold and limit hazardous to health. Therefore, the deployed instrument should be able to detect these given the fact that those concentrations will be reached in the scope of application.
2.5.4

2.5.5 Meteorological monitoring

The devices used in the exemplary works of [Hal12] in order to collect meteorological data are listed in the following. With respect to this very project, these two kinds of measurement devices were also deployed in the field works during the performance of the dynamic olfactometry on-site. In fact, they were united in a portable weather station called "Kestrel 5500 Fire Weather Meter Pro". More

information on this particular device, like the data fact sheet and visual impressions of the instrument, can be found in subsection 3.1.3.

Wind logger (anemometer)
A wind logger provides average speed, wind gust and average direction. It can measure the wind speed in the range of $0-67\,\mathrm{m\,s^{-1}}$ with an accuracy of $\pm 2\,\%$ and measures the wind direction with an accuracy of $\pm 22.5^\circ$.
It works on the same principle as an anemometer. It is a cup-type anemometer mounted on a vertical axis and is provided with a sensor to log the wind speed and direction.

Wind rose
The data obtained from the anemometer was used to produce a wind rose to get a better understanding of the wind direction and speed for each day. A freeware available online called the WRPlot View developed by the Lakes Environmental Software was used for this purpose. This provides visual wind rose plots, frequency analysis, and plots for several meteorological data formats.
A wind rose depicts the frequency of occurrence of winds in each of the specified wind direction sectors and wind speed classes for a given location and time period.

2.6 Odor dispersion modeling

In general, for the application of an atmospheric dispersion model, at least three different kinds of input data are needed [Cen17]: *meteorological, emission and topographical.*
Furthermore, it should be based on spatial and temporal dimension, and consider a relation between purely physically measurable parameters and biologically-effective ones since odor perception is not just representable by concentration without a conversion. For more details on the SOP see [Cen17, p.86 and p.131 et seq.].
According to [Cap+13, ch. 5 "Electronic Nose"], electronic noses could be useful for odor impact assessment purposes in cases where dispersion modeling is hardly applicable. More details on that can be found in subsection 2.5.3.

2.6.1 Air pollution emission plumes

According to [Wikg], air pollution emission plumes are the flow of pollutant in the form of vapor or smoke released into the air. Plumes are of considerable importance in the atmospheric dispersion modeling of air pollution. There are three primary types of air pollution emission plumes:

Buoyant plumes
: are lighter than air because they are either at a higher temperature (e.g. flue gas stacks of industrial furnaces) and lower density than the ambient air which surrounds them, or because they are at about the same temperature as the ambient air but have a lower molecular weight (e.g. methane) and hence lower density than the ambient air.

Dense gas plumes
: are heavier than air because they have a higher density (e.g. carbon dioxide) than the surrounding ambient air for opposite reasons as mentioned above with respect to buoyant plumes.

Passive or neutral plumes
: are neither lighter or heavier than air.

2.6.2 Characterization of atmospheric turbulence

Following [Wikg], the effect of turbulence on dispersion is the increase of the entrainment and mixing of unpolluted air into the plume and thereby acts to reduce the concentration of pollutants in the plume (i.e. enhances the plume dispersion). It is therefore important to categorize the amount of atmospheric turbulence present at any given time. This type of dispersion is scale dependent, such that for flows where the cloud of pollutant is smaller than the largest eddies present, there will be mixing. There is no limit on the size on mixing motions in the atmosphere and therefore bigger clouds will experience larger and stronger mixing motions. And hence, this type of dispersion is scale dependent. In the following a list of parameters defining the stability classes is presented:

The Pasquill atmospheric stability classes
are the oldest and, for a great many years, the most commonly used method of categorizing the amount of atmospheric turbulence present was the method developed by Pasquill in 1961. He categorized the atmospheric turbulence into six stability classes named A, B, C, D, E and F, with class A being the most unstable or most turbulent class, and class F the most stable or least turbulent class. Compared to other more advanced methods it is quite inaccurate using only some meteorological parameters for categorization.

Richardson number
is a dimensionless number [Wikh] that expresses the ratio of the buoyancy term to the flow shear term:

$$\mathrm{Ri} = \frac{\text{buoyancy term}}{\text{flow shear term}} = \frac{\mathrm{g}}{\rho} \frac{\nabla \rho}{(\nabla u)^2} \tag{8}$$

where g is gravity, ρ is density, and u is a representative flow speed. If the Richardson number is much less than unity, buoyancy is unimportant in the flow. If it is much greater than unity, buoyancy is dominant (in the sense that there is insufficient kinetic energy to homogenize the fluids). If the Richardson number is of order unity, then the flow is likely to be buoyancy-driven: the energy of the flow derives from the potential energy in the system originally.

Bulk Richardson number
(BRN) is an approximation of the Gradient Richardson number [Wikb]. The BRN is a dimensionless ratio in meteorology related to the consumption of turbulence divided by the shear production (the generation of turbulence kinetic energy caused by wind shear) of turbulence. It is used to show dynamic stability and the formation of turbulence.

Monin–Obukhov length
which results from the Monin-Obukhov similarity theory. The Obukhov length [Wikf] is used to describe the effects of buoyancy on turbulent flows, particularly in the lower tenth of the atmospheric boundary layer. It is also known as the Monin–Obukhov length because of its important role in the similarity theory developed by Monin and Obukhov. A simple definition (and physical interpretation) of the Monin-Obukhov length is that height at which turbulence is generated more by buoyancy than by wind shear.

Surface roughness length
z_0 is a parameter of some vertical wind profile equations that model the horizontal mean wind speed near the ground [Wiki]. In the log wind profile, it is equivalent to the height at which the wind speed theoretically becomes zero. In reality the wind at this height no longer follows a mathematical logarithm. It is so named because it is typically related to the height of terrain roughness elements. Whilst it is not a physical length, it can be considered as a length-scale a representation of the roughness of the surface.

Boundary layer height

δ is the distance across a boundary layer from the wall to a point where the flow velocity has essentially reached the 'free stream' velocity, u_0. This distance [Wika] is defined normal to the wall. It can be distinguished between laminar y turbulent boundary layers when calculating δ.

Mixing height:

When an inversion aloft is formed [Wikg], the atmospheric layer between the Earth's surface and the bottom of the inversion aloft is known as the mixing layer and the distance between the Earth's surface and the bottom of inversion aloft is known as the mixing height. Any air pollution plume dispersing beneath an inversion aloft will be limited in vertical mixing to that which occurs beneath the bottom of the inversion aloft (sometimes called the lid). Even if the pollution plume penetrates the inversion, it will not undergo any further significant vertical mixing. As for a pollution plume passing completely through an inversion layer aloft, that rarely occurs unless the pollution plume's source stack is very tall and the inversion lid is fairly low.

Other variables to be considered are

- wind speed,
- temperature gradient and
- fluctuations in wind direction.

2.6.3 Model types

General overview

According to [Cen17], two classes of dispersion models are currently used for (regulatory) odor dispersion: *Gaussian and Lagrangian models.*
Both model classes belong to the so-called non-CFD (computational fluid dynamics) models. Non-CFD models do not explicitly resolve fluid-dynamics equations but physical processes are parameterized. Regulations of different countries propose air dispersion modeling as a method for odor impact assessment and this is currently the most frequently used approach (Capelli et al., 2013). It was found that internationally, several studies have already demonstrated the capability of air dispersion models to estimate odor impact from various sources (Busini et al., 2012; Chemel et al., 2012; Mantovani et al., 2010). Numerous modeling approach has been applied to simulate the impact of odor generated from various sources. Most popular models are

- Gaussian steady state plume models (e.g. AERMOD, ISCST3, ADMS-Urban),
- Gaussian non-steady state puff models (e.g. CALPUFF),
- Fluid dynamic models, i.e. CFD models, and
- Lagrangian particle models (Capelli et al., 2013).

Out of them, the Gaussian dispersion models are found to be the most frequently used for simulation of odor dispersion with satisfactory performance. More details on the different models can be found on [Cen17, p.132 et seq.].

Advanced models

In [Cap+13] several models for pollutant dispersion into the atmosphere are described.

Analytical stationary plume models:

These are the simplest models, among them, Gaussian models, for which turbulent dispersion is parameterized with empirical coefficients derived from experimental campaigns, are the most traditional ones and very cheap for computation (Gifford, 1959; Pasquill, 1961; Smith, 1995). Critical conditions for the use of such models are low winds (calm conditions) and complex terrain (Luhar, 2011; Thomson and Manning, 2001).

Hybrid models:

These models are more advanced. Dispersion is parameterized directly from meteorological data giving information about the thermal and mechanical structure of the lower atmospheric layers (Ganguly and Broderick, 2010).

Puff models

(Cao et al., 2011; Lamb and Neiburger, 1971) are improved from Gaussian plume models to be applied to non-stationary and non-homogeneous flow by representing a plume by a series of independent elements (puffs) that evolve in time as a function of temporally and spatially varying meteorological conditions (Jung et al., 2003). Puff models applied to odor dispersion are able to simulate the instantaneous characteristics of odor perception (De Melo Lisboa et al., 2006). First applications of puff models for odor dispersion are linked to studies of Högström (1972).

Lagrangian particle models and Eulerian grid models (3-D models)

are more advanced tools for atmospheric dispersion simulation. The first simulate the dispersion of the emitted pollutants with computational particles moving in the wind field and three-dimensional turbulence field. The latter numerically solve the diffusion equations of the pollutant emitted in the three-dimensional domain subdivided in grids of variable dimensions (Nguyen et al., 1997). Their limits consist in the incomplete knowledge of the turbulence mechanisms and the very high computational time required for complex simulations (Lagzi et al., 2004; Franzese, 2003; Raza et al., 2002; Wilson and Sawford, 1996).

Fluid dynamic models (CFD)

are the most complex models (i.e. CFD: Computational Fluid Dynamics), which solve three-dimensional equations for wind, temperature, humidity and concentrations (Pontiggia et al., 2009). Such models are used for extremely time and spatially detailed simulations, considering the presence of obstacles or buildings explicitly in the model, and are currently applied also to odor dispersion modeling (Maïzi et al., 2010; Lin et al., 2007).

Steady-state and more sophisticated models

In general, all the above mentioned model typologies, in some cases with opportune precautions, may be successfully applied to the simulation of odor dispersion [Cap+13, p.733]. The choice of the most adequate model for a given application should be evaluated case by case based on several factors (Turner, 1979).

Steady-state models

(i.e. simple or advanced Gaussian plume models) can successfully be applied when the requested outcome is the worst-case condition. In general, the models that are most commonly used for odor dispersion modeling purposes are Gaussian models (e.g. AERMOD) and CALPUFF.

Recent studies tend to prefer CALPUFF, due to the limitations of Gaussian models, including the inability to handle calm and stagnation conditions, lack of three-dimensional meteorology and steady-state assumption (Barclay and Borissova, 2013). Nevertheless, AERMOD has already included 3D-meteorology to a certain extent, and apart from that it can handle also complex terrain. Moreover, other studies prove AERMOD to significantly overestimate concentrations, especially during stable atmospheric conditions (Dresser and Huizer, 2011; Busini et al., 2012). On the other hand, the importance of these issues also depends strongly on the scope of application in every individual project: for instance, when the odor is transported especially through turbulent advection and the location is situated in a rather windy region, or even the season comprises of increased wind speeds in general, the aforementioned constraint carries no weight. This is the case for this project, as the WWTP Camping San Fernando is located directly next to the seashore and shows significant stable wind patterns all year round.

More sophisticated models
include more complex parameterizations. They also require more meteorological input, more computer time and more expertise. Whether it is worth to spend extra efforts to gather both data and expertise depends on the type of application, the locations of the sources and receptors, source types, complexity and variability of the meteorology, desired accuracy of the results and averaging time (Escoffier et al., 2010).

For more details on "Modeling of Odor-Potential Produced in WWTP Process Units, Integrated WWTP Process Modeling and Atmospheric and Dispersion Models" see [Car+14, p.6 et seq.].

Forward dispersion modeling
If some pollutants are responsible of the odor (and the annoyance), these compounds can be followed as tracers for odor activity and in that way, a *dispersion model* can be used with measured concentrations as inlet data [Cap+13, p.735]. Of course, for modeling purposes, chemical measurements must be carried out including all data and physical measurements required for the model. In a classical way of dispersion, the source is characterized and measurements in the environment give data to estimate the precision of a model. This approach is also the one of the modeling with AERMOD carried out in this project.

Inverse dispersion modeling If the source cannot be characterized, the pollution is measured in the field and with so-called reverse dispersion, the emission rate is estimated but in that case, no real validation can be proposed, because the calculated results cannot be compared with unknown emission data [Cap+13, p.735 et seq.].

2.6.4 Model input

The following general input variable explanations were extracted from [Cap+13], where more details can be found.

Meteorological data:
The acquisition and pre-processing of meteorological data is of crucial importance for atmospheric dispersion modeling purposes. In general, the meteorological data required for dispersion modeling include wind speed, wind direction, and information about the atmospheric stability conditions which can be derived from other meteorological parameters, such as humidity, temperature and wind speed profiles, as well as cloud covering or global or net solar radiation. For more

information about AERMOD's meteorological preprocessor AERMET, please see subsection 3.2.3.

Emission Rate:

As for the simulation of dispersion of any pollutant, also in the case of the dispersion of odors, it is not sufficient to consider the pollutant (odor) concentration, but it is necessary to account for the air flow associated with the monitored odor source. In the case of odor, the parameter to be considered for dispersion modeling purposes is the Odor Emission Rate (OER), which is expressed in odor units per second ($\mathrm{OU_E}$ /s) and is obtained as the product of the odor concentration and the air flow associated with the source (EN 13725, Capelli et al., 2013). As a matter of course, usually the odorant concentrations are still measured in traditional units, such as ppm or mg/m^3, since they are recorded as gaseous chemical compounds and not in their quality of odor generation. For instance, the AERMOD model still requires emission rate input based on classical chemical concentrations.

Topographical parameters:

The spatial domain of the simulation has been setup as per actual mean sea level including all the emission sources to be studied, as well as the data requirement for odor dispersion modeling receptors that are believed to be impacted by the emitted odors, and their geographical coordinates, i.e. latitude and longitude usually given in the UTM- WGS84 (Universal Transverse of Mercator - Word Geodetic System 1984). In order to get more information about AERMOD's terrain preprocessor AERMAP, please see subsection 3.2.4.

2.6.5 Measures for model validation

As already mentioned [Cap+13], dispersion models can be more or less complex. Independently from model complexity, model validation is an important aspect that cannot be set aside. Indeed, "strict" validation studies are limited in literature (Hayes et al., 2006). One difficulty is that chemical analyses, which are easily carried out at the source or close to the source, are hardly applicable for model validation due to the low, or even very low, level of pollutants, which is often below the analytical detection threshold. Exactly this happened throughout the first measuring campaign in 2018 at the WWTP Camping San Fernando, when a lot of measuring efforts further away from the main emission source led to pure 0 or below-accuracy concentrations (see 3.1.1).
Limitations are due also to the fact that the provenance of the detected compounds is not always unequivocally identifiable. For this reason, dispersion modeling based on chemical measurements at the source and in the environment should be focused on the identification of specific tracer compounds. In some cases, it is possible to identify a limited number of compounds that can be linked to the source, such as hydrogen sulfide (Latos et al., 2011; O'Shaughnessy and Altmaier, 2011), sulfur dioxide (Dresser and Huizer, 2011) or ammonia (Blanes-Vidal et al., 2012).

Tracer (SF_6)

Following up on this, another solution is to introduce a new tracer. Sulfur hexafluoride (SF_6) is a compound that is typically used as a tracer for dispersion experiments (Connan et al., 2011; Van Dorpe et al., 2007). The advantages of using SF_6 as a tracer for dispersion modeling purposes are mainly three:

1. The warranty of specificity due to the fact that this compound is not present in the environment,
2. it is stable (non-reactive or inert), and

3. specific detection techniques (which are generally based on optical measurements) allow to reach very low detection levels (μg m^{-3} - level).

Radioactive tracers (natural or anthropogenic) have been also used for atmospheric dispersion studies (Sykora and Froehlich, 2010). Of course, validation studies with radioactive compounds or other hazardous chemicals need authorizations and must be carried out by experts used to manipulate such compounds.

Wind tunnel scale studies If a tracer injection cannot be carried out on field, a small scale study can be developed into a wind tunnel. Of course, the scale factor with respect to odor cannot be easily estimated, but such studies are generally designed with the purpose of understanding diffusion and transportation of compounds around buildings or other obstacles. Typically, a small scale area representative of a real one can be constructed. In that case, dispersion at urban street canyons and intersections is studied (Ahmad et al., 2005). Moreover, wind tunnel study results can be compared with field observations as shown by Aubrun and Leitl (2004). In their study the authors demonstrate the ability to replicate the unsteady properties of a dispersion process inside a wind tunnel. Depending on the concept of the wind tunnel, different parameters can be controlled (e.g. air humidity and temperature), and heating devices can simulate solar radiation. Wind tunnel studies can also be linked with emission experiments whereby a wind tunnel is designed for simulating a source of odorous pollutants and to test emission models as a first step of the dispersion process (Santos et al., 2012).

3 Methods

In the method section, the interested reader is going to be informed about all measurement instruments, modeling techniques and data employed in order to accomplish this research project.

3.1 Measuring instruments

In this subsection all measuring devices are going to be listed and described thoroughly which were deployed during the entire research project. First, the gas measurement apparatus will be portrayed, followed by the olfactometry device and the accompanying mobile weather station. Finally, the volume flow meter is going to be explained.

3.1.1 Gas detector "Dräger Polytron 7000"

The gas detector model "Polytron 7000" from the company "Dräger" (see official web page of this instrument under [Drä]) was deployed during both measurement campaigns 2018 and 2019 for measuring both odorant concentrations of interest in the field at various locations on-site.
Generally, the Polytron 7000 can record maximum one measurement per minute. The measured values are constantly saved in an external register device connected via cable to the Dräger Polytron 7000, as it can be seen in figure 31.

As for safeguarding the correct calibration, it is recommended it in appropriate time intervals, especially when being constantly exposed to heat, i.e. strong solar irradiation. To avoid this problem, the devices should be placed in the shade or at least protected against the sun with any kind of cover. In the case of this project, this was attained by slipping plastic buckets over the sensors whenever it was impossible to place them in the shade due to the limited range of the cables of maximally 30 meters (see figure 32).

These sensor cables allow the experimenter to mount the sensors remote from the emission source of interest, which in turn enables the user to read, configure and operate the transmitter from a safe and more convenient area when aiming to detect toxic gases.
As far as detectable gases are concerned, the Dräger Polytron 7000 can detect over 100 different species. Moreover, Dräger sensors are specifically designed for the demands of 24 hours per day, 365 days per year operation. The built-in sensor data memory containing all the relevant gas and calibration information, together with on board temperature and pressure compensation. This also allows the Polytron 7000 to accept pre-calibrated sensors, with minimal operator intervention, the Dräger Polytron 7000 is a virtually maintenance free transmitter.
Finally, turning to the two species of interest, namely $\mathrm{H_2S}$ and $\mathrm{NH_3}$, in the following two separate paragraphs are going to be dedicated for their description as their data sheets are distinct.

Figure 31: Photograph of the Dräger Polytron 7000 gas measuring devices situated in the shade along with their associated data register. The black cables represent the air-sucking system transporting the odorant-laden air to the sensors, which then send their measurement result digitally via the light gray cables to the registry.

Figure 32: In this photograph, the makeshift sun protection of the sensors by utilizing plastic buckets is demonstrated. To that end, they were slipped over the top of them. Besides, in the left part of the picture one can locate the sensor cables which were fixed by the weight of a medium-sized brick put on top of them. As for the weight, the cables are still passable. To ensure this, the endings of the sensor cables always protruded a few centimeters from the brick.

Comment on cross sensibility:
According to Carlos Lafita López, for conducting the gas concentration measurements in the field there is not equipment available which particularly measures other reduced sulfuric compounds, such as methyl mercaptan (MESH), dimethyl sulfide (DMS), etc. On the other hand, the Dräger Polytron 7000 H_2S detector measures these compounds together with H_2S. The general unit employed when referring to concentrations in this context are "parts per million" (ppm) which stands for a volumetric mixing ratio, i.e. 1 volume unit of the chemical compound of interest for every million units of air, or whichever the surrounding medium is. Following up on this, the measuring device does not register a 1:1 relation of the chemical compounds due to cross-sensibility of the sensor to similar compounds. Besides, the relation of these confused compounds to measured units of the actually desired compounds is not 1:1. In the case of H_2S these could be other reduced sulfuric compounds, e.g. 1 ppm of mercaptans would lead to an increase in measured H_2S concentration, but not necessarily to the same extent of another 1 ppm, but rather less than that. Generally, these effects cannot be distinguished by the measuring apparatus which leads to the conclusion that all concentrations obtained for e.g. H_2S are not unequivocally caused by pure H_2S. This will be also true for the NH_3 measurements.

Hydrogen sulfide:
According to the data sheet (see figure 33) delivered along with the Dräger Polytron 7000 extension for hydrogen sulfide, the reliable measuring range goes from 1 to 100 ppm which is applicable to typical values within the measuring range of new sensors and ambient conditions of 20°C (68°F), 50% relative humidity and 1013 mbar. Moreover, the measurement accuracy is either $\leq \pm 3\%$ or $\leq \pm 0.5\,\mathrm{ppm}$

whichever is the greater value.
As can later be seen in the data sheet of ammonia (see 34), the H_2S extension is more sensitive as the limit detection value and its associated measurement accuracy and uncertainty are lower than those of ammonia. This is recommended since H_2S has both a significantly lower perception threshold and limit hazardous to health, which can be corroborated when looking in subsection 2.2.3, particularly table 1 for the perception threshold.

Calibration interval	
default	6 months
Adjustment range min/max	1 day/12 months
Warm-up time	
ready for operation after max.	15 minutes
ready for calibration after max.	520 minutes
when using SensorReady®	<3 minutes
Measurement accuracy *	
measurement uncertainly (of meas. value) or	≤ ±3 %
minimum (whichever is the greater value)	≤ ±0.5 ppm
Loss of sensitivity *, per year	≤ –3 %
Expected service life, in ambient air	>36 months
Environmental conditions	
Temperature, min./max.	–40/65 °C (–40/149 °F)
Rel. humidity, min./max.	5/95 %
Ambient pressure	±3 %
Storage conditions	
packed, min./max.	0/40 °C (32/104 °F)
Cross-sensitivities	existing, for information contact Dräger Safety
Order Nos.:	
DrägerSensor H_2S LC	68 09 610
Dust filter	68 09 595
Calibration adapter V	68 10 536
Calibration cylinder for ampoule calibr.	68 03 407
Test gas ampoule 10 ppm H_2S	68 08 140
Test gas ampoule 20 ppm H_2S	68 08 141
Test gas ampoule 40 ppm H_2S	68 08 142
Test gas ampoule 100 ppm H_2S	68 08 143

Additional technical data
Available on Internet at www.draeger.com or on request from your Dräger Safety dealer.

Figure 33: Data sheet of the Dräger Polytron 7000 H_2S LC - 6809610 extension (Edition 09 - 03/2007). Among other facts, it comprises the measurement accuracy which specifies the distinction between the general measurement uncertainty (of measured values) and the minimum uncertainty depending on whichever is the greater value.

Ammonia:

In accordance with the data sheet (see figure 34) provided along with the Dräger Polytron 7000 extension for ammonia, the reliable measuring range goes from 1 to 300 ppm which is, in the same way as mentioned before with regard to hydrogen sulfide in figure 33, applicable to typical values within the measurement range of new sensors and ambient conditions of 20°C (68°F), 50% relative humidity and 1013 mbar. Besides that, the measurement accuracy is either $\leq \pm 5\%$ or $\leq \pm 1.5\,\mathrm{ppm}$ whichever is the greater value. As already mentioned previously related to the $\mathrm{H_2S}$ extension, the ammonia measuring accuracy and uncertainty are higher since the limit values of perception and health impairment are considerably higher than hydrogen sulfide (compare 2.2.2 and 2.2.3).

Intervalo de calibración	
preajustado	6 meses
Rango de ajuste mín./máx.	1 día/12 meses
Tiempo de calentamiento	
Operativo después de máx.	15 minutos
Listo para calibración después de máx.	60 minutos
Precisión de la medición *	
Inseguridad de medición (del valor de medición) o	≤ ±5 %
Mínima (aplica el valor mayor)	≤ ±1,5 ppm
Pérdida de sensibilidad, al año	≤ -15 %
Vida útil esperada, en el aire ambiental	>24 meses
Condiciones ambientales	
Temperatura, mín./máx.	-40/65 °C
Humedad rel., mín./máx.	15/95 %
Presión ambiental	±1 %
Condiciones de almacenamiento	
Empaquetado, mín./máx.	0/40 °C
Sensibilidades cruzadas	disponibles. Datos mediante solicitud a Dräger
Números de referencia:	
DrägerSensor NH_3 TL	68 13 095
Filtro de polvo	68 12 224
Adaptador de calibración V	68 10 536
Botella de calibración para la calibración de ampollas	68 03 407
Ampolla de gas de prueba 50 ppm NH_3	68 07 924

9 Otras características técnicas

En www.draeger.com o solicitando la información necesaria a la filial competente de Dräger.

Figure 34: Data sheet of the Dräger Polytron 7000 NH_3 TL 6813095 extension (Edition 04 - 10/2015) for availibility reasons in the Spanish version. Inter alia, it contains the measurement accuracy ("precisión de la medición" in Spanish) which specifies the distinction between the general measurement uncertainty (of measured values) ("inseguridad de medición (del valor de medición)" in Spanish) and the minimum uncertainty depending on whichever is the greater value ("mínima (aplica el valor mayor)" in Spanish).

3.1.2 Dynamic olfactometer "Nasal Ranger"

In accordance to the information obtained from Carlos Lafita López, the dynamic field-olfactometer can measure every 2 to 3 minutes, even though this time display strongly depends on the operator, i.e. the panelist, because fatigue should caused by repeated measurement should be strictly avoided. The following information about this olfactometry measurement device can be found on the official website of Nasal Ranger [Nas]. For further information about dynamic olfactometry and the Nasal Ranger deployment in another research project, please see subsection 2.5.3.

In addition, in order to transform the European Odor Units per cubic meter into intensities or offensiveness, the conversion table 6 is to be used.

Table 6: Classification of olfactometry measurement units in odor intensity and offensiveness. The measurements are taken with the Nasal Ranger field olfactometer (see fig. 35 and 36). OU_E stands for "European Odor Units".

Odor concentration ($OU_E\,m^{-3}$)	Odor intensity	Offensiveness
> 15 - 60	5	Very strong
> 7	4	Strong
> 5	3	Moderate
> 3	2	Weak
< 3	1	Very weak

In the following, the component diagram 35 and the associated data sheet of the measurement device 36 are displayed.

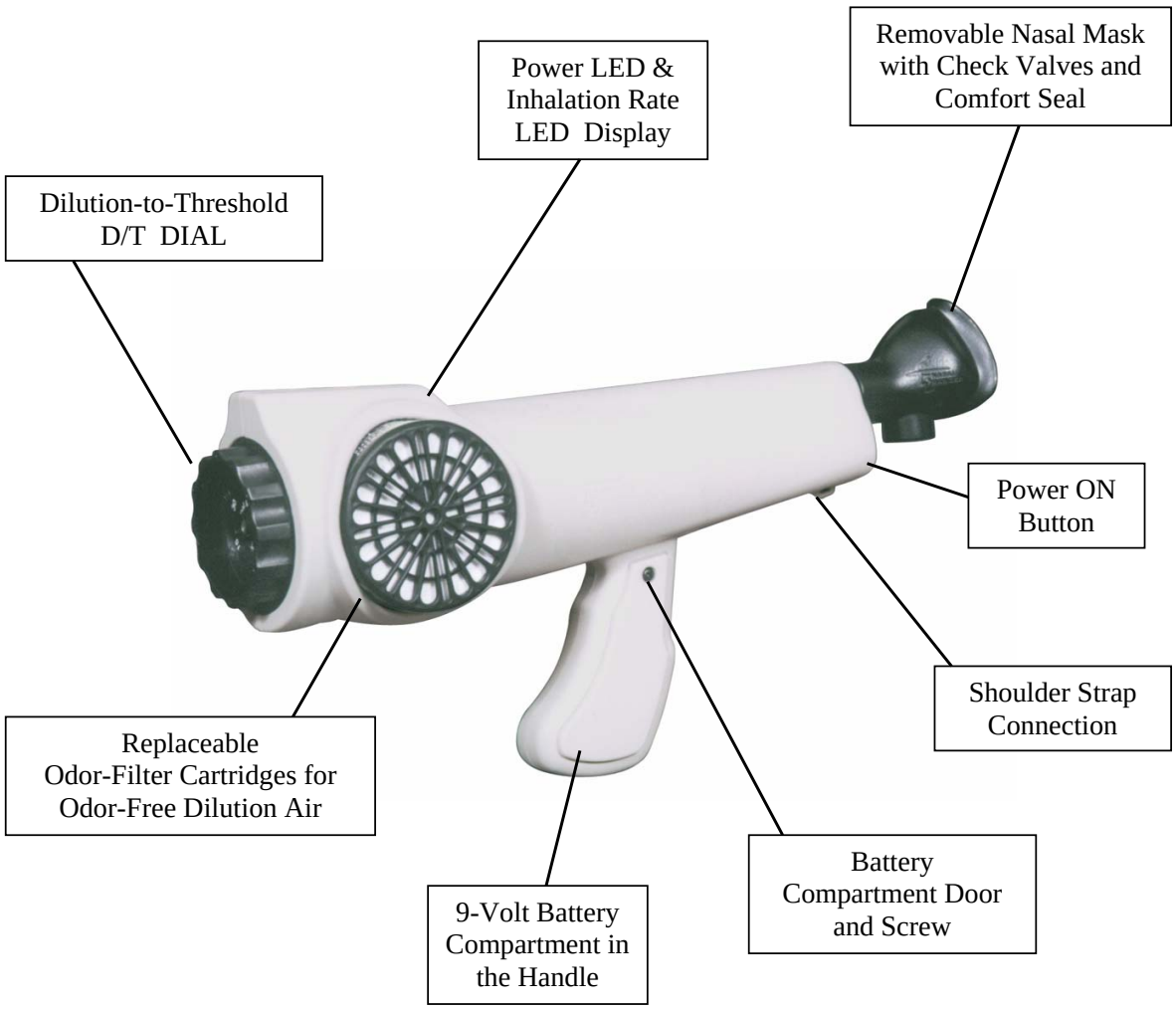

Figure 35: Component diagram of the Nasal Ranger field olfactometer.

Nasal Ranger® Field Olfactometer
Technical Specifications

Detection Technique:	Human Nose
Discrete Dilution Ratios:	2, 4, 7, 15, 30, 60 D/T's (Standard Dilution-to-Threshold Ratios)
Response Time:	As fast as 3-seconds (2 inhalations)
Accuracy:	+/- 10% of D/T
Repeatability:	+/- 2%
Inhalation Rate:	16-20 liters per minute
Operating Temperature Range:	32° to 104°F, 0° to 40°C
Power Requirements:	Standard 9-Volt Alkaline Battery
Dimensions:	14"(L) x 7.5"(H) x 4"(W) (35.5 x 19 x 10 cm)
Weight:	2.0 lbs (0.91 kg)
Materials of Construction:	PTFE and Polymer Alloys
Odor Filter Cartridge:	3.5" diameter x 1.5" (H) (8.9 cm diameter x 7 cm)
Nasal Mask:	2.75" (H) x 2.25" (W) (7 cm x 5.7 cm)
Patent:	U.S. Patent No.: 6,595,037
Calibration Verification:	Recommended Annually
EMC Verification:	Emissions: EN 61326: 1997, Class B Immunity: EN 61326:1997, Industrial Location
Markings:	89/336/EEC (EMC) 92/59/EEC (General Product Safety) CE

Figure 36: Table of technical specifications of the Nasal Ranger field olfactometer.

Moreover, figure 37 shows a live photograph shot during a field application of the Nasal Ranger.

Figure 37: Close-up shot during dynamic field olfactometry measurements on the WWTP site using the Nasal Ranger equipment (see fig. 35) on 3 August 2018. Here, the outgoing odors from the bioreactor toward the closest dwellings were measured.

Usually, the measuring session for each spot lasted around 8 to 10 minutes and comprised of approximately 4 measurements.

3.1.3 Mobile weather station "Kestrel 5500 Fire Weather Meter Pro"

During the on-site olfactometry measurements, carried out by the panelists Fernando Andrés Tomas and Carlos Lafita López, a mobile weather station was employed in order to obtain simultaneous wind direction and speed data of the same location where the olfactometry data was being taken. On the official website [com] the subsequent details regarding the Kestrel mobile meteorological station provided by the figures 38, 39 and 40 can be inspected.

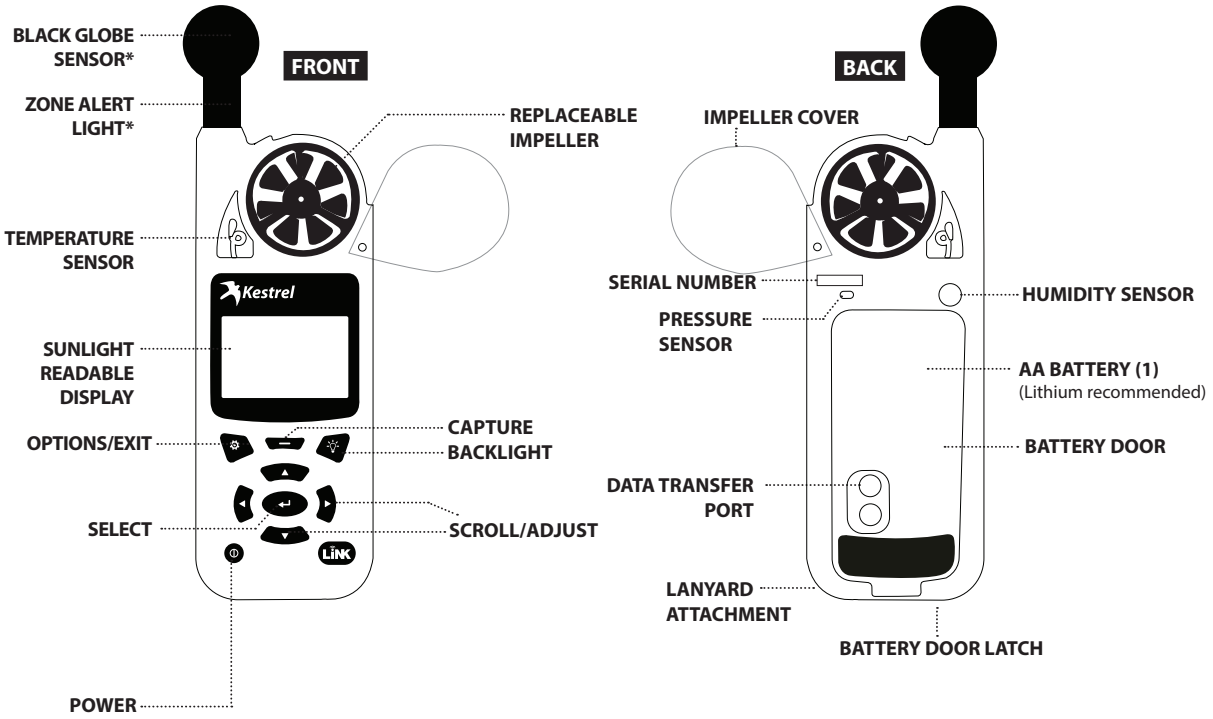

*Only available on 5400 Fire Weather Pro WBGT.

Figure 38: Front and back layout of the Kestrel-5-series.

SENSOR	ACCURACY (+/-)	RESOLUTION	SPECIFICATION RANGE	NOTES
Wind Speed |Air Speed	Larger of 3% of reading, least significant digit or 20 ft/min	0.1 m/s 1 ft/min 0.1 km/h 0.1 mph 0.1 knots 1 B* 0.1 F/S*	0.6 to 40.0 m/s 118 to 7,874 ft/min 2.2 to 144.0 km/h 1.3 to 89.5 mph 1.2 to 77.8 knots 0 to 12 B* 2-131.2*	1 inch|25 mm diameter impeller with precision axle and low-friction Zytel® bearings. Startup speed stated as lower limit, readings may be taken down to 0.4 m/s |79 ft min|1.5 km/h |.9 mph |.8 kt after impeller startup. Off-axis accuracy -1% @ 5º off axis; -2% @ 10º; -3% @ 15º. Calibration drift < 1% after 100 hours use at 16 MPH |7 m/s. Replacement impeller (NK PN-0801) field installs without tools (US Patent 5,783,753). Wind speed calibration and testing should be done with triangle on impeller located at the top front face of the Kestrel. Measuring wind speeds above 60 m/s / 134.2 mph can damage the impeller.
Ambient Temperature	0.9 °F 0.5 °C	0.1 °F 0.1 °C	-20.0 to 158.0 °F -29.0 to 70.0 °C	Airflow of 2.2 mph|1 m/s or greater provides fastest response and reduction of insolation effect. For greatest accuracy, avoid direct sunlight on the temperature sensor and prolonged sunlight exposure to the unit in low airflow conditions. Calibration drift is negligible for the life of the product. For further details, see Display & Battery Operational Temperature Limits.
Relative Humidity	2%RH	0.1 %RH	10 to 90% 25°C non-condensing	To achieve stated accuracy, unit must be permitted to equilibrate to external temperature when exposed to large, rapid temperature changes and be kept out of direct sunlight. Calibration drift is typically less than ±0.25% per year.
Pressure	1.5 hPa|mbar 0.044 inHg 0.022 PSI	0.1 hPa|mbar 0.01 inHg 0.01 PSI	25°C/77°F 700-1100 hPa|mbar 20.67-32.48 inHg 10.15-15.95 PSI	Monolithic silicon piezo-resistive pressure sensor with second-order temperature correction. Between 1100–1600 mbar, unit will operate with reduced accuracy. Sensor may not operate above 1600 mbar and can be damaged above 6,000 mbar or below 10 mbar. Calibration drift is negligible for the life of the product.
Compass	5°	1° 1/16th Cardinal Scale	0 to 360°	2-axis solid-state magneto-resistive sensor mounted perpendicular to unit plane. Accuracy of sensor dependent upon unit's vertical position. Self-calibration routine eliminates magnetic error from batteries or unit and must be run after every full power- down (battery removal or change). Readout indicates direction to which the back of the unit is pointed when held in a vertical orientation. Declination/variation adjustable for True North readout.

Figure 39: Sensor specifications from the Kestrel-5-series data sheet.

MEASUREMENT	ACCURACY (+/-)	RESOLUTION	SENSORS EMPLOYED
Air Density	0.0002 lb/ft3 0.0033 kg/m3	0.001 lbs/ft3 0.001 kg/m3	Temperature, Relative Humidity Pressure
Air Flow	6.71%	1 cfm 1 m3/hr 1 m3/m 0.1m3/s 1 L/s	Air Speed, User Input (Duct Shape & Size)
Altitude	typical: 23.6 ft/7.2 m from 750 to 1100 mBar max: 48.2 ft/14.7 m from 300 to 750 mBar	1 ft 1 m	Pressure, User Input (Reference Pressure)
Barometric Pressure	0.07 inHg 2.4 hPa|mbar 0.03 PSI	0.01 inHg 0.1 hPa|mbar 0.01 PSI	Pressure, User Input (Reference Altitude)
Crosswind & Headwind/ Tailwind	7.1%	1 mph 1 ft/min 0.1 km/h 0.1 m/s 0.1 knots	Wind Speed, Compass
Delta T	3.2 °F 1.8 °C	0.1 °F 0.1 °C	Temperature, Relative Humidity Pressure
Density Altitude	226 ft 69 m	1 ft 1 m	Temperature, Relative Humidity, Pressure
Dew Point	3.4 °F 1.9 °C 15-95% RH. Refer to Range for Temperature Sensor	0.1 °F 0.1 °C	Temperature, Relative Humidity
Evaporation Rate	0.01 lb/ft2/hr 0.06 kg/m2/hr	0.01 b/ft2/hr 0.01 kg/m2/hr	Wind Speed, Temperature Relative Humidity Pressure, User Input (Concrete Temperature)
Heat Index	7.1°F 4.0°C	0.1 °F 0.1 °C	Temperature, Relative Humidity
Moisture Content | Humidity Ratio (“Grains”)	4.9 gpp 0.7 g/kg	0.1 gpp 0.01 g/kg	Temperature, Relative Humidity Pressure
Probability of Ignition (PIG)	PIG Accuracy dependent on proximity of inputs to reference table steps.	10%	Temperature, Relative Humidity
THI (NRC)	1.5 °F 0.8 °C	0.1 °F 0.1 °C	Temperature, Relative Humidity
THI (Yousef)	2.3 °F 1.3 °C	0.1 °F 0.1 °C	Temperature, Relative Humidity
Relative Air Density	0.3%	0.1%	Temperature, Relative Humidity Pressure
Wet Bulb Temperature - Psychrometric	3.2 °F 1.8 °C	0.1 °F 0.1 °C	Temperature, Relative Humidity Pressure
Wet Bulb Temperature – Naturally Aspirated (NWB TEMP)	1.4 °F 0.8 °C	0.1 °F 0.1 °C	Wind Speed, Temperature Globe Temperature, Relative Humidity, Pressure
Wind Chill	1.6 °F 0.9 °C	0.1 °F 0.1 °C	Wind Speed, Temperature

Figure 40: Measurement specifications from the Kestrel-5-series data sheet.

Furthermore, the two following shots 41 and 42 depict the device in action during the olfactometry measurements next to the WWTP's main emission source, i.e. the canalization entrance into the bioreactor. The first figure 41 is a close-up showing how the blade is adjusting to the wind direction whereas the small wind wheel integrated into the top of the instrument is measuring the associated speed.

Figure 41: Close-up shot of the Kestrel mobile meteorological weather station next to the former canalization entrance deployed by the olfactometry panelists from the collaborating company Global Omnium S.L.

Next, in the second photo 42 the apparatus is shown while both the sludge recirculation inlet in the foreground and the two canalization pipes in the background are letting out liquid sludge and sewage water during the current pumping cycle.

Figure 42: Another view of the Kestrel mobile meteorological weather station along with an active outflow of the canalization and the sludge recirculation into the bioreactor.

3.1.4 Volume flow meter

Finally, the in advance firmly installed volume flow meter (see picture 43) is also included into this instrument listing. The device registers the accumulated outflow of the entire WWTP, i.e. after having passed through the decanter and being chlorinated. In the end of every working day, an employee passes by for reading off the current number given in cubic meters.

Figure 43: Photo of the fixedly installed volume flow meter which allows for reading off the currently accumulated volume outflow of the entire WWTP complex in cubic meters.

3.2 AERMOD atmospheric dispersion model

As for the versions of AERMOD itself and its pre- and postprocessors, which were employed in this project, they are listed in the following:

AERMOD: 18081

AERMAP: 18081

AERMET: 18081

AERSURFACE: 13016

As an aside, during the last stage of this project newer versions of AERMOD and AERMET were released. They are called "19191" referring also to the release year 2019, just like the versions utilized in the theses are from 2018 as the nomenclature indicates.
What is more, as far as time zone conventions are concerned, all data was converted into the Spanish local standard time, which is during winter from the end of October until the end of March UTC+1, and in the rest of the year the zonal daylight saving time UTC+2. In view of this project, all field campaigns were carried out during daylight saving time (UTC+2).

3.2.1 General model overview

According to [EA, p.43], AERMOD is a steady-state plume model in that it assumes that concentrations at all distances during a modeled hour are governed by the temporally averaged meteorology of the hour. Thus, as mentioned on [EA, p.38], AERMOD can use only a single value of each meteorological parameter to represent the boundary layer, which is why additional effective parameters are calculated to make up for that.
Generally, the steady state assumption yields useful results since the statistics of the concentration distribution are of primary concern rather than specific concentrations at particular times and locations ([EA, p.43]). Furthermore, following the model overview given in [EA, p.7], it assumes the concentration distribution to be Gaussian in both the vertical and horizontal in the stable boundary layer (SBL). In the convective boundary layer (CBL), the horizontal distribution is also assumed to be Gaussian, but the vertical distribution is described with a bi-Gaussian probability density function (pdf). This behavior of the concentration distributions in the CBL was demonstrated by Willis and Deardorff (1981) and Briggs (1993). Additionally, in the CBL, AERMOD treats "plume lofting", whereby a portion of plume mass, released from a buoyant source, rises to and remains near the top of the boundary layer before becoming mixed into the CBL. AERMOD also tracks any plume mass that penetrates into the elevated stable layer, and then allows it to re-enter the boundary layer when and if appropriate. For sources in both the CBL and the SBL AERMOD treats the enhancement of lateral dispersion resulting from plume meander.
As for the terrain handling, AERMOD uses a relatively simple approach and incorporates current concepts about flow and dispersion in complex terrain. Where appropriate, the plume is modeled as either impacting and/or following the terrain. All terrain is handled in a consistent and continuous manner while considering the dividing streamline concept (Snyder et al. 1985) in stably- stratified conditions.
Furthermore, following the model overview on [EA, p.8], AERMOD is able to characterize the PBL through both surface and mixed layer scaling. AERMOD constructs vertical profiles of required meteorological variables based on measurements and extrapolations of those measurements using similarity (scaling) relationships. Vertical profiles of wind speed, wind direction, turbulence, temperature, and temperature gradient are estimated using all available meteorological observations. AERMOD is designed to run with a minimum of observed meteorological parameters. AERMOD requires only a single surface measurement of wind speed (measured between 7z o and 100m - where z o is the surface roughness height), wind direction and ambient temperature. Moreover, AERMOD needs observed cloud cover, but in case it is not available (e.g. from an on-site monitoring program) two vertical measurements of temperature (typically at 2 and 10 meters), and a measurement of solar radiation can be employed for substitution. Additionally, a full morning upper air sounding (rawinsonde) is required in order to calculate the convective mixing height throughout the day. Also, surface characteristics (surface roughness, Bowen ratio, and albedo) are needed in order to construct similarity profiles of the

relevant PBL parameters. As far as the vertical inhomogeneity of the PBL is concerned, AERMOD accounts this in its dispersion calculations. This is accomplished by "averaging" the parameters of the actual PBL into "effective" parameters of an equivalent homogeneous PBL.

3.2.2 Information flow, processing and involved parameters

According to [EA, p.8f], the modeling system consists of one main program (AERMOD) and two pre-processors (AERMET and AERMAP), which are treated shortly in the forthcoming subsections 3.2.3 and 3.2.4. As for the information flow within the main model, the scheme 44 visualizes the processing.

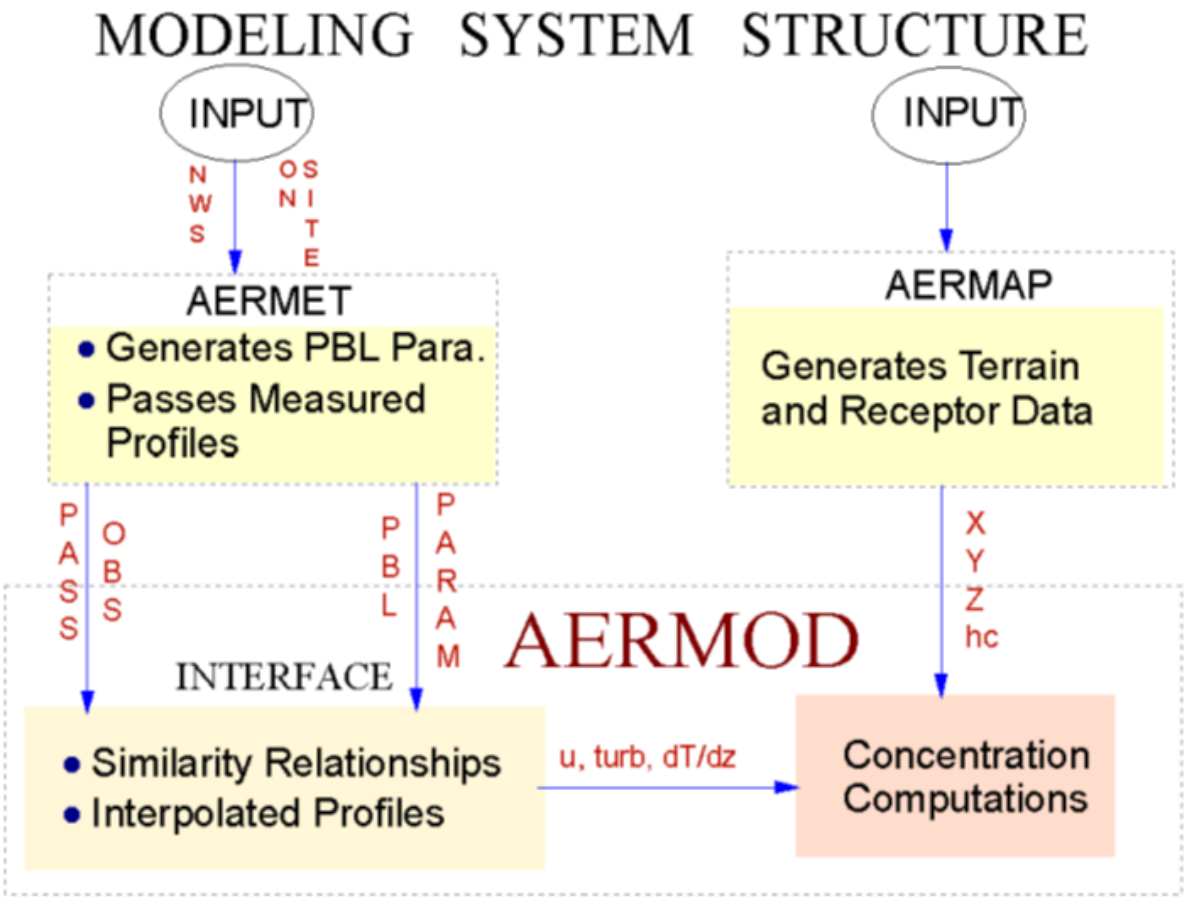

Figure 44: Flow chart of the data processing in the AERMOD modeling system with its most important preprocessors (quoted from [EA, p.9]).

Apart from the flow depiction 44, two more detailed process diagrams (45 and 46) are going to display the overall workflow and interdependences between the main model AERMOD and its preprocessor models AERMET, AERMAP, AERSURFACE and BPIBPRIME utilized in this thesis.

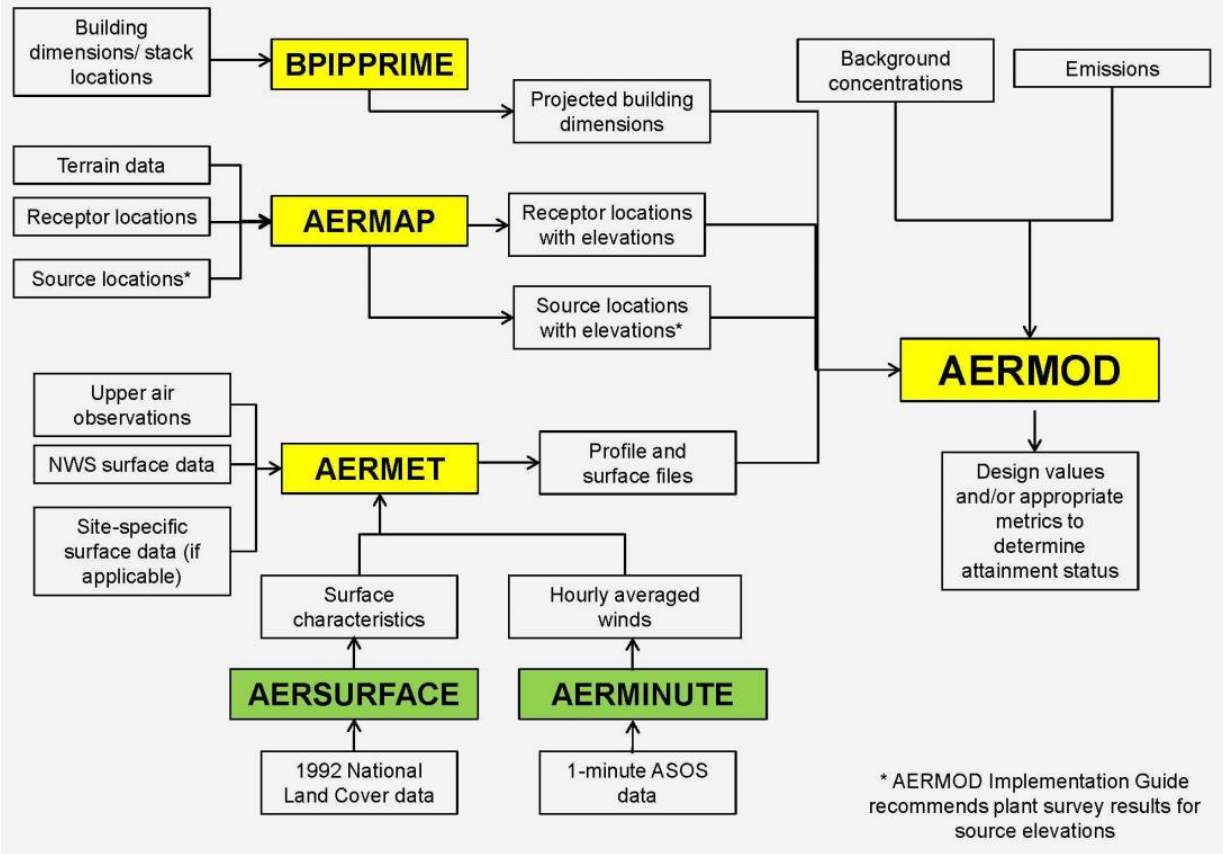

Figure 45: Scheme of the entire AERMOD-workflow extracted from [Vil17, p.54].

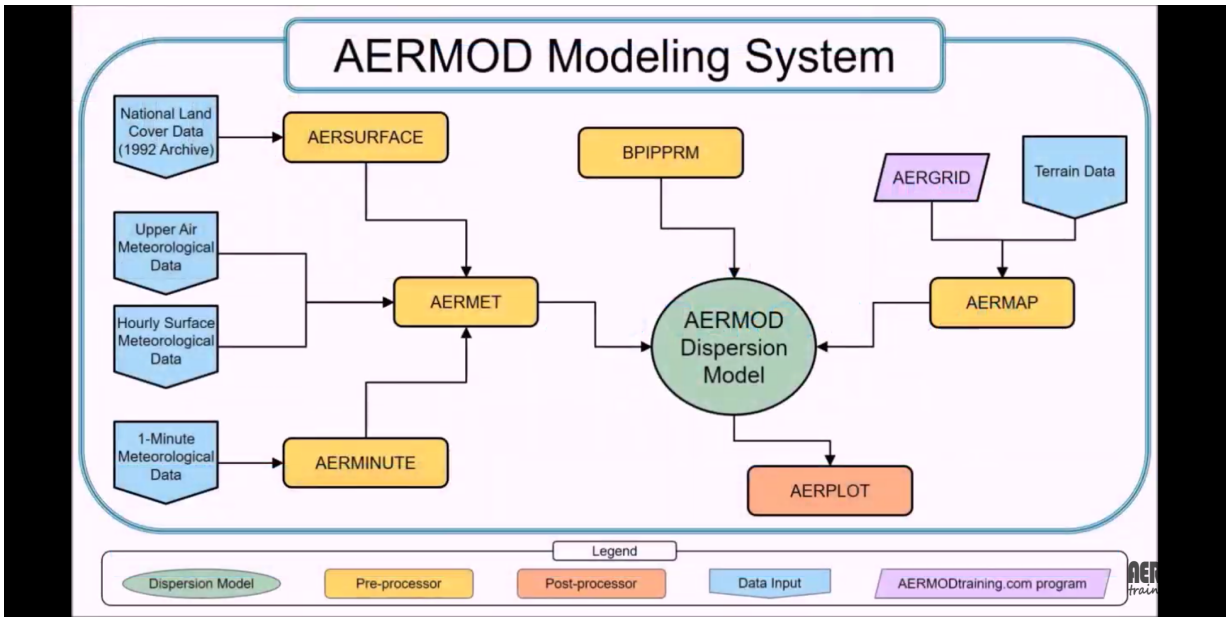

Figure 46: Another version of the AERMOD-workflow (compare fig. 45) to give a quick overview of the AERMOD main model in conjunction with its associated preprocessors (screenshot from instruction videos on [AER16]).

Finally, in order to retrace which options were used in the AERMOD-specific control file in this project, please inspect subsection 3.2.8 for further details.

3.2.3 AERMET

The major purpose of AERMET ([EA, p.9]) is to calculate boundary layer parameters for use by AERMOD. The meteorological interface, internal to AERMOD, uses these parameters to generate profiles of the needed meteorological variables. In addition, AERMET passes all meteorological observations to AERMOD. Input variables for AERMET, depending on the file formats of the radiosonde upper air and the surface data, are listed in the following.

Upper air input data in the FSL-format:

The main input variables, apart from other standard features such as the timestamp of each observation, the meteo-station number etc., are itemized in what follows.

- Atmospheric pressure at the current height of the registering balloon in millibars,
- Height above sealevel in meters related to the ascending registering balloon,
- Temperature in degrees Celsius,
- Dew point temperature in degrees Celsius,
- Wind direction in angular degrees, and
- Wind speed in meters per second.

It is paramount to note that the final units of each input variable could be decimal fraction or multiple of 10 of the general unit owing to the fact that the plain text input file should not comprise of decimal separators.

Surface input data in the SCRAM-format:
The SCRAM (MET 144) format consists of fewer weather variables. The file is composed of one record per hour, with all weather elements reported in an 28-column card image. The format is as follows:

- Ceiling height in feet,
- Wind direction in angular degrees,
- Wind speed in knots,
- Dry bulb temperature in degrees Fahrenheit,
- Total cloud cover, and
- Opaque cloud cover.

Hereafter, a further description of some variables shall be made:
At first, when talking about "ceiling height", it is meant the height of the cloud base above local terrain. Secondly, when referring to "cloud cover", in the SCRAM meteorological data files there are two cloud cover parameters called "opaque" and "total" cloud cover. Both parameters identify the amount of cloud cover measured in tens of percent, and are classified as follows:
0 = clear or less than 10%, e.g. 4 = 40-49%, and finally '-' or 10 = overcast or 100%.

General explanations:
Surface characteristics in the form of albedo, surface roughness and Bowen ratio, plus standard meteorological observations (wind speed, wind direction, temperature, and cloud cover), are input to AERMET. AERMET then calculates the PBL parameters: friction velocity (u^*), Monin-Obukhov length (L), convective velocity scale (w^*), temperature scale (θ^*), mixing height (z_i), and surface heat flux (H) . These parameters are then passed to the interface (which is within AERMOD) where similarity expressions (in conjunction with measurements) are used to calculate vertical profiles of wind speed (u), lateral and vertical turbulent fluctuations (σ_v , σ_w), potential temperature gradient ($d\theta/dz$), and potential temperature (θ). In order to see which options were used in the AERMET-specific control file in this project, please inspect subsection 3.2.8 for further details.

3.2.4 AERMAP

The AERMIC terrain pre-processor AERMAP ([EA, p.9f]) uses latticed terrain data to calculate a representative terrain-influence height (h_c), also referred to as the terrain height scale. The terrain height scale h_c , which is uniquely defined for each receptor location, is used to calculate the dividing streamline height. The latticed input data required by AERMAP is selected from Digital Elevation Model (DEM) data. AERMAP is also used to create receptor grids. The elevation for each specified receptor is automatically assigned through AERMAP. For each receptor, AERMAP passes the following information to AERMOD: the receptor's location (x_r , y_r), its height above mean sea level (z_r), and the receptor specific terrain height scale (h_c). For comprehending which options were used in the AERMAP-specific control file in this project, please inspect subsection 3.2.8 for further details.

3.2.5 Treatment of building downwash

Pursuant to [EA, p.73f], AERMOD incorporates the Plume Rise Model Enhancements (PRIME) (Schulman et al. 2000) algorithms for estimating enhanced plume growth and restricted plume rise for plumes affected by building wakes (U.S. Environmental Protection Agency, 1995). PRIME partitions plume mass between a cavity recirculation region and a dispersion enhanced wake region based 73upon the fraction of plume mass that is calculated to intercept the cavity boundaries. These boundaries are established from estimates of the locations of the lateral and vertical separation streamlines. Further information can be found following the in-depth description on [EA, p.74ff].

3.2.6 Source characterization

As mentioned in [EA, p.78f], AERMOD gives the user the ability to characterize a source as either a point, an (even irregularly shaped) area, or a volume. Regarding the project, the WWTP Camping San Fernando was found to comprise of one sole point source. Point sources are characterized exactly as in the ISC3 model (U.S. Environmental Protection Agency, 1995). In this case, the input to the model includes the location, elevation, emission rate, stack height, stack gas temperature, stack gas exit velocity, and stack inside diameter. The temperature, exit velocity, and diameter are required for plume rise calculations.

3.2.7 General remarks for further reading

Finally, according the content of [EA, p.10], a comprehensive description of the basic formulation of the AERMOD dispersion model including the INTERFACE, AERMET, and AERMAP can be found in the document [EA], which is the official AERMOD model formulation and evaluation. Inter alia, the document encompasses the following points:

1. A complete description of the AERMET algorithms that provide quantitative hourly PBL parameters
2. The general form of the concentration equation with adjustments for terrain
3. Plume rise and dispersion algorithms appropriate for both the convective and stable boundary layers
4. Handling of boundary layer inhomogeneity
5. Algorithms for developing vertical profiles of the necessary meteorological parameters
6. A treatment of the nighttime urban boundary layer
7. Treatment of building downwash (incorporation of the PRIME model)
8. Enhancement of lateral dispersion due to plume meander

3.2.8 Input control files - employed options of each model part

Before the listing of the input options of each control file used in the AERMOD model starts, it is noteworthy that not every comment, indicated by "**", and every option is included. Only those which matter and could even be chosen differently by the user. Moreover, the real filepaths were replaced by the generic term "filepath". Following, the control options employed in this thesis are going to be listed subsequently; first for the main model AERMOD, then for all the included preprocessors AERMAP, AERMET and AERSURFACE. The building downwash handling software BPIPPRM was not utilized.

AERMOD control file content

** +++ Control Pathway Keywords and Parameters +++
CO STARTING

** DFAULT - Specifies that regulatory default options will be used. Specification of DFAULT option will override non-regulatory options that may be specified.
** CONC - Concentration values will be calculated
** ELEV - Default option of assuming elevated terrain will be used.
MODELOPT DFAULT CONC ELEV

** AVERTIME Time1 Time2 . . . TimeN MONTH PERIOD/ANNUAL
** The different average time possibilities (listed in the syntax above are):
** - TimeN: Nth optional averaging time (1, 2, 3, 4, 6, 8, 12, or 24-hr)
** - PERIOD: averages of the entire data period (for the MULTYEAR option, the summary of highest PERIOD averages is based on the highest PERIOD average across the individual years processed with MULTYEAR)
AVERTIME 1 PERIOD

** If necessary: FLAGPOLE - Default value for height of (flagpole) receptors above local ground, a default value of 0.0 meters is used if this optional parameter is omitted
** Note: FLAGPOLE = Receptor Height Above Ground: This may be used to model impacts at "flagpole" receptors. A flagpole receptor is defined as any receptor located above ground level, e.g.,

to represent the roof or balcony of a building. The default value is assumed to be 0.0 meters (i.e., ground-level receptors).
FLAGPOLE 1.7

** Specifies name of detailed error listing file (default = ERRORS.LST)
ERRORFIL filepath
CO FINISHED

** +++ Source Pathway Keywords and Parameters +++
SO STARTING
** SOURCE LOCATION AND STACK-IDs
** ELEVUNIT - defines input units for source elevations (defaults to METERS, already included in AERMAP-source file included below)
** LOCATION - Identifies name, type and coordinates for particular source
** Syntax: SrcID Srctyp Xs Ys (Zs) = elevation above mean sea level
** LOCATION STACK1 POINT 0.00 0.00 3.26
** Note: Instead of the ELEVUNIT and LOCATION keywords, the AERMAP-source-output is being imported:
INCLUDED filepath

** 1) EMISUNIT - Optional unit conversion factors for emissions, concentrations
** The default emission rate units for the AERMOD model are grams per second for point and volume sources,
** and grams per second per square meter for area sources. By default, the model converts these input units to output
** units of micrograms per cubic meter for concentration calculations. This is accomplished by applying a default
** emission rate unit factor of 1.0E06 for concentration.
** NOTE: The defaults for concentration outputs are: " EMISUNIT 1.0E3 GRAMS/SEC MICROGRAMS/M**3"
** Syntax: Emifac (emission rate unit factor) Emilbl (emission unit label) Conlbl (output concentration calc. unit label)
EMISUNIT 1.0E3 GRAMS/SEC MILLIGRAMS/M**3

** SOURCE PARAMETERS
** 2) Showcase of the syntax for a point source
** SRCPARAM - Identifies source parameters for a particular source. The keywords are, depending on the source type:
** - SrcID: Source identification code
** - Ptemis: emission rate for point sources (g/s) -> Caution: conversion from concentrations to mass flow necessary!
** - Stkhgt: source stack physical release height above ground (m)
** - Stktmp: stack gas exit temperature (K) -> Caution: in Kelvin (conversion necessary usually)
** - Stkvel: stack gas exit velocity (m/s) -> Caution: Again use of SI-units
** - Stkdia: stack diameter (m)
** SourceID 'STACK1_2018' of source type 'POINT':
** SRCPARAM syntax: SrcID Ptemis (g/s) Stkhgt Stktmp (K) Stkvel (m/s) Stkdia

SRCPARAM STACK1_2018 2.2110621710020966e-05 0.3 300.47156546330615 0.24230464827850506 0.16

** 3) Variable source parameters implemented via previously calculated values included into an external text file
** HOUREMIS - Option for specifying hourly emission rates in a separate file
** -> This keyword is crucial to avoid a general constant approach to provide a scalar emission rate
** Column features of the AERMOD hourly emission (HOUREMIS) file: ['Source pathway', 'Keyword', 'Year', 'Month', 'Day', 'Hour', 'SourceID', 'Emission rate (g/s)', 'Gas exit temperature (K)', 'Gas exit velocity (m/s)']
HOUREMIS filepath STACK1_2018

** SrcGrpID: Group ID (Grpid = ALL specifies group including all sources) -> here: only one stack source given
SRCGROUP ALL
SO FINISHED

** +++ Receptor Pathway Keywords and Parameters +++
RE STARTING
** Includes the receptor network output generated by AERMAP - nothing else needed to specify
INCLUDED filepath
RE FINISHED

** +++ Meteorology Pathway Keywords and Parameters +++
ME STARTING
SURFFILE filepath
PROFFILE filepath
** Weather station data specifications - Syntax affects SURFDATA, UAIRDATA and SITEDATA as follows:
** Keyword Stanum Year (Name) (Xcoord) (Ycoord)
SURFDATA 83650 2018 Denia 38.832995 0.116995
UAIRDATA 08430 2018 Murcia 38.001895 -1.170805

** Base elevation (above MSL) for the potential temperature profile (unit defaults to METERS)
PROFBASE 15.0 METERS
ME FINISHED

** +++ Output Pathway Keywords and Parameters +++
OU STARTING
FILEFORM FIX
** "Allave" means "all averaging periods"
RECTABLE ALLAVE 1-5
MAXTABLE ALLAVE 3
DAYTABLE ALLAVE
** Unit in milligrams per cubic meters, perception threshold of hydrogen sulfide

MAXIFILE 1 ALL 0.0007 filepath
RANKFILE 1 5 filepath
SEASONHR ALL filepath
POSTFILE 1 ALL PLOT filepath
** The PLOTFILEs were used in order to produce the receptor network maximum value outputs overlaid on Google Earth satellite pictures
PLOTFILE 1 ALL 1ST filepath
SUMMFILE filepath
OU FINISHED

AERMAP control file content

CO STARTING
TITLEONE "Using 1.0 arc-second SRTM (NED GeoTIFF) data for OLIVA, SPAIN"
TITLETWO "CRS: WGS 84 for UTM Anchor Point coordinates"
** Two types possible: NED (National Elevation Dataset, GeoTIFF) and DEM (Digital Elevation Model data including 7.5-minute, 15-minute, and/or 1-degree) and the additional secondary..
** ..keyword FILLGAPS which only applies to DEM data, NOT to NED (GeoTIFF) data
DATATYPE NED

** Here: Use SRTM-1-arcsec DEM data starting with the OLIVA file, secondly DENIA and then the completion of the square out of 4 files in the North (Valencia and its gulf basin)
** CAUTION with AERMAP.INP - syntax: accepts only double quotation marks like ", not single ones like '
DATAFILE "filepath1" tiffdebug
DATAFILE "filepath2" tiffdebug
DATAFILE "filepath3" tiffdebug
DATAFILE "filepath4" tiffdebug

** Determines the terrain heights from the DEM data files provided (default)
TERRHGTS EXTRACT

** ANCHORXY-syntax: Xauser Yauser Xautm Yautm Zautm NADA
** (Xauser,Yauser) = any geogr. location, such as the origin (0,0) in the user coord. system
** (Xautm,Yautm,Zautm) = (Easting,Northing,Zone) UTM coordinates for the aforementioned user location
** NADA = 0 -> no datum switch outside the US since usually terrain data are referenced to the WGS84 datum
** OLIVA Bioreactor entrance: Zone = 30 S, Easting = 756163.09 m E, Northing = 4308576.55 m N
ANCHORXY 0.0 0.0 756163.09 4308576.55 30 0

CO FINISHED

** Source pathway (here: canalization entrance)
SO STARTING
** LOCATION Srcid Srctyp Xs Ys (Zs) <- elevation optional, will be derived from input DEM files automatically
** Srcid = source ID (up to 8 alphanumerical characters)
** Srctyp = source type (POINT, VOLUME, AREA, AREAPOLY or AREACIRC)
** Xs and Ys are the x-coordinate (East) and y-coordinate (North) of the source location in meters, and Zs is the optional source elevation in meters above mean sea level
** Comment: Here, the anchor point ANCHORXY is the same as the only source point, thus has the same UTM coordinates
LOCATION STACK1 POINT 0 0
SO FINISHED

** Receptor pathway for building one OR SEVERAL receptor networks
** -> DISTANCE UNIT of the grids are in METERS, indicate floats with a "." after the integer part of the number
RE STARTING
GRIDCART RECT1 STA
** Rectangular grid chosen to be a square of 400.0m edge length
** Start (Xinit, Yinit) = (x_source - 200.0m, y_source - 200.0m)
** Initial coords relative to the AnchorXY-point defined previously
** Xinit Xnum XDelta Yinit Ynum YDelta
RECT1 XYINC -200.0 80 5.0 -200.0 80 5.0
GRIDCART RECT1 END
RE FINISHED

OU STARTING
RECEPTOR filepath
SOURCLOC filepath
DEBUGHIL filepath
DEBUGREC filepath filepath filepath
DEBUGSRC filepath filepath filepath
OU FINISHED

AERMET control file content

Stage 1: surface data

JOB
REPORT filepath
MESSAGES filepath

SURFACE
DATA filepath SCRAM
EXTRACT filepath
QAOUT filepath
XDATES 2019/04/03 TO 2019/06/03

** Station info (extracted from the file "083650-99999-DENIA-SPAIN-metadata.txt"):
** USAF-WBAN-ID STATION NAME COUNTRY STATE LATITUDE LONGITUDE ELEVATION
** ———— ———————— ———————————————-
** 083650 99999 DENIA SPAIN +38.833 +000.117 +0015.0
LOCATION 83650 38.833N 0.117E 0 15

Stage 1: upper air data

JOB
REPORT filepath
MESSAGES filepath

UPPERAIR
** Data from weather station located in Murcia, Spain
DATA filepath FSL
EXTRACT filepath
QAOUT filepath

** Decrease the lower limit of the feature PRESSURE to 0 mbar instead of the default 5000 mbar in order to include more levels per sounding
RANGE UAPR 0 <= 11000 99999
** Raise the upper limit of the feature HEIGHT to 30000 m instead of the default 5000 m in order to include more levels per sounding
RANGE UAHT 0 <= 30000 99999

XDATES 2019/04/03 TO 2019/06/03

** Station info (complete): SPM00008430 (short version from Spain: 08430), 38.00277778N 1.16944444W
** Data can be obtained from: `http://radiosonde.eu/RS00-S/RS02K-S.html#ancre27265`
** Comment: The latitude and longitude values have been adapted for the data within the provided text file, which differ slightly from the aforementioned information
** Data from weather station located in Murcia, Spain

LOCATION 08430 38.00N 1.17W 0

Stage 2: merge surface and upper air data

JOB
REPORT filepath
MESSAGES filepath

UPPERAIR
QAOUT filepath

SURFACE
QAOUT filepath

MERGE
OUTPUT filepath
XDATES 2019/04/03 TO 2019/06/03

Stage 3: produce AERMOD-ready surface and profile outputs

JOB
REPORT filepath
MESSAGES filepath

METPREP
DATA filepath
OUTPUT filepath
PROFILE filepath

XDATES 2019/04/03 TO 2019/06/03

** ++++ METHODS USED IN THE FOLLOWING ++++

** REFLEVEL - substitution of NWS (National Weather Service) data
** SUBNWS - allows substitution of NWS data for missing ONSITE wind and/or temp data (other parameters automatically substituted).
** NOTE: this option must be used if no ONSITE data are provided, as it is the case in the OLIVA project
METHOD REFLEVEL SUBNWS

** WIND_DIR (not applicable to 1-min ASOS data, which is only available for locations in the US anyway) - processing of NWS wind directions:
** RANDOM - randomize (NWS) wind directions (default).
METHOD WIND_DIR RANDOM

** STABLEBL - specify option for SBL (stable boundary layer) processing:

** 1) BULKRN - Bulk Richardson Number - This option requires onsite measurements of temperature difference
** 2) ADJ_U* - Option to adjust U* (surface friction velocity) for low wind/stable conditions.
** For applications without the BULKRN option, the ADJ_U* option is based on Qian and Venkatram (2011).
** For applications with the BULKRN option, the ADJ_U* option is based on Luhar and Rayner (2009).
METHOD STABLEBL ADJ_U*

** NWS_HGT - (NWS) instrument height, in meters, for the specified variable
** NOTE: Mandatory if METHOD REFLEVEL SUBNWS is specified, as it is the case here
** NOTE on origin of this height: it is the height of the surface weather station in Dénia
** Syntax: variable_name (only valid variable_name is WIND) instrument_height (above ground in meters)
NWS_HGT WIND 15.0

** UASELECT - selecting upper air sounding
** SUNRIS(E) - select upper air sounding based on local sunrise
METHOD UASELECT SUNRISE

** Syntax: AERSURF primary_surfchar_filename
** primary_surfchar_filename: Contains the surface characteristic inputs for the primary surface data location (FREQ_SECT , SECTOR, and SITE_CHAR keywords)
AERSURF filepath

AERSURFACE control file content

filepath ** Land use data file
filepath ** Output file with sfc values for AERMET Stage 3
LATLON ** Coordinate type (UTM, LATLON)
58.5314 ** Latitude
-79.0018 ** Longitude
NAD83 ** Datum
1.0 ** Study radius for surface roughness (km)
Y ** Vary by sector? (Y/N)
12 ** Number of sectors
M ** Temporal resolution (A=ANNUAL, M=MONTHLY, S=SEASONAL)
N ** Continuous snow cover at least one month? (Y/N)
Y ** Reassign months to seasons? (Y/N)
1 2 ** Late autumn after frost and harvest, or winter with no snow
3 4 ** Transitional spring (partial green coverage, short annuals)
5 6 7 8 9 ** Midsummer with lush vegetation

10 11 12 ** Autumn with unharvested cropland
N ** Airport? (Y/N)
N ** Arid region? (Y/N)
A ** Surface Moisture (A=Average, W=Wet, D=Dry)

Comment on the AERSURFACE input TIFF file

As it was not possible to find a proper GeoTIFF from a Spanish national entity which provides high resolution satellite orthophotos for the surroundings of Dénia also into the sea away from the shore, the resolution of the employed graph was not decreased to the AERSURFACE-native 30x30 m^2, but maintained at the PNOA-native 0.25x0.25 m^2. In order to make AERSURFACE work, only the corresponding GeoTIFF-header-TAG was changed to 30x30 m^2. This has as a consequence, that the default gathering ground of 10 kilometers radius is in reality around 100 meters, which could be improved by finding other georeference satellite data which can be land-cover-classified at the lower AERSURFACE-resolution of 30x30 m^2, which in turn would allow, in the case of Dénia and its surroundings, for considering also the large water masses of the adjacent sea when estimating surface roughness length, Bowen ratio and and the albedo. It is likely that the AERMET input values, i.e. the AERSURFACE output, would have differed.

AERPLOT control file content

;- meta
version=2
origin = UTM

; Extracted from AERMAP source-file output: ** ANCHORXY 0.0 0.0 756163.09 4308576.55 30 0
easting = 756163.09
northing = 4308576.55
utmZone = 30

inNorthernHemisphere = true
; These two parameters will be used for 'origin=LL'. (If origin=UTM, they do not matter.)
originLatitude = 0.0
originLongitude = 0.0

; Note that all seven UTM+LL parameters must be set, but only five will be used for UTM, or three for LL will be used.
;- altitude parameters
; ====================
; Receptors can be plotted relative to the ground,
; or at a specific height level above or below sea level.

; If the ZELEV field can be isolated, "flagpole" also can be used as relativeToGround
altitudeChoice = flagpole

; The altitude of the receptors is offset from the height indicated in the .PLT file.
; (Note: Specify an expected altitude even if 'flagpole' is the altitudeChoice.
; This parameter is part of the calculation for the height of the initial viewpoint.)
altitude = 0

;- the source data file
; ====================
; The input file name, that is, the plotfile.
PlotFileName = filepath

; If one wishes to plot the sources as well, set this to the aermod.inp file.
SourceDisplayInputFileName = filepath

;- output parameters
; ==================
; Pick a name for this run, and it will be applied to a number of files, plus the objects that may be manipulated within Google Earth.
OutputFileNameBase = name

; The name that will be displayed in Google Earth for the dataset.
NameDisplayedInGoogleEarth = name

;- control parameters on the procedure
; ====================================
sDisableProgressMeter = false
sDisableEarthBrowser = true

;- receptor display
; =================
IconScale = 0.70

; The sIconSetChoice color scheme for the concentration scale.
sIconSetChoice = redBlue

;- concentration binning (for receptors and contours)
; ======================
; The user has the choice between a "Linear" or "Log" color scale. The user also can provide one of their own.
minbin = data
maxbin = data
binningChoice = Linear

; These examples could be realistic binning schemes.
customBinningElevenLevels = 1,2,3,4,5,6,7,8,9,10,11

;- concentration legend (for receptors and contours)
; ====================
; The program will insert this line into the HTML used to create the legend.
contourLegendTitleHTML = $C\ O\ N\ C\ E\ N\ T\ ...$
$...R\ A\ T\ I\ O\ N\ S$

;- line mappings (for contours and gradients)
; ============
; To plot any of the lines, an evenly spaced grid needs to be constructed by means of a combination of interpolating the data and extending the data.
; The following values are the default:
numberOfGridCols = 400
numberOfGridRows = 400

numberOfTimesToSmoothContourSurface = 1

; Note that the smoothing applies to both the contour and the gradient.
;- contour parameters
; ==================
; The parameter 'makeContours' enables ("TRUE") or disables ("FALSE") contours.
makeContours = true

; The contour lines seem less sensitive to the edge than the gradient.
; (If set to 0.0 or less, most lines won't be drawn.)
; (If set to 9999999, then all lines will be drawn.)
; - Contour is the way to go, gradient does not work so well
; - Values: 0 is nothing, 1 is only the source, 4 is more and 10 is almost everything
contourExtension = 4

;- gradient parameters
; ====================
; The parameter 'makeGradients' enables ("TRUE") or disables ("FALSE") gradients.
makeGradients = false

gradientExtension = 0.0

;- gradient binning
; ================
gradientMaxBin = data
gradientMinBin = data
gradientBinningChoice = Log

customGradBinElevenLevels = 1,2,3,4,5,6,7,8,9,10,11
gradientLegendTitleHTML = $Gradient\ Magnitudes$

;- hidden_grid
; ==========
; For display of evenly spaced grid. Debugging purposes only.

provideEvenlySpacedInterpolatedGrid = false

; end

3.3 Terrain data

The term terrain data refers usually to processed satellite pictures measured in different sets of frequencies (or bands) which are then employed for different scopes.

3.3.1 AERSURFACE - Multiband Orthophoto for land cover classification

Apart from the digital elevation data passed to the principal terrain preprocessor AERMAP (see 3.2.4), there is another part within the preprocessing of AERMOD where terrain data need to be introduced: In order to carry out the land cover classification fed to the AERSURFACE terrain preprocessor model of AERMET, which for its own part stands for the meteorological preprocessor of the main AERMOD dispersion model, the most up-to-date PNOA orthophoto (from Spanish "Ortofoto PNOA máxima actualidad") was downloaded from the corresponding website [Cen]. The institution responsible for the production and distribution of these orthoimages is the National Aerial Orthophotography Plan (from Spanish "Plan Nacional de Ortofotografía Aérea" (PNOA)), which can be inspected in further detail under [Pla].
In the latter web page it can be found that those high-resolution digital orthophotos of PNOA flights (as of 2004) comprise of a pixel size 0.25 or 0.50 meters and are provided either as TIFFs or ECWs along with the corresponding world file (TFW) georeferencing. As for the geodetic reference system the European Terrestrial Reference System 1989 (ETRS89) has been employed for continental Spain and the adjacent Balearic Islands. Following [Wikd], the ETRS89 is an Earth-Centered and Earth-Fixed (ECEF) geodetic Cartesian reference frame, in which the Eurasian Plate as a whole is static. In addition, ETRS89 is the EU-recommended frame of reference for geodata for Europe. Moreover, it is the only geodetic datum to be used for mapping and surveying purposes in Europe. Consequently, it plays the same role for Europe as NAD-83 for North America.
A chronological overview about the different land use classifications utilized in the National Water Quality Assessment (NAWQA) of the USA from 1976 till today is given under the web page [Unib] of the United States Geological Survey (USGS). From there, the required classification "National Land Cover Data Set 1992 (NLCD)" was adopted as it is the one which needs to be used in conjunction with the AERSURFACE terrain preprocessor for AERMET. The detailed meaning of each category and their subclasses is explained on the web page [Unic], which stands for the Enhanced National Land Cover Data Set 1992 (NLCDe 1992) and includes some additional subcategories in comparison to the land use classification "NLCD 1992" employed in AERSURFACE.
Within the scope of this project, superfluous categories are omitted, i.e. those which practically do not occur in the examined region or are rather hard to distinguish from another more dominant category. As a consequence of narrowing down the needful classes, the resulting table 7 was employed in AERSURFACE.

Table 7: Minimum of necessary categories defined in the land use classification "NLCD 1992" (see USGS web page [Unib]) implemented in this project. For each class so-called training-polygons were assigned which were overlaid over the PNOA orthophoto of the region in question with the aim to conduct a supervised land cover classification using a GIS-tool of choice (e.g. ArcGIS or the open-source tools QGIS and gvSIG).

Code	Gen	Description
11	wa	Open Water
21	ur	Low Intensity Residential
22	ur	High Intensity Residential
23	ur	Commercial/Industrial/Transportation
31	un	Bare Rock/Sand/Clay
43	un	Mixed Forest
51	un	Shrubland
61	un	Orchards/Vineyards/Other
85	ur	Urban/Recreational Grasses

3.3.2 AERMAP - Digital Elevation Model (DEM)

Shuttle Radar Topography Mission (SRTM) elevation data offer worldwide coverage of void filled data Digital Elevation - Shuttle Radar Topography Mission (SRTM) 1 Arc-Second Global at a resolution of 1 arc-second (30 meters) and provide open distribution of this high-resolution global data set. The DEM data type which was evaluated to be the most adequate for this project due to its highest resolution and up-to-dateness. The mentioned open distribution of high-resolution digital elevation data was produced by the Shuttle Radar Topography Mission (SRTM) which offers worldwide coverage of void filled data at a resolution of 1 arc-second (30 meters). More details can be found under [Unid]. The DEM-data was downloaded in the GeoTIFF-format from the interactive global geographical satellite data base provided by the United States Geological Survey (USGS) through their "Earth Explorer" [Unia].

3.4 Meteorological data

In order to provide AERMET, the meteorological preprocessor of AERMOD, with the required input data, essential variables such as wind speed, wind direction, atmospheric sealevel pressure, temperature etc. were obtained from various surface meteo-stations and one upper air radiosonde station. Moreover, other variables were contained in the plain text files as well, e.g. concerning the atmospheric stability conditions, which were in parts derived from other meteorological parameters, such as humidity, temperature and wind speed profiles, as well as cloud coverage or global and net solar radiation.
In general, the data stem from various sources and comprise of different temporal resolutions, such as 5-min, 10-min and daily.
Also, it must be pointed out that the distinct surface meteo-stations had an order of preference when being implemented into the model and related computations. The preferred station for every purpose was "AVAMET - Dénia Platja de Pego" due to both highest temporal resolution and proximity to the WWTP-site. All wind roses and other sorts of statistics plots presented in the section 4.4 are based on these data. Just for the special purpose of creating the AERMOD-ready hourly emission rate file, other data were considered in order to get the most complete set of hourly surface meteo data. In this case, the second preference had the official "Hourly Surface Data" from Dénia located around 14 kilometers

down the coast. Third, the other AVAMET station in "Oliva poble" situated a bit inland, and finally the data measured at some surfing schools up to 20 kilometers northward along the coast line.

3.4.1 Murcia airport - Upper air radiosonde data

The data are provided via data bases maintained by the National Oceanic and Atmospheric Administration (NOAA) of the USA, formerly the National Climatic Data Center (NCDC) as stated on [NOAb]. From this website the Integrated Global Radiosonde Archive (IGRA) can be accessed, in particular the raw data can be downloaded under [NOAa]. As for the scope of the IGRA, it consists of radiosonde and pilot balloon observations at over 2700 globally distributed stations (cited on 4 July 2019). The earliest data date back to 1905, and recent data become available in near real time. Observations are available at standard and variable pressure levels, fixed- and variable-height wind levels, and the surface and tropopause. Variables include pressure, temperature, geopotential height, relative humidity, dew point depression, wind direction and speed, and elapsed time since launch.
Moreover, the recommended uses in accordance to [NOAb] is the general aptitude as input to air pollution models, for studies of the detailed vertical structure of the troposphere and lower stratosphere, for assessing the atmospheric conditions during a particular meteorological event, and for many other analyses and operational applications. Scientists from the National Centers for Environmental Information (NCEI) have applied a comprehensive set of quality control procedures to the data to remove gross errors.
Regarding the origin of the employed radiosonde data in this project, the weather station at the Murcia Airport with the WMO station number SPM00008430 (or just "08430") was chosen, which is situated approximately 139 kilometers beeline from the WWTP according to the Google Earth Pro distance measuring tool. On the other hand, the second next upper air weather station is located in Son Bonet, Mallorca about 250 kilometers beeline from the WWTP, wherefore Murcia Airport was the preferred choice. An exhaustive list of all radiosonde weather stations in Western Europe can be found under the official website [EU].

3.4.2 Dénia - Hourly Surface Data

The Integrated Surface Database (ISD), provided by the National Centers for Environmental Information (NCEI) of the NOAA, is the source for the hourly surface data of a AERMET-specific format for this very same meteorological preprocessor of AERMOD. From the official website [NOAc], were the data can be downloaded at large scale in ASCII format via File Transfer Protocol (FTP), more detailed information on the data can be obtained. In summary, the Integrated Surface Database (ISD) consists of global hourly and synoptic observations compiled from numerous sources into a single common ASCII format and common data model. Beyond that, the database includes over 35000 stations worldwide, with some having data as far back as 1901. Currently (status 05-07-2019), there are over 14000 "active" stations updated daily in the database. ISD includes numerous parameters such as wind speed and direction, wind gust, temperature, dew point, cloud data, sea level pressure, altimeter setting, station pressure, present weather, visibility, precipitation amounts for various time periods, snow depth, and various other elements as observed by each station.
With regards to this project, the closest weather station integrated in the aforementioned ISD is Dénia with a beeline distance of about 14.3 kilometers southward along the coast from the WWTP site in accordance with the distance measurement tool provided by Google Earth Pro. The data delivered from this very meteorological station [AEM] with the ID "83650" is apt for the direct implementation into the AERMET model, i.e. is offered in the recognized ISHD-format.

3.4.3 AVAMET - Dénia Platja de Pego

The station [AVAa] disposes of a resolution of 5 minutes, and the data range from 01-02-2018 till 31-12-2018 which were download on 15-01-2019. The data were made available by the competent and helpful technician Sergi Segura i Llópez (administrador@avamet.org) working for AVAMET (Associació Valenciana de Meteorologia).
This weather station is the closest to the WWTP Camping San Fernando, with a distance of about 2.71 kilometers according to Google Maps, and has the highest temporal resolution in addition. Furthermore, apart from the standard features such as mean and maximum wind speed, its corresponding direction and mean temperature the data even comprises of relative humidity, mean air pressure at sea level and precipitation. The data are quite complete throughout the whole year of 2018 except for April where some 3 weeks are missing. During the gas and olfactometry measuring period, i.e. between 16 July and 15 October 2018, there are some data gaps in the range of 1 hour. If necessary, these can be filled with other meteorological data from distinct stations nearby, which are mentioned in the following for the sake of completeness, even though this station will be used mainly. All things considered, these data are the best for carrying out the modeling.

3.4.4 AVAMET - Oliva poble

The alternative weather station [AVAb] comprises of a resolution of 5 minutes akin to the above-mentioned station of Platja de Pego. as well. The data range from 01-02-2018 till 31-12-2018 and were also made available by technician Sergi Segura i Llópez (administrador@avamet.org) of AVAMET, downloaded on 15-01-2019. The distance of about 6.74 kilometers according to Google Maps is a little bit further from the WWTP than the other AVAMET station Dénia Platja de Pego. These data are overall more complete than the aforementioned data from Dénia Platja de Pego, but due to the position of the respective weather station Dénia Platja de Pego is preferred over Oliva poble since the former is closer to the WWTP and additionally has similar conditions for being situated directly next to the seashore, whereas the "Oliva Poble" weather station is located in the outskirts of the small town Oliva being positioned further from the beach and closer to a bigger residential and urban area.

3.4.5 Windguru - Surf school "GandiaSurf"

On the Czech semi-commercial web page `www.windguru.cz` two weather stations further northward on the beach could be located. These stations measure with a temporal resolution of 10 minutes apart from occasional interruptions or data loss. The data extracted from this particular station [Winb] ranges from 13-05-2018 till 08-09-2018. Before the receipt of the data from AVAMET stated previously these data were the only existent with a higher resolution than 1 day. However, its distance to the examined WWTP amounts to about 18.83 kilometers northward along the coast according to Google Maps' direct distance measurement tool. As the weather station stopped measuring on 8 September 2018, it was necessary to request data from the operator Windguru from another station nearby called "DKPiles", which is also closer to the WWTP. Because Windguru is commercial, the willingness of providing more data for free had its limits which is why the data of "DKPiles" could not be conceived for the entire gas measuring period from 16 July till 15 October 2018. Owing to this reason, apart from being located far further from the WWTP and comprising of a lower temporal resolution, the final decision was made in favor of the AVAMET data from Platja de Pego.

3.4.6 Windguru - Surf school "DKPiles"

For the previously mentioned reasons concerning the initial high resolution meteorological data set of the other station "Gandiasurf" ([Winb]) it was necessary to ask for data from another station nearby [Wina]. The data obtained range from 08-09-2018 till 25-10-2018. The temporally overlapping data of the first few hours on 08-09-2018 are taken from the "GandiaSurf"-data, which generally seem more reliable, especially in terms of temperature patterns. However, the distance to the WWTP amounts to about 8.54 kilometers northward along the coast according to Google Maps' direct distance measurement tool, which is significantly closer as the aforementioned "GandiaSurf"-station.

3.4.7 Project on-site meteorological data

Apart from the aforementioned sources, also proper on-site meteorological data were measured by Carlos and Fernando using the Kestrel mobile weather station (see in subsection 3.1).

4 Results and discussion

In this section, the gas measurement data of both measurement campaigns 2018 and 2019 are going to be analyzed under different aspects and by means of various graphics. Also, the meteorological data will receive special attention, as especially the wind data play a crucial role in this research. Finally, the modeled hydrogen sulfide concentrations are going to be presented and discussed.

4.1 Overview of measurement campaign 2018

4.1.1 Spatial distribution of gas measurements

To start with, the gas measuring results of both odorants H_2S and NH_3 summarized from 16 July till 15 October 2018 are displayed as the 75% quantiles in the following labeled scheme of the WWTP site 47. As for the sample sizes of the distinct measurement periods of 1 up to 14 days, 1 complete day stands for 1440 samples, since one sample per minute was measured, and thus 14 days consist of 20160 samples.

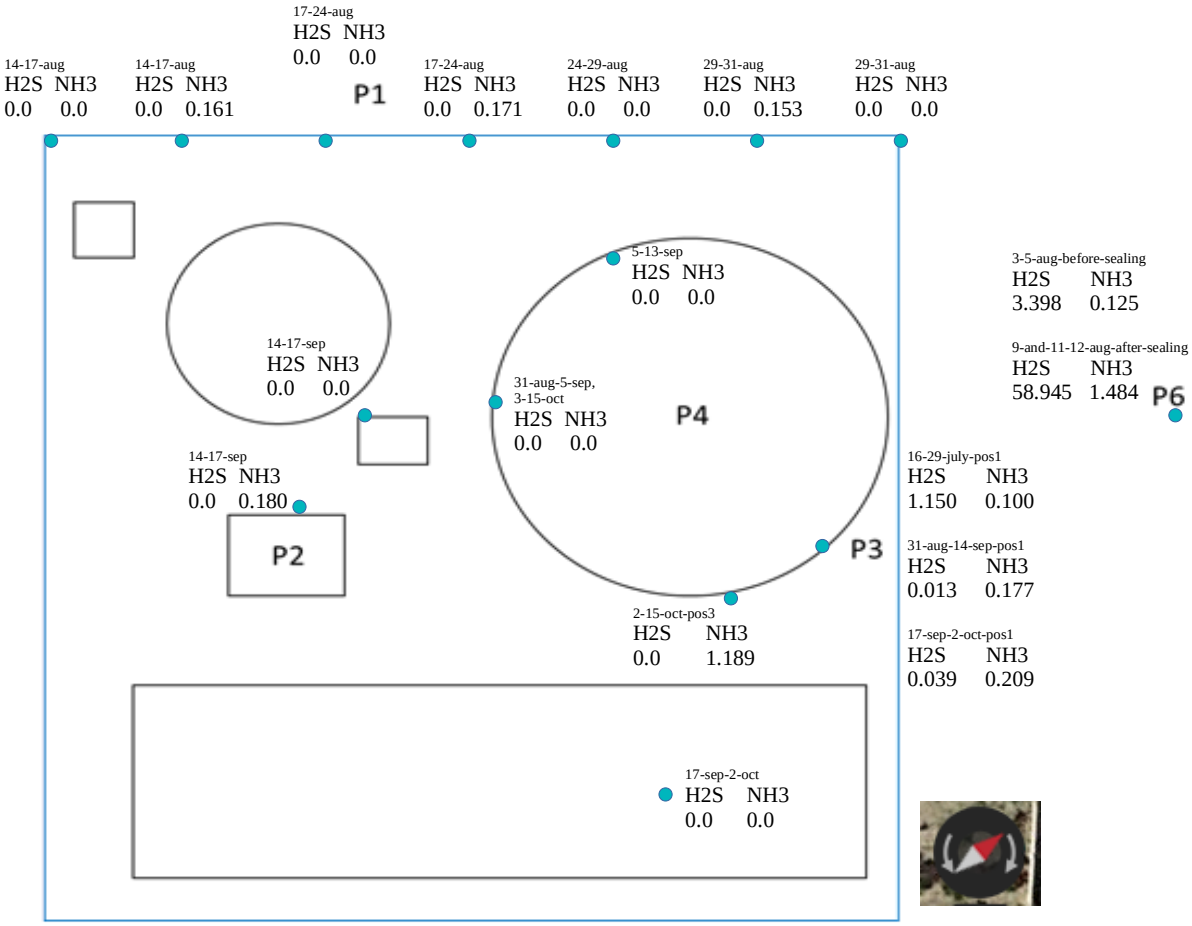

Figure 47: Schematic top view of the WWTP Camping San Fernando in Oliva (Comunidad Valenciana, Spain). Here, measurement periods and the respective 75% quantiles of H_2S and NH_3 are assigned to every measurement spot. The corresponding concentration unit is uniformly given in "parts per million" (ppm).

By and large, it can be concluded that the only relevant odorant emission sources are the canalization entrance into the bioreactor "P3" and possibly the Pumping Station 2 "P6". As for hydrogen sulfide (H_2S), the instruments could practically not detect any non-zero value in any of the other measuring points, whereas ammonia (NH_3) was measured basically entirely below any threshold of perception or health impairment and even below the measurement accuracy of the deployed instrument (see subsection 3.1.1). Since after the sealing no further odor was perceived when carrying out olfactometry measurements next to the sealed well (see figure 48) and due to the danger of damaging the sensors again, no further gas measurements were undertaken at the well assuming that the sealing resolved the possible problem of leaking odorants. As a consequence, the only odorant emission source of the WWTP Camping San Fernando is the canalization entrance "P3".
Following up on this and taking the concentration limits of ammonia (see 2.2.2) and hydrogen sulfide (see 2.2.3) into account, it is obvious that the only pollutant of concern in this project is H_2S. Therefore, the modeling will be based on H_2S concentration data exclusively. Generally, in order to give the concentration values of a pollutant (here H_2S and NH_3) a meaning, it is vital to relate them to their specific perception and toxicity thresholds as they were listed under 2.2.3 and 2.2.2. It is important to note that the 75%-quantile representation does not include isolated peak concentrations which occurred on a regular basis at the canalization entrance (see figure with the ECDFs of H_2S 49). As a matter of course, it is conceivable that with unfortunate wind conditions these maximum gas concentrations could arrive at the nearby housings. This hypothesis will be investigated in the modeling results section 4.7.

Comments
As an aside, regarding the values from Pumping Station 2 measured in the beginning of August, they were measured both before and after sealing the well. During the time after sealing, the sensors got damaged by water intake which led to extremely high and moreover constant concentrations for hours so that these values can just be considered as a hint that high concentrations could accumulate occasionally within the sealed well and thus, technical workers should be careful when opening and entering the well. Besides that, the sensors cannot be installed in a humid place for a long time since a too high amount of condensed water within the tubes can lead to malfunctions, faulty measurements and damage the instruments ultimately as happened in the case of the period between 9 and 12 August 2018.
Apart from that, the fact that two distinct sensor pairs were used simultaneously as of 14 August 2018 until the end of the first measuring campaign can be verified by looking at the results of the 7 spots located at the WWTP site's wall toward the adjacent street, which are not included here since they comprise solely of insignificant values: one pair of sensors was not able to detect anything at all whereas the other one detected either some or continuous non-zero NH_3 values and isolated non-zero H_2S-values. Thus, it was clear that the sensitivity of both sensor pairs were different from each other when measuring in ranges below the measuring instrument accuracies.

4.1.2 Spatial distribution of olfactometry measurements

The olfactory measurements are based on a panelist employing the dynamic olfactometer, the calibration to the panelist of this device and the simultaneous use of a mobile weather station. For more details, see subsection 3.1.
The relation between the olfactometry units for the odor concentration and the odor intensity along with its offensiveness can be understood via table 6. In the same way as done with the gas measurements in figure 47, the panelists' measuring results summarized from 16 July till 15 October 2018 are visualized in the following graph 48.

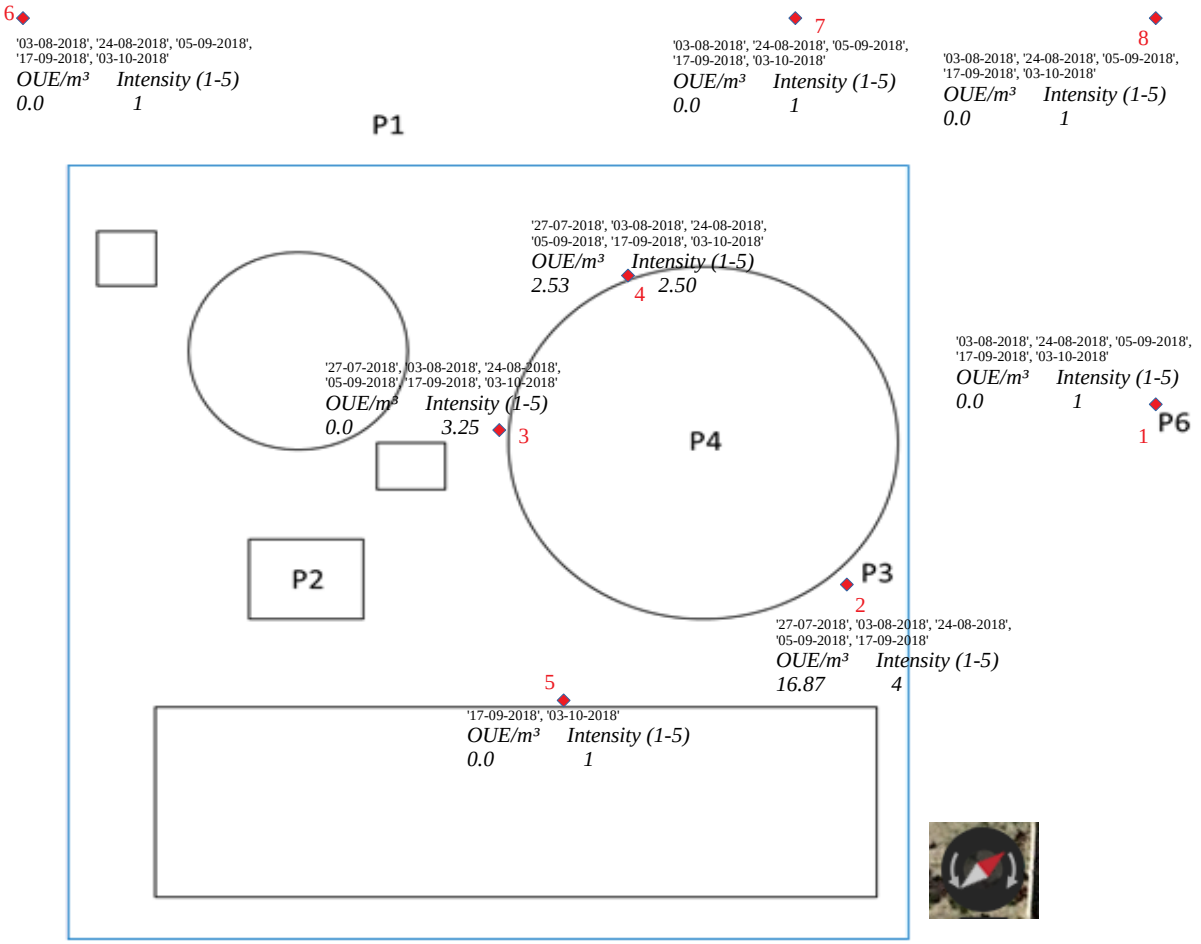

Figure 48: Schematic top view of the WWTP comprising the measurement days and their respective 75% quantiles of odor concentrations given in European Odor Units ($\mathrm{OU_E}$) along with their associated intensity classification, which can be revisited in table 6.

Again, similarly to the gas measurements in graphic 47, the 75% quantiles of the olfactometry measurements are assigned to every measurement point in conjunction with the measuring period. These values in $\mathrm{OU_E/m^3}$ are converted D/T-values in "European Odor Units" per cubic meter. Here, the "dilution threshold", or in short "D/T"-value, depends on the respective panelist's calibration as every individual perceives odors in another way.
Generally speaking, 1 measuring session at 1 point usually stands for about 4, rarely 8 samples, which were taken normally within 10 minutes approximately.
The aim of these olfactometry measurement was to enable the panelists to tell whether or not bad odors existed in each place, and if so, how offensive they were. Besides that, another objective was to strive for finding a reliable correlation between olfactometry and conventional concentration measurements by utilizing simultaneously taken samples in the same place and taking the wind conditions into account. The results related to this attempt are going to be presented in subsection 4.5.

4.2 Empirical cumulative distribution functions (ECDFs) of selected measuring points

In the graphics displayed in the following, the concentrations of the perception thresholds and their associated long-term recommended exposure limits (or long-term RELs, see 2.2.3) of the respective pollutant are depicted, along with the measurement accuracy of each sensor, which can be revisited under 3.1.1. These characteristic values are inlaid into the figures as either horizontal or vertical lines, depending on the axis labeling. Moreover, if the limit values are far outside the range of the measured values, they have been put into the legend with their associated concentration value given in ppm.
Generally, an ECDF contains all measured values ordered by size from the smallest to the highest. The highest value is assigned to 1, the lowest to 0 and all the others are assigned to their associated fraction of the present entirety of recorded values. In this way, quantiles can be read easily and in addition the distribution of the values can be deduced visually.
In the subsequent plots, characteristic quantiles are delineated for simplifying the reading. The relative values from 0 to 1 lie on the ordinate, whereas the concentrations are plotted on the abscissa in parts per million (ppm). With respect to the measuring periods at main emission source during both measuring campaigns 2018 and 2019, the following list registers them ordered by time:

1st period: 16 - 29 July 2018

2nd period: 31 August - 14 September 2018

3rd period: 17 September - 2 October 2018

4th period: 3 April - 3 June 2019

4.2.1 Main emission source: Bioreactor entrance

In this subsection, the statistical empirical distributions of odorant concentrations are plotted in the unit of parts per million (ppm) on the abscissa, whereas the quantiles from 0 to 1 are displayed on the ordinate. As far as the measuring period is concerned, in figures 49 and 50 all periods are included. These periods have been listed under 4.2). Also, it must be mentioned that zero-valued concentrations were filtered out of the data previously, as they comprised in some cases a considerable percentage of the provided data.

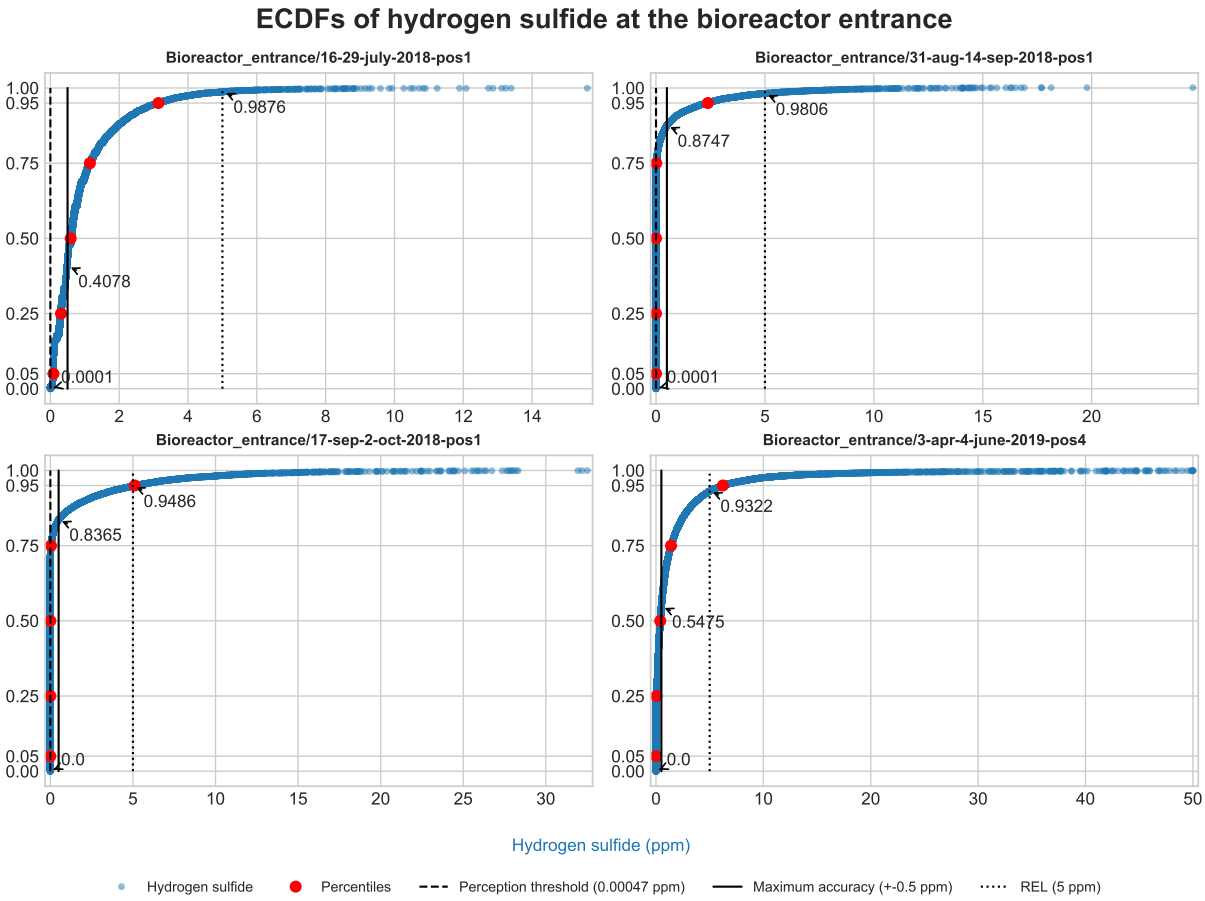

Figure 49: ECDFs of hydrogen sulfide concentrations given in ppm at the main emission source during all 4 relevant measuring periods. As for the legend, particular concentration limits in ppm are embedded into the graphic; namely the recommended long-term exposure limit (or long-term REL) and perception threshold of the odorant, mentioned in subsection 2.2.3, and the maximum accuracy of the deployed measuring instruments explained in 3.1.1.

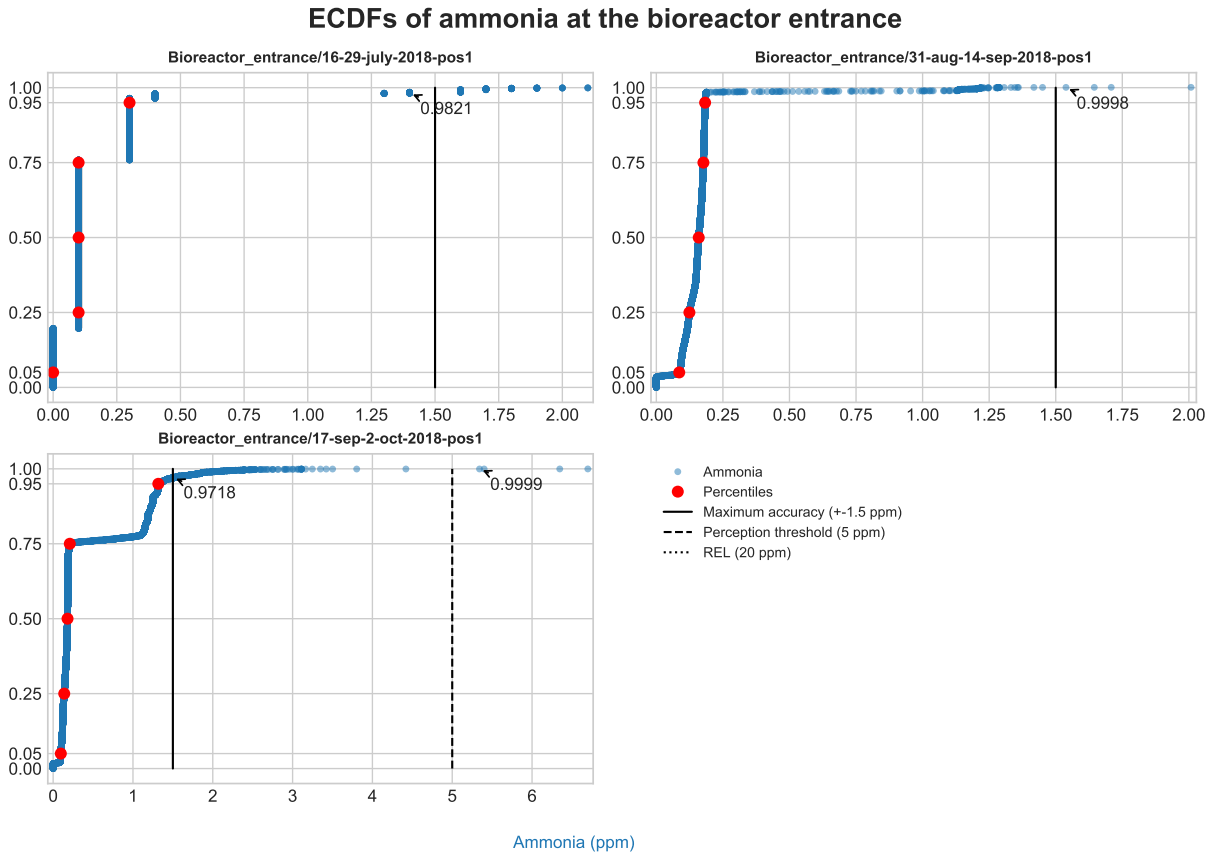

Figure 50: ECDFs of ammonia concentrations in ppm at the main emission source during all 3 relevant measurement periods of the first measuring campaign 2018. As opposed to hydrogen sulfide, it was not measured anymore during the second campaign. Regarding the legend, particular concentration limits in ppm are embedded into the graphic; namely the recommended long-term exposure limit (or long term-REL) and perception threshold of the odorant, mentioned in subsection 2.2.2, and the maximum accuracy of the deployed measuring instruments explained in 3.1.1.

From the ECDF subplots of figure 50, one can derive that ammonia can be discarded as an potential odorant in this investigation which could play a role in the odor nuisance in the vicinity of the WWTP Camping San Fernando. At almost any time, despite looking at the main emission source data, its concentration remained below the perception limit of 5 ppm, and apart from this even below the measurement accuracy of the deployed instrument.
On the other hand, the data associated with hydrogen sulfide shows clearly that almost all data measured at the canalization entrance exceeds the perception limit of only 0.00047 ppm, and also the measuring accuracy of 0.5 ppm (see 3.1.1). Thus, H_2S will be considered as the remaining odorant in question for this entire investigation project. With respect to the recommended long-term exposure limit (or long-term REL) of 5 ppm (see 19), this was exceeded regularly by the emission peaks which comprises in each of the data sets around 5 percent of the data, depending on the season and data set. Following up on that, one can estimate that the possibility of causing odor nuisance in the surroundings under unfortunate meteorological conditions is given. Moreover, regarding physical health problems, it seems rather unlikely that a few occasional peaks above the long-term REL of 5 ppm measured directly at the main emission source can lead to extended exposure to concentrations above this hazardous limit value as well in a distance of more than 40 meters, i.e. where the residential dwellings are situated.

Apart from that, it appears plausible that workers on-site, which stay close at a short distance of a few meters to the main emission source, could be intermittently affected by higher concentrations dangerous to health. Notwithstanding, this needs to be proven by the AERMOD model whose results are going to be presented later on in subsection 4.7.
Albeit getting direct physical health problems through inhalation of concentrations above the long-term REL of 5 ppm (defined in 19) seems unlikely, the psychological health afflicted by odor nuisance at lower, but still perceptible concentrations, cannot be underestimated nor neglected. As a consequence, it is crucial to estimate the average frequency of incidents related to odor nuisance at the nearby dwellings, which can be found in detail in subsection 4.7.

4.2.2 Pump Station 2

Next, the second potential emission source was examined both before and after its sealing. This subsection is about the pumping well of Pump Station 2 located around 65 meters beeline toward the seashore from the on-site canalization entrance into the bioreactor of the WWTP. While the distribution before the sealing, depicted in graph 51 behaved similarly to those seen in 49, the values after the sealing in figure 52 show extremely high and even constant concentrations, which demonstrate the damaging process of the sensors during that measuring period. The tubes were submerged into the sealed well, and thus too much condensed water entered the sensor tubes which finally broke them. As a consequence, the well was not investigated further apart from outer olfactometry measurements which corroborated the functioning of the sealing, i.e. that no directly perceptible odor could be smelled outside at the adjacent parking lot.

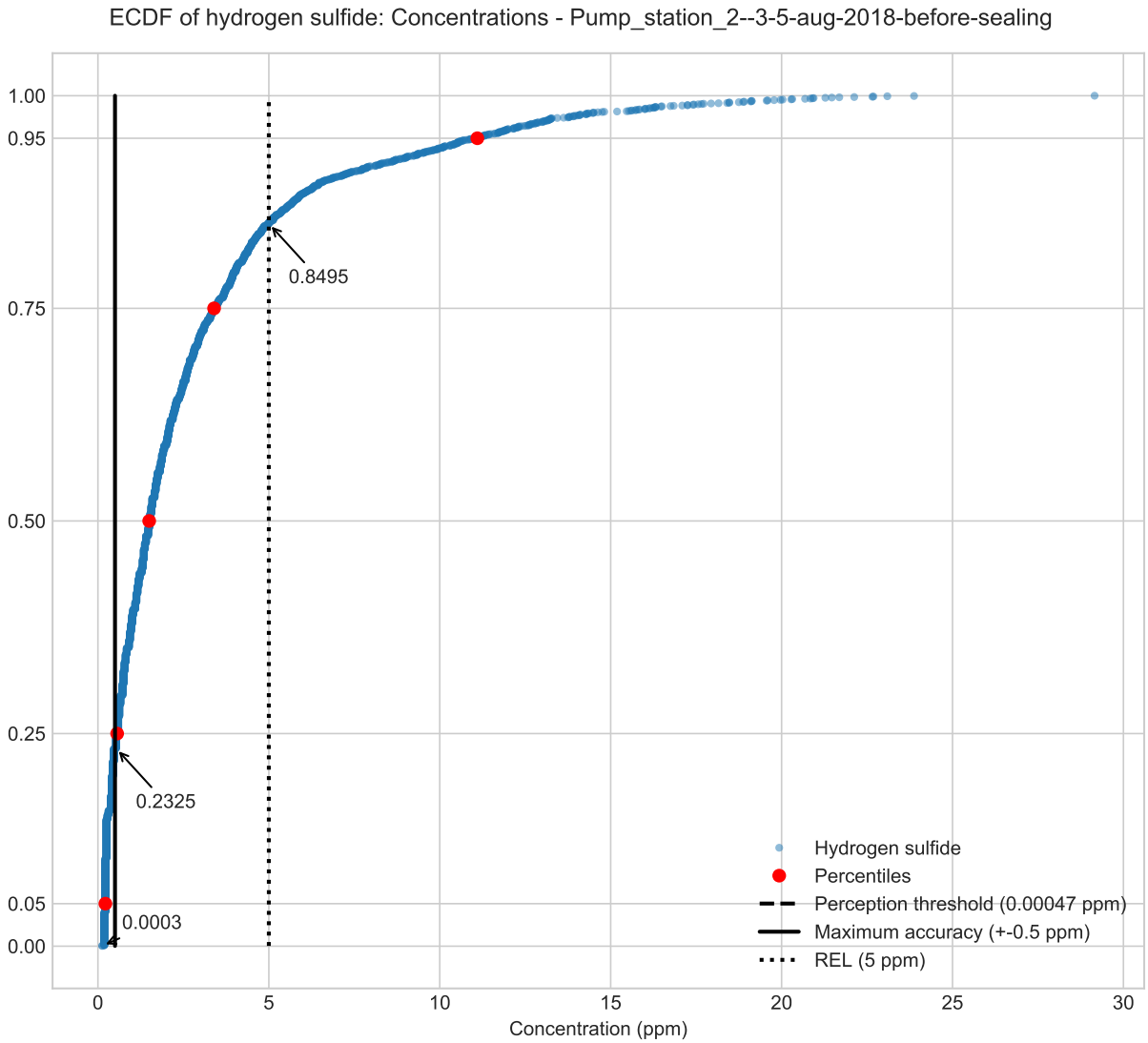

Figure 51: ECDF of hydrogen sulfide concentrations in ppm at the grid which formerly covered the well of Pumping Station 2 before it was finally sealed. The associated period was from 3 till 5 August 2018. Concerning the legend, particular concentration limits in ppm are embedded into the graphic; namely the recommended long-term exposure limit (or long-term REL) and perception threshold of the odorant, mentioned in subsection 2.2.3, and the maximum accuracy of the deployed measuring instruments explained in 3.1.1.

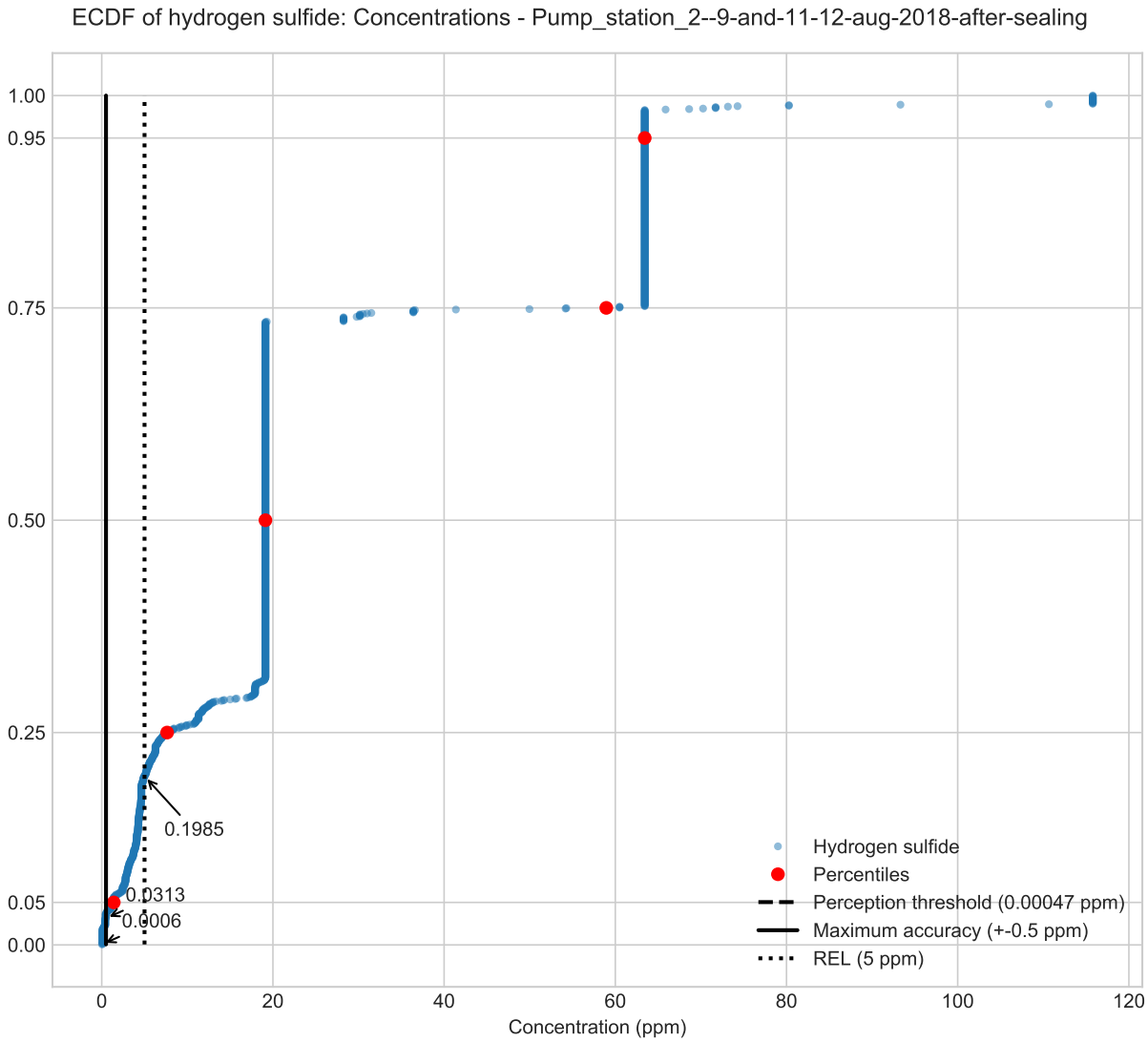

Figure 52: ECDF of hydrogen sulfide concentrations in ppm after sealing the pumping well. The measuring period was from 9 to 12 August 2018. As for the legend, particular concentration limits in ppm are embedded into the graphic; namely the recommended long-term exposure limit (or long-term REL) and perception threshold of the odorant, mentioned in subsection 2.2.3, and the maximum accuracy of the deployed measuring instruments explained in 3.1.1.

Hereinafter, these peculiar measuring results from the well of Pump Station 2 are going to be analyzed.

Measuring period before sealing: 3-5 August 2018

Before the sealing of the well on 5 August 2018, it was solely covered by a coarse grid through which evidently gases were able to leak, as it can be seen in photo 14. After the sealing, the well entrance looks from outside as depicted in figure 16. The difference to the main emission source of the WWTP at its canalization entrance was that the inlet pipes were located right above the open water surface from where the turbulent gas masses could propagate readily into the surrounding air, whereas within

the well of about 3 meter depth the contaminated air parcels needed to rise to the well top first to be taken up by surface-near wind. As hydrogen sulfide is heavier than air, it rather accumulates at the well ground, while ammonia is lighter than air and thus would rise to the well top over time.
Nevertheless, ammonia concentrations remained below the perception threshold again, wherefore the graph will not be included here as it only confirms the aforementioned statement that it does not contribute significantly to the odor nuisance in the surroundings.
On the contrary, the H_2S concentrations are located almost completely above the perception threshold. Moreover, the quantile between approximately 85% and 100% exceeds even the long-term REL of 5 ppm, which is defined in 19.
Consequently, despite being heavier than air and thus trapped inside the well, it was of concern to seal it in order to safeguard that the well cannot contribute to public odor nuisance.

Measuring period after sealing: 9, 11 and 12 August 2018
After the sealing operation, the measurements were difficult to accomplish since the sensor tubes needed to be hung inside the sealed well. Then, in the course of the measurement period from 9 to 12 August 2018, the sensors suffered moisture damage along with the incidence of data loss. As a result, the values were extremely high and for many hours even constant (see figure 52).

Thus, these values cannot be taken seriously, but nevertheless there are two useful outcomes to state:
Firstly, when sealing the well high concentrations could occur due to enhanced gas accumulation, which in turn needs to be taken into account when opening the well, e.g. for maintenance works. Secondly, the tubes should be installed in a way that prevents interior accumulation of condensed water which could consequently be sucked into the tube until it arrives at the sensors. To prevent sensor damage as it happened during the measurements of the data associated to figure 52, the tubes should face downward to make use of gravity working against sucking in water drops. In addition, moist environments without proper ventilation should be avoided, if possible.

4.3 Temporal patterns at the main emission source

In this subsection, the chronological sequences of both odorant concentrations are displayed in various ways in order to give another perspective on characteristic patterns within the data. To begin with, in figure 53 hydrogen sulfide concentrations were mostly greater than the perception threshold of 0.00047 ppm (see table 1) and sometimes even above the long-term REL limit of 5 ppm (defined under 19), as it was already confirmed via the ECDF 49. In addition, this type of plot purports that there must be some daily patterns hidden in the data, which will be revealed later in subsection 4.3.1 and 4.3.2. It seems that there are characteristic peaks produced within a certain frequency range of several minutes, and the height of these peaks also changes with a lower frequency at daily scale. With respect to the high frequency periodicity, this will be discussed more thoroughly by means of graphics 55 and 56.

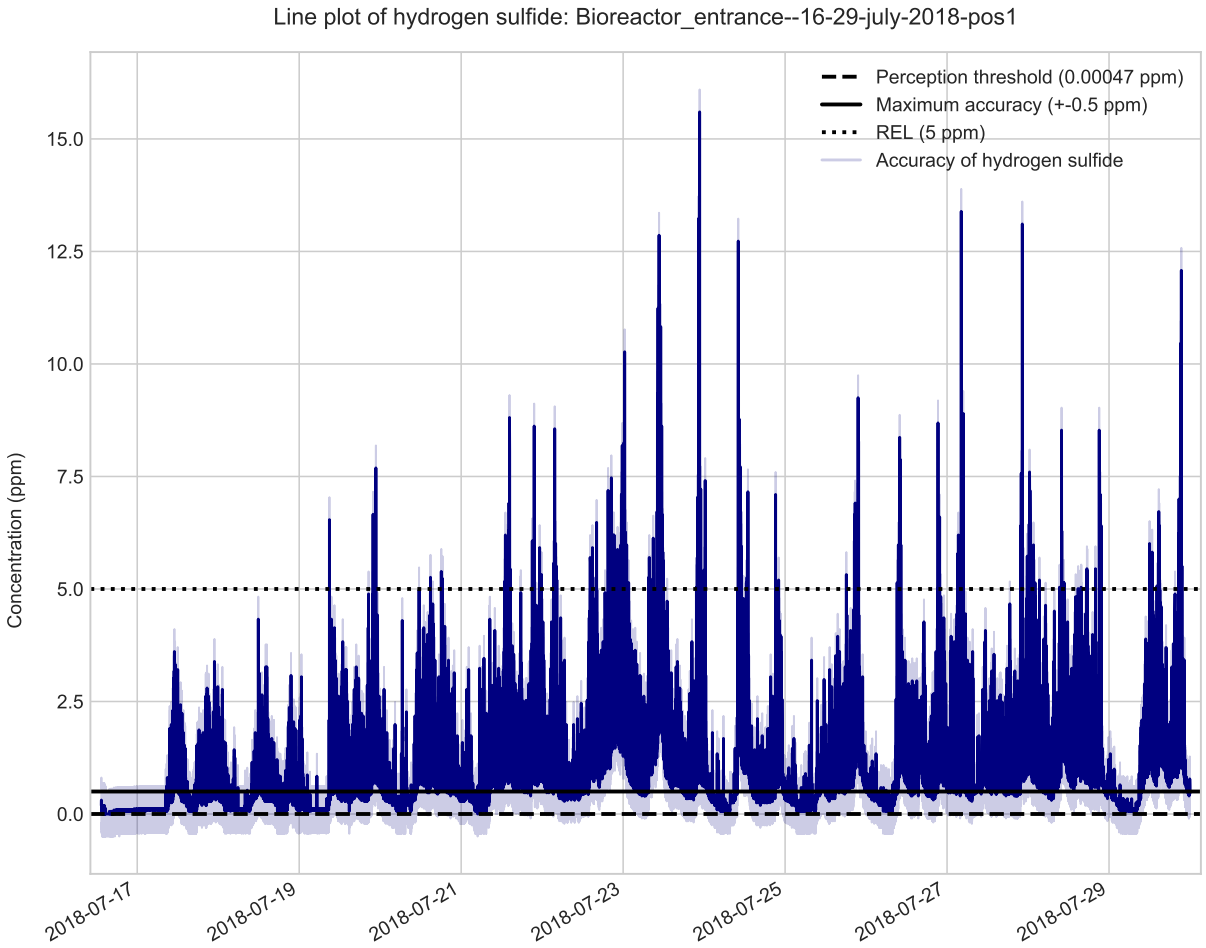

Figure 53: This line plot displays the temporal changes of H_2S concentrations in ppm measured at the main emission source at the canalization entrance in ppm. The temporal resolution was 1 minute apart from exceptional malfunctions of the measurement equipment (see 3.1.1), when either less data were recorded or even data loss occurred. With regard to the legend, particular concentration limits in ppm are embedded into the graphic; namely the recommended long-term exposure limit (or long-term REL) and perception threshold of the odorant, mentioned in subsection 2.2.3, and the maximum accuracy of the deployed measuring instruments explained in 3.1.1. Also, the measuring accuracy band associated with each value is included in transparent blue.

Following up on what was mentioned before about ammonia (see fig. 50), in the line plot 54, which shows the chronological sequence of its concentrations in ppm from 16 till 29 July 2019, it can be acknowledged again that ammonia does not play a role in terms of odor generation at the WWTP. As one can deduce from graph 54, the measurement accuracy of the apparatus of at least 1.5 ppm leads to uncertainties in the low concentration measurements, that the ammonia concentrations could very well be even negative, which does not make sense. Moreover, the measured values lie clearly below the perception threshold of 5 ppm and even further below the recommended long-term exposure limit (or long-term REL) of 20 ppm, which is quoted from the official status explained in 18. Thus, it can be said in advance that the ammonia measurements could not be considered for modeling. For a further explanation on the measurement accuracy, see 3.1.1.

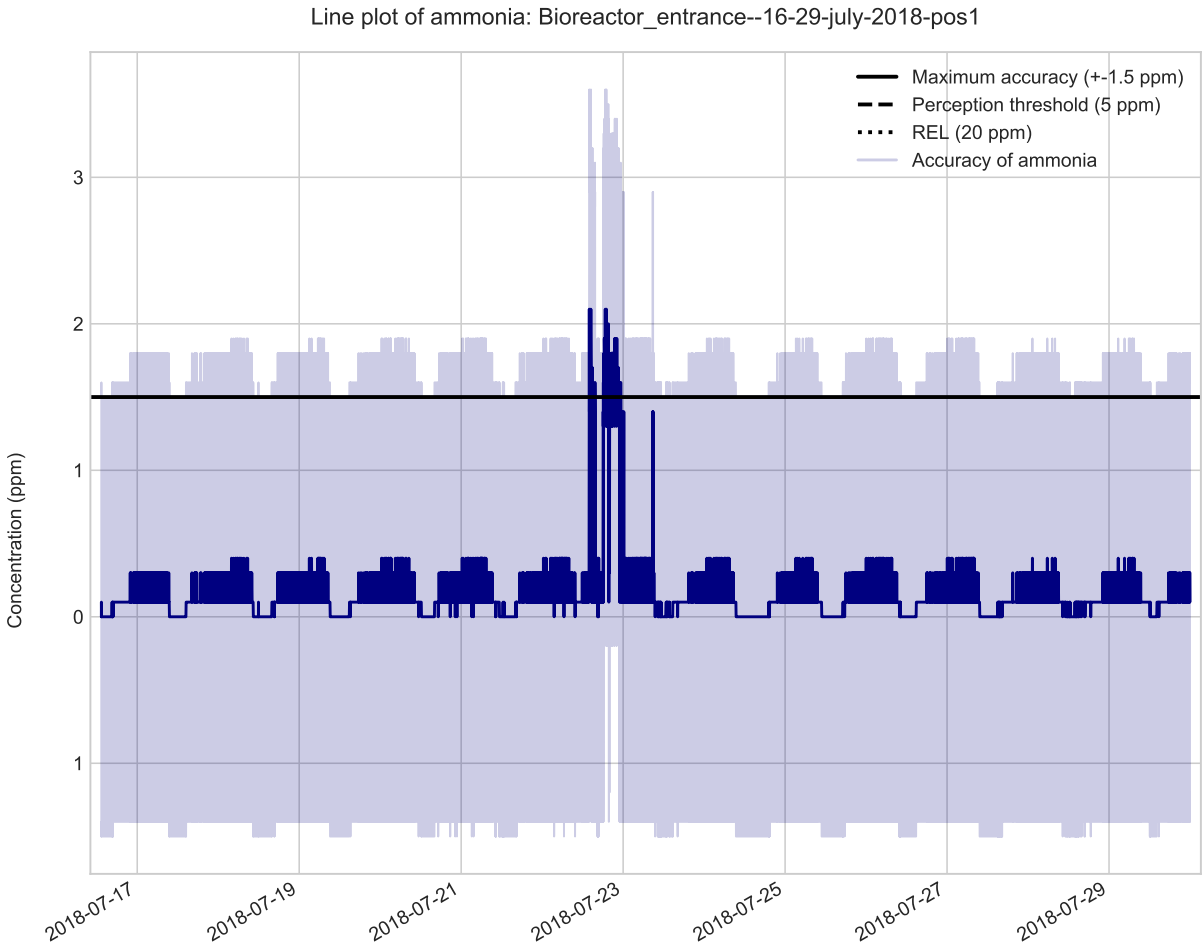

Figure 54: Similarly to figure 53, the chronological sequence of ammonia concentrations in ppm is shown. With respect to the legend, particular concentration limits in ppm are embedded into the graphic; namely the recommended long-term exposure limit (or long-term REL) and perception threshold of the odorant, mentioned in subsection 2.2.2, and the maximum accuracy of the deployed measuring instruments explained in 3.1.1. What is more, the measuring accuracy band associated with each value is plotted in transparent blue.

As an aside, the choice fell on the measuring period from 16 to 29 July 2018 since the patterns were similar to those registered in the second period at the canalization entrance from 31 August to 14 September 2018.
Furthermore, the concentration measurements of ammonia seem rather quantized than continuous. That is presumably owing to the fact that the measured values, if considered valid as they are well below the instrument accuracy (see 3.1.1), were integer multiples of some minimum value which could still be resolved by the instrument.
Next, in order to understand the intermittency of the H_2S peaks alluded before, one needs to take a closer look at the pumping rhythm of the mentioned Pumping Station 2, which is responsible for these characteristic odorant peaks. Those are caused by the intermittent sewage outflow of the canalization entrance into the bioreactor and their frequency could be derived from the time deltas extracted between all adjacent maxima within the data sets of certain periods (see following figures 55 and 56).

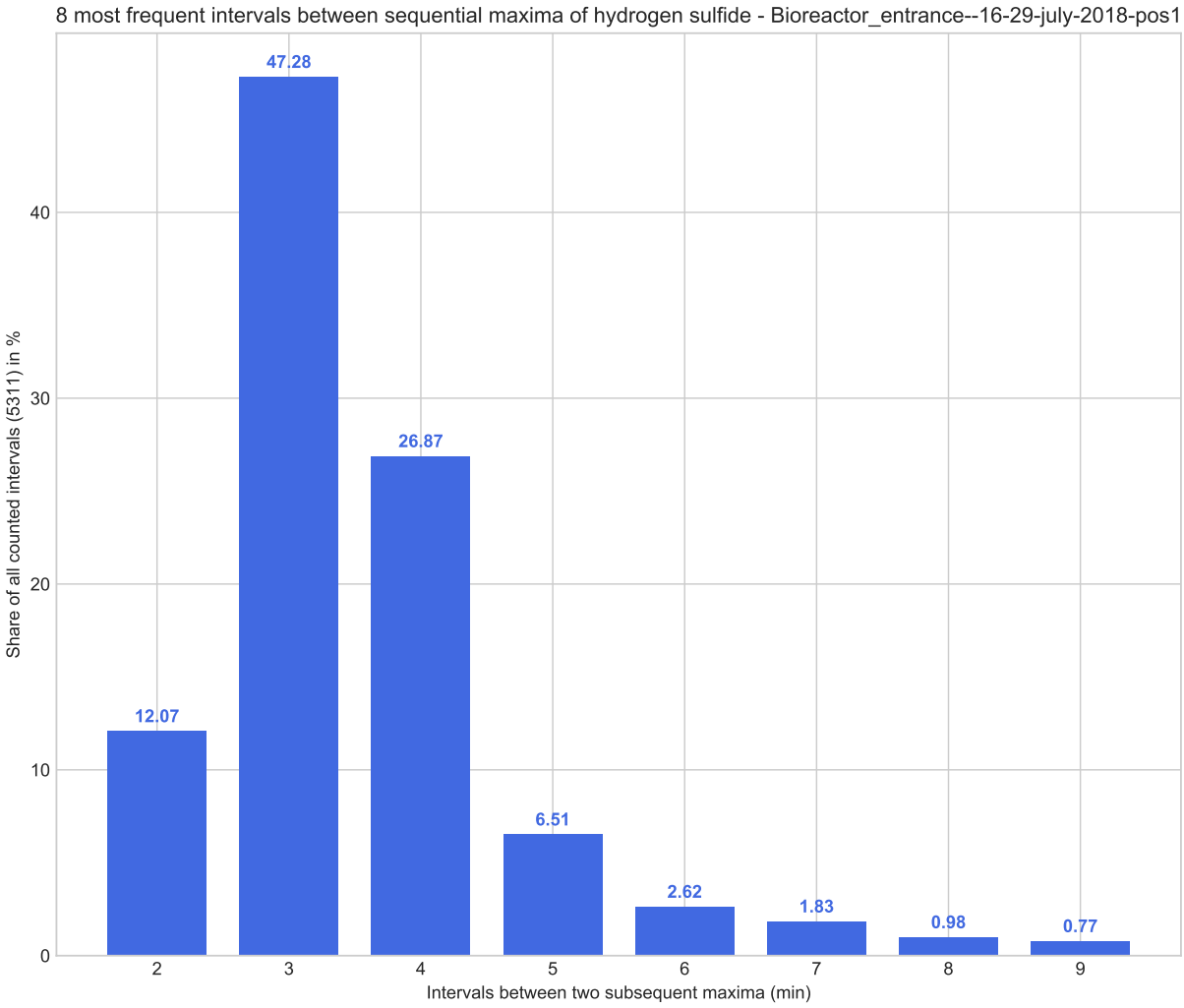

Figure 55: Bar chart of the 8 most frequent pumping frequencies during the high summer measurement period from 16 till 29 July 2018. The frequencies are displayed on the horizontal axis as intervals between two successive concentration maxima in minutes. On the vertical axis, the share of all counted intervals are given in percent. Besides, the total number of considered intervals is provided in parenthesis within the y-axis label.

As can be inferred from comparing the results of the bar charts 55 and 56, the average pumping frequency was higher during the high summer season and dropped from around every 3 minutes in July to a more uniform distribution between 3 and 10 minutes in September, even though the principal frequency remained 3 minutes. It happens due to the higher volume flow during the high summer seasons which makes the pumping well fill up more quickly. This in turn triggers the pump to transport the accumulated sewage into the bioreactor of the WWTP, which consequently causes the characteristic H_2S peaks (see fig. 53) at the canalization entrance, i.e. the main emission source of the plant.

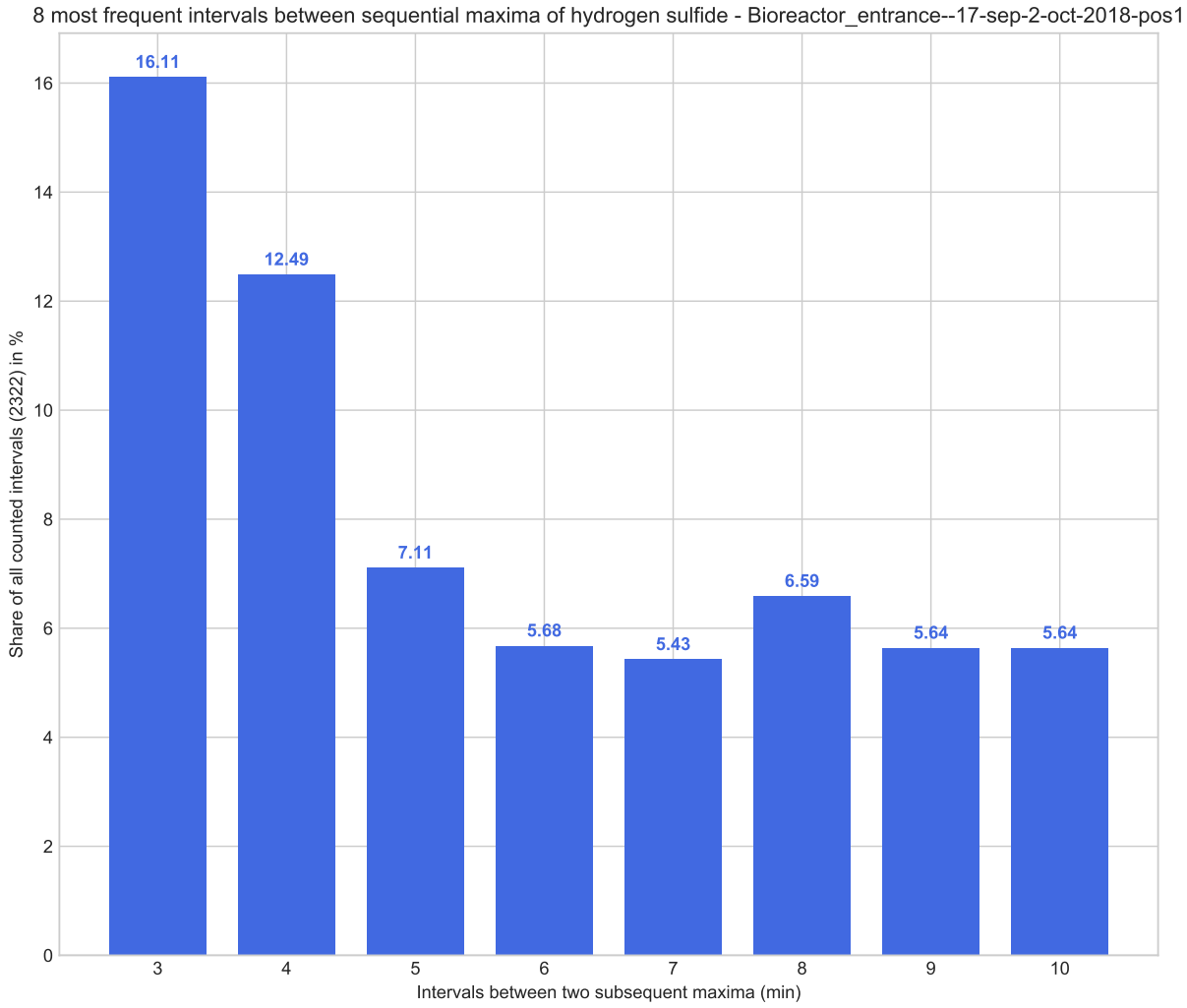

Figure 56: Bar plot of the 8 most frequent pumping frequencies during the beginning of autumn from period from 17 September till 2 October 2018. The frequencies are displayed on the horizontal axis as intervals between two successive concentration maxima in minutes. On the vertical axis, the share of all counted intervals are given in percent. Besides, the total number of considered intervals is provided in parenthesis within the y-axis label.

Hereafter, the daily patterns of both odorants are going to be examined more thoroughly with the aid of showing their daily overlaid aggregated hourly means in 4.3.1 and 4.3.2.

4.3.1 Ammonia

As a side note, it shall be mentioned that ammonia was not measured during the second measuring campaign anymore, since it was already evident after the data analysis of the first campaign, that it does not contribute to the odor nuisance. Thus, the graphics consisting of NH_3 data do not comprise of the period from 3 April to 3 June 2019, as opposed to those belonging to hydrogen sulfide. Next, yet in spite of the comments on the validity of the ammonia concentration values, the descriptive summary statistics related to NH_3 measurements will be presented in the following to make the picture complete.
To start with, graphic 57 portrays the moving hourly averages of every day during the first measuring

period from 16 to 29 July (compare 4.2) overlaid on a daily basis. As can be derived from the figure, except for the 22 July 2018, the pattern followed a stable daily rhythm far below the measurement accuracy (see 3.1.1) and even further below perception and health hazard limits.

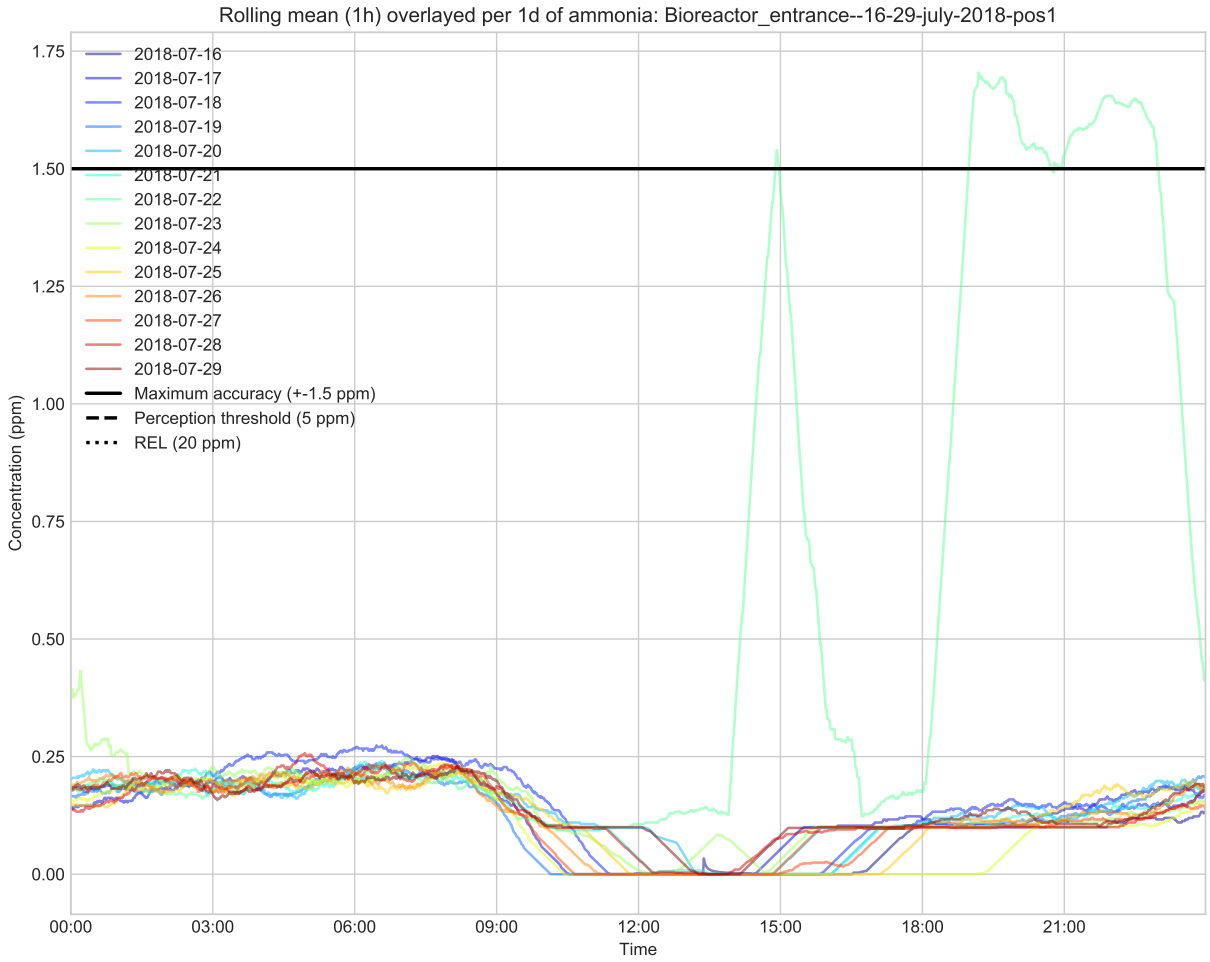

Figure 57: Chronological sequence of moving hourly means of ammonia concentrations in ppm overlaid on a daily basis. With regard to the legend, particular concentration limits in ppm are embedded into the graphic; namely the recommended long-term exposure limit (or long-term REL) and perception threshold of the odorant, mentioned in subsection 2.2.2, and the maximum accuracy of the deployed measuring instruments explained in 3.1.1.

Next, the figure 58 depicts the findings of the above rolling mean lineplot 57 in another way: Here in figure 58, the averages were made over every hourly time step from 0 to 23 o'clock during a 24-hour day over all days of each period during the entire project. More precisely explained, if one picks the value at noon, it represents the mean over all daily values at noon of the entire sample. Of course, before carrying out the final averaging computation, each day needed to be averaged previously on an hourly basis as the values were measured with a resolution of once per minute.

From the behavior of the 95% confidence interval (CI) in graph 58 it can be verified that generally the values were quite uniform during the first 10 hours of the day during the measuring period from 16 till 29 July 2018. The same applies to the last 9 hours of the day during the period from 31 August to 14 September. By contrast, the outliers on 22 July 2019, which are readily visible in figure 57 are responsible for the broadening of the 95%-CI during the same day times in the corresponding

subplot. As for the rest, the values showed a greater variance. Moreover, in figure 58 the subplot at the bottom right called "Bioreactor entrance position 1 complete" depicts the totality of the ammonia concentrations during the first measuring campaign obtained at the main emission source. This graphic serves for certifying the aforementioned interpretations, as they are in a broader sense generally applicable to all 2-week periods of $\mathrm{NH_3}$ measurements carried out in 2018.
In order to ensure that during the periods apart from 16 to 29 July 2018 there were no important peaks obscured by computing the means, the maxima of all periods are illustrated in the subplots of figure 59. It can be derived that apart from one exceptional maximum at 11 o'clock during the period in the end of September 2018, none of the values exceeded the perception threshold of 5 ppm, and almost half of the maxima did not even surpass the measurement accuracy of the deployed Dräger Polytron 7000 measuring instrument (see 3.1.1).

To sum up, ammonia concentrations remained generally below any threshold or limit concentration, even below the measurement instrument accuracy, which reinforces the inference that ammonia cannot be considered relevant in resolving the question whether or not the nearby residents can be objectively affected by odor nuisance. In addition, it shall be mentioned for the sake of completeness, that at several other gas measuring points, such as the site's surrounding wall and the worker's control house, daily ammonia patterns were recorded, although their concentration ranges lied even further below the measurement accuracy, which is why they won't be discussed here.
Now, in the next subsection, the results of the important pollutant $\mathrm{H_2S}$ will be further examined, which are quite distinct to the just discussed results concerning ammonia concentrations.

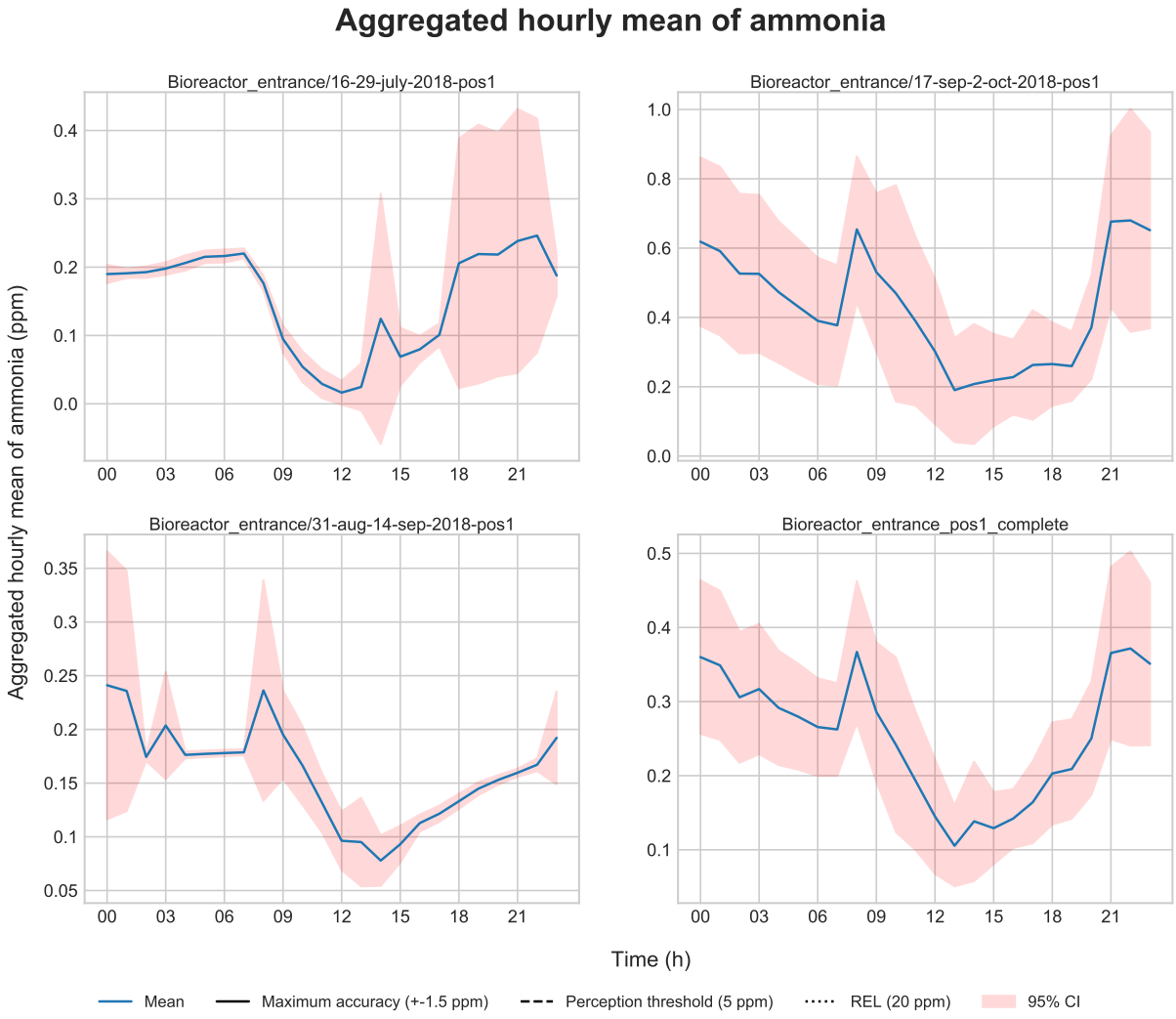

Figure 58: Aggregated hourly means of ammonia concentrations in ppm during the first measurement campaign of 2018 at the main emission source. Regarding the legend, particular concentration limits in ppm are embedded into the graphic; namely the recommended long-term exposure limit (or long-term REL) and perception threshold of the odorant, mentioned in subsection 2.2.2, and the maximum accuracy of the deployed measuring instruments explained in 3.1.1.

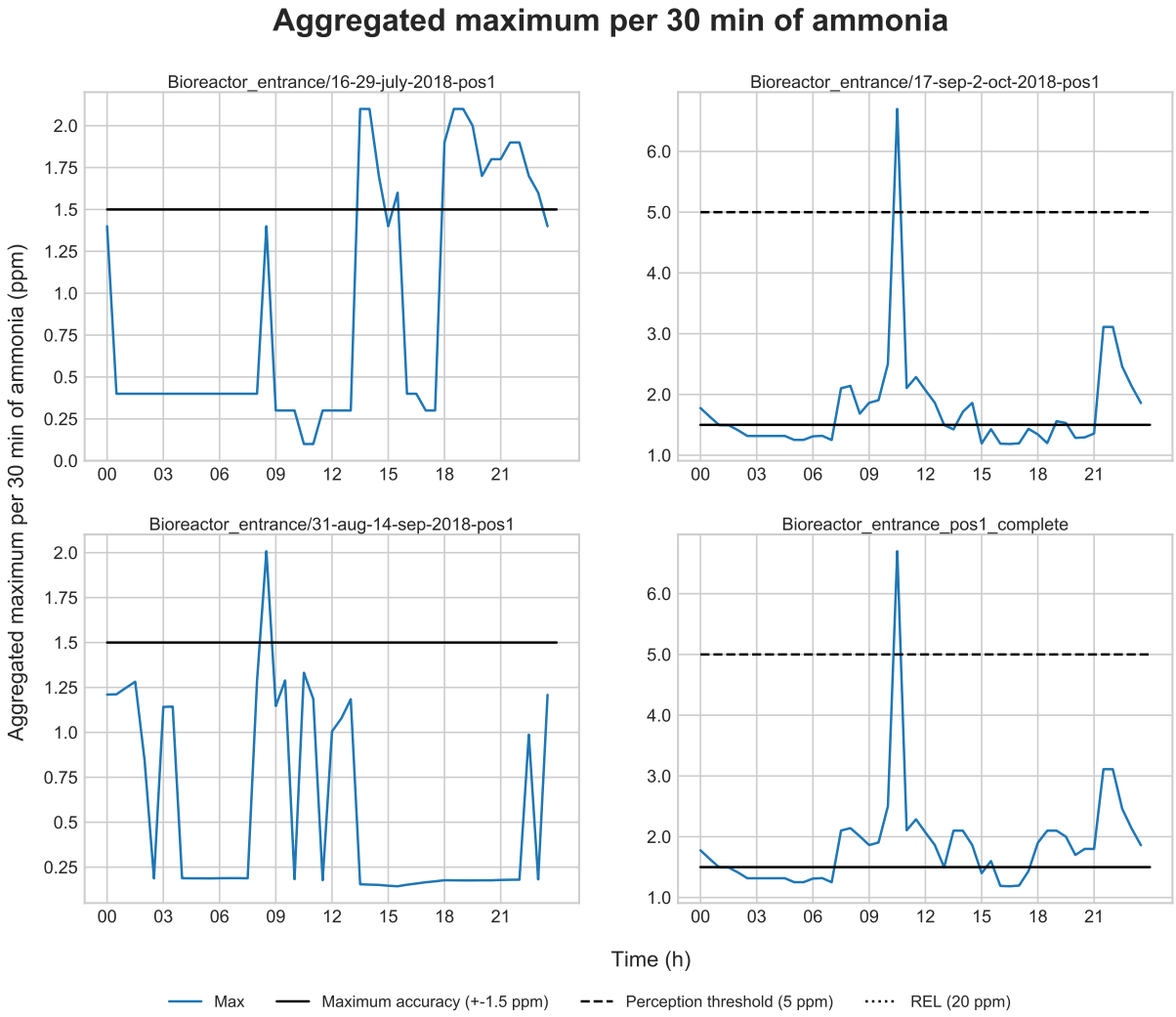

Figure 59: Aggregated half-hourly maxima of ammonia concentrations in ppm during the first measurement campaign of 2018 at the main emission source. Concerning the legend, particular concentration limits in ppm are embedded into the graphic; namely the recommended long-term exposure limit (or long-term REL) and perception threshold of the odorant, mentioned in subsection 2.2.2, and the maximum accuracy of the deployed measuring instruments explained in 3.1.1.

4.3.2 Hydrogen sulfide

Following the structure given in the previous subsection 4.3.1 covering the daily patterns of ammonia concentrations at the main emission source, the results related to hydrogen sulfide are going to be presented similarly from here.
Initially, the figure 60 displays the moving hourly averages of every day during the first measuring period (see 4.2) overlaid on a daily basis. Apart from the already discussed threshold exceedances, it can be deduced already that on average concentrations peak in the morning, the evening and the early night.

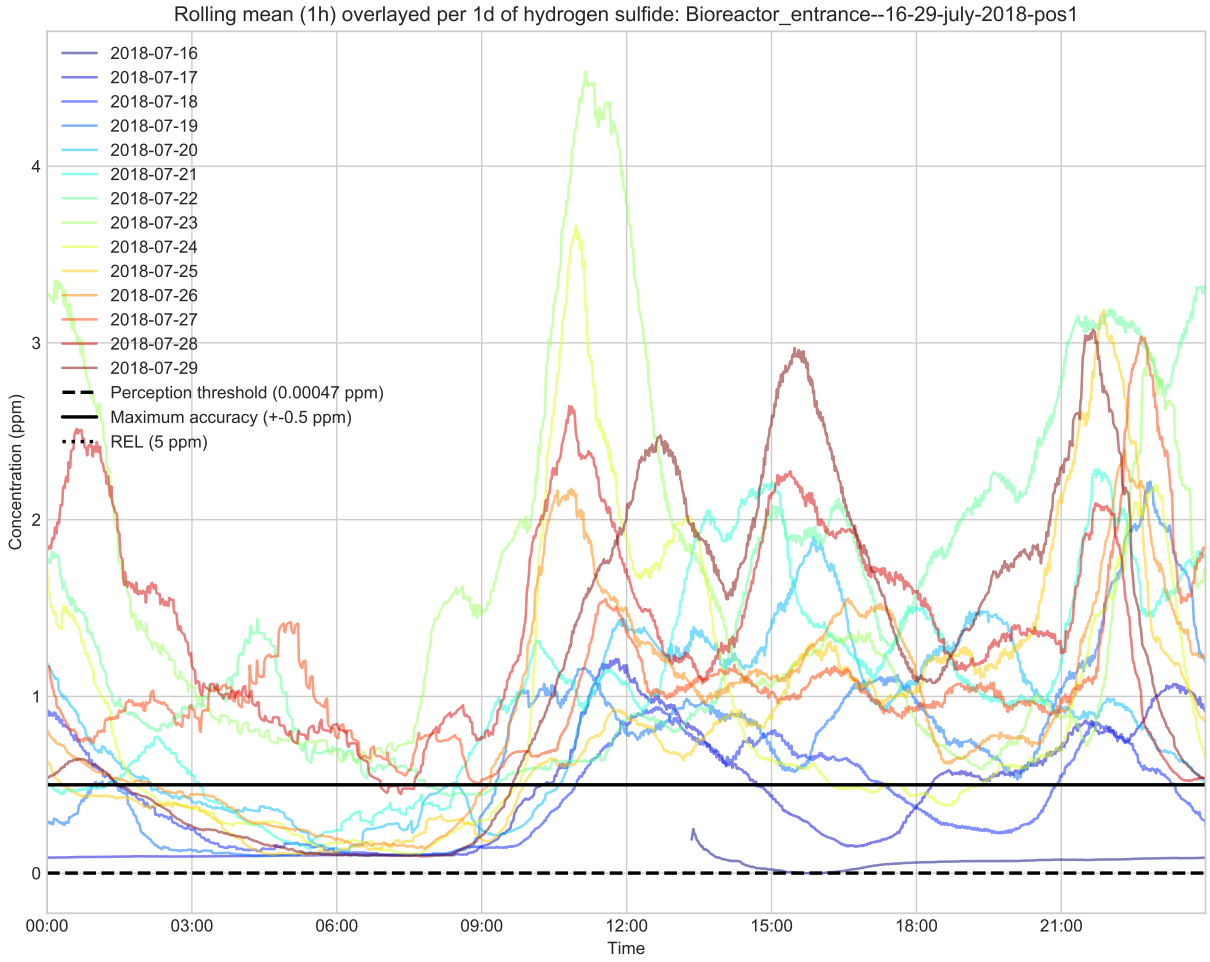

Figure 60: Line plot of moving hourly means of hydrogen sulfide concentrations in ppm overlaid on a daily basis. With respect to the legend, particular concentration limits in ppm are embedded into the graphic; namely the recommended long-term exposure limit (or long-term REL) and perception threshold of the odorant, mentioned in subsection 2.2.3, and the maximum accuracy of the deployed measuring instruments explained in 3.1.1.

This conclusion will be substantiated by means of the graph 61, where the high frequency fluctuations are averaged out and represented via a 95% confidence interval, similarly to the previously discussed figure 58 related to ammonia concentrations. As a quick inference, one could argue that when the local residents are either sleeping at night or are out during the day, concentrations go down, especially at night. Then, when they start the day in the morning, or come home in the evening, the highest peaks can be expected.
More explicitly, in the course of the night, from sunset to sunrise, the curve tends toward its global minimum. When the sun rises, concentrations also start to rise toward the first global maximum during the day before noon. Then, during the afternoon, the concentration shows two dips with a smaller peak around 15 o'clock, and finally concentration levels ascend to the second global maximum at about 21 o'clock on average, before it drops again throughout the nighttime.
Following up on this, graph 61 illustrates the mean concentrations of hydrogen sulfide considering all measurement periods (see 4.2) during the first and second measuring campaign in 2018 and 2019 obtained from the main emission source.

It can be noticed that the pattern during the first measurement campaign does barely change, while from 3 April till 3 June 2019 the second global maximum in the evening seems to be displaced to the early night. What is more, the data give evidence that the averaged non-zero H_2S concentrations at the emission source are always above the perception threshold of 0.00047 ppm (see table 1), and only during some hours of the night below the highest measurement accuracy (see 3.1.1) of 0.5 ppm; during the first measurement campaign. All of this is opposed to what could be derived from the ammonia data.
On the other hand, due to displaying pure mean values, the frequent peaks transcending the long-term REL of 5 ppm (see 19) were averaged out. Consequently, the graphs based on hourly averages 60 and 61 serve rather for a general pattern examination. To cope with this, apart from the means for all measuring periods at the emission source displayed in fig. 61, the half-hourly maxima are shown in fig. 62. There, one can see that the maxima lie almost entirely above the recommended long-term exposure limit (or long-term REL) of 5 ppm, which is defined in 19. In addition, it can be deduced that high emission peaks can virtually occur at any time of the day, even though the main daily patterns discussed based on the mean concentrations are still preserved to a great extent. These extreme events are of great interest concerning the worst case scenario as a high initial odorant emission rate at the source clearly plays an important role in the probability that perceptible concentrations arrive at the dwellings. Of course, for this to happen, more variables need to play their role also, but a noticeably high initial concentration is essential.
If all absolute non-aggregated values are of interest, the reader might want to take a look at the graphics 53 and 49. As a matter of fact, the absolute values are paramount for the creation of worst case scenarios, whereas the mean values are better when examining periodic patterns. As for giving the patterns a meaning, when assuming a short transportation time of recently produced sewage by the households to the nearby bioreactor, it seems logical to deduce a correlation to the commonplace working hours, as it was mentioned before. Following up on this, generally people are at home in the morning preparing to leave for work and in the evening they return. Because the highest concentration peaks observed occur around 10 and 21 o'clock, along with the constantly declining curve in the course of the night, the previously elaborated inference appears sensible.

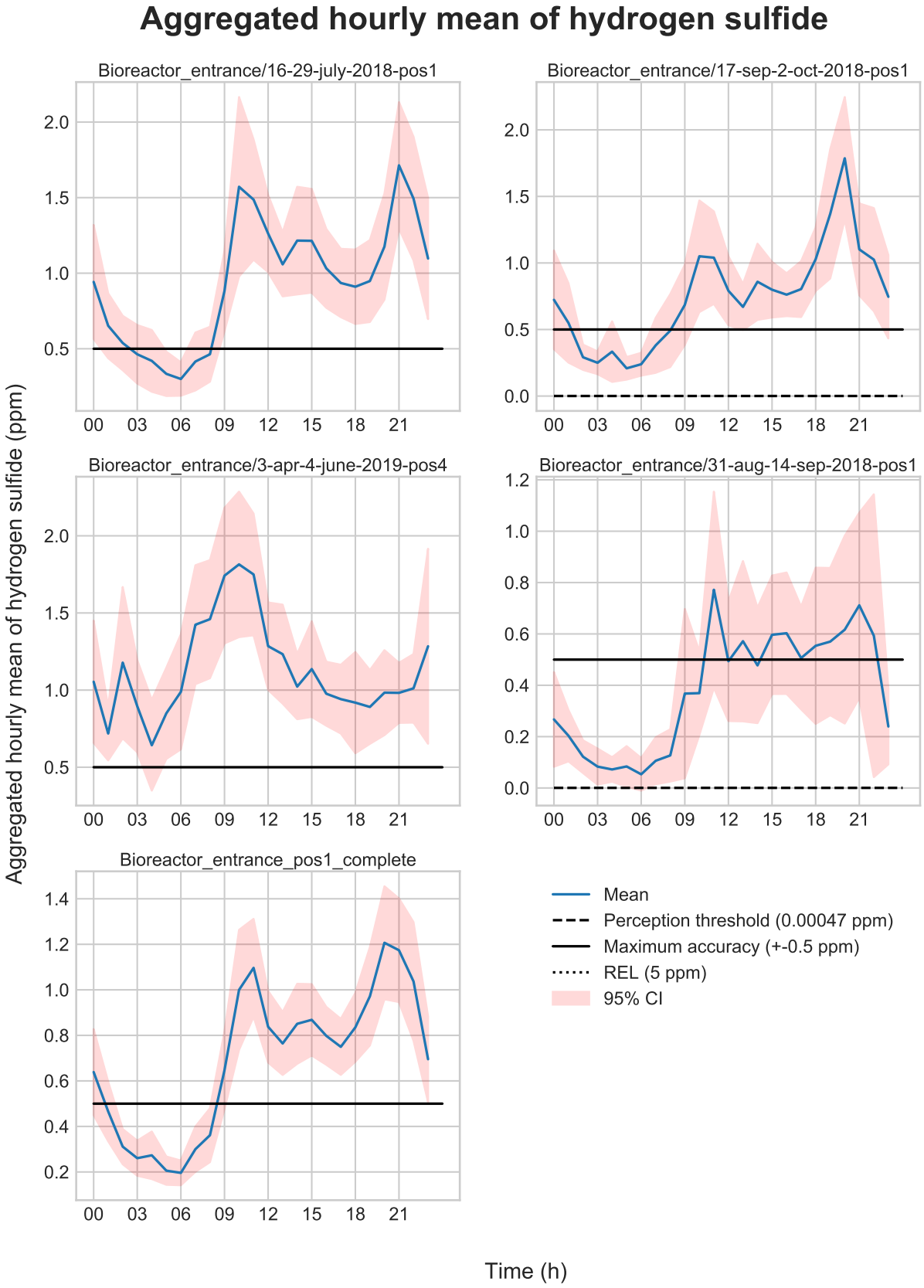

Figure 61: Aggregated hourly means of hydrogen sulfide concentrations in ppm during both measurement campaigns of 2018 and 2019 at the main emission source. With regard to the legend, particular concentration limits in ppm are embedded into the graphic; namely the recommended long-term exposure limit (or long-term REL) and perception threshold of the odorant, mentioned in subsection 2.2.3, and the maximum accuracy of the deployed measuring instruments explained in 3.1.1.

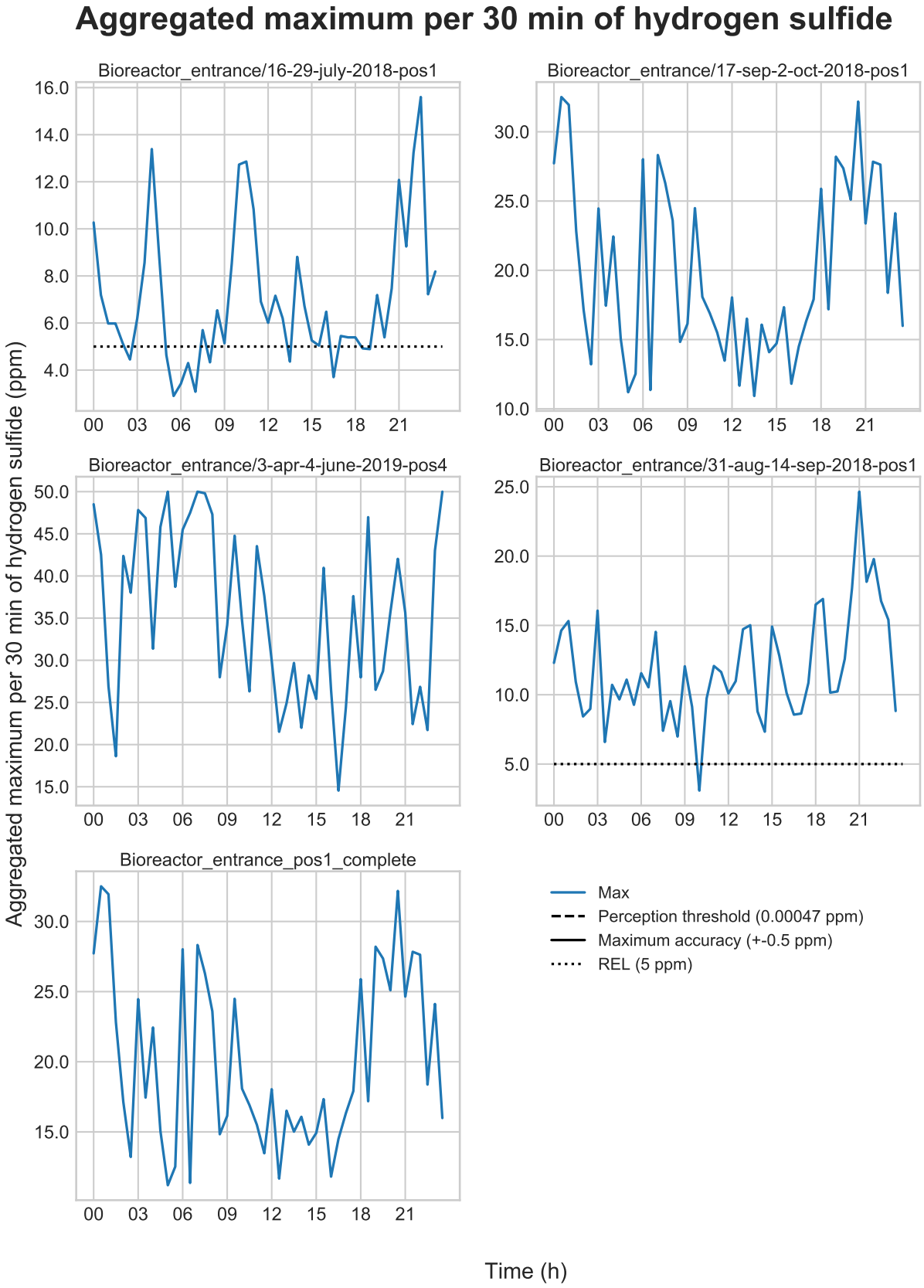

Figure 62: Aggregated maxima per 30 minutes of hydrogen sulfide concentrations in ppm during both measurement campaigns of 2018 and 2019 at the main emission source. As far as the legend is concerned, particular concentration limits in ppm are embedded into the graphic; namely the recommended long-term exposure limit (or long-term REL) and perception threshold of the odorant, mentioned in subsection 2.2.3, and the maximum accuracy of the deployed measuring instruments explained in 3.1.1.

4.4 Meteorological variables

In what follows, the most important meteorological variables "wind speed", "wind direction" and "temperature" are displayed for every month during the entire year of 2018, as annual averages and the wind speed filtered for the wind directions pointing toward the residential areas. As for the graphic type, a similar approach as above regarding NH_3 and H_2S concentrations was chosen. The values were aggregated either half-hourly or hourly, then overlaid every 24 hours to facilitate spotting daily patterns. As far as the aggregation methods are concerned, the mean was generally employed, whereas the maximum was utilized were appropriate. With respect to the means, where applicable, a 95% confidence interval was plotted along with the mean in order to give an idea of the variability associated with each feature of interest. With regard to their naming in the upcoming plots, they can contain the suffix "mean" even though they were not aggregated by the investigator, but used as raw data instead. This is due to the fact that the original data are already provided as means, because their resolution of 5 minutes is based on averages of even higher resolved recordings of the meteorological equipment, but for saving disk memory, they have been stored every 5 minutes.
At first, the monthly wind and temperature patterns are going to be presented in figure 63, 64 and 65.

4.4.1 Wind and temperature patterns during the year 2018

When looking at the subplots of the mean wind speed in graph 63, one can observe a clear difference in terms of stability during the summer and winter period. During summer, i.e. from May to September, the 95%-CI band is wrapped rather tightly around the mean values, whereas in the other months the band is considerably broader, which tells the reader an increased variance of the wind speeds during winter. What is more, while the daily average minima are almost equal throughout the year, the maxima are up to 2 m/s higher on average during summer. Generally, a constant pattern can be observed during almost all months except for January, February and March: wind speeds increase from the early morning till reaching their daily maximum in the evening, then show a subsequent drop toward their daily minimum in the end of the night. This pattern is exceptionally stable during the high summer season, wherefore it can already be speculated that the odorants can travel the furthest from the main emission source in the evenings.
After having discussed the wind speeds, the wind directions are also of high interest for the model. Similarly, they are depicted in graph 64 and more stable conditions during summer as well, which can be confirmed again when looking at both the mean values and their associated confidence interval. The narrower it is, the less the variance of the variable. As an universally valid assertion throughout the entire year, it can be deduced from figure 64 that during the afternoon and evening, the wind blows in direction of the dwellings, i.e. coming from a range between approximately 65 to 170 angular degrees. Again, this is especially true for the particularly stable summer months. The wind direction toward the residential housings of interest coincides temporally with the increase of wind speed from morning till evening (see fig. 63), and also with the global maxima of H_2S mean concentrations in the evenings (compare fig. 61). Consequently, one can infer that the highest probability of being subjected to perceptible odorant concentrations at the dwellings should be during the evening and early night.
As far as the mean temperatures are concerned (see figure 65), they show very stable patterns over the course of the entire year. This is owing to the fact that Oliva lies at the Mediterranean coast comprising of long stable summers under the influence of the subtropical high pressure belt, and more rain and cloud formation during the winter. Thus the confidence intervals are a bit broader during winter, indicating more variance in the temperature variable, but generally the overall picture states a rather stable climate almost the entire year. As a matter of course, the temperatures are on average 15 degrees higher in high summer compared to the lowest temperatures in February, which

has a direct effect on the on the biological activity of the sulfur-reducing bacteria (SRB). As stated in 2.3.5, "each degree Celsius increase in temperature represents a 7 percent increase in SRB activity (up to 30° C)". As a result, this circumstance increases the odorant production during the high summer season considerably, since odor nuisance due to elevated odorant emission rates is much likelier then.

By and large, just from looking at the 3 most important meteorological data, one can already draw an anticipated conclusion that the highest probability of being exposed to perceptible odorant concentrations is during the hottest months of the year in the evenings and early nights. This could be inferred by discussing hourly aggregated wind speed, wind direction and temperature data overlaid on a daily scale for each month of the year 2018.

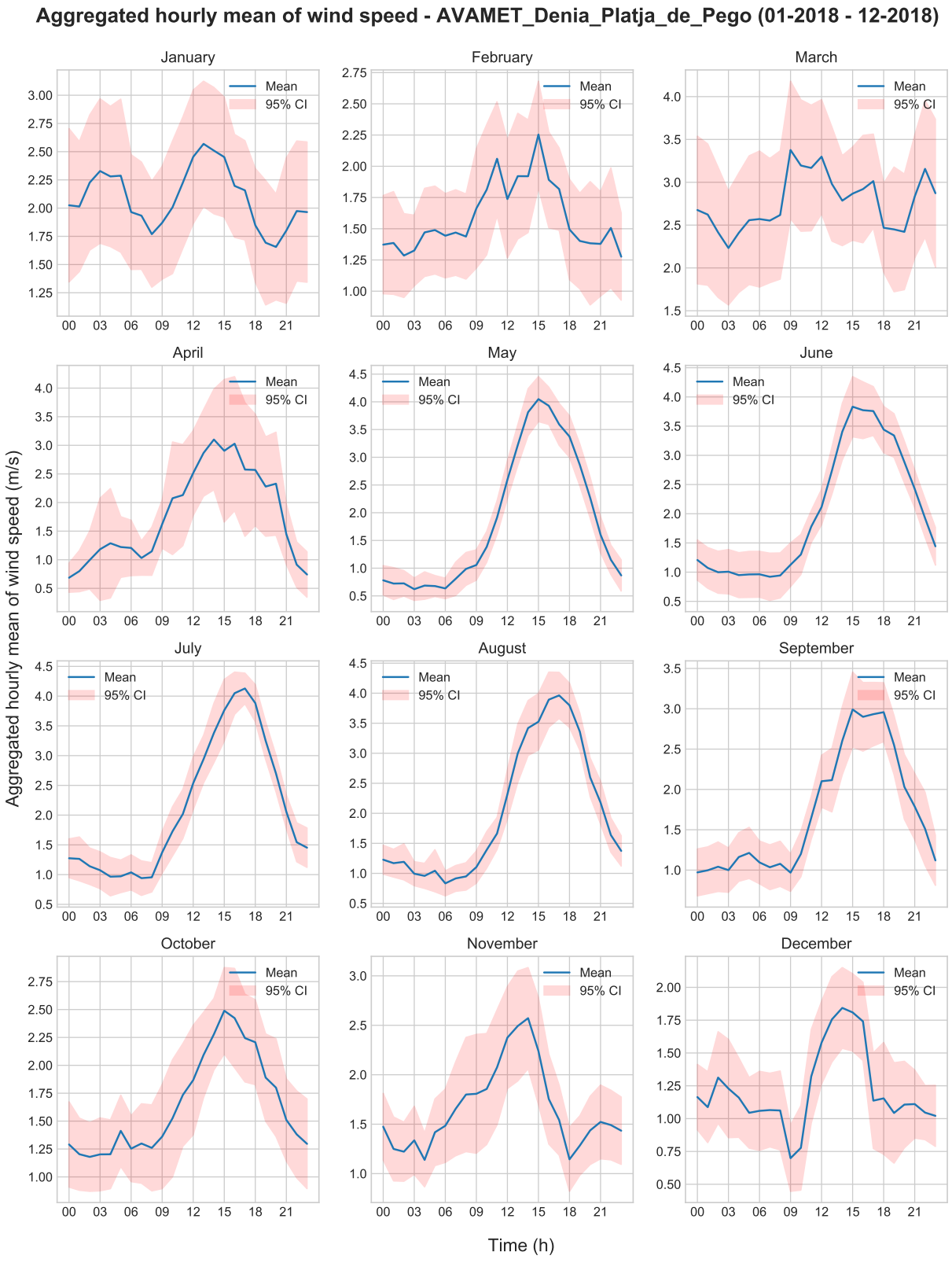

Figure 63: Subplots of the aggregated hourly means of the wind speed given in m/s. Each subplot represents one month of the year 2018 and comprises of the hourly mean and the associated 95%-CI band calculated from every of the 24 mean values related to each hour of the day from 0 to 23 hours.

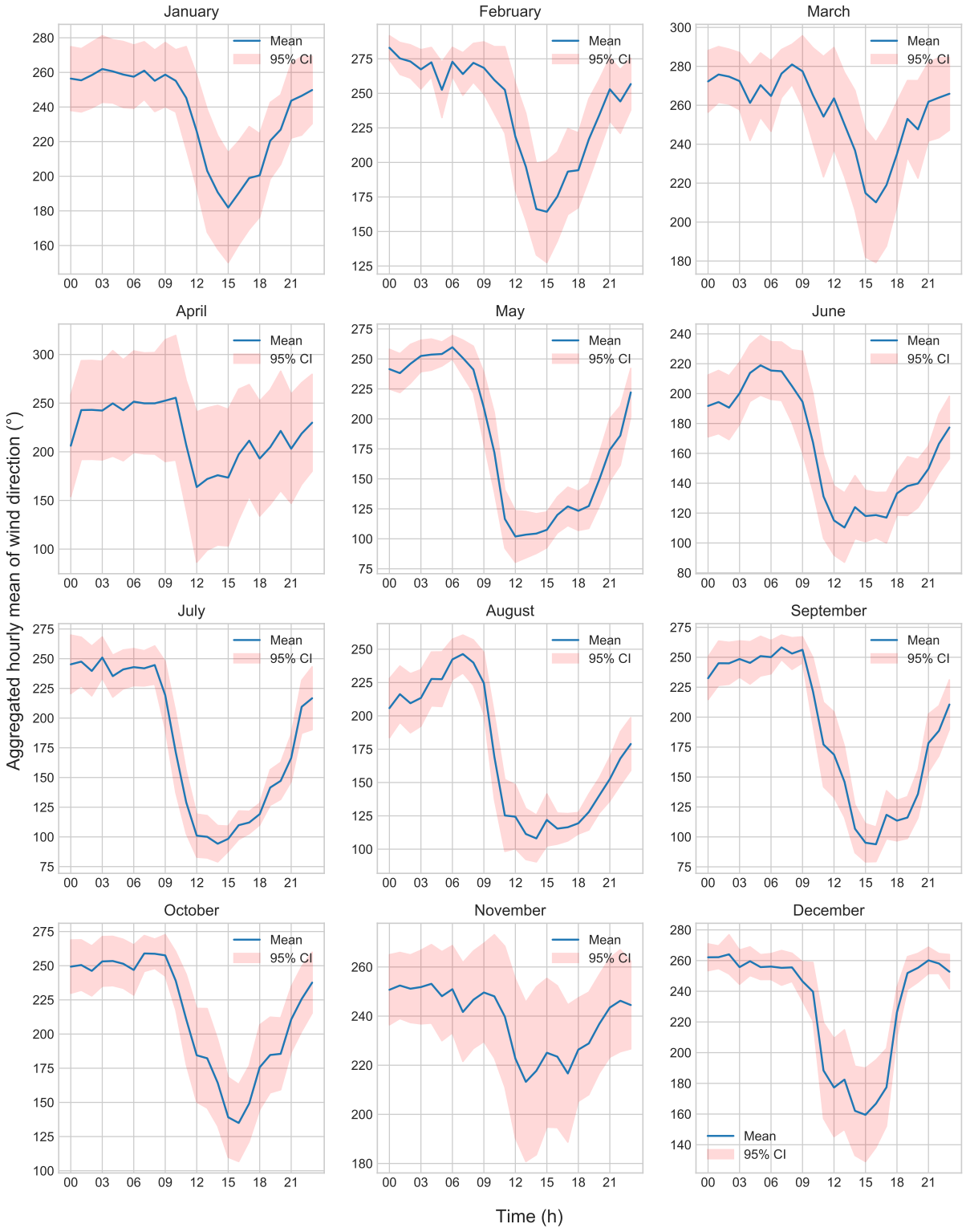

Figure 64: Subplots of the aggregated hourly means of the wind direction given in angular degrees. Each subplot displays one month of the year 2018 and consists of the hourly mean and its associated 95%-CI band computed from every of the 24 mean values related to each hour of the day from 0 to 23 hours.

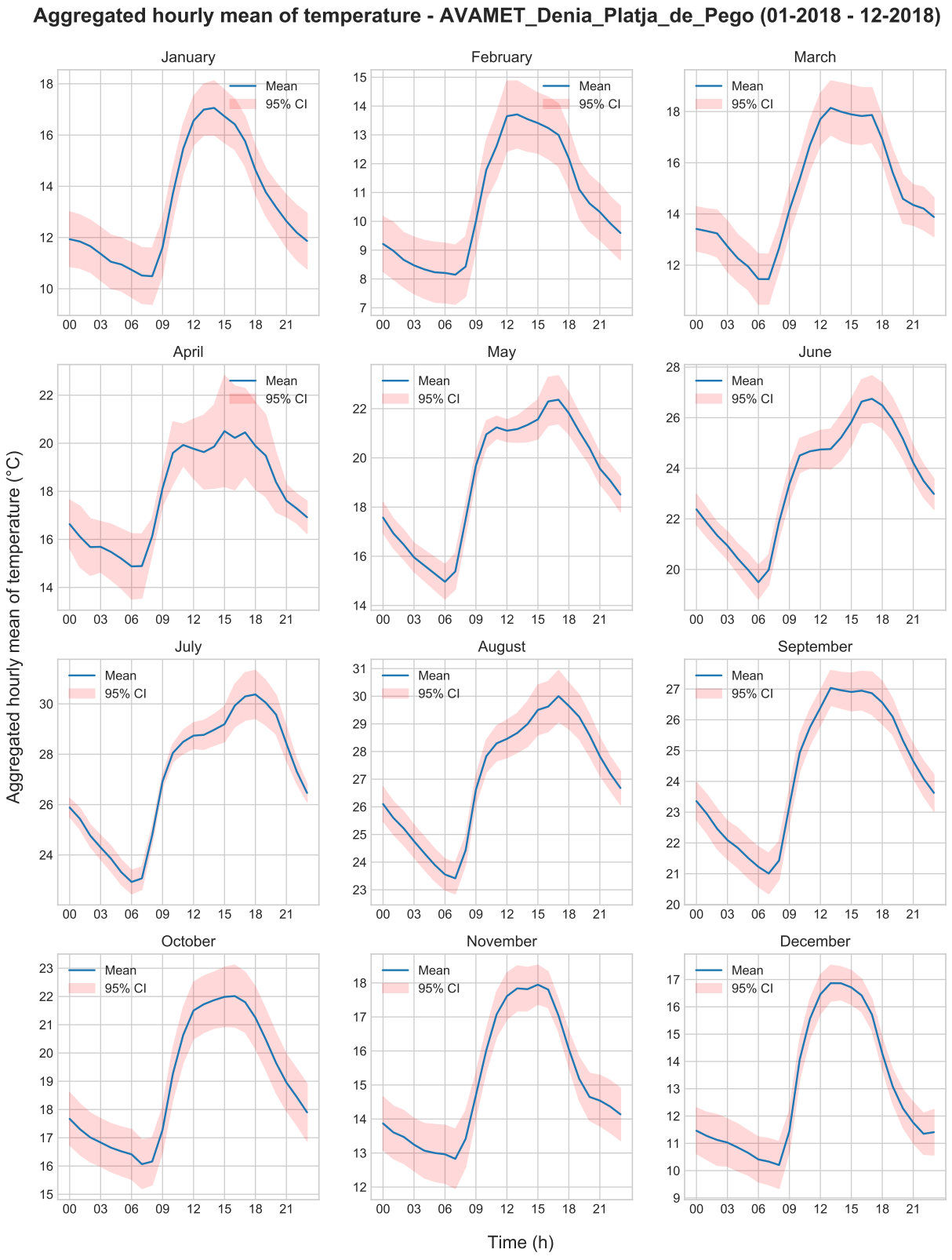

Figure 65: Subplots of the aggregated hourly means of the temperature given in degrees Celsius. Each subplot depicts one month of the year 2018 and contains the hourly mean and its associated 95%-CI band obtained from every of the 24 mean values related to each hour of the day from 0 to 23 hours.

4.4.2 Wind speed filtered for direction of the affected residential housings

Since the complaints came from one specific direction (see labeled Google Maps screenshot 4) in the residential area surrounding the WWTP site Camping San Fernando, a crucial variable to help understand this circumstance was the wind. As being a vector quantity, when talking about wind both its direction in space and speed are of importance. This stems from the fact that advection is the main means of airborne transportation at distances between say 40 and 100 meters, which represents the proximity of the affected housings to the emission source. On the other hand, if the wind blew into the opposite direction, it would be rather unlikely that the odorants arrived in a sufficient quantity at the afflicted dwellings.
As for the direction of interest, starting from the only pollutant emission source of the WWTP toward the residential dwellings in question, it ranges from about 65 to 170 angular degrees. This circumstance can be readily derived by looking at the wind roses embedded into the Google Maps satellite picture of the WWTP in figure 68 and 69. At this point it is vital to note that the convention in determining wind directions is to refer to the direction where the wind comes from, not in which direction it blows. More concretely, if the wind needs to blow from the emission source toward the buildings in a direction of X degrees, one needs to add 180 degrees to it in order to obtain the corresponding wind direction.

Having said that, one of the most important variables, the mean wind speed, is going to be examined more thoroughly in what follows. To this end, similar plots as in the previous subsection 4.4.1 discussing the general wind and temperature patterns were included, but this time with a previously applied filter for the wind directions pointing directly toward the residential dwellings, where the complaints stem from.
To start with, in figure 66 the annual hourly mean overlaid from 0 to 23 o'clock is displayed. From this it appears evident that the wind speed shows a stable increase from morning to evening year round, with its global maxima in the late afternoon and its global minima in the early morning (compare also fig. 63).
Furthermore, the monthly data are displayed in the subplots of graph 67, which sustain the general conclusions made from the annual averages in fig. 66, except for the very irregular month of November. As an aside, it must be mentioned that the 95%-CI band can only be plotted, when there are enough values for every hour during the day, which is not always the case due to the reduced data set caused by the filtering for a certain range of wind directions. Also, it can be seen that this filtered data subset does not comprise of this high stability all year round which could be observed previously in the entire data set (see fig. 63). Notwithstanding, it is clear to see that again in the summer months, the already derived daily pattern holds as well when taking only the wind speed into account which are directed toward the residential dwellings. This in turn corroborates the anticipated conclusion again, that it is most likely for these residents to be affected by odors in summer during the evening and early night.

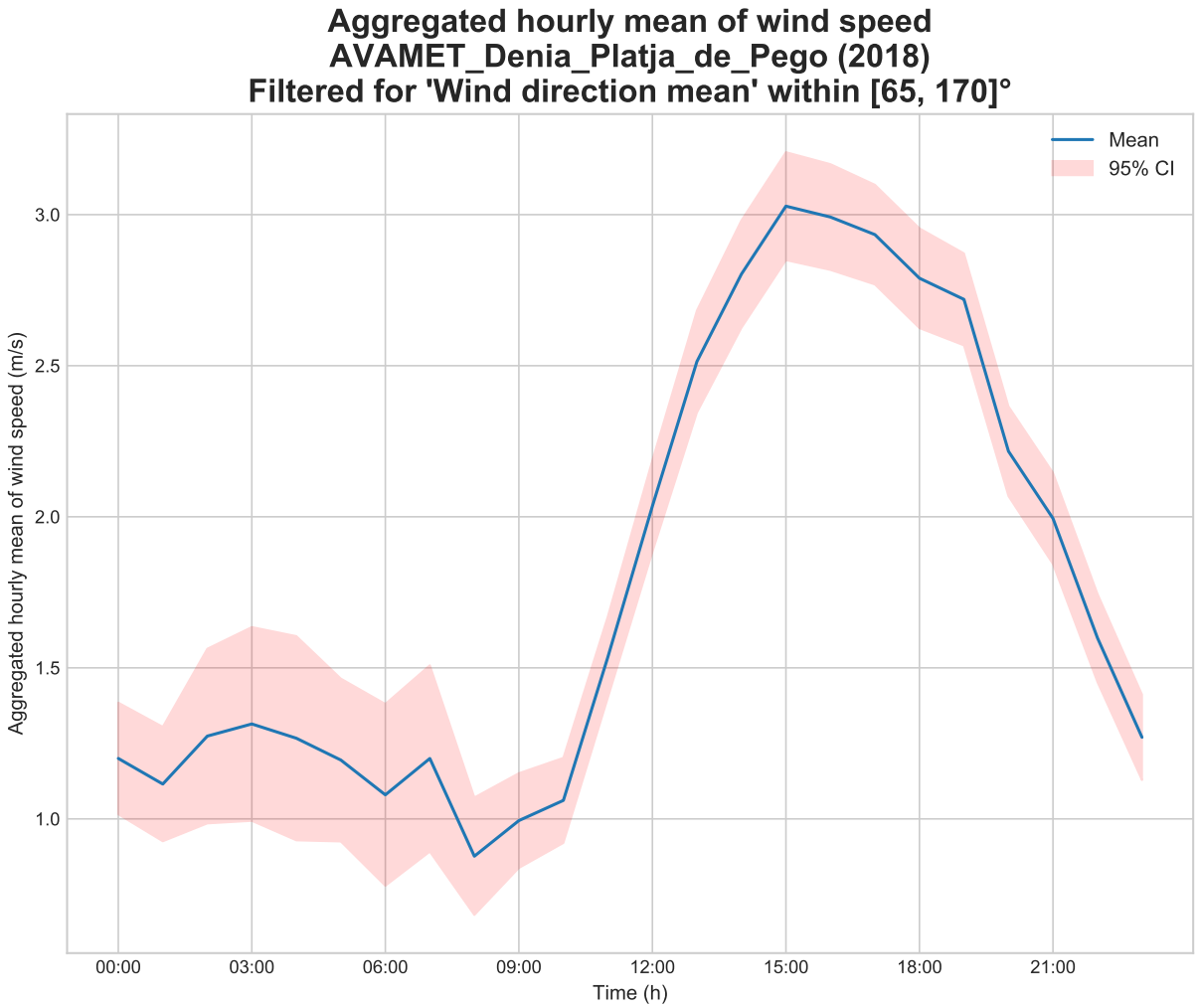

Figure 66: Direction-filtered hourly mean wind speed of the year 2018 displayed in m/s on the ordinate against the daytime from 0 to 23 hours on the abscissa. The data was obtained from an AVAMET meteo station called "Denia - Platja de Pego". Apart from the hourly mean, an associated 95% confidence interval is plotted calculated from each of the mean values in order to show the variance in the data.

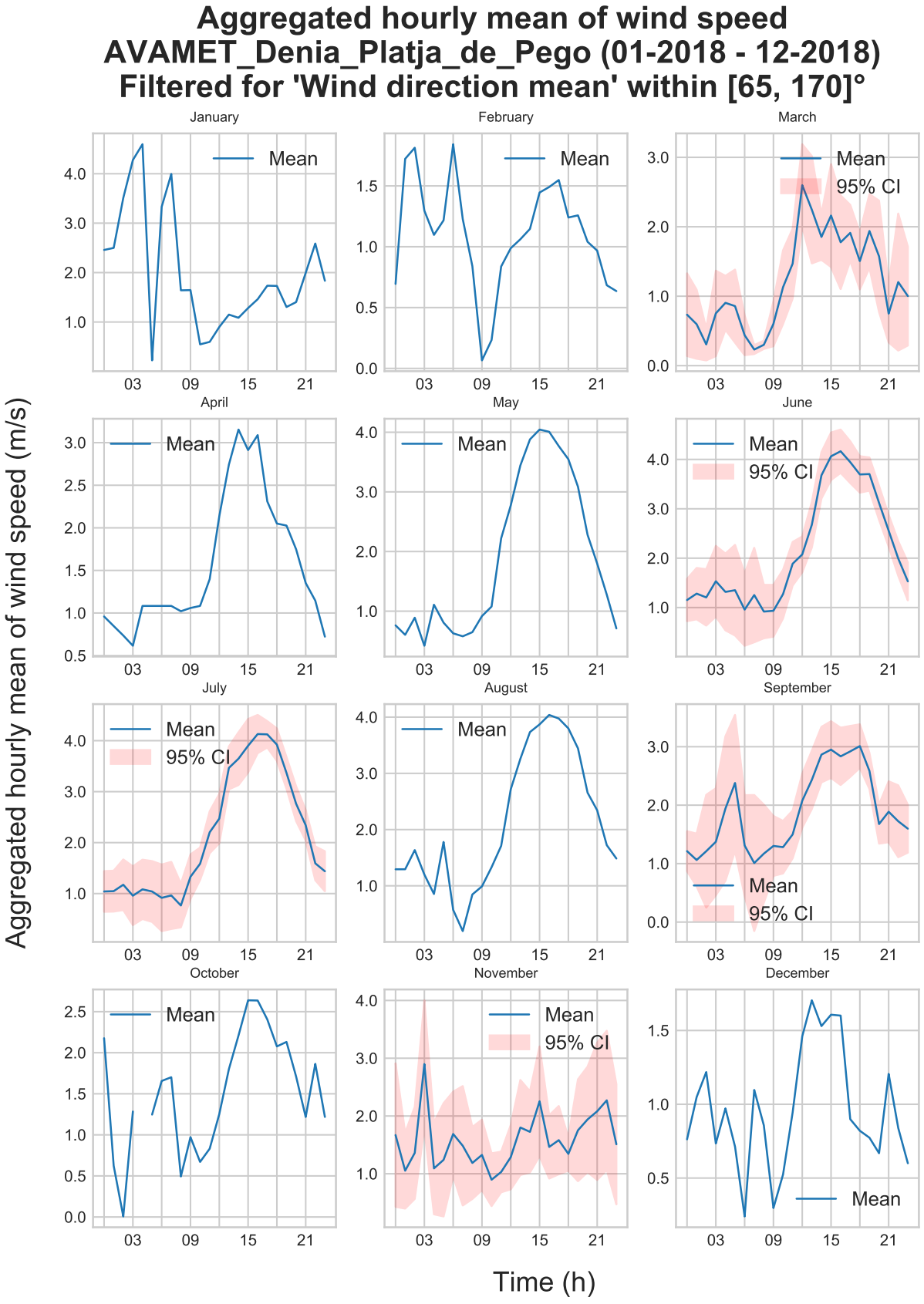

Figure 67: Subplots of the aggregated hourly means of the wind speed given in m/s; this time filtered by the wind directions ranging from 65 to 170 angular degrees pointed toward the residential housings, as opposed to the unfiltered data illustrated in fig. 63. Regarding the above-stated wind direction range, this means that the wind blew from these directions, not toward them. What is more, each subplot represents one month of the year 2018 and comprises of the hourly mean and the associated 95%-CI band calculated from every of the 24 mean values related to each hour of the day from 0 to 23 hours.

4.4.3 Wind roses overlaid on satellite top view of the WWTP

In addition, in order to visualize the wind speed and direction distribution during a representative short time period in the high summer season, in figure 68 the WWTP top view extracted from Google Maps was overlaid by a wind rose depicting the conditions during the month of July 2018. Again, the bars indicate the directions were the wind comes from, not toward which direction it blows.

Figure 68: Wind rose displaying the wind speeds occurred in July 2018 from light to dark blue in m/s and the corresponding wind directions divided in the 8 main compass points N, N-E, E, S-E, S, S-W, W and N-W starting from the North "N" clockwise over East "E" and South "S" to West "W". The graph is overlaid on top of the satellite picture from Google Maps showing the top view of the WWTP and its surroundings, including the affected dwellings in between WSW and NNW. Furthermore, the concentric rings are labeled with the percentages each of the plotted bars comprises with respect to the totality of wind speed observations of the dataset.

As an aside, regarding all wind rose figures 68, 69, 70 and 71 the conversion from the integrated main compass points N, N-E, E, S-E, S, S-W, W and N-W works as stated in the following: North or "N" equals 0 and 360 angular degrees and represents therefore both start and end of the clockwise enumeration of the directions from 0 to 360 degrees. According to this convention, East or "E" stands for 90, South or "S" for 180 and West or "W" for 270 angular degrees.
Having said that, hereafter the graphic 69 intents to give a better understanding on how the wind direction and force are statistically distributed throughout the entire example year of 2018. The two figures 69 and 69 lead to the conclusion that during the high summer season, the winds are mainly orientated toward the dwellings comprising statistically of the highest speeds on top. On the other hand, the annual distribution in fig. 69 shows clearly that even though most winds blow from the dwellings toward the WWTP site, overall there is a significant share regarding both wind direction and speed toward the residential area all year round (compare also fig. 67). In the end, these two overlaid windrose graphics verify again that the residential housings in question can be affected most of all during the high summer season, i.e. from May till September which is substantiated by figure 63 and 64 owing to the fact that both wind direction and speed are consistently stable and comparable during the aforementioned summer months.

Figure 69: Wind rose displaying the wind speeds occurred during the entire year of 2018 from light to dark blue in m/s and the corresponding wind directions divided in the 8 main compass points N, N-E, E, S-E, S, S-W, W and N-W starting from the North "N" clockwise over East "E" and South "S" to West "W". The graph is overlaid on top of the satellite picture from Google Maps showing the top view of the WWTP and its surroundings, including the affected dwellings in between WSW and NNW. Moreover, the concentric rings are labeled with the percentages each of the plotted bars comprises with respect to the totality of wind speed observations of the dataset.

4.4.4 General wind roses during periods of interest in 2018

Hereafter, with the aim to underpin the previously drawn conclusions, figure 70 and 71 depict the wind variables' distributions during the summer months of the first measuring campaign in 2018 and also all months of the same year as subplots. In graph 70 it can be seen that the wind patterns are very similar from July to August and from September to October. What all these months have in common is that the wind blew proportionally stronger from the east toward the dwellings which is

based on the fact that the wind speed increases toward its maximum in the evening and the direction turns simultaneously toward the dwellings, as could be derived from figure 63 and 64.
Next, in graphic 71 it can be confirmed again that the statistical distributions of both wind direction and speed are comparable in particular in June, July and August during the high summer season. Then, over September to March, the share of winds blowing from East toward the dwellings decreases until it rises significantly again from April evolving into the predominant wind direction with also the highest wind speeds during summer. Yet in spite of the fact that the winds blow largely from the opposite direction during winter, the share in toward the housings never vanishes completely and with respect to the associated the wind speed distribution they comprise mainly of average and higher-than-average values. In a nutshell, one can observe that if the wind blows in winter toward the affected buildings, it blows often above average speed. This in turn increases the chance during those moments to receive perceptible odor concentrations at the dwellings.

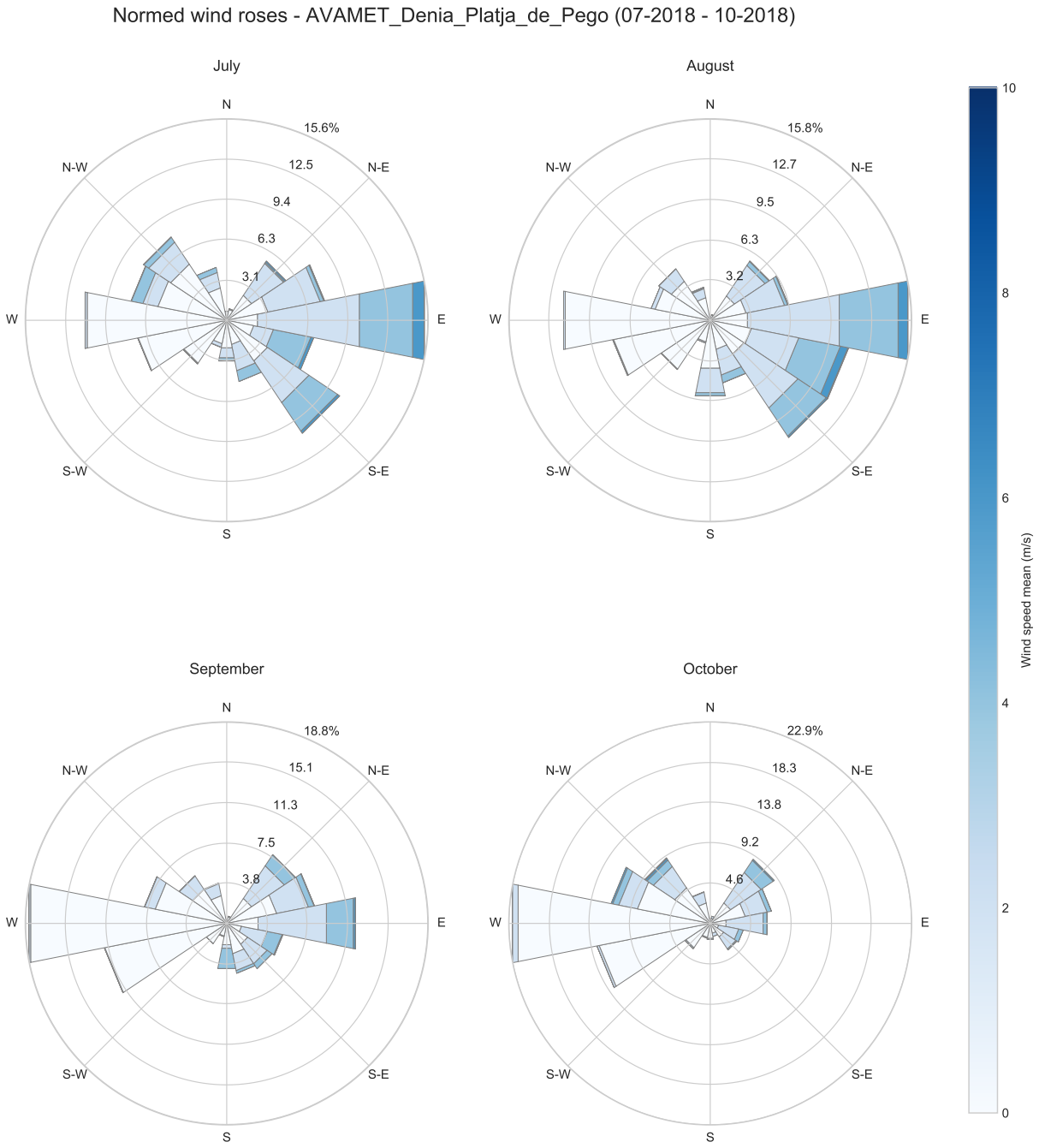

Figure 70: Subplots of wind roses which display the wind speeds occurred during the 4 months in summer 2018 when the first measuring campaign was carried out. The wind speeds are shown from light to dark blue in m/s and the corresponding wind directions divided in the 8 main compass points N, N-E, E, S-E, S, S-W, W and N-W starting from the North "N" clockwise over East "E" and South "S" to West "W". Apart from that, the concentric rings are labeled with the percentages each of the plotted bars comprises with respect to the totality of wind speed observations of the dataset.

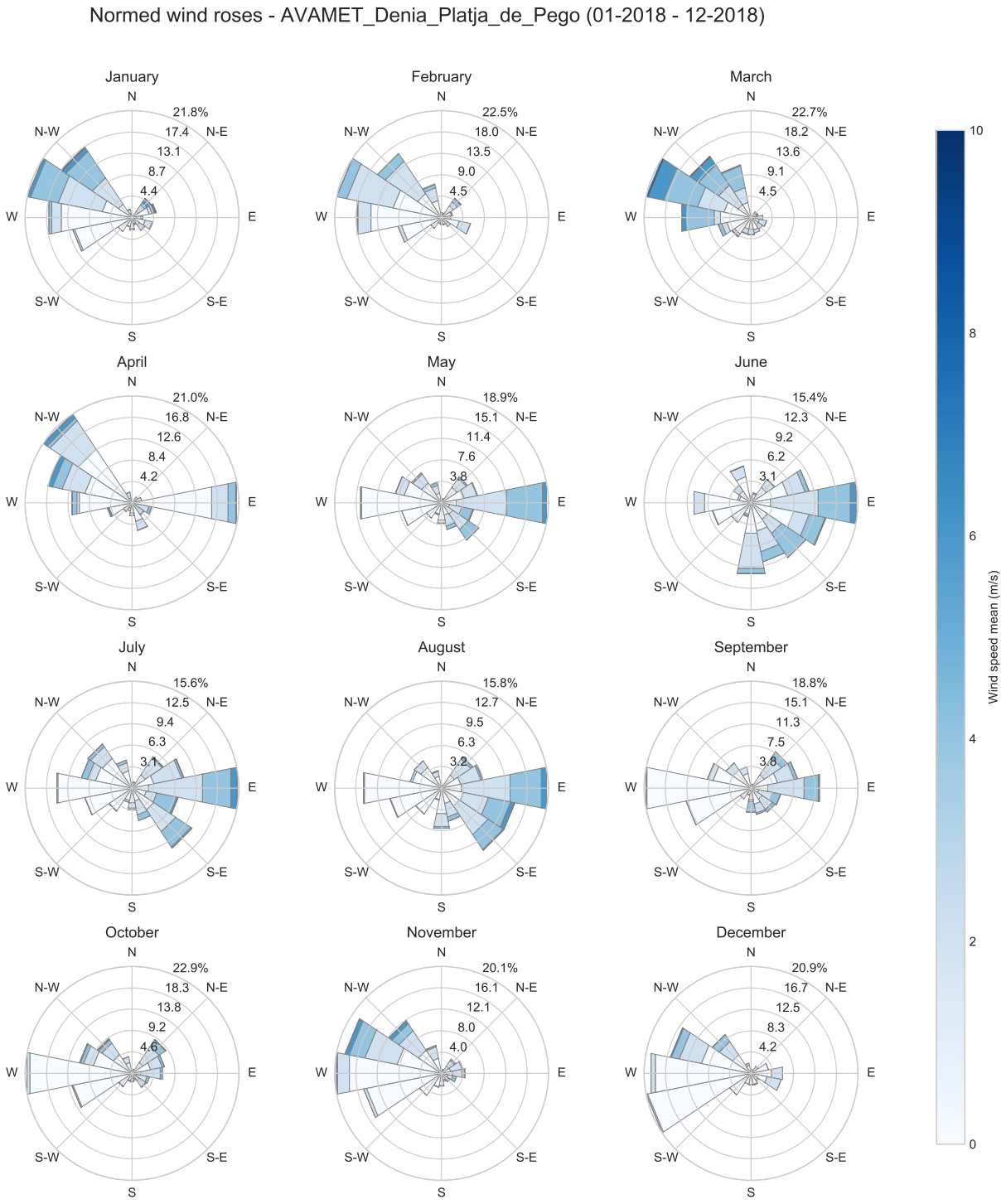

Figure 71: Subplots of monthly wind roses which display the wind speeds occurred during the whole year of 2018. The wind speeds are shown from light to dark blue in m/s and the corresponding wind directions divided in the 8 main compass points N, N-E, E, S-E, S, S-W, W and N-W starting from the North "N" clockwise over East "E" and South "S" to West "W". Besides that, the concentric rings are labeled with the percentages each of the plotted bars comprises with respect to the totality of wind speed observations of the dataset.

4.5 Correlations between olfactometry measurements and H_2S concentrations

Generally speaking, odorant and odor concentrations represent two ways of expressing odors, i.e. conventional chemical gas concentrations and human perception units in terms of offensiveness and intensity (for more details, see subsection 2.5.2). Therefore, correlations were sought between the olfactometry measurements in European Odor Units (OU_E) per m^3 and both examined gaseous pollutants NH_3 and H_2S (compare figure 72), in order to find a way to convert from odor to odorant concentrations and vice versa. However, only the graphic related to the main and only relevant odorant in the context of this project will be discussed in what follows, since the rather unreliable ammonia data below the instrument accuracy (see 3.1.1) cannot be considered valid for examining correlations to other variables.

With the aim to look for correlations between H_2S concentrations and olfactometry measurements, several aspects had to be taken into account. At first, the temporal proximity was paramount, i.e. the closest simultaneously gas recording was selected, preferably right before the olfactometry measuring was undertaken. Secondly, the spatial proximity needed to be considered while including simultaneous wind speed and direction. This means that the filtering code respected the exact GPS position of the panelists next to the odorant source.

As visible from graphic 72, there were not many measuring points to correlate owing to the small quantity of 37 non-zero olfactometry recordings during the first measuring campaign in 2018. In addition, some of these were taken when either no gas measurements were being carried out at the same time or due to distance and wind conditions no sound correlation could be found. Hence, after having taken the measurements, it became clear that in order to obtain a reliable and meaningful correlation between both variables, the statistics need to be strongly improved. That means, that the panelists need to take either much more measurements, especially when an offensive odor can already be perceived naturally which would guarantee a non-zero measurement, or alternatively opt for the most advanced cutting-edge method and deploy electronic noses (see 2.5.3). The latter would be able to measure on a continuous basis in the same way as the conventional measurement instruments, such as the Dräger Polytron 7000 (see 3.1.1 put to measure in this project.

To repeat the principal benefit of electronic noses, it shall be mentioned that such a measuring device could be deployed continuously in the field which obviously cannot be accomplished by human panelists. Apart from that, its ability of distinguishing different kinds of odorants simultaneously is another feature which cannot be accomplished by panelists, who merely measure levels of offensiveness (see table 6) of the current airborne mixture of odorants.

To conclude, panelists can give a rather general hint whether or not an odor nuisance exists in a certain location, but with regard to creating a proper data base for statistics, let alone calculating correlations to other variables, it seems to be a rather inappropriate method. It would cost a lot more time and effort, e.g. when sending larger groups of panelists more often to the site in question, or even let people live nearby for a while noting down their findings in an "odor diary" or logbook, but these methods would be quite expensive.

Besides that, given the fact that the sample size were large enough to calculate sensible correlations, the investigator is advised to take into account both the wind direction and speed, since these meteorological quantities are essential to safeguard attaining coherent results. To give an illustrative example on this, the reader could imagine a smoker standing next to another person: as long as the wind is blowing away from the latter person, perception of the bad smell is rather unlikely, if not impossible. On the contrary, given that the wind blows directly into this person's direction, the smoke odor would be clearly perceptible.

To sum up, regarding the correlation results of olfactometry and gas measurements in this project the statistics are rather insufficient, and thus solely permit a very rough linear estimate for a conversion

between conventional odorant concentrations and olfactometry odor units.

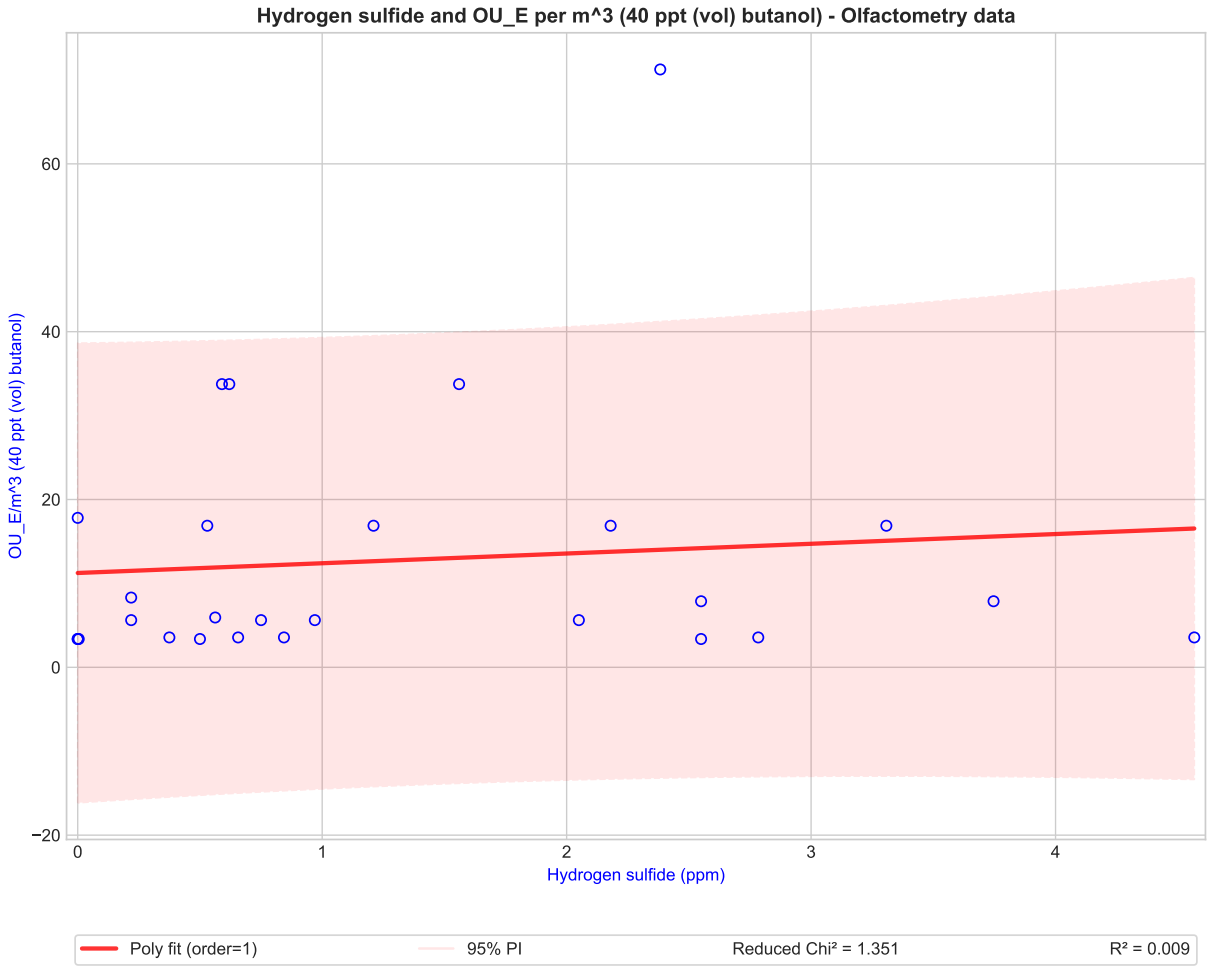

Figure 72: Linear correlation plot of hydrogen sulfide concentrations in ppm and olfactometry measurements in European Odor Units (OU_E), which were calibrated with 40 ppt butanol. For further explanations regarding the dynamic olfactometer and its calibration, please revisit the subsection 3.1.2 and list 2.2.1.

4.6 Correlation of the daily mean H_2S concentrations and WWTP volume outflows

On top of the aforementioned intertwined factors leading to an increased possibility of experiencing odor nuisance during the end of the day, the enhanced presence of the residents through the last hours before sunset produces increased amounts of sewage flowing from the canalization into the WWTP, which as a consequence gives rise to an even more increased probability of suffering from odor nuisance. In addition, as Oliva is a tourist region, the number of non-permanent residents increases during the summer season, which results in higher volume in- and outflows of the WWTP.
However, when looking at the results of the following correlation subplots in figure 73, these quite intuitive assumptions cannot be undoubtedly verified by means of the available variables " H_2S concentration at the WWTP entrance" and "Volume outflow at the WWTP exit". The reason why it seems difficult to check the logical correlation between maximum concentrations and outflows is for one thing the different temporal resolution of 1 measurement per minute (concentration) compared

to one measurement per day (volume flow). What is more, the concentration peaks can occur with every pumping cycle which lies, depending on the season, between once per 1 up to 10 minutes. Provided that the pump is activated by the accumulation of a certain wastewater volume in the well, the pumping rhythm increases, but not necessarily does this have as a consequence the single concentrations peaks are higher. Then again, when the pumping frequency rises, the daily WWTP outflow must also increase. Therefore, the variable don't need to be directly correlated; also, because the response of every pumping cycle is not necessarily the outflow of the same amount of water out of the plant, i.e. instantaneous or somehow direct within the entire system. This in turn could explain why the correlation got lost when crossing the concentration measurements with high resolution volume outflow measurements with a joint resolution significantly higher than 6 hours down to 1 minute. Conclusively, a better approach would be to measure the volume inflow into the plant since this is the actual emission source of the odorants. Moreover, as a matter of fact also chemical sewage system variables play their determining role in the question how high the peaks at the emission source can be. In addition, the state of the pipes, their filling levels and other conditions, which promote increased production and accumulation of sewer gases, are correlated to peaking $\mathrm{H_2S}$ concentrations at the canalization outflow, i.e. the entrance to the WWTP.
Yet in spite of the aforementioned arguments and open questions, the intuitive positive correlation between volume flow and $\mathrm{H_2S}$ concentration can be found in the first measuring period between 16 and 29 July 2018, but on the other hand the remaining periods don't show a positive or any correlation.

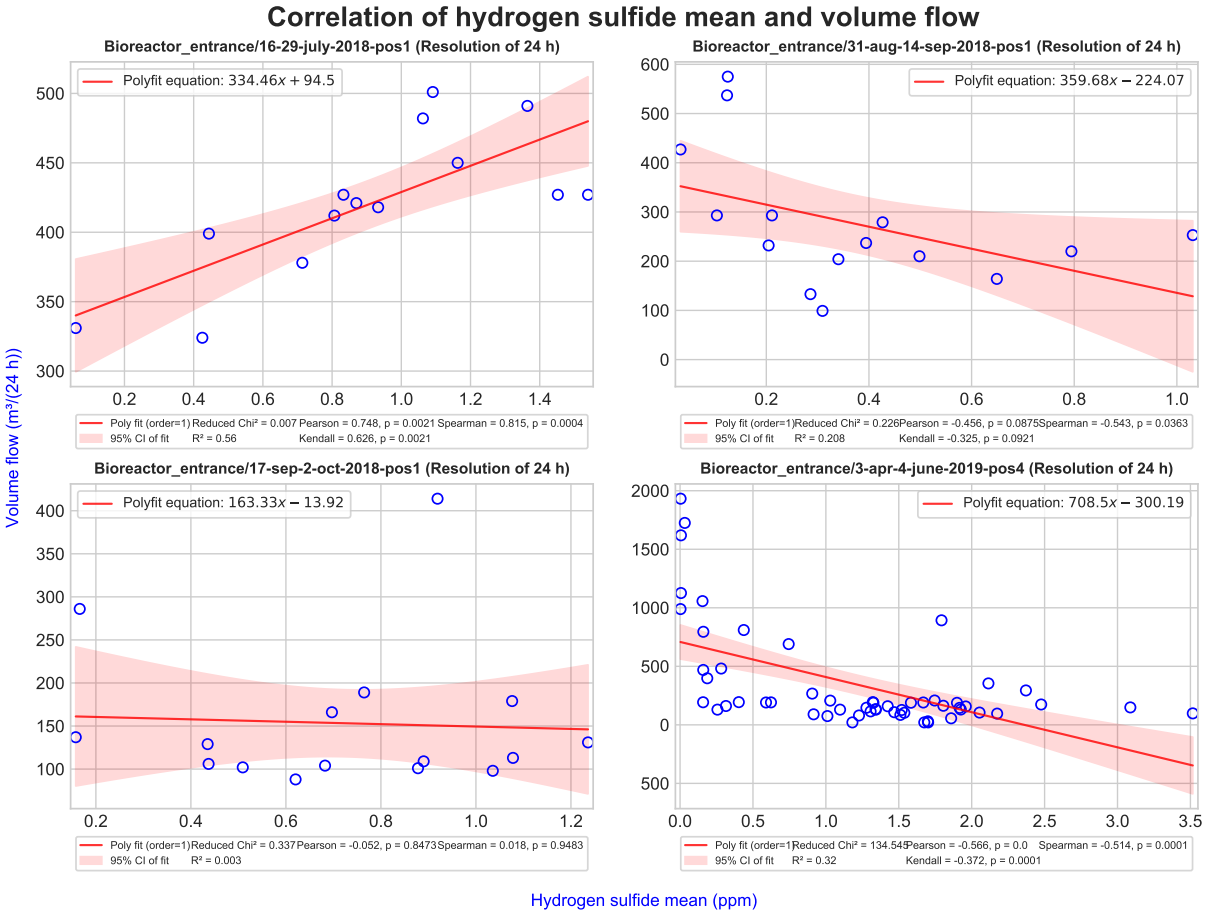

Figure 73: Linear correlations of daily volume outflow of the WWTP in cubic meters per day and the daily mean of hydrogen sulfide concentrations in ppm during the both measurement campaigns 2018 and 2019. The gas data were recorded directly at the main emission source, i.e. the canalization entrance into the bioreactor.

Additionally, apart from the daily volume flow data shown in fig. 73, there were also high resolution data available measured every 10 seconds from 16 to 22 May 2019. Since the H_2S concentration data measured simultaneously has a resolution of 1 minute, it was possible to aggregate the means of both quantities to several rather short time steps of interest. The correlations between four selected time steps are depicted in figure 74.

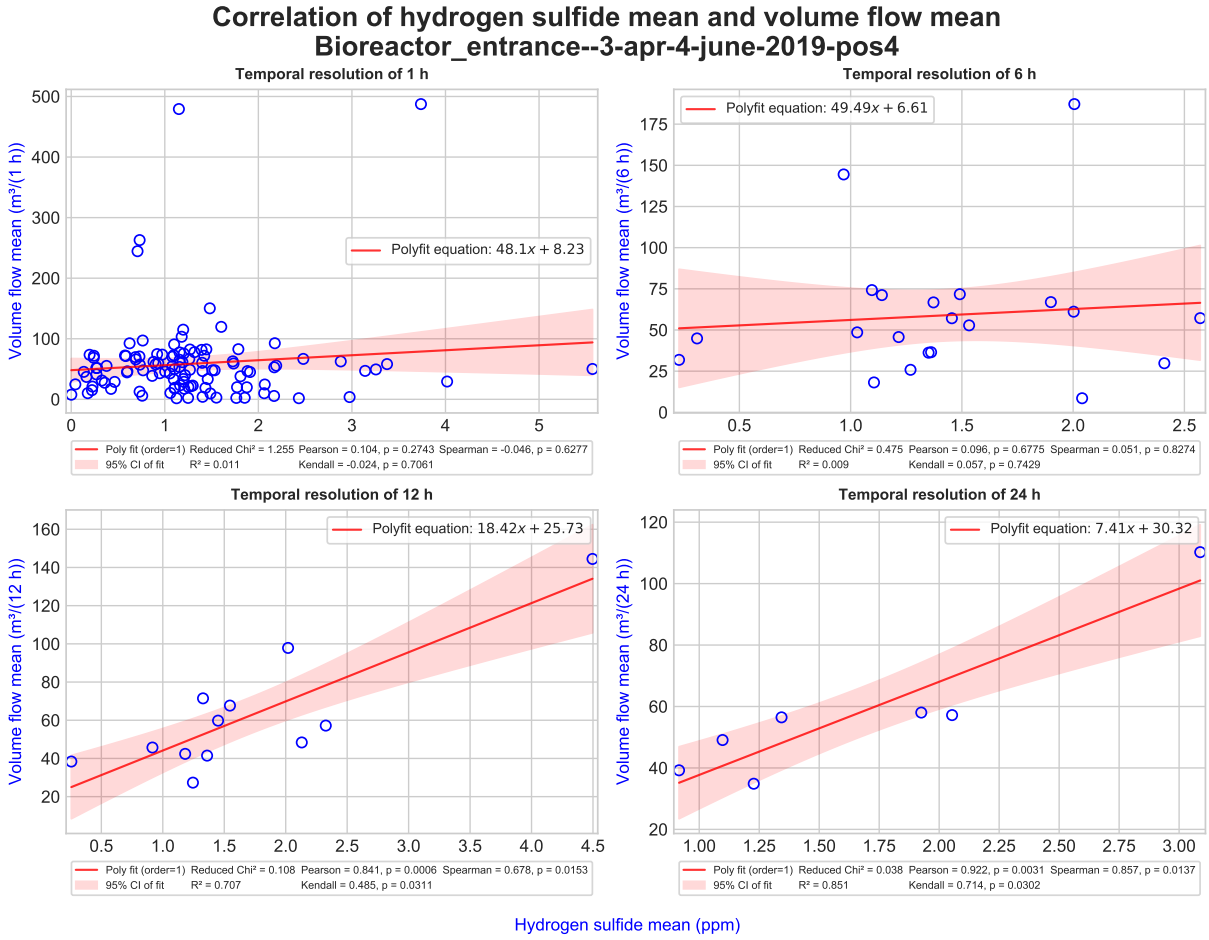

Figure 74: Linear correlations of the means of high resolution volume outflow data in cubic meters per time unit, and the hydrogen sulfide mean concentrations in ppm averaged over the corresponding time unit. These time units were chosen to be 1, 6, 12 and 24 hours. The high resolution volume outflow data were recorded from 16 to 22 May 2019, wherefore the related gas measurement period was the 2-month time from 3 April till 4 June 2019, i.e. during the second measuring campaign.

From the graph 74 it can be concluded that the correlation between the aggregated means seems to be positive for 12- and 24-hour resolutions, but as for lower resolutions than 12 hours, the correlation vanishes.
To sum up, a clear positive correlation between (mean) hydrogen sulfide concentrations at the principal emission source and daily or mean volume outflows could not be confirmed. Perhaps, by measuring the volume inflow at the entrance at the same temporal resolution as the gas concentrations it would be more likely to find a correlation as it makes intuitively sense that the more wastewater there is, the more likely higher concentration peaks will be produced. For further investigation, one could compare hourly means overlaid every 24 hours such as done previously with the meteorological and gas variables, in order to check for correlations. Moreover, one could take a look at the medians in order to safeguard that no outliers alter the correlation.

Next, after having finished the analysis and discussion of the measured data, the AERMOD modeling results are going to be presented in what follows.

4.7 AERMOD modeling results

In this subsection, various plot types are going to be utilized to illustrate the modeling results for two scenarios. One is based on the most realistic approach where the emission rate and source outflow speed is based on the daily volume outflow data of the WWTP. The second modeling results rest on a rather generic assumption of a constant flow calculated via geometric pipe parameters and average volume flows. This very constant for the geometric pipe conditions of 2018 resulted in a number more than one order of magnitude higher than the median of all daily volume flows provided. This in turn led to output $\mathrm{H_2S}$ concentrations at times up to two orders of magnitude higher than in the more realistic model approach.
Generally, it shall be anticipated here, that in the best approach available, the modeled $\mathrm{H_2S}$ concentrations never exceeded the threshold concentration of 0.00047 ppm (see table 1) in the residential area of interest. By contrast, in the approach assuming a constant sewage outflow, numerous events were modeled which exceeded this perception threshold, but in no case reached levels hazardous to health. As far as the nomenclature of the following modeling results is concerned, they will be distinguished by using the names "Best modeling results" and "Alternative modeling results".
Hereinafter, odor maps with contour plots are going to be displayed.

4.7.1 Odor contour maps

In this subsection, the focus will lie on the most suitable model approach based on daily volume flow data. In the end, one exemplary period will be shown which was produced by the less reasonable input data in order to give the reader an idea of the differences regarding the modeled concentration ranges. The graphics stem from Google Earth figure outputs with an overlaid georeferenced receptor network produced by AERPLOT, which is a post-processor of AERMOD. AERPLOT creates Google Earth-native kmz-files with the output data containing the maximum values of each receptor point of the network. These maxima will then make up the diamond-like colored points superimposed to the Google Earth satellite picture. As for the colors, they are automatically created by AERPLOT with the aim to map the concentration range from highest in dark red to lowest in dark blue. The legend labels were not automatically created wherefore it was necessary to label them by hand. To this end, receptor points of the same color were compared value-wise, then a value was assigned to the color. Nonetheless, especially concerning the low values in dark blue, it needs to be mentioned here that the partitioning is not very exact: for instance, some values in dark blue could be around 0.0008 mg/m^3 and other around 0.00001, in particular those receptor locations further away from the source. To put more emphasis on the higher values and consequently the closer receptor points, the dark blue values were labeled according to the higher end of the range among the locations assigned with this color.
Regarding the concentration unit, here, as opposed to the rest of this document, they are given in milligrams per cubic meter (mg/m^3), as the AERMOD output is designed as decimal powers of grams per cubic meter. The limit perception value in this unit is then 0.0007 mg/m^3, which is equivalent to the aforementioned 0.00047 ppm (see table 1).

Best modeling results

To begin with, the first period (see fig. 75) during the high summer season in July 2018 does not show any non-zero $\mathrm{H_2S}$ concentrations apart from 5-10 meters next to the main emission source, whereas the other three measuring periods (depicted in figure 76, 77 and 78) comprise of more variation and thus also of a real contour map which contains dropping concentrations with growing distance to the canalization entrance. Regarding the model results of the period in July 2018, it can

be speculated that it might have been due to missing meteorological input data just in hours of high odorant potential. This scenario makes sense since especially the upper air radiosonde data for the vertical atmospheric profile consisted of a higher percentage of missing values than usual during this period, and as a consequence, AERMOD skips these hours and puts out a concentration of 0 at all receptor locations without further calculation.

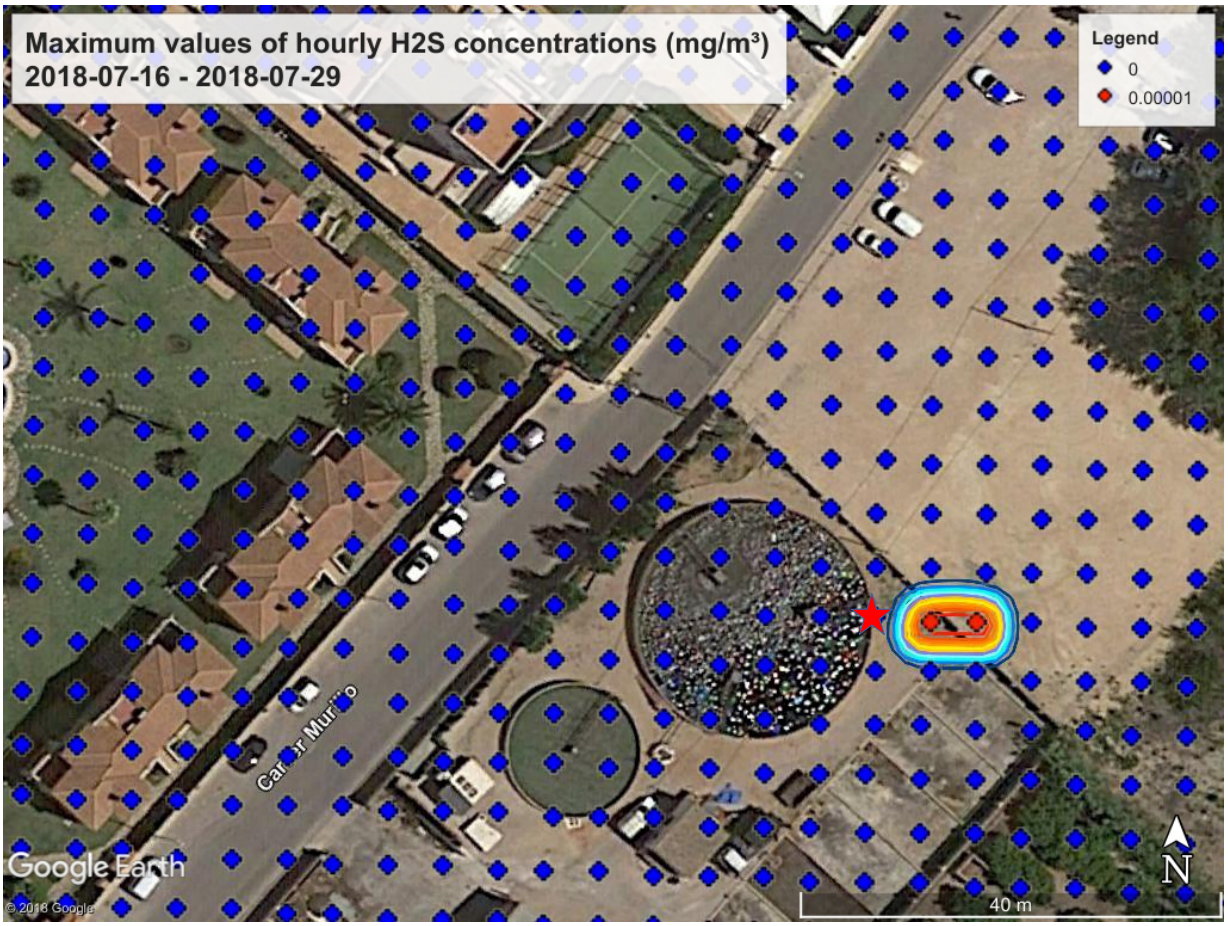

Figure 75: Contour map of modeled H_2S concentrations in mg/m³ during the first measurement period from 2018-07-16 till 2018-07-29. The square receptor grid has a spatial resolution of 5x5 m² and an edge length of 400 meters. Additionally, the point source, i.e. the canalization entrance, is marked with a red star. Regarding the legend, the colors go from dark blue to dark red in ascending order from the lowest to the highest gas concentrations. The values assigned to each color listed in the legend represent an average value; in other words, not all receptor points marked with say dark blue actually have the very same value of the associated legend label.

According to the modeled concentrations (see fig. 76) based on data between 31 August and 14 September 2018, perceptible odorant concentrations occurred at least once in the direct surroundings of the main emission source. This can be seen when looking at the legend, which contains concentration values all above the threshold limit of 0.0007 mg/m³ except for the darkest blue color, i.e. the uppermost legend element. This very color is associated to the majority of the receptor points depicted in graph 76 and thus lie outside the last contour line. This in turn means, that, according to the model results, the residential area was not affected by perceptible odorant concentrations during that period in the end of the high summer season 2018.

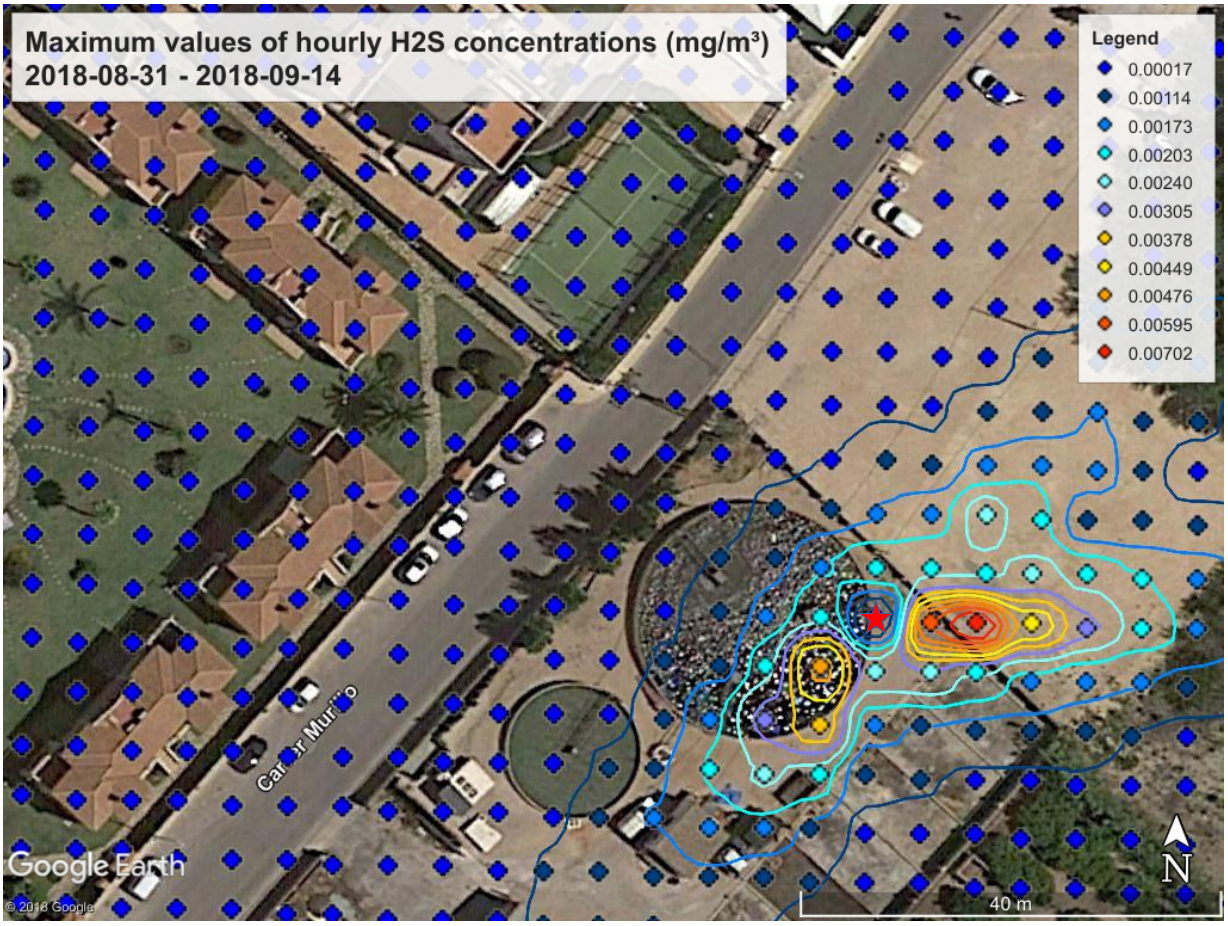

Figure 76: Contour map of modeled H_2S concentrations in mg/m³ during the second measurement period from 2018-08-31 to 2018-09-14. The square receptor grid has a spatial resolution of 5x5 m² and an edge length of 400 meters. Additionally, the point source, i.e. the canalization entrance, is marked with a red star. Regarding the legend, the colors go from dark blue to dark red in ascending order from the lowest to the highest gas concentrations. The values assigned to each color listed in the legend represent an average value; in other words, not all receptor points marked with say dark blue actually have the very same value of the associated legend label.

For the last period from 17 September till 2 October (see fig. 77) of the first measurement campaign in 2018 the same holds true as for the period in the beginning of September displayed in graph 76. Both the value range and spatial extension of the contours are comparable.

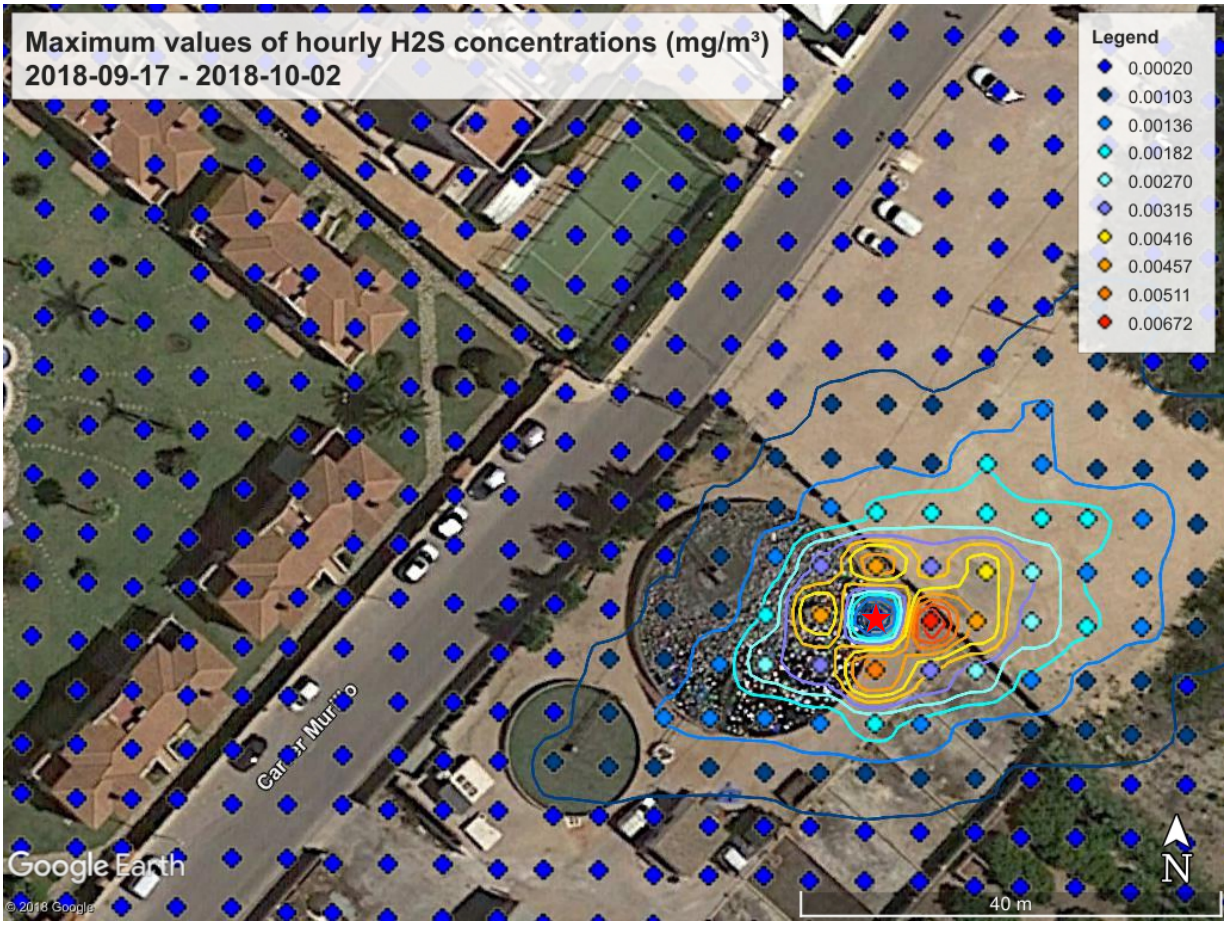

Figure 77: Contour map of modeled H_2S concentrations in mg/m³ during the third measurement period from 2018-09-17 to 2018-10-02, which was the last of the first measuring campaign in 2018. The square receptor grid has a spatial resolution of 5x5 m² and an edge length of 400 meters. Additionally, the point source, i.e. the canalization entrance, is marked with a red star. Regarding the legend, the colors go from dark blue to dark red in ascending order from the lowest to the highest gas concentrations. The values assigned to each color listed in the legend represent an average value; in other words, not all receptor points marked with say dark blue actually have the very same value of the associated legend label.

As opposed to the just mentioned graphs 76 and 77, the one and only period of the second measuring campaign in 2019 from 3 April till 3 June (see fig. 78) shows a wider range of concentration values. Moreover, the spatial extension of the contours which represent perceptible odorant concentrations above 0.0007 mg/m³ is larger as well.
This might surprise at first, as the previously listed periods were during the middle and end of the summer season. On the other hand, taking into account that AERMOD's highest resolution is 1 hour and that it does not calculate anything during each hour during which e.g. some meteorological or concentration input variable is missing, it can be understood that a longer modeling period increases the probability of events to be recorded and then modeled. This could have been the case when contrasting the 2-month period in 2019 and the three isolated 2-weeks periods in 2018.

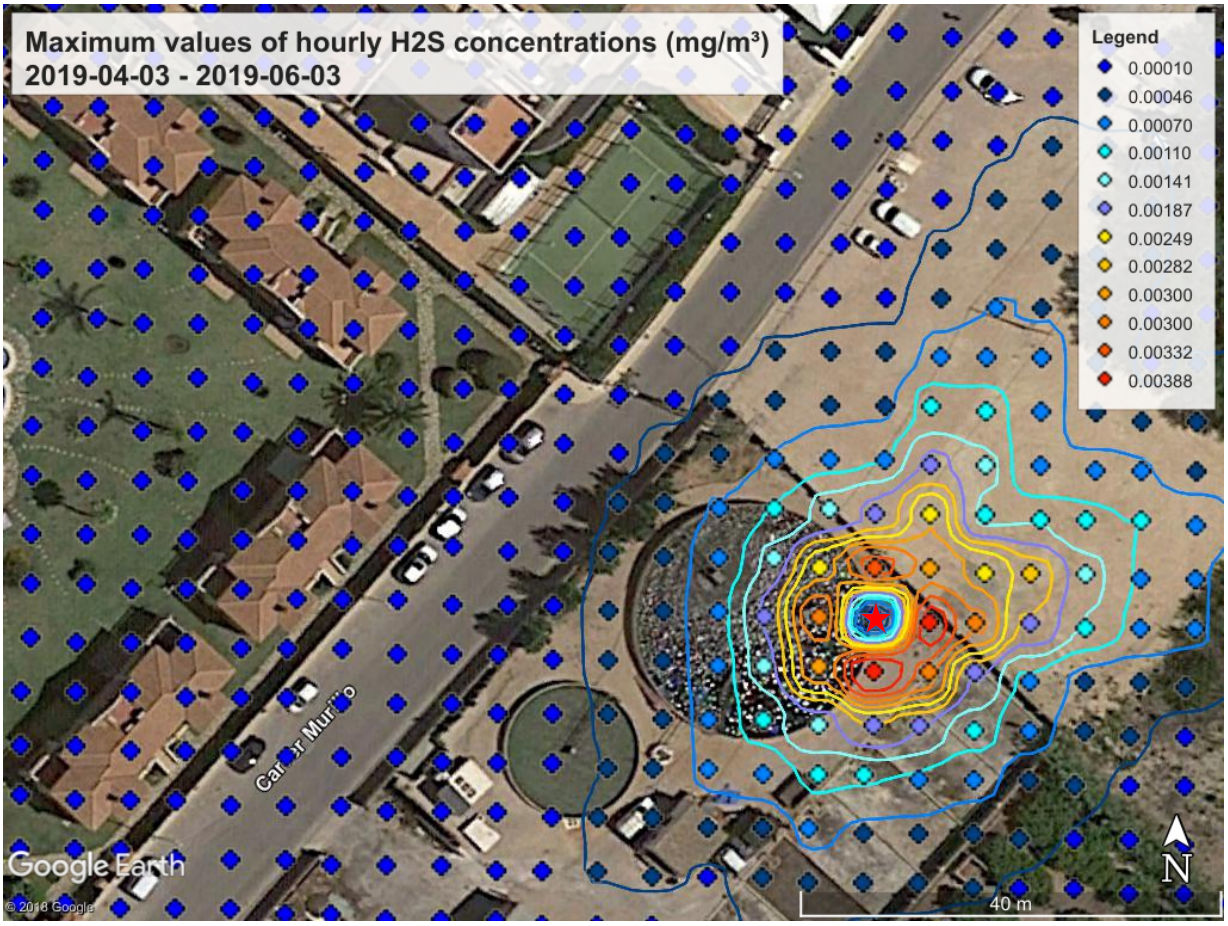

Figure 78: Contour map of modeled H_2S concentrations in mg/m³ during the only measurement period of the second campaign from 2019-04-03 to 2019-06-03. The square receptor grid has a spatial resolution of 5x5 m² and an edge length of 400 meters. Additionally, the point source, i.e. the canalization entrance, is marked with a red star. Regarding the legend, the colors go from dark blue to dark red in ascending order from the lowest to the highest gas concentrations. The values assigned to each color listed in the legend represent an average value; in other words, not all receptor points marked with say dark blue actually have the very same value of the associated legend label.

Alternative modeling results

In the following, the maximum value model outputs for each receptor location of the rectangular receptor network modeled during the first 2-week measuring period in July 2018 is displayed (see fig. 79).

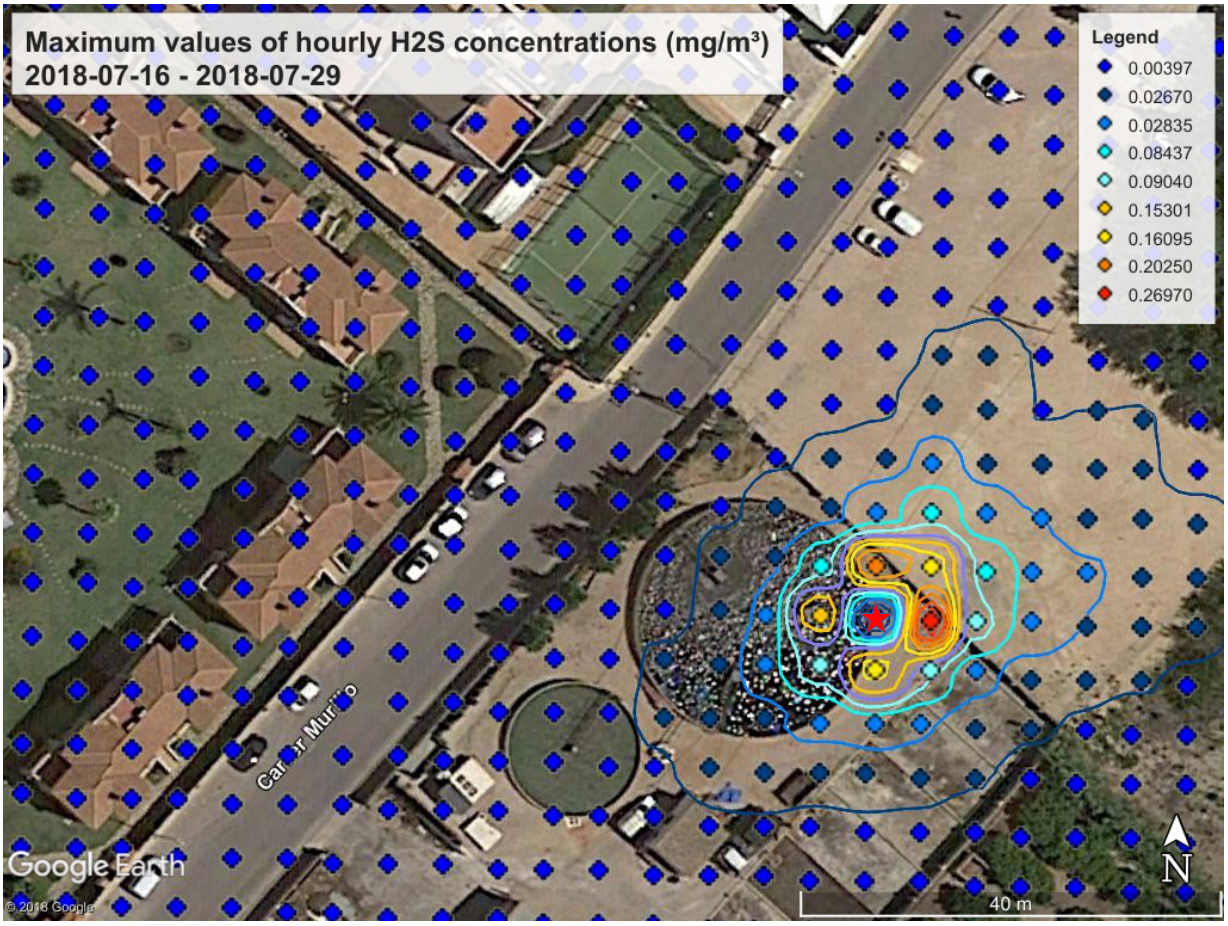

Figure 79: Contour map of modeled H_2S concentrations in mg/m³ during the first measuring period from 2018-07-16 till 2018-07-29; this time with the alternative model output data. The concentrations are up to two orders of magnitude higher compared with those in figure 75, 76, 77 and 78. As before in the previously listed figures, the square receptor grid has a spatial resolution of 5x5 m² and an edge length of 400 meters. Additionally, the point source, i.e. the canalization entrance, is marked with a red star. Regarding the legend, the colors go from dark blue to dark red in ascending order from the lowest to the highest gas concentrations. The values assigned to each color listed in the legend represent an average value; in other words, not all receptor points marked with say dark blue actually have the very same value of the associated legend label.

From this graph it is evident that the concentration values are significantly higher; even the maxima at the receptor locations of the nearest buildings show H_2S values above the perception threshold of 0.0007 mg/m³. Under these circumstances, it would be straightforward to argue that the complaints due to odor nuisance can be validated by the model. However, it is paramount to bear in mind that these results are based on the rather imprecise assumption of a constant volume inflow which was derived by annual average flow rates and pipe geometry, whereas the other results were calculated by employing the daily volume outflow data. As the reader can see, with the first approach modeled concentrations were always below the perception threshold at the residential dwellings, whereas in the second output version (see e.g. fig. 79) this threshold was crossed on a regular basis during the modeled periods.
At any rate, in the following both output data versions are going to be considered, as due to more non-zero concentration values the second (rather unrealistic) approach serves for deriving connected

meteorological conditions, which in combination with airborne odorant emissions give rise to odor nuisance also in the residential areas.

4.7.2 Descriptive statistics based on 5 specific receptor locations

In the following, several descriptive statistics graphics on the basis of 5 particular receptor locations, which are depicted in figure 80, are going to be displayed. These points were chosen in order to properly represent the emission source, the control house of the WWTP-site workers and the closest boundary of the affected residential area beginning from the other side of the street "Carrer Murillo" (see also fig. 79). As for the nomenclature, the relative coordinates are given as usual in a Kartesian 2D-system like (x, y).

"Bioreactor entrance": (5.0, 0.0)

"Control house entrance": (-20.0, -20.0)

"Hotel sporting place": (-30.0, 40.0)

"Domicile 1 closest": (-50.0, 5.0)

"Domicile 2 toward hotel" (-45.0, 25.0)

As an aside, these coordinates are defined relative to the origin (0, 0) which represents the only emission source of the WWTP Camping San Fernando: the canalization entrance. What is more, the subplots related to each point of interest are ordered by distance to the emission source in ascending order within each graphic. This order is the same as in the aforementioned list 4.7.2.

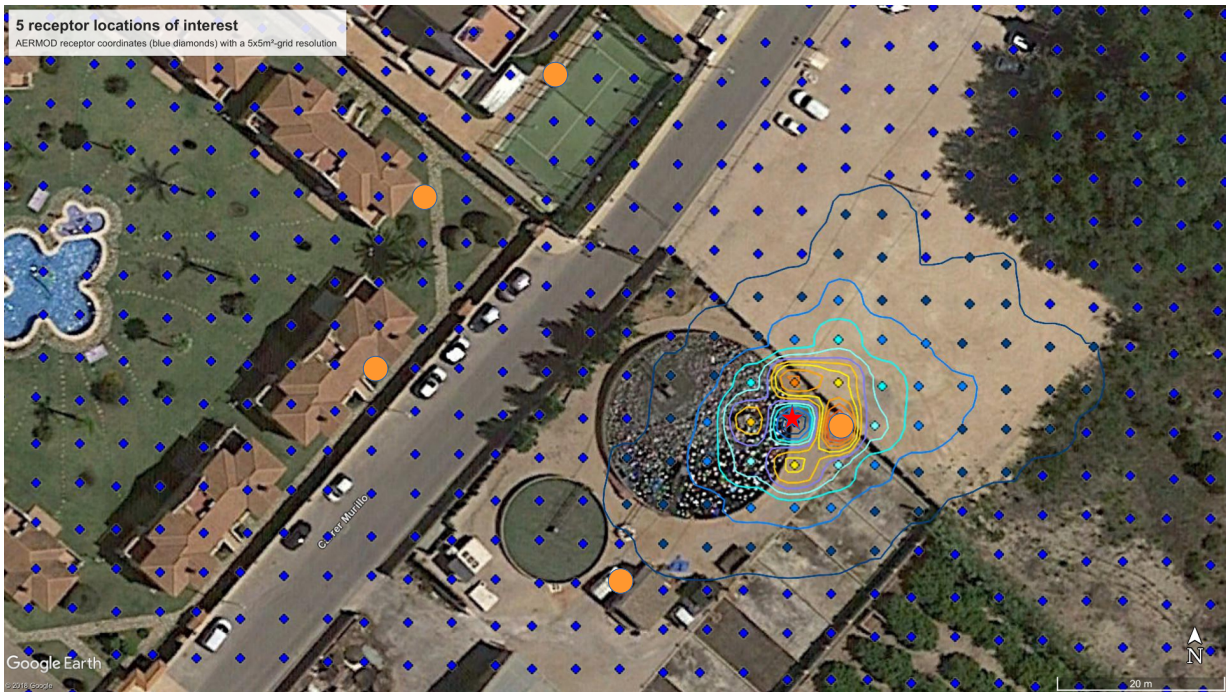

Figure 80: Contour map with focus on 5 receptor locations of interest highlighted as non-transparent orange circles. The relative receptor coordinates can be revisited in the list 4.7.2. Besides, the point emission source is marked again with a red star.

Hereinafter, in paragraph 4.7.2, aggregated hourly mean and maximum concentration values are superimposed at daily scale in order to illustrate possible daily recurring patterns.

Aggregated hourly mean and maximum $\mathbf{H_2S}$ concentrations displayed at daily scale

In this paragraph, not only the hourly H_2S means, but also the maxima of the same modeling periods are going to be outlined. This additional way of displaying the daily patterns shall underline the fact that the previously shown means did not obscure any important H_2S peaks. The latter effect happened when examining the *measured* data from the main emission source by employing mean and maximum aggregation methods: as the peaks were so selective, the mean was mainly dominated by the commonly low concentrations.
To avoid this possibility, the hourly maxima are illustrated in figure 82, 84 and 86. Of these figures, the first is associated with the best model results on the basis of daily volume flow data, whereas the latter two graphics are related to the alternative output data.

To begin with, the most accurate modeling output will be presented.

Best modeling results

As for the other two periods of the first measurement campaign in 2018, similar results as displayed in 81 have been obtained. By contrast, during the 2-month period of the second campaign 2019, only the receptor location directly next to the canalization entrance showed a few non-zero H_2S-concentrations, wherefore no graphic for this particular period was generated.
As another side note it shall be mentioned, that in the case of the most meaningful model approach only output data of 2018 was available as during the second measuring campaign in 2019 all values were zero except for some concentrations directly adjacent to the canalization entrance. Consequently, just the first measuring period during July 2018 is portrayed in figure 82.
Besides that, as the non-zero output data has not been sufficient for each of the chosen points of interest in order to compute a 95%-confidence interval, particularly the points further from the emission source lack the CI-bands at times.

Next, when looking at the 5 different spots in the graphic 81, it can be seen that only the hourly mean H_2S concentrations which exceed the perception threshold of 0.00047 ppm (see table 1) belong to the receptor directly next to the bioreactor entrance. On the contrary, the other locations showed constantly imperceptible mean concentrations. Not even the hourly maximum concentrations of the other points of interest portrayed in figure 82. exceeded the perception limit, apart from the maximum at the control house entrance occurred at 22 o'clock. Only next to the canalization entrance, the maxima during the night were all above the perception threshold. It can also be seen, when looking at the morning hours from 3 to 6 o'clock, that the 95%-confidence interval of the mean plotted in figure 81 is notably influenced by outlying maxima (compare fig. 82).

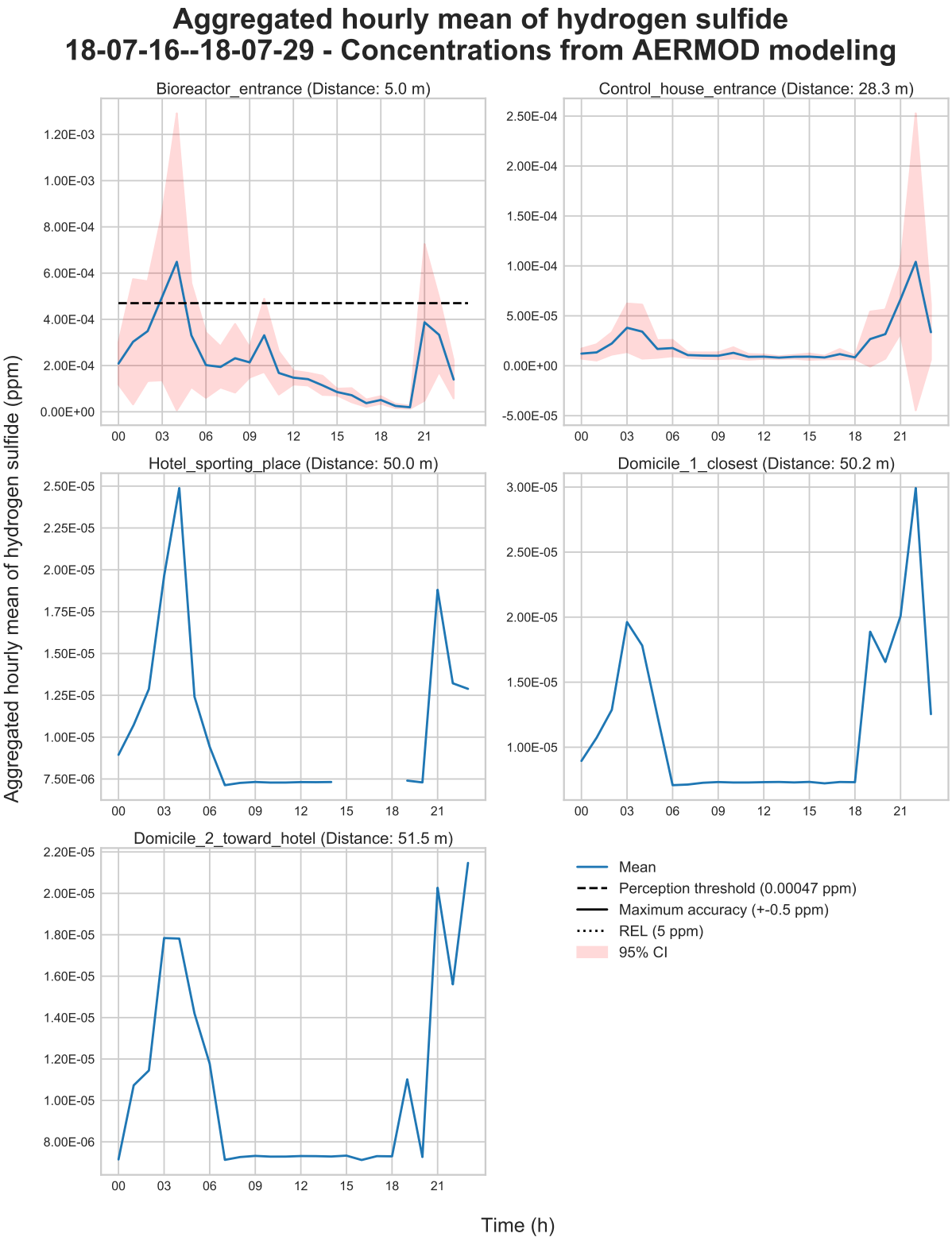

Figure 81: In this figure, each subplot belongs to one the 5 receptor locations of interest (see list 4.7.2 and map 80) sorted by distance to the emission source in ascending order from top to bottom. The plotted variable is the aggregated hourly mean concentration of hydrogen sulfide in ppm overlaid on a daily scale from hour 0 till 23; based on the modeling results of the first measurement period from 16 to 29 July 2018. The corresponding concentration values in mg/m³, obtained from the most sound modeling approach, are shown as an overlaid contour map in figure 75. With regard to the legend, particular concentration limits in ppm are embedded into the graphic; namely the recommended long-term exposure limit (or long-term REL) and perception threshold of the odorant, mentioned in subsection 2.2.3, and the maximum accuracy of the deployed measuring instruments explained in 3.1.1. The latter is still kept in the legend to maintain consistence and to enable the comparison with all previous characteristic values. Also, it is included the hourly mean and its associated 95%-CI band computed from every of the 24 mean values related to each hour of the day from 0 to 23 hours, where applicable.

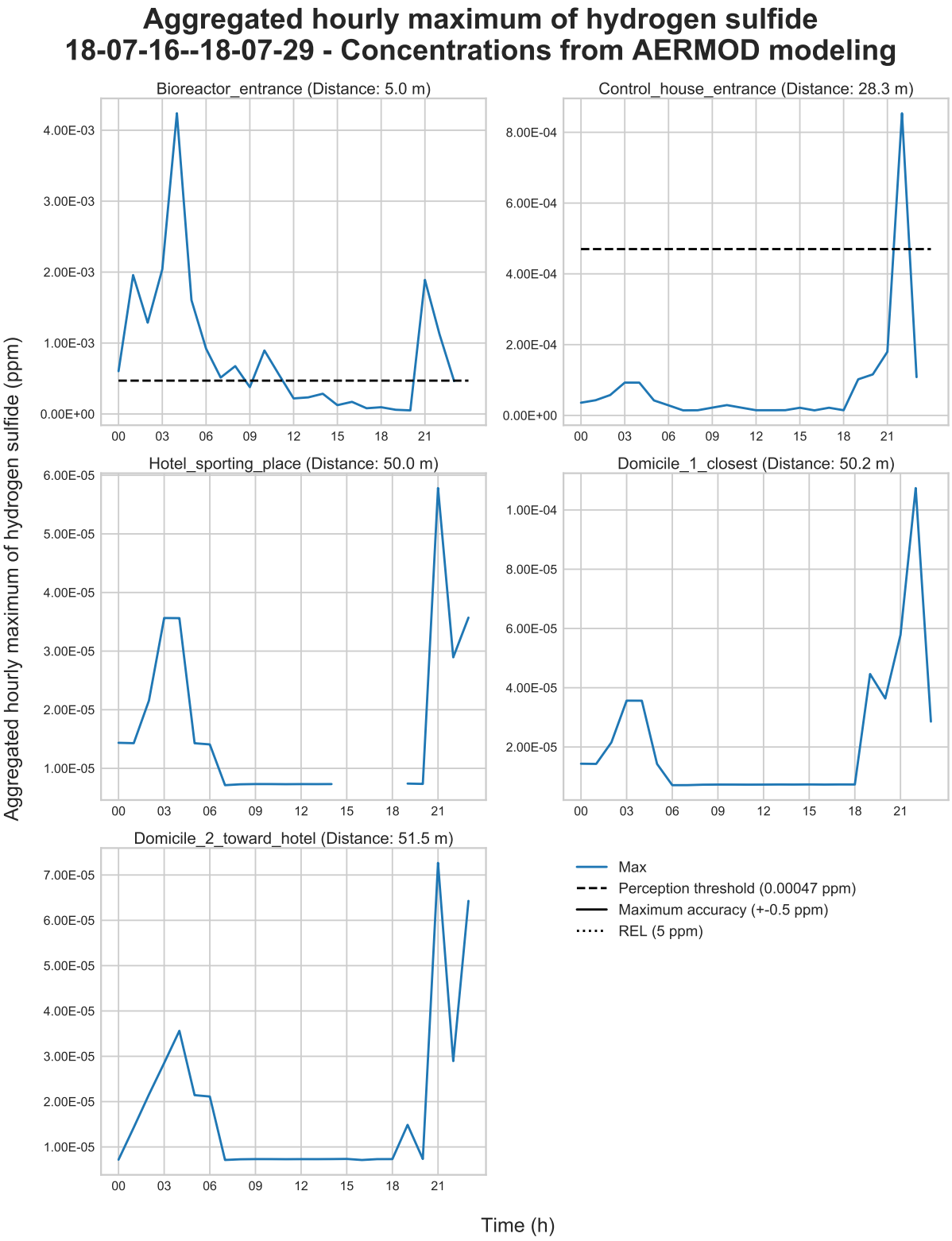

Figure 82: In this graphic, each subplot belongs to one the 5 receptor locations of interest (see list 4.7.2 and map 80) sorted by distance to the emission source in ascending order from top to bottom. The plotted variable is the aggregated hourly maximum concentration of hydrogen sulfide in ppm overlaid on a daily scale from hour 0 till 23; based on the modeling results of the first measurement period from 16 to 29 July 2018. The corresponding concentration values in mg/m³, obtained from the most sound modeling approach, are shown as an overlaid contour map in figure 75. With regard to the legend, particular concentration limits in ppm are embedded into the graphic; namely the recommended long-term exposure limit (or long-term REL) and perception threshold of the odorant, mentioned in subsection 2.2.3, and the maximum accuracy of the deployed measuring instruments explained in 3.1.1. The latter is still kept in the legend to maintain consistence and to enable the comparison with all previous characteristic values.

Alternative modeling results

In what follows, the mean and maximum statistics for the less plausible model results are going to be shown and discussed. The graphics 83 and 84 illustrate the aggregated hourly means and maxima of the same modeling period from 16 till 29 July 2018 as in the preceding paragraph.
It is apparent that, in comparison to the former figures 81 and 82 related to the best modeling approach, the alternative output comprises of mean concentrations around a bit more than one order of magnitude higher (see fig. 83). In fact, the distributions of the means are comparable to the maxima of the best model approach. As a consequence, the modeled $\mathrm{H_2S}$ means at the bioreactor entrance are almost entirely above the perception threshold. In addition, when looking at the hourly maxima 82 of the same measuring period in July 2018, even at the three distant spots located at the boundary of the residential area the late evening maxima surpass the threshold while the maxima during the night get close to it.

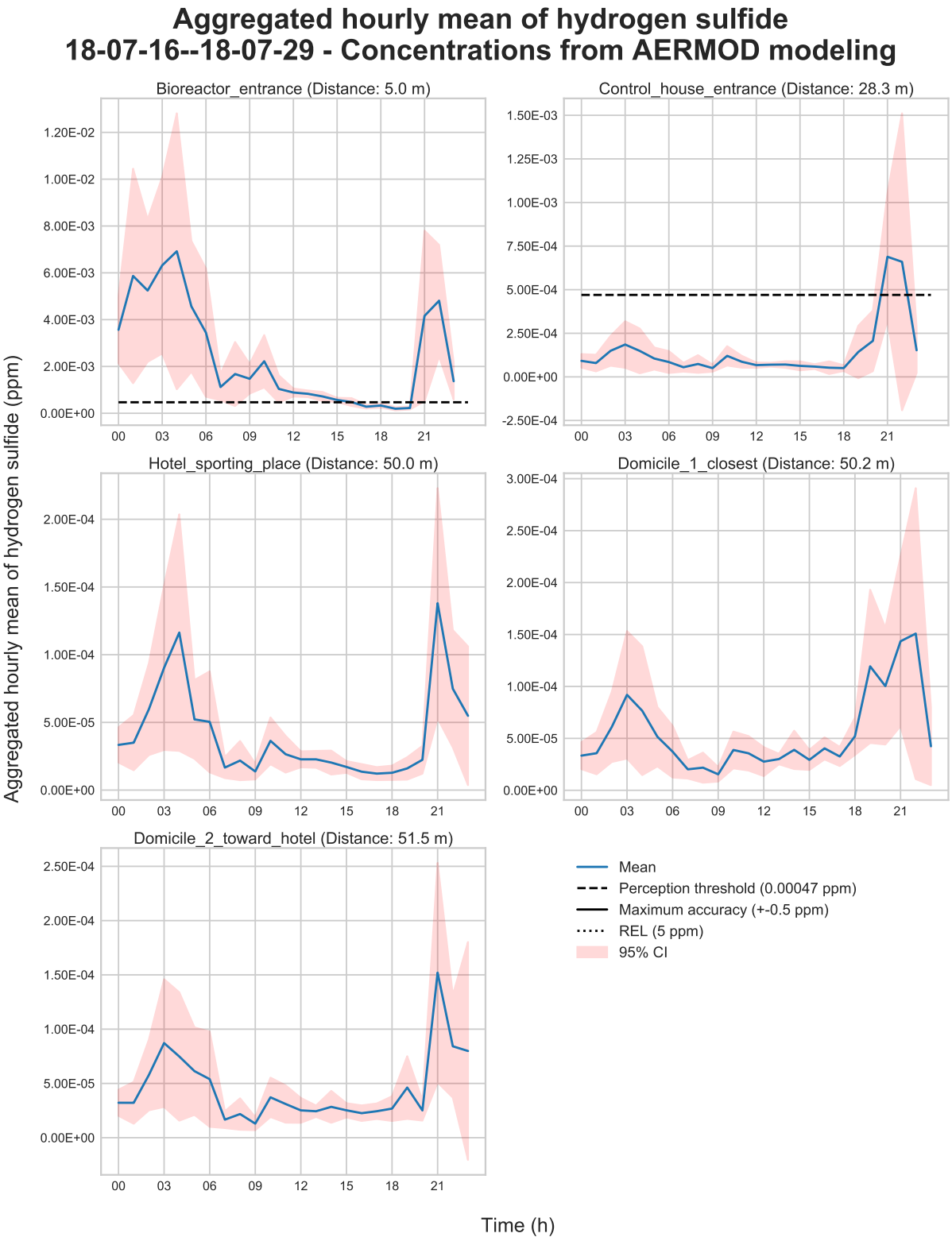

Figure 83: In this graph, each subplot belongs to one the 5 receptor locations of interest (see list 4.7.2 and map 80) sorted by distance to the emission source in ascending order from top to bottom. The plotted variable is the aggregated hourly mean concentration of hydrogen sulfide in ppm overlaid on a daily scale from hour 0 till 23; based on the modeling results of the first measurement period from 16 to 29 July 2018. The corresponding concentration values in mg/m³, obtained from the alternative modeling approach, are shown as an overlaid contour map in figure 79. With regard to the legend, particular concentration limits in ppm are embedded into the graphic; namely the recommended long-term exposure limit (or long-term REL) and perception threshold of the odorant, mentioned in subsection 2.2.3, and the maximum accuracy of the deployed measuring instruments explained in 3.1.1. The latter is still kept in the legend to maintain consistence and to enable the comparison with all previous characteristic values. Also, it is included the hourly mean and its associated 95%-CI band computed from every of the 24 mean values related to each hour of the day from 0 to 23 hours.

Figure 84: In this figure, each subplot belongs to one the 5 receptor locations of interest (see list 4.7.2 and map 80) sorted by distance to the emission source in ascending order from top to bottom. The plotted variable is the aggregated hourly maximum concentration of hydrogen sulfide in ppm overlaid on a daily scale from hour 0 till 23; based on the modeling results of the first measurement period from 16 to 29 July 2018. The corresponding concentration values in mg/m³, obtained from the alternative modeling approach, are shown as an overlaid contour map in figure 79. With regard to the legend, particular concentration limits in ppm are embedded into the graphic; namely the recommended long-term exposure limit (or long-term REL) and perception threshold of the odorant, mentioned in subsection 2.2.3, and the maximum accuracy of the deployed measuring instruments explained in 3.1.1. The latter is still kept in the legend to maintain consistence and to enable the comparison with all previous characteristic values.

Next, the modeling results of the 2-month period in 2019 from 3 April till 3 June are depicted in figure 85 and 86. When comparing the means in 85 with the former means in figure 81 one can see that all in all the concentrations are distributed over similar ranges, albeit especially the receptor locations more distant to the canalization entrance show more higher concentration events on average, which brings them closes to the threshold limit and lets them even exceed it during the most critical hours in the late evening and at night. Thus, as can be verified when looking at the hourly maxima in graph 86, they exceed the perception threshold at virtually every hour during the late evening and at night, even at the boundary of the residential dwellings.

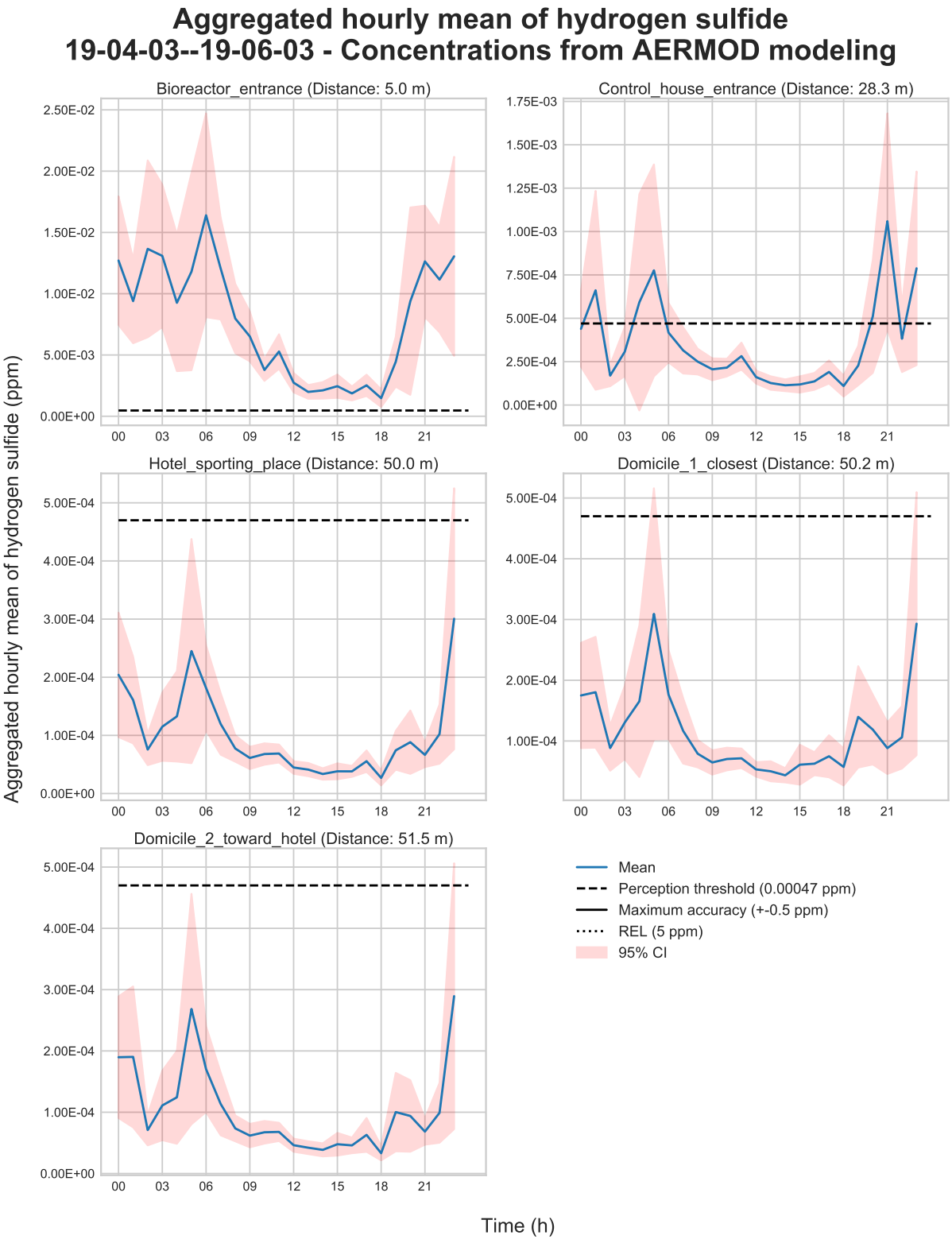

Figure 85: In this figure, each subplot belongs to one the 5 receptor locations of interest (see list 4.7.2 and map 80) sorted by distance to the emission source in ascending order from top to bottom. The plotted variable is the aggregated hourly mean concentration of hydrogen sulfide in ppm overlaid on a daily scale from hour 0 till 23; based on the alternative modeling results of the second measurement campaign from 3 April to 3 June 2019. With regard to the legend, particular concentration limits in ppm are embedded into the graphic; namely the recommended long-term exposure limit (or long-term REL) and perception threshold of the odorant, mentioned in subsection 2.2.3, and the maximum accuracy of the deployed measuring instruments explained in 3.1.1. The latter is still kept in the legend to maintain consistence and to enable the comparison with all previous characteristic values. Also, it is included the hourly mean and its associated 95%-CI band computed from every of the 24 mean values related to each hour of the day from 0 to 23 hours.

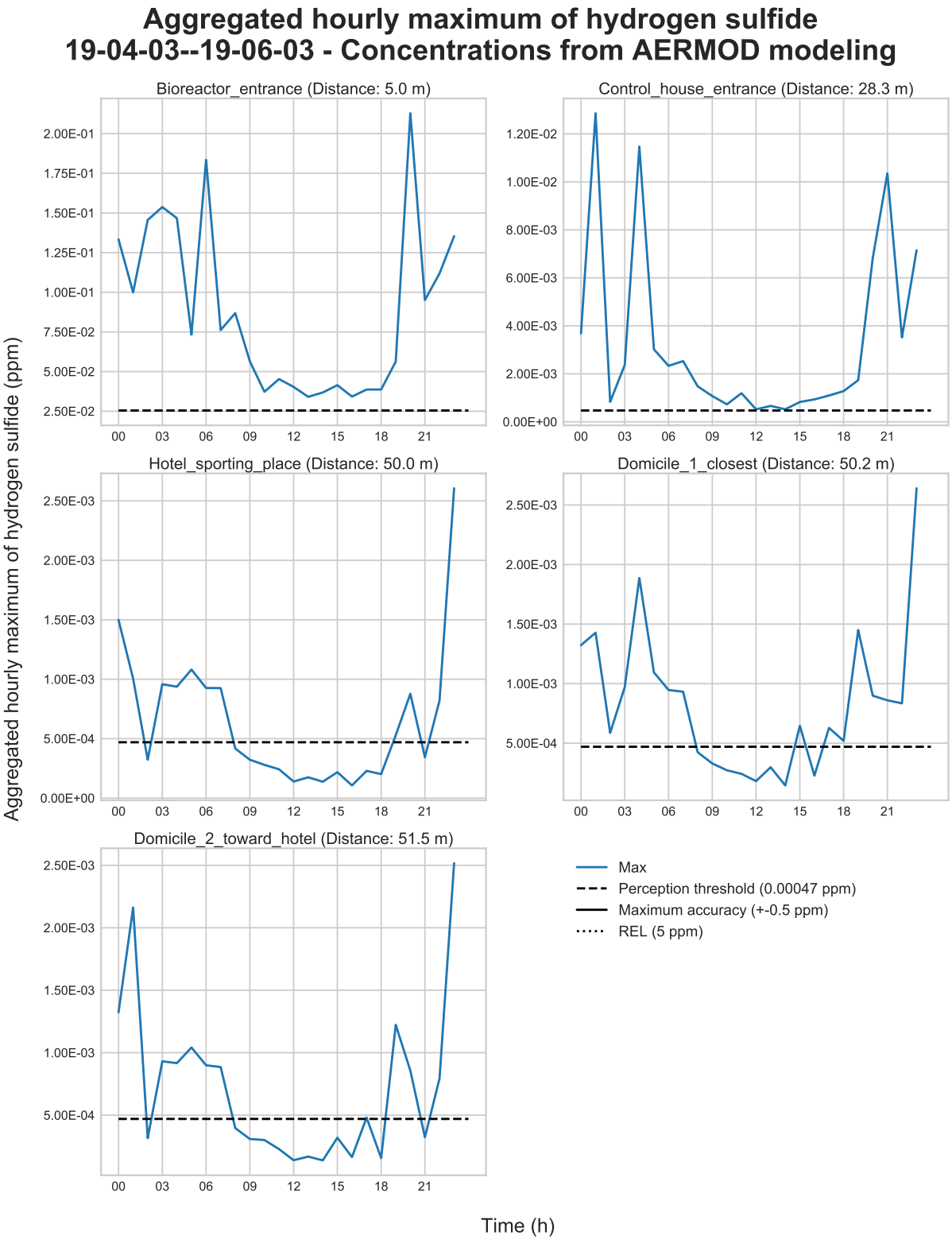

Figure 86: In this figure, each subplot belongs to one the 5 receptor locations of interest (see list 4.7.2 and map 80) sorted by distance to the emission source in ascending order from top to bottom. The plotted variable is the aggregated hourly maximum concentration of hydrogen sulfide in ppm overlaid on a daily scale from hour 0 till 23; based on alternative the modeling results of the second measurement campaign from 3 April to 3 June 2019. With regard to the legend, particular concentration limits in ppm are embedded into the graphic; namely the recommended long-term exposure limit (or long-term REL) and perception threshold of the odorant, mentioned in subsection 2.2.3, and the maximum accuracy of the deployed measuring instruments explained in 3.1.1. The latter is still kept in the legend to maintain consistence and to enable the comparison with all previous characteristic values.

As an anticipated conclusion it can be deduced that, by considering the less realistic model approach as a worst case scenario for the WWTP Camping San Fernando, it is possible that residents living in the dwellings of concern are able to perceive odors caused by hydrogen sulfide emissions from the canalization entrance into the open-air bioreactor of the WWTP. This is particularly true for the hours between around 19 and 7 o'clock, i.e. from the evening until the early morning.
On the other hand, the most accurate modeling results based on the daily volume flow data state that the above-mentioned dwellings do not receive sufficiently high odorant concentrations in order to be perceptible by the residents.

Modeled hydrogen sulfide concentration distributions at 5 spots of interest

Finally, in order to sustain the just mentioned arguments in terms of the probability that perceptible H_2S concentrations do or do not reach the residential areas, depending on the model approach, empirical cumulative distribution functions (ECDFs) of the same data as discussed before were created. In graphic 87, all modeled non-zero H_2S concentrations are plotted sorted from minimum to maximum at each of the 5 points of interest during the period from 16 to 29 July. It can be seen that almost 88% of the data next to the emission source lie below the perception threshold, whereas at the other spots practically all values lie below this limit.
In figure 88 though, during the 2-month period in 2019 assuming the alternative modeling input, it can be derived that at every place a clear non-zero percentage of the events lies above the perception limit; even at the residential dwellings of concern.

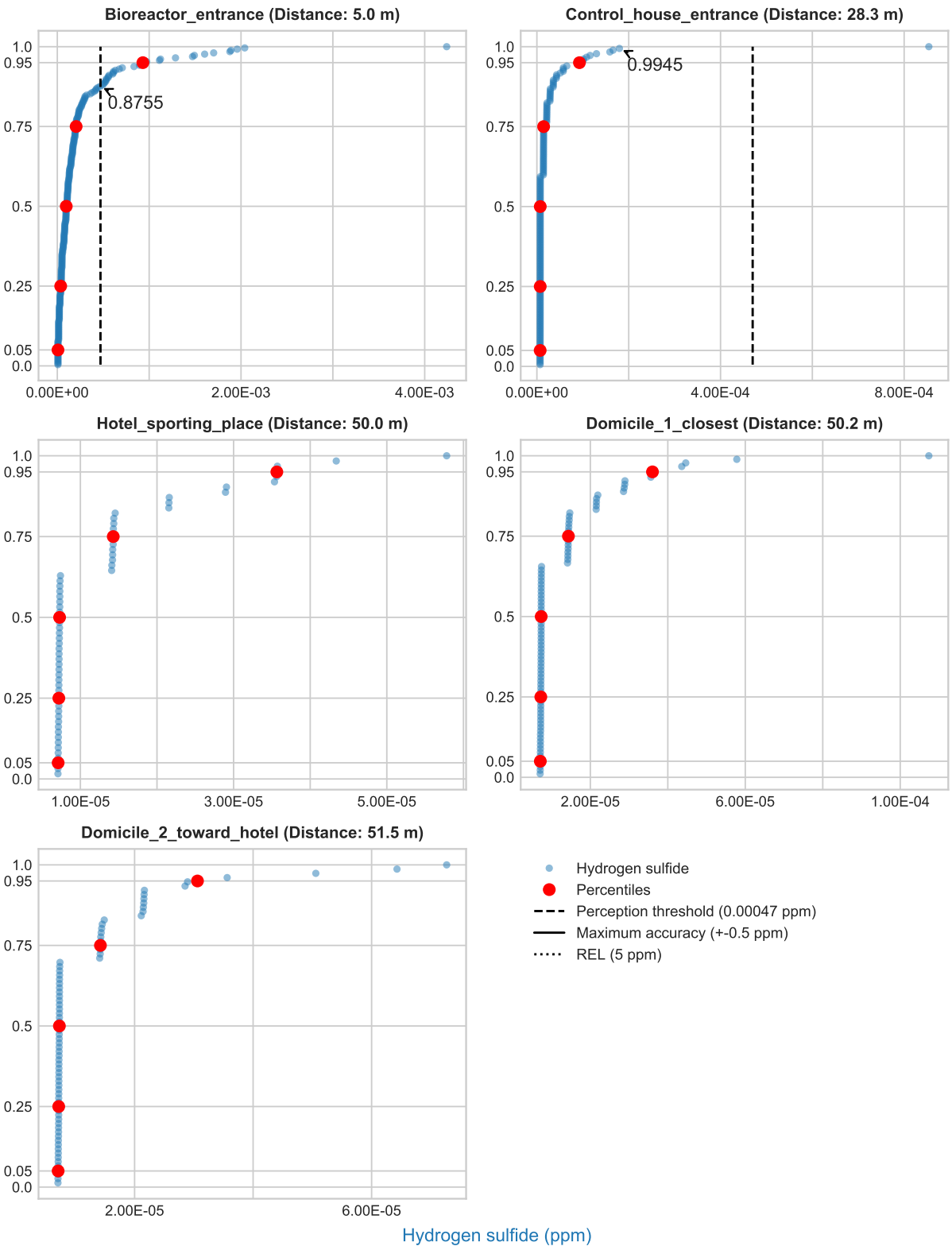

Figure 87: In this figure, each ECDF-subplot belongs to one the 5 receptor locations of interest (see list 4.7.2 and map 80) sorted by distance to the emission source in ascending order from top to bottom. The plotted variable is the modeled concentration of hydrogen sulfide in ppm, whereby the zero-values are not part of the dataset employed here, in the same way as the other model output graphics before. These data stem from the modeling results of the first measurement period from 16 to 29 July 2018. The corresponding concentration values in mg/m³, obtained from the most sound modeling approach, are shown as an overlaid contour map in figure 75. With regard to the legend, particular concentration limits in ppm are embedded into the graphic; namely the recommended long-term exposure limit (or long-term REL) and perception threshold of the odorant, mentioned in subsection 2.2.3, and the maximum accuracy of the deployed measuring instruments explained in 3.1.1. The latter is still kept in the legend to maintain consistence and to enable the comparison with all previous characteristic values.

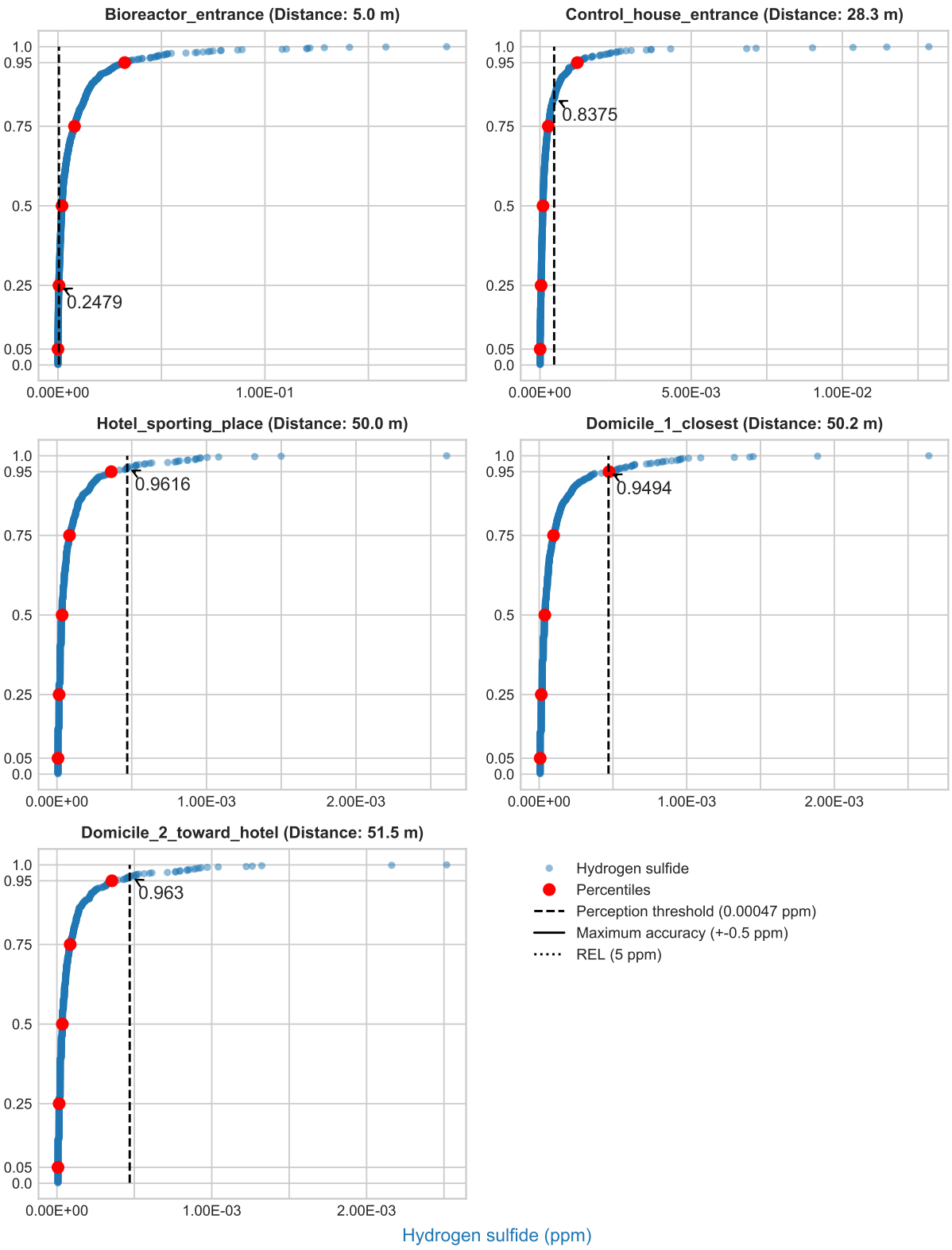

Figure 88: In this graph, each ECDF-subplot belongs to one the 5 receptor locations of interest (see list 4.7.2 and map 80) sorted by distance to the emission source in ascending order from top to bottom. The plotted variable is the modeled concentration of hydrogen sulfide in ppm, whereby the zero-values are not part of the dataset employed here, in the same way as the other model output graphics before. These data stem from the alternative modeling results of the last measurement period from 3 April to 3 June 2019. With regard to the legend, particular concentration limits in ppm are embedded into the graphic; namely the recommended long-term exposure limit (or long-term REL) and perception threshold of the odorant, mentioned in subsection 2.2.3, and the maximum accuracy of the deployed measuring instruments explained in 3.1.1. The latter is still kept in the legend to maintain consistence and to enable the comparison with all previous characteristic values.

4.7.3 Alternative model data filtered spatially for the residential area - Coincident modeled and measured hydrogen sulfide, wind and other data

As mentioned before in subsection 4.7.1 which showed the odor contour maps, the AERMOD-native concentration output unit are decimal powers of grams per cubic meter (mg/m^3). By contrast, the values provided by the gas measuring instruments were all in parts per million (ppm). Therefore, a conversion of the AERMOD output via the ideal gas law to ppm was indispensable in order to compare the measured and modeled H_2S concentrations soundly in the same graphics. To this end, the 5-minute meteorological data measured at the AVAMET station "Dénia Platja de Pego" was utilized to compute the molar volume of H_2S, in particular the atmospheric surface pressure and the associated temperature. This time, as opposed to paragraph 4.7.2, not a discrete selection of points but an entire area was picked out of the total provided by the rectangular 5x5 m^2 - resolution grid with an edge length of 400 meters encompassing the WWTP-site and the adjacent residential areas. The selected area comprises of the residential dwellings where the complaints due to odor nuisance came from. Graph 89 displays the area of interest covered in transparent orange, beginning from the opposite side of the street "Carrer Murillo" from the perspective of the WWTP-site.

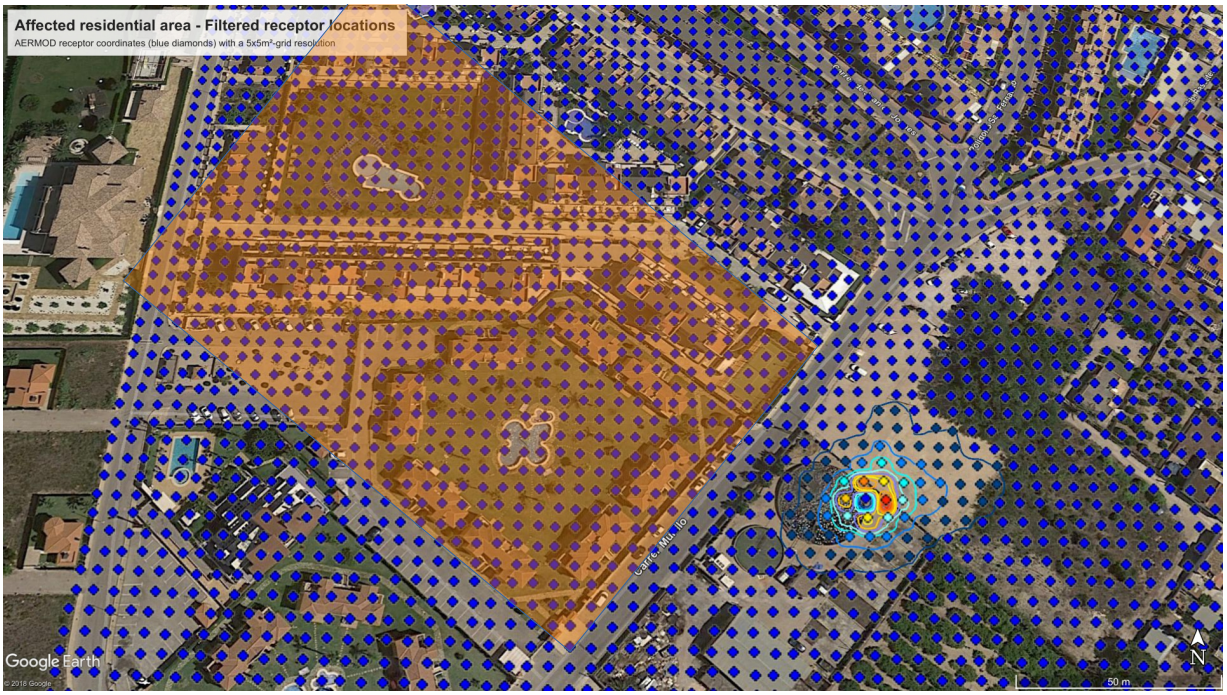

Figure 89: Satellite top view of the WWTP Camping San Fernando and its surroundings with the receptor network overlaid. The network grid comprises a spatial resolution of 5x5 m^2 and an edge length of 400 meters. The focus here lies on the residential area in question marked in transparent orange. The complaints due to odor nuisance were lodged from housings within the highlighted area, rather in the eastern part toward the WWTP site, which can be distinguished by means of the center of the plotted contours.

First and foremost, it must be said clearly that the filtering results of all modeled H_2S concentrations of the residential area of interest were entirely zero with the modeling output obtained from the most realistic approach, i.e. no concentrations above the threshold of 0.00047 ppm (see table 1) happened in none of the four measuring periods in 2018 and 2019.
Hence, the following graphics are based on the alternative modeling outputs. As stated before, those

rest upon an assumption of a constant sewage flow around 1 order of magnitude higher than the median of the daily volume flow data for the entire periods. This assumption affects directly the emission rate and its related outflow speed at the emission source.
Notwithstanding, the graphs related to the two exemplary periods "18-07-16–18-07-29" (see fig. 90 and 91) and "19-04-03–19-06-03" (see graphs 92 and 93) allow for interpreting correlations between several input and output variables, wherefore they are of significance despite the fact that the alternative model outputs were employed.
Before starting with the detailed discussion, it shall be mentioned previously what kind of data are going to be seen in these plots. The applied filters were both spatial and concentration related, i.e. all modeled $\mathrm{H_2S}$ concentration above the perception threshold of 0.00047 ppm (see table 1) and all receptor locations situated in the residential area of interest were admitted, the rest discarded. Now, the related wind direction, wind speed and hourly maxima of the measured $\mathrm{H_2S}$ concentrations were plotted along with the filtered receptor points and modeled concentrations. Finally, apart from the output variable "Hydrogen sulfide modeled", the derived "Distance" from the main emission source based on the two-dimensional rectangular receptor network, and the hourly aggregated model input variables "Wind speed mean", "Wind direction mean" and "Hydrogen sulfide hourly maxima", the associated "Hour" of each of these observations is plotted as well in order to derive daily patterns. Furthermore, the continuous variables "Distance" and "Hydrogen sulfide modeled" appear as a rather smooth continuous ECDF which is due to the fact that all values stem from unique observations within the employed compound data frame, whereas the model input variables (wind and gas measurements) are hourly aggregated data which occur repeatedly for different modeling receptor points (x, y) which showed a different modeled $\mathrm{H_2S}$ concentration at the same timestamp. In other words, as the same input values of one specific timestamp are assigned to all output $\mathrm{H_2S}$ values occurring individually at all receptor locations, the result is that there are many more unique values in the output than in the input, which can be derived from the forthcoming graphics in this subsection.
As for the plot types, both periods "18-07-16–18-07-29" and "19-04-03–19-06-03" and the just mentioned variables are depicted as ECDFs to show their values' distributions and as chronological sequences with one shared time axis. The intention of this is to facilitate the intercomparison of these related input and output variables.

Measurement period: 16 - 29 July 2018

To begin with, the period from 16 till 29 July 2018 was chosen as it is representative for high summer season conditions, which is characterized by early morning, night and late evening $\mathrm{H_2S}$ concentration peaks in comparison to lower values during the day. As can be seen in graphic 90, the hourly maximum input concentrations at the emission source were mainly above the long-term REL ("Recommended Exposure Limit", see 2.2.3), which leads to the conclusion that there must be a considerable $\mathrm{H_2S}$ peak at the emission source in order to have a perceptible effect in the residential area. Apart from that, the distribution of the hours clearly demonstrates that around 85% of the odor incidents at the residential dwellings happened during the last 4 hours of the day. The remaining events occurred during the night and during daytime there was no event at all. When assuming commonplace working and school schedules, the residents can be affected especially in the evening and early night, when they are supposedly at home. Particularly in summer, when windows are left open and people normally spend time outside on their balcony, their terrace or garden, the probability of being subjected to an odor nuisance is even higher.
Regarding the wind speed, according to the data it does not seem necessary for a strong wind to blow; it is rather the present direction which is important. For example in the current figure 90,

approximately 95% of the hourly mean wind speeds were below 5 m/s. In addition, the direction pointed in around 50% of the cases exactly in direction of the dwellings, but also in almost 1 out of 4 incidents in the opposite direction.

Following up on the discussion about the wind directions, it can be derived that during the summer period the wind directions indeed stabilize often toward the residential area in question, especially during the evening and early night (see subsection 4.4.1). On the other hand, the wind directions sometimes do not fit directly the direction from the emission source toward the dwellings, which could be explained by turbulence considerations and other effects which differ from the current mean wind direction. Apart from that, it is also noteworthy that the model's minimum time delta is one hour which leaves out temporal information about possible wind direction changes within every hour as it assumes a mean value instead. Moreover, the wind data were not measured directly on-site, but from meteorological stations mentioned above (see subsection 3.4). The input surface meteorological data was constructed as a mixture of these stations in the order of preference, as listed in the aforementioned subsection 3.4, in order to obtain low percentage of "missing meteo data" in the AERMOD model. Usually, the conditions at these different stations were sufficiently comparable, but nevertheless it is possible that the wind direction might differ in some occasions.

A better understanding regarding the discrepancy of some mean wind directions related to odor events at the dwellings gives figure 91. Here, the depiction of the chronological sequence allows for drawing new conclusions which were not visible in the empirical cumulative distributions displayed in graph 90.

For instance, the number of threshold-exceeding odorant concentrations at distinct receptor coordinates differs a lot with changing wind direction and speed. It could be interpreted that the wind speed needs to be higher, when the direction does not fit the orientation from the source toward the dwellings, in order to transport the gas a longer trajectory with still perceptible concentrations. This can be seen in the last days of the time line, from 28 till 30 July 2018.

On the other hand, lower mean wind speeds can also be sufficient to carry the gas a long way, provided that the wind blows exactly in the direction of the dwellings as seen from the emission source, As a general tendency, it can be verified when looking at the values related to approximately 23 July 2018 (in figure 91).
In addition, as one might assume, the initial concentration emitted at the source also plays a role in the question how far away the pollutant can still be perceived. Nevertheless, when looking at the various incidents displayed in figure 91, the wind is the determining factor. This can be seen in certain events, such as on 28 July 2018, when the odorant traveled further with a lower initial concentration at the source than in another event, which can then be explained by the increased wind speed during that moment of time.

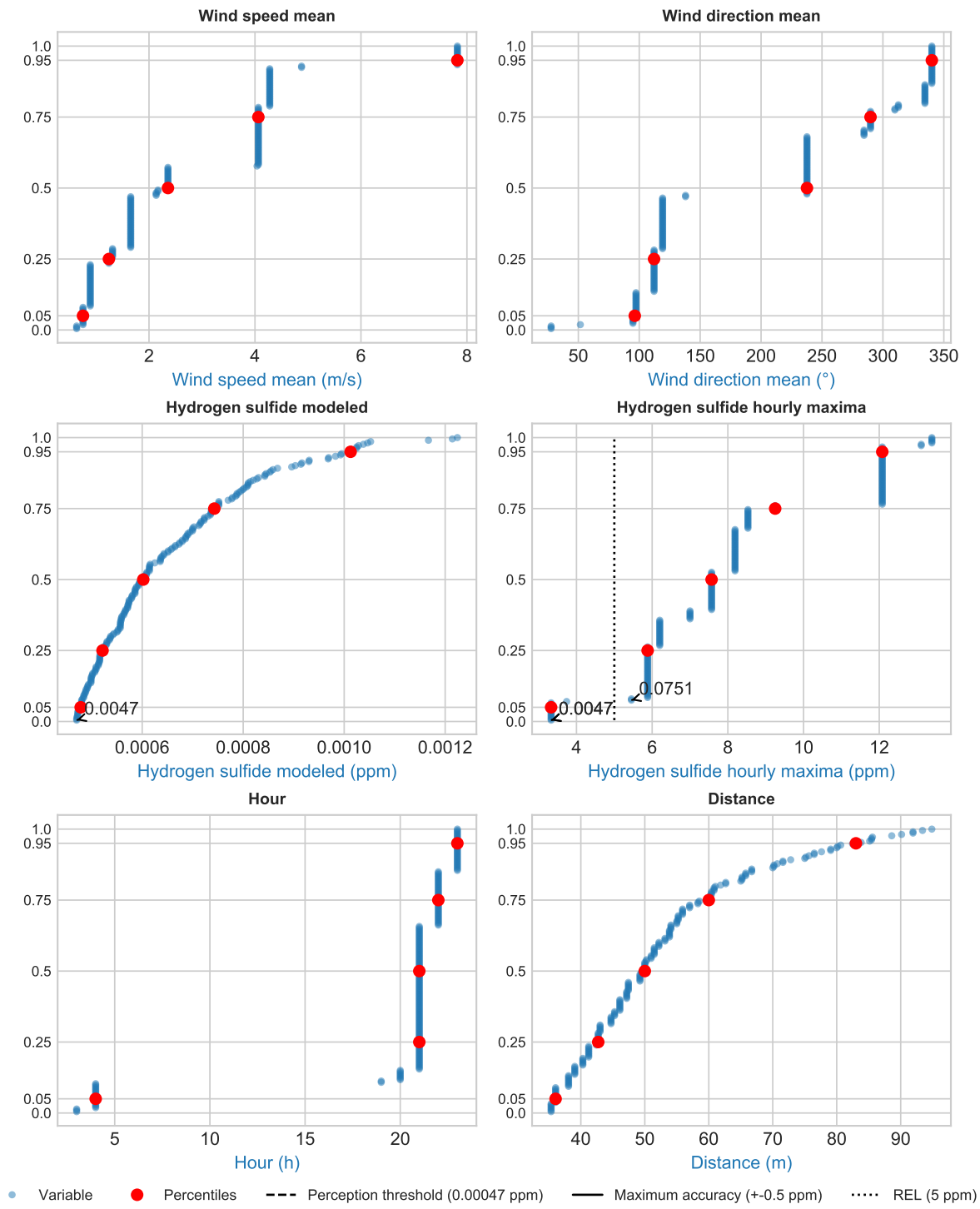

Figure 90: In this figure, each ECDF-subplot belongs to one of the characteristic variables; namely wind speed in m/s and wind direction in angular degrees, modeled hydrogen sulfide concentrations and the corresponding input maxima in ppm, the associated hour and distance in meters to the main emission source of each event. The modeled hydrogen sulfide concentrations stem from the alternative model approach, and is filtered both by the residential area of interest (see map 89) and by the perception threshold of 0.00047 ppm (see 2.2.3). All the other variables belong to these double-filtered model concentrations from the the first measurement period from 16 to 29 July 2018. With regard to the legend, particular concentration limits in ppm are embedded where suitable; namely the recommended long-term exposure limit (or long-term REL) and perception threshold of the odorant, mentioned in subsection 2.2.3, and the maximum accuracy of the deployed measuring instruments explained in 3.1.1. Finally, in the two H_2S-subplots, the quantile of the closest data point to the limit values in the legend is annotated, if applicable.

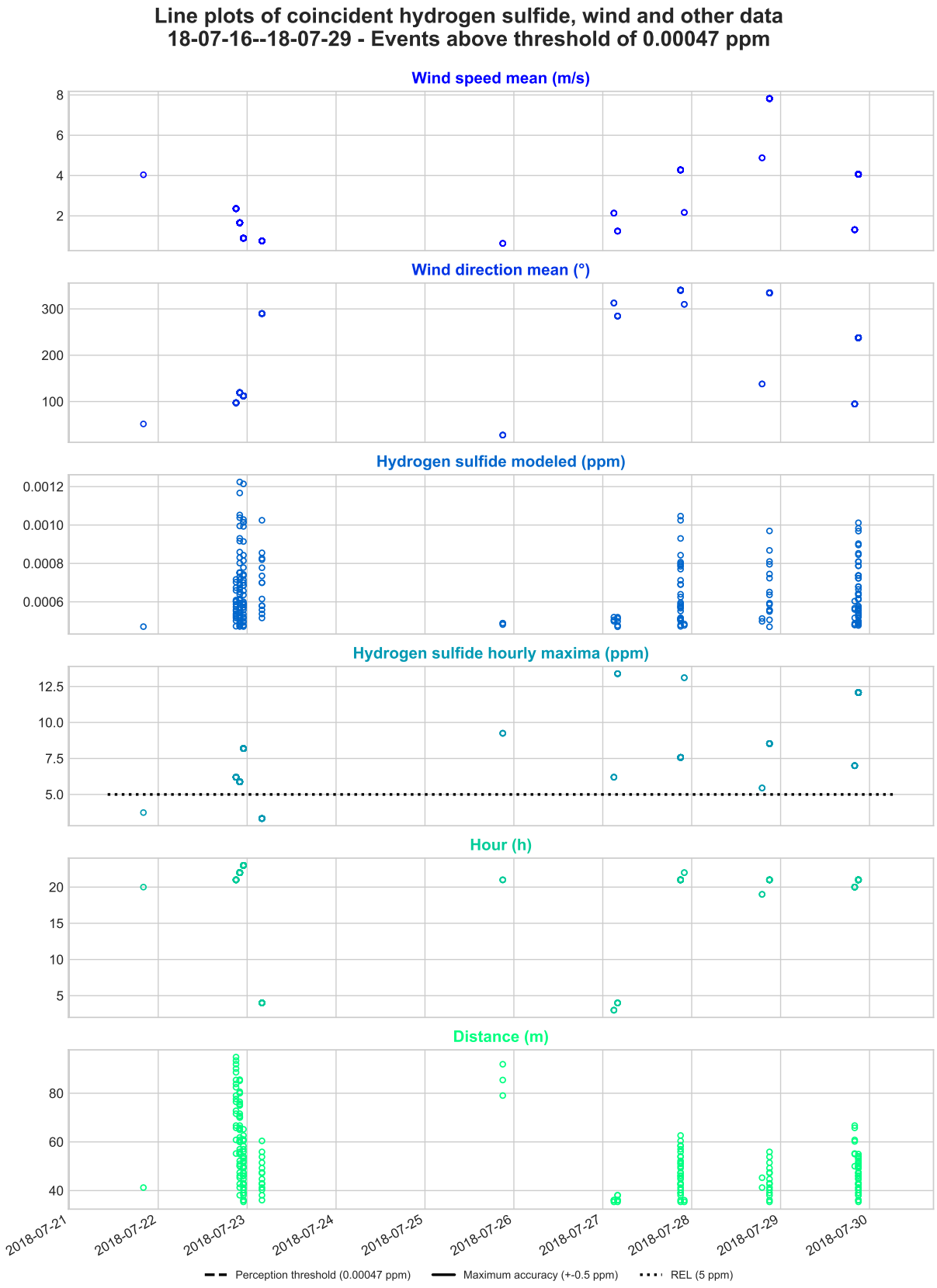

Figure 91: In this figure, each time series belongs to one of the characteristic variables; namely wind speed in m/s and wind direction in angular degrees, modeled hydrogen sulfide concentrations and the corresponding input maxima in ppm, the associated hour and distance in meters to the main emission source of each event. The modeled hydrogen sulfide concentrations stem from the alternative model approach, and is filtered both by the residential area of interest (see map 89) and by the perception threshold of 0.00047 ppm (see 2.2.3). All the other variables belong to these double-filtered model concentrations from the the first measurement period from 16 to 29 July 2018. With regard to the legend, particular concentration limits in ppm are embedded where suitable; namely the recommended long-term exposure limit (or long-term REL) and perception threshold of the odorant, mentioned in subsection 2.2.3, and the maximum accuracy of the deployed measuring instruments explained in 3.1.1.

Measurement period: 3 April - 3 June 2019

After having discussed the characteristics of the first measurement campaign in 2018, similar aspects are going to be developed from here on with respect to the second measuring campaign from 3 April till 3 June 2019. Compared to the above-stated plot 90, graphic 92 shows some similarities, even though the circumstances of the installations have changed significantly during the winter from 2018 (see 6) to 2019 (see 7).
Despite the different season of late spring and early summer and the temporal expansion of the data of about 2 months, in comparison to the rather selective 2 weeks of the graphic 90 before, the times of odor nuisance appear still concentrated from around 19 o'clock in the evening till about 7 in the morning.
In general, the characteristics found and discussed in figure 90 and 91 are also applicable here. However, a difference can be found in the mean wind direction distribution, which is much more uniformly distributed than the previous sharp patterns.

As an aside, it should be mentioned that the maximum concentration setting of the gas measuring instrument during this period was 50 ppm, wherefore the this value appears discontinuously in extremes of the value range displayed in the subplot "Hydrogen sulfide hourly maxima" in figure 92. Concentration peaks exceeding 50 ppm were simply recorded as 50 ppm.

As already discussed regarding figure 91, the simultaneously displayed variables give rise to correlation derivations, which are similar in graphic 93. For the sake of spotting patterns, the chronological sequence of the period "18-07-16–18-07-29" was more suitable to explore the patterns and correlations between the chosen input and output variables due to the shorter period of 2 weeks and the more stable meteorological conditions during the high summer season.

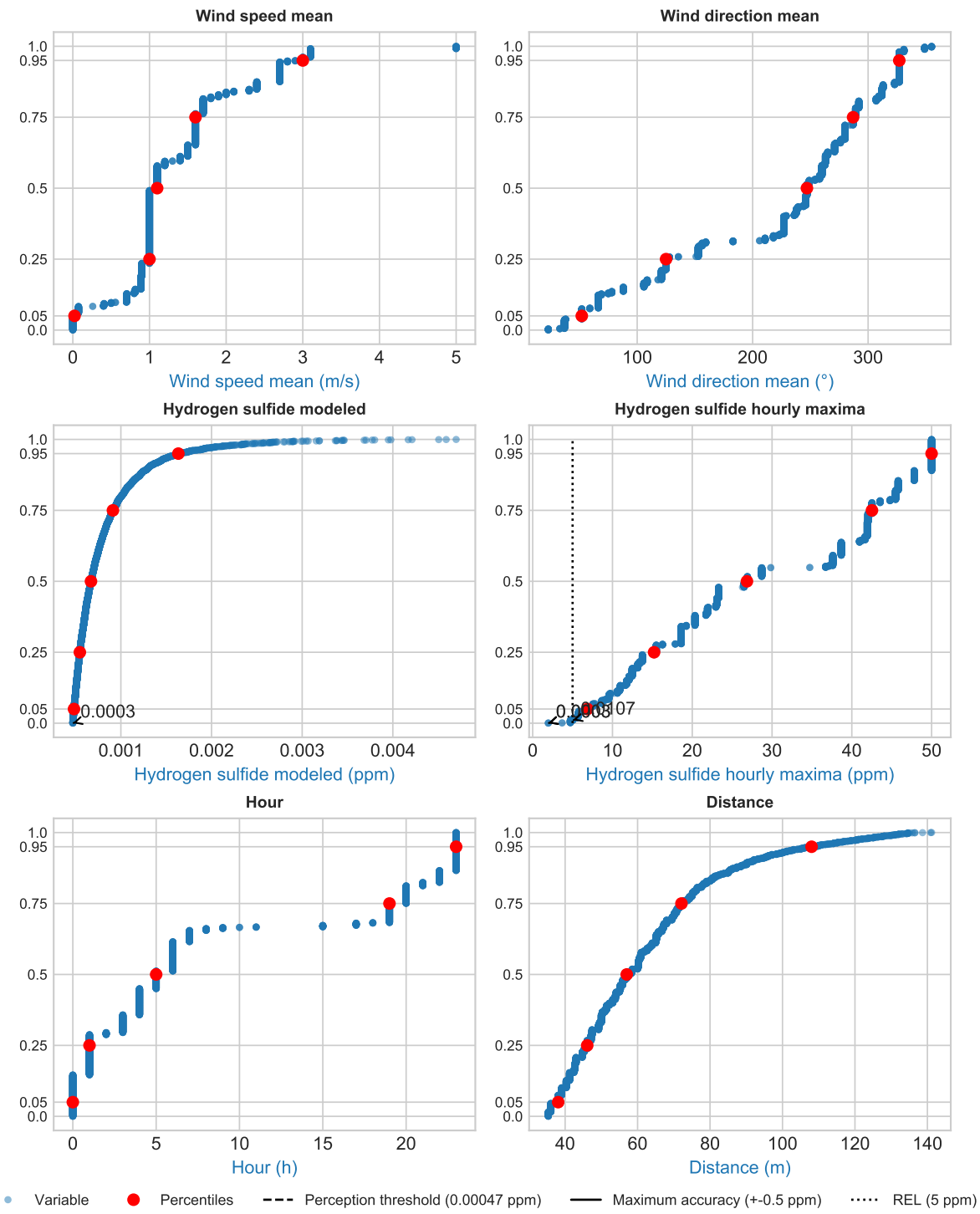

Figure 92: In this figure, each ECDF-subplot belongs to one of the characteristic variables; namely wind speed in m/s and wind direction in angular degrees, modeled hydrogen sulfide concentrations and the corresponding input maxima in ppm, the associated hour and distance in meters to the main emission source of each event. The modeled hydrogen sulfide concentrations stem from the alternative model approach, and is filtered both by the residential area of interest (see map 89) and by the perception threshold of 0.00047 ppm (see 2.2.3). All the other variables belong to these double-filtered model concentrations from the the last measurement period from 3 April to 3 June 2019. With regard to the legend, particular concentration limits in ppm are embedded where suitable; namely the recommended long-term exposure limit (or long-term REL) and perception threshold of the odorant, mentioned in subsection 2.2.3, and the maximum accuracy of the deployed measuring instruments explained in 3.1.1. Finally, in the two H_2S-subplots, the quantile of the closest data point to the limit values in the legend is annotated, if applicable.

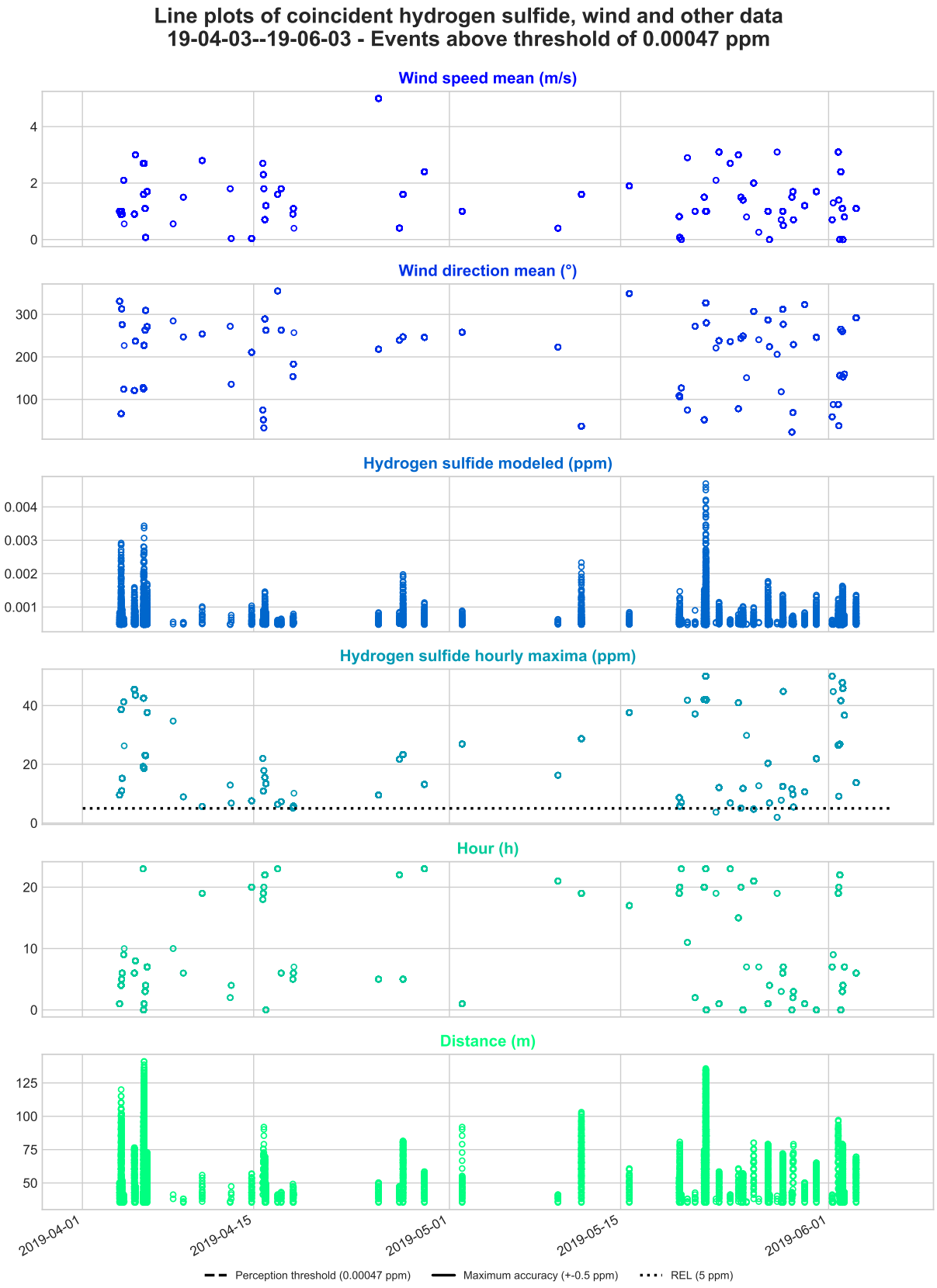

Figure 93: In this figure, each time series belongs to one of the characteristic variables; namely wind speed in m/s and wind direction in angular degrees, modeled hydrogen sulfide concentrations and the corresponding input maxima in ppm, the associated hour and distance in meters to the main emission source of each event. The modeled hydrogen sulfide concentrations stem from the alternative model approach, and is filtered both by the residential area of interest (see map 89) and by the perception threshold of 0.00047 ppm (see 2.2.3). All the other variables belong to these double-filtered model concentrations from the the last measurement period from 3 April to 3 June 2019. With regard to the legend, particular concentration limits in ppm are embedded where suitable; namely the recommended long-term exposure limit (or long-term REL) and perception threshold of the odorant, mentioned in subsection 2.2.3, and the maximum accuracy of the deployed measuring instruments explained in 3.1.1.

5 Conclusions

In the following, the answers to the main research questions, additional findings and recommendations are going to be illustrated.

5.1 Main research questions

The principal problem to resolve in this study is how likely it is for local people to be affected by odor emissions from the WWTP, and in case of being affected, what are the conditions leading to the nuisance.
According to the results from the analysis and discussion of both the measured and modeled data, the months during the year with the highest probability that the residents in the area of complaints can be affected by perceptible odorant concentrations range from May till September, especially the high summer season from June till August. Concerning the time, residents can be affected above all during the evening, night and early morning; in other words from about 7 p.m. to 7 a.m. This is due to the stable wind patterns during these months with increasing wind speed toward their housings in the evening, and the similarly on average elevated hydrogen sulfide ($\mathrm{H_2S}$) concentration peaks in the end of the day. Moreover, the temperature plays an essential role in both the exalted population burden due to the tourists in the high summer season, and also in the increased biological activity of sulfur-reducing bacteria ("SRB"): For one thing, the summer season attracts more tourists to the region for beach tourism, which in turn increases the daily volume inflow of the WWTP. As there is a positive correlation assumed between sewage volume flow and $\mathrm{H_2S}$ concentrations, the increased population in summer is as a consequence positively correlated with the probability of perceiving odor nuisance. On the other hand, the aforementioned SRB increase their biological activity with rising temperatures within the typical temperature ranges occurring in Oliva, producing more $\mathrm{H_2S}$. Therefore, the temperature is again positively correlated with odorant emissions, apart from the beach tourism factor.
As far as the two investigated odorants are concerned, ammonia could be ruled out since practically all concentrations lied significantly below the perception threshold of 5 ppm and even below the measurement accuracy of the deployed instrument. On the contrary, $\mathrm{H_2S}$ was found to be emitted in high peaks from the canalization entrance with concentrations up to 50 ppm, wherefore hydrogen sulfide was identified as the central pollutant for investigating the odor nuisance. Next, when taking into account the dynamic olfactometry and gas measurements away from the canalization entrance, i.e. the main emission source, $\mathrm{H_2S}$ concentrations remained zero during all measurement times and odor recordings especially when they were taken outside the WWTP site. What is more, the most realistic modeling results from AERMOD confirm that in the residential area of interest the $\mathrm{H_2S}$ perception limit of 0.00047 ppm (see table 1) was never surpassed during any of the measurement periods. However, the worst-case model scenario showed that indeed perceivable odors caused by $\mathrm{H_2S}$ can occur at the dwellings. The general difference between both model outputs was how the WWTP volume outflow was employed as input variable for the model: In the most realistic approach, the daily volume flow values were downsampled to hourly scale which was used for calculating both emission rates and flow speed at the source. By contrast, in the alternative approach a constant volume outflow was estimated by means of the inflow pipe geometry and general average volume flows. The resulting constant was more than one order of magnitude higher than the median of the daily volume flows, which also led finally to modeled $\mathrm{H_2S}$ concentrations up to two orders of magnitude higher than with the most realistic approach. Yet in spite of that, the maximum $\mathrm{H_2S}$ values from the alternative model output remain below 1 ppm even next to the emission source, even when taking into consideration the maximum odorant peaks at the emission source of up to 50 ppm. It can be concluded that rather small

gas outflow volume leads to a rapid dispersion and thus decrease of ambient pollutant concentrations, which in turn supports the assumption of a point source in the AERMOD modeling system. Following up on this, since the recommended short-term exposure limit (or short-term REL) for $\mathrm{H_2S}$ is 10 ppm, and not even in the worst case scenario concentrations surpass this limit, the safety can be guaranteed for both local residents and also the staff of the WWTP working on-site close to the canalization entrance. As an aside, the short-term REL of 10 ppm stands for the maximum short-term exposure limit of average hydrogen sulfide concentrations for 15-minute continuous exposure, which is defined by the Spanish National Institute of Occupational Health and Safety (INSST) (see 19). Following this definition that the maximum exposure limit as specified as an average concentration of a 15-minute duration, when bearing in mind the pumping rhythm, which lied, depending on the season, between every 2 and 10 minutes, it is not plausible to be exposed to more than 10 ppm on average during 15 consecutive minutes time; not even when staying next to the canalization entrance. Thus, as the only inconvenience, WWTP site workers could be subjected to perceptible odors intermittently when being close to the emission source while the sewage is pumped into the bioreactor, but certainly not to concentrations above the limits hazardous to health.
The aforesaid safety statements are underpinned by the fact that also the $\mathrm{H_2S}$ measurements were recorded as 0 ppm at all measuring locations apart from the emission source, along with measurements of zero odor units outside the WWTP site by the olfactometry panelists.
Nevertheless, the results of the worst case scenario indicates the possibility of the occurrence of perceptible $\mathrm{H_2S}$ concentrations at the dwellings in question. This does not contradict the above-mentioned arguments, as the olfactometry measurements were not taken during the evening or night in the high summer season; i.e. the most probable time for odor nuisance according to the analysis of the meteorological and concentration data. Apart from that, since the measurement accuracy of the employed Dräger Polytron 7000 for $\mathrm{H_2S}$ concentrations lies around 0.5 ppm, but the perception threshold around 0.00047 ppm, this instrument was able to show that no values hazardous to health occurred away from the emission source, but it could not exclude the possibility that a perceptible $\mathrm{H_2S}$ concentration can occur at the other locations where it was deployed; in particular at the wall bordering the WWTP site toward the housings. Consequently, considering that the perception threshold lies approximately three orders of magnitude below the measurement accuracy of the utilized instrument, and that the olfactometry measurements were too selective and limited in temporal coverage, the chance of noticing odors at the dwellings cannot be ruled out entirely. It can only be said that in accordance with the measured data and the most realistic modeling results it is very unlikely to perceive odors at the dwellings around 40 meters and more from the canalization entrance. On the other hand, it is safe to say that neither the on-site workers nor the residents are at risk of being exposed to odorant concentrations hazardous to health.

5.2 Additional inferences

Worker safety at Pumping Station 2
Following up on the safety topic for the staff with respect to the by now sealed pumping well, due to the high hydrogen sulfide and even ammonia concentrations measured within - putting aside the damaging of the measurement equipment during the measurements carried out within the sealed well - these results give a clear hint that workers who ought to open or even enter the well are strongly advised to protect themselves. This could be accomplished by several precaution measures, e.g. previously ventilating the well and pollutant concentration measurements. Apart from that, it is recommended to install a small ventilation stack with a filter inside in order to avoid high odorant concentrations due to accumulation within the well on the one hand, and on the other hand to prevent odor nuisance near the pumping well zone.

Unfavorable wind conditions
As for stating a certain minimum wind speed value capable of transporting still perceptible hydrogen sulfide concentrations to the dwellings, it can be seen from figure 91 and 93, which are based on the alternative modeling input data, that already small wind speeds of around 0.5 m/s could be sufficient; especially, when the wind direction origin lies in a range from 65 to 170 angular degrees blowing directly from the emission source toward the residential area in question. On the other hand, it can also be deduced that in the case of higher wind speeds from 4 to 8 m/s, it is also possible to perceive odors at the dwellings despite the fact that the simultaneous mean wind direction points almost in the opposite way.

Minimum concentration at source
In addition, as far as any minimum concentrations at the point source are concerned, which could be considered necessary to produce a perceivable odor at the dwellings, it can be interpreted by means of the same aforementioned graphics that these initial peaks comprised of concentrations at least as high as the associated long-term REL of 5 ppm.

Nuisance frequency assuming alternative model results
Besides, regarding the frequency of odor nuisances, the alternative model scenario results used to create the above-cited graphs 91 and 93 testify that, depending on the season and circumstances, it can be possible to have incidents up to twice a day, or also just once a week, but certainly on a regular basis.

Correlation between odors and odorant concentrations
As thoroughly discussed in subsection 4.5, the correlation results of olfactometry and gas measurements in this project state that the olfactometry datasets are too incomplete for proper statistics, and thus solely permit a very rough linear estimate. This is due to the fact that the data set of olfactometry measurements is scarce in observations and moreover biased since it does not cover the full spectrum of times, especially not the most important ones during the evening and night, in accordance with the data analysis results based on the wind data. Furthermore, the measurements can result in zero just due to the current wind conditions, whereas at a alter time the situation could already be entirely different. For more details, the reader is referred to subsection 4.5 and the following recommendations 5.3, where the issues related to the olfactometry measurements are more profoundly described.

5.3 Recommendations

Generally, the possible problems, which can challenge the successful accomplishment of such a project, were listed in the subsection 2.5.2. Following this, hereinafter the project-related experiences and from there derived recommendations are going to be noted down.

5.3.1 Odor control and mitigation measures

In order to corroborate or refute the results of this study, a long-term monitoring would have to be carried out which includes, according to the US Environmental Protection Agency (EPA) regulations, at least 12 consecutive months, better even 2 or 3 years in order to make comparisons between similar seasons. Regarding this study, the data from 4 June until the end of July 2019 was lost which is why the comparison with the first measuring period from 16 till 29 July 2018 could not be accomplished. Also, according to paragraph 2.4, it would be a good approach to employ continuous monitoring of the emission source in conjunction with on-site meteorological data measurements. Even better on

top would be to upload these data in real-time to a server where dispersion modeling software, such as AERMOD, give a live overview of the current nuisance potential at the nearby residential housings.
What is more, instead of temporally too sporadic and consequently biased olfactometry measurements by human panelists, a more modern approach of deploying an electronic nose would be the method of choice. This way, just like installing a permanent gas measuring instrument, an odor measurement apparatus would take data continuously and thus produce a proper data base with statistically more complete temporal coverage and resolution. More details on this direct odor measurement method were stated under 2.5.3 and can be obtained via [Cap+13, ch. 5 "Electronic Nose"].
Apart from this, as perceiving odor intensity and offensiveness is a highly individual matter, a survey involving the local residents is recommended in order to get another perspective of the nuisance, since measured and modeled chemical concentrations is only one aspect in terms of assessing this kind of disturbance. More details regarding the population investigation method were mentioned under 2.5.3.
By contrast, if values hazardous to health occurred, the situation would be entirely different, since people at times cannot even recognize pollutant concentrations hazardous to health, depending on the particular odorant and its concentration.
Strictly speaking, when referring to health, regular perceivable odor nuisance can also have adverse health effects in an indirect way since it gives rise to psychological stress and discomfort. In this study though, according to the modeled concentration data in both input approaches, it could be assured that the odorant concentrations are not continuously perceivable at the housings, if at all.

Moreover, regarding additional odor mitigation and control measures, other cleaning processes mentioned in subsection 2.4 and the info graphics 24 and 25 do not seem adequate in the case of WWTP Camping San Fernando, since the obtained data give evidence that neither the gas outflow rate nor the odorant concentration are sufficiently high that it would be worth the effort.
As a result and final advice with respect to the WWTP Camping San Fernando, continuous monitoring and application of dispersion modeling is the method of choice.
Apart from the aforesaid recommendations, the plant operators have changed the conditions to the better with respect to the now submerged canalization entrance with an automatic rotation sieve (see picture 7) in comparison to the previous rather simple open-air installation, as can be confirmed in photograph 6. Moreover, an additional sight protection fence was built on top of the previous wall surrounding the WWTP-site (see photo 26). The latter contributes not only to visual protection of the open-air WWTP, but creates also a nicer appearance as seen from the outside. These psychological factors can play a decisive role when it comes to perceiving odors, or the general toleration of the mere existence of the WWTP embedded in the residential area. In that sense, the operators are already on a good path and in case of carrying out ongoing monitoring and modeling in the future, a sound and holistic approach would be achieved and that way it could be guaranteed that the odor nuisance will be even better understood and under control.

5.3.2 Olfactometry

As for the field measurements during this study, both the temporal and the spatial resolution of these measurements need to be higher in order to have more significance. Moreover, the measurements should rather be carried out when a smell is already noticeable with the bare nose instead of measuring anyways. Next, and based on the previous argument, if it is intended to obtain a reliable conversion between a chemical concentration and (European) Odor Units per cubic meter, it is recommended to adapt the olfactometry measuring to the gas emission rhythm in order to safeguard a sound statistics. By virtue of the fact that, depending on the wind speed and direction, the odor can be completely imperceptible even though the panelists stand next to the source, they should stand rather in the

current wind direction in order to actually evaluate the intensity of the possible nuisance. When the aim is to measure these rare events, the chance should be increased to actually measure them, otherwise the result will remain zero in spite of the fact that at times the nuisance occurs. Furthermore, when taking into account that after a certain periodic time interval odorants are emitted from the canalization entrance, this condition demands thus measurements at the same time or immediately after the gas emission took place in order to obtain a non-zero olfactometry measuring result. Otherwise the opportunity to measure a non-zero odorant concentration would be missed. This was the case in this project due to the pumping rhythm of a frequency usually between 1 and 4 minutes, depending on the season and day time.
Finally, it is important to mention that finding correlations between odor units and single gas concentrations is not trivial due to cross-effects with other odorants and gases (for more details see subsection 2.5.2). The presence of various odorants and other gases in real field situations is the common situation, whereas only in laboratory conditions pure odorant gases can be achieved.

On the other hand, since it is clear that if there is an odor nuisance at the said dwellings, it most likely happens between 19 and 7 o'clock according to the wind direction and wind speed statistics along with the general modeling results. This time range did not intersect with the site visiting schedules, wherefore the field olfactometry measurements were not carried out as ideally desired during the aforementioned most critical time window. Instead, they were conducted when the meteorological conditions are the most favorable as they statistically occur around noon. Then again, it is comprehensible that the working hours of the panelists are not between 19 and 7 o'clock.
Apart from that, as the incidents could occur rather intermittently than regularly while taking into account the quite selective olfactometry recordings, the possibility of the worst case cannot be clearly discarded that, when all comes together, perceptible odorant concentrations can arrive at the dwellings.
In terms of alternative direct odor measuring approaches to the established dynamic olfactometry through human panelists, the cutting-edge method is the electronic nose described in subsection 2.5.3, as it is an automatized direct odor measurement. By contrast, human panels cannot collect as much data as a fixedly deployed instrument. Also, in comparison with traditional gas measurements which measure the chemical concentrations of specific odorants, i.e. indirect odor measurements (compare subsection 2.5.4), electronic noses measure odors directly.

5.3.3 Gas measurements

Due to the low concentrations of hydrogen sulfide smaller than 1 ppm when not measured directly next to the main emission source, i.e. the canalization entrance, it is paramount to dispose of the appropriate measuring equipment with a precision and accuracy (see 3.1.1) still high enough to measure and resolve these concentrations reliably, as the human perception limit lies around 0.00047 ppm (see table 1). Instead, during the project the measurements were accomplished with an instrument comprising a maximum accuracy of 0.5 ppm for hydrogen sulfide, which was primarily apt for safeguarding that no long- or short-term REL of 5 or 10 ppm was surpassed.
Additionally, with regard to the arrangement of the gas measuring sensor tubes, it is recommended to install them with their ends facing downwards to prevent possible humidity damage, as it happened twice in the course of the measuring campaigns. With this, the mere gravitational force could be able to hinder any water drop entered into the tube from advancing until the sensor. Besides that, miscellaneous unforeseeable complications due to force majeure occurred during the measuring campaigns at the WWTP Camping San Fernando, such as sensor damaging during heavy rainfalls and thunderstorms, and recurrent relocation of gas sensor tubes due to construction and other works on the WWTP-site, which involved heavy machines and vehicles that disturbed the ongoing measurements as a result. As a matter of fact it is virtually impossible to prevent all these inconveniences from happening, let

alone data loss of the on-site register equipment, but nevertheless, with sound preparation, they can be significantly reduced. Of course it is easier when the investigator visits the site him- or herself on a regular basis, as it can be difficult to communicate complex instructions and questions via e-mail or telephone. Also, it is indispensable to obtain an own impression of the real situation on-site, as from the distance, and by means of emails one cannot fully assess the local circumstances. For example, sensors could be fixed at any other place but the one actually desired, or one does not take into account important conditions which can only be realized being on-site yourself. No matter how much good will all the people involved show, sometimes communication simply fails, which happens naturally.
Next, with respect to the evaluation of the measurements undertaken at the WWTP Camping San Fernando, the ammonia measurement instruments were adequate as the perception threshold lies around 5 ppm, the measurement accuracy at around 1.5 ppm (see 3.1.1), whereas in particular the main odorant $\mathrm{H_2S}$ could have been measured far better if it had been possible to dispose of more accurate and precise measuring instruments. This statement is based on the fact that the measuring accuracy lied around 3 orders of magnitude higher than the minimum perception limit. Notwithstanding, it was possible to conduct a proper modeling with AERMOD since this model solely requires one point source as a minimum in terms of emission sources. Nevertheless, it would be more accurate to dispose of several emission sources or spatially distributed concentration measurements, but as mentioned before the $\mathrm{H_2S}$ concentrations were too low to be detected with the deployed apparatus.
As a consequence, the investigator should make sure to be aware which odorant is being measured and which concentration ranges are expected, and following up on this also where it shall be measured (see subsection 2.5.4). For example, the concentrations at the canalization entrance of the WWTP Camping San Fernando ranged up to even more than 50 ppm, whereas with regard to the perimeter analysis of the plant, an apparatus with an accuracy of down to parts per billion (ppb) would have been paramount. As every odorant has a distinct associated perception threshold and limit hazardous to health, the deployed instruments should be able to detect these provided that these concentrations are expected to be reached in the scope of application.

5.3.4 Building downwash effects

As far as building downwash effects in the AERMOD model (see subsection 3.2) due to nearby obstacles are concerned, it is indirectly included in the complex terrain hill height calculations of AERMAP (compare subsection 3.2.4), which are based on the DEM-data input in form of GeoTIFFs. The proper building downwash effects would have to be treated with the only AERMOD preprocessor not used in this project called "Building Profile Input Program for PRIME" (BPIPPRM), which in turn is called "Plume RIse Model Enhancements" (PRIME). For instance, the surrounding wall of the WWTP Camping San Fernando with about 2 meters height could be taken into special consideration this way. On the other hand, the flagpole parameter of the AERMOD model was already set to 1.7 meters above ground in order to factor in the height of an average person. Besides that, the building heights of the residential area have already been taken into consideration by AERMAP through processing the high-resolution digital elevation model data provided by the satellite orthophoto inputs as GeoTIFFs. Thus, the additional functionality of BPIPPRM is the building downwash effect of obstacles close to the emission source(s), wherefore it is recommended to utilize it, if applicable.

5.3.5 AERMOD and other model alternatives

According to the opinion of experts in the field of odor treatment associated with the collaborating firm Global Omnium S.L., the AERMOD model is principally designed for distances below 50 kilometers which fits well with the application of the current project. On the other hand, with respect to the

treatment of odor emissions, Lagrangian models, or advanced Gaussian puff models such as CALPUFF etc., could lead to more exact results than Gaussian models due to the fact that they can handle low wind speeds more accurately, which is sometimes necessary to describe the odor nuisance under calm wind conditions. Especially CALPUFF can include better the influence of large adjacent water bodies, such as lakes or the sea.
Besides that, in the listing under 2.6.3 based on [Cap+13], these and other model types are further explained, such as Lagrangian particle models and Eulerian grid models (3-D models), and also Computational Fluid Dynamic models (CFD). As a general rule, the more complex the model, the more exact and realistic the results will be, provided that the input data are of high spatial and temporal resolution and sufficiently complete, i.e. of high quality. Because these input data are most likely not achievable due to time and monetary costs, the rather cheap, but still reliable and in many fields of applications well-proved Gaussian models can also do the job, such as AERMOD. Nevertheless, in order to improve the results, but still maintain input requirements simple and computation times short enough, it is recommended to try CALPUFF as a comparison to AERMOD since it is widely used in the field of odor dispersion modeling, can deal better with calm wind conditions and has other improved features.
Apart from this, it shall be mentioned that the current state of the art in the field of atmospheric odorant dispersion modeling are high-resolution 3D-models based on the real physical partial differential (Navier-Stokes) equations, in particular the computational fluid dynamic models (see 2.6.3). Nevertheless, due their aforesaid advantages the Gaussian models are still widely used in science and also for commercial and public applications.

5.3.6 Automation of the model AERMOD

Albeit the model comes prefabricated as open-source FORTRAN code, it is still a long way to go until one can actually run the model concerning all its input data requirements, let alone those of the preprocessor models. The main and its preprocessor models are controlled by plain ASCII so-called "control files". In order to run each model in a user-defined way with different custom input data and settings, it is recommended to automatize the data import, modification of the input text files and execution of each model in the right order. It can take a lot of time and effort, but in the end it pays off since the entire model is then operable almost as if it were an application, just that the interface are textfiles, i.e. it is not a real graphical user interface (GUI).
As a side note regarding the AERMOD simulation settings, the exhaustive listing of the employed control input file contents of all pre- and postprocessors and the principal model AERMOD was mentioned in subsection 3.2.8. Incidentally, by saying "preprocessors", it is referred namely to AERMET, AERSURFACE and AERMAP, whereas "postprocessor" means actually AERPLOT. Another important detail to mention, concerning the modeling, is that in the case of hydrogen sulfide being the pollutant, AERMOD is run assuming mass conservation without any sort of decay or other reactions of the pollutant.

5.3.7 Choosing an appropriate model

In hindsight, it would have been an easier approach to first and foremost determine which model to use. This would allow for evaluating in the beginning which input variables one exactly needs, where you can get them from or how you measure them. In the case of this project, measurements were done with the equipment available in summer 2018, and afterwards it was thought more about the employability of model classes, then narrowing down subsequently which models could be used. The conclusion is that one should not underestimate the complexity of established models and their usage,

and also their input requirements. Despite the fact that it can be often read that Gaussian models are based rather on simple assumptions in comparison with cutting-edge models like computational fluid dynamic (CFD) models etc., it can result in quite a lot of work just to collect all the input data necessary to run AERMOD and pass them on to it in the correct way. As just mentioned, AERMOD input requirements are very specific and US-centric; particularly regarding the meteorological data. As the data retrieved from meteorological stations outside the US is usually not provided with all necessary input variables, let alone having the correct input format, one ought to search in a lot of places until receiving the data needed. Apart from that, with respect to the correct input format, which is very inflexible concerning AERMOD, AERMET, AERMAP, AERSURFACE, etc., it is paramount to possess the knowledge - or the time to acquire it - to manipulate, separate, merge, aggregate, and, if necessary, interpolate the data previous to passing them on to the models. As a matter of course, these procedures should be done under the central premise to evaluate responsibly whether a custom approach is scientifically acceptable or not.

By and large, it would be the best to fix quite early during the project which model is going to be used, and what kind of requirements it has for being able to weigh all available options and decide which requirements can be fulfilled in the first place. In the opposite case it could happen at times, as occurred while carrying out this study, that sudden difficulties arise, such as the initial unavailability or incompleteness of necessary data to proceed in executing the model. On the other hand, despite all possible careful planning, unforeseen occurrences throughout the study are inherently part of the game. Whatever the case, in the end one needs to decide the most suitable way for oneself and make the best out of it. Apart from that, the proverb "where there is a will, there is a way" is always valid.

List of Figures

List of Tables

References

[CDC94] CDC (Centers for Disease Control and Prevention). *Ammonia*. 1994. URL: https://www.cdc.gov/niosh/idlh/7664417.html (visited on 10/15/2018).

[SR01] Jeff Staudinger and Paul V Roberts. "A critical compilation of Henry's law constant temperature dependence relations for organic compounds in dilute aqueous solutions". In: *Chemosphere* 44.4 (Aug. 2001), pp. 561–576. ISSN: 0045-6535. DOI: 10.1016/S0045-6535(00)00505-1. URL: https://www.sciencedirect.com/science/article/pii/S0045653500005051.

[Hvi+02] T Hvitved-Jacobsen et al. "Sewer microbial processes , emissions and impacts". In: *Sewers process and networks* (2002), p. 13.

[Age04] Agency for Toxic Substances and Disease Registry. *Public Health Statement for Ammonia*. 2004. URL: https://www.atsdr.cdc.gov/PHS/PHS.asp?id=9%7B%5C&%7Dtid=2 (visited on 10/15/2018).

[SS05] Zarook Shareefdeen and Ajay Singh. *Biotechnology for Odor and Air Pollution Control*. Ed. by Zarook Shareefdeen and Ajay Singh. Berlin, Heidelberg: Springer, Berlin, Heidelberg, 2005, p. 409. ISBN: 978-3-540-27007-2. DOI: https://doi.org/10.1007/b138434.

[Hea07] New Jersey Department of Health. "Hazardous Substance Fact Sheet Ammonia". In: (2007). URL: https://nj.gov/health/eoh/rtkweb/documents/fs/0084.pdf.

[Sme+07] Monique A.M. Smeets et al. "Odor and irritation thresholds for ammonia: A comparison between static and dynamic olfactometry". In: *Chemical Senses* 32.1 (2007), pp. 11–20. ISSN: 0379864X. DOI: 10.1093/chemse/bjl031.

[Lev08] National Research Council (US) Committee on Acute Exposure Guideline Levels. *Acute Exposure Guideline Levels for Selected Airborne Chemicals: Volume 6*. 6th ed. Washington (DC): National Academies Press (US), 2008. URL: https://www.ncbi.nlm.nih.gov/books/NBK207883/.

[Suc+08] Kirsten Sucker et al. "Odor frequency and odor annoyance. Part I: Assessment of frequency, intensity and hedonic tone of environmental odors in the field". In: *International Archives of Occupational and Environmental Health* 81.6 (2008), pp. 671–682. ISSN: 03400131. DOI: 10.1007/s00420-007-0259-z.

[Wat09] Water Environment Federation. *Following the Flow: An inside look at wastewater treatment*. Tech. rep. Water Environment Federation, 2009, p. 20. URL: https://www.wef.org/resources/for-the-public/public-information/.

[KRH11] Dong-kyu Kim, Yong-wan Roh, and Kwang-seok Hong. "A Method of Multiple Odors Detection and Recognition". In: *Human-Computer Interaction. Interaction Techniques and Environments*. Ed. by Julie A. Jacko. Vol. 6762. 14th International Conference, HCI International 2011, Orlando, FL, USA. Berlin, Heidelberg: Springer, Berlin, Heidelberg, 2011. Chap. A Method o, pp. 464–473. ISBN: 978-3-642-21604-6. DOI: 10.1007/978-3-642-21605-3. URL: http://link.springer.com/10.1007/978-3-642-21605-3.

[Hal12] Natasha Halageri. "Odor Monitoring at Wastewater Treatment Plants". In: *University of New Orleans Theses and Dissertations* (2012), p. 64. URL: https://scholarworks.uno.edu/td/1580.

[Cap+13] Laura Capelli et al. “Measuring odours in the environment vs. dispersion modelling: A review”. In: *Atmospheric Environment* 79 (2013), pp. 731–743. ISSN: 13522310. DOI: 10.1016/j.atmosenv.2013.07.029. URL: http://dx.doi.org/10.1016/j.atmosenv.2013.07.029.

[Car+14] Fabio Carrera-Chapela et al. “Modeling the odor generation in WWTP: An integrated approach review”. In: *Water, Air, and Soil Pollution* 225.6 (2014). ISSN: 15732932. DOI: 10.1007/s11270-014-1932-y.

[Che+15] C. A.L. Chernicharo et al. “Anaerobic sewage treatment: state of the art, constraints and challenges”. In: *Reviews in Environmental Science and Biotechnology* 14.4 (2015), pp. 649–679. ISSN: 15729826. DOI: 10.1007/s11157-015-9377-3.

[AER16] AERMODtraining.com. *AERMOD Training YouTube-Channel*. 2016. URL: https://www.youtube.com/watch?v=o8y7cUD2Ef4 (visited on 06/30/2019).

[Kim16] Ki Hyun Kim. “The need for practical input data for modeling odor nuisance effects due to a municipal solid waste landfill in the surrounding environment”. In: *Environment international* 87 (2016), pp. 116–117. ISSN: 18736750. DOI: 10.1016/j.envint.2015.11.004. URL: http://dx.doi.org/10.1016/j.envint.2015.11.004.

[Cen17] Central Pollution Control Board (CPCB). “Odour Monitoring & Management in Urban MSW Landfill sites”. In: *Central Pollution Control Board (CPCB), Ministry of Environment , Forests & Climate Change, Government of India* CUPS/86/ 2.Control of Urban Pollution Series (2017), p. 231. URL: www.cpcb.nic.in.

[Guo+17] Hanwen Guo et al. “Characteristics of volatile compound emission and odor pollution from municipal solid waste treating/disposal facilities of a city in Eastern China”. In: *Environmental Science and Pollution Research* 24.22 (2017), pp. 18383–18391. ISSN: 16147499. DOI: 10.1007/s11356-017-9376-8.

[Vil17] German Villar. “Estudio de modelos de dispersión y su aplicación al control industrial”. PhD thesis. Universidad de Alcalá (Escuela Politécnica Superior), 2017, p. 156. URL: https://ebuah.uah.es/dspace/bitstream/handle/10017/30263/PFC%20Villar%20Lagos%202017.pdf?sequence=1%7B%5C&%7DisAllowed=y.

[Dia18] Diari Oficial de la Generalitat Valenciana. *Conselleria de Agricultura, Medio Ambiente, Cambio Climático y Desarrollo Rural - DECRETO 228/2018, de 14 de diciembre*. 2018. URL: http://www.dogv.gva.es/datos/2018/11/12/pdf/2018%7B%5C_%7D10400.pdf.

[Fis+18a] R. M. Fisher et al. “Emissions of volatile sulfur compounds (VSCs) throughout wastewater biosolids processing”. In: *Science of the Total Environment* 616-617 (2018), pp. 622–631. ISSN: 18791026. DOI: 10.1016/j.scitotenv.2017.10.282. URL: https://doi.org/10.1016/j.scitotenv.2017.10.282.

[Fis+18b] Ruth M. Fisher et al. “Framework for the use of odour wheels to manage odours throughout wastewater biosolids processing”. In: *Science of The Total Environment* 634 (Sept. 2018), pp. 214–223. ISSN: 0048-9697. DOI: 10.1016/J.SCITOTENV.2018.03.352. URL: https://www.sciencedirect.com/science/article/pii/S0048969718311124.

[God+18] Ana Flavia Locateli Godoi et al. “Human exposure to hydrogen sulphide concentrations near wastewater treatment plants”. In: *Science of the Total Environment* 610-611 (2018), pp. 583–590. ISSN: 18791026. DOI: 10.1016/j.scitotenv.2017.07.209. URL: https://doi.org/10.1016/j.scitotenv.2017.07.209.

[Mat+18] Rita Ventura Matos et al. “Assessment of sulfide production in a full scale wastewater sludge rising main”. In: *Journal of Environmental Management* 209 (2018), pp. 505–514. ISSN: 10958630. DOI: 10.1016/j.jenvman.2017.12.073.

[Pra+18] Ademir A. Prata et al. “A critical review on liquid-gas mass transfer models for estimating gaseous emissions from passive liquid surfaces in wastewater treatment plants”. In: *Water Research* 130 (Mar. 2018), pp. 388–406. ISSN: 0043-1354. DOI: 10.1016/J.WATRES.2017.12.001. URL: https://www.sciencedirect.com/science/article/pii/S004313541730996X.

[Raj+18] Ishan Raj et al. “Recent advancements in the mitigation of obnoxious nitrogenous gases”. In: *Journal of Environmental Management* 205 (2018), pp. 319–336. ISSN: 10958630. DOI: 10.1016/j.jenvman.2017.09.064. URL: https://doi.org/10.1016/j.jenvman.2017.09.064.

[Can19] Canadian Centre for Occupational Health and Safety. *Converting Occupational Exposure Limits from mg/m3 to ppm : OSH Answers*. 2019. URL: https://www.ccohs.ca/oshanswers/chemicals/convert.html (visited on 07/03/2019).

[Ins19] M.P. Instituto Nacional de Seguridad y Salud en el Trabajo (INSST), O.A. *Límites de Exposición Profesional para Agentes Químicos 2019*. 2019. URL: http://www.insst.es/catalogopublicaciones/.

[AEM] AEMET. *Hourly Surface Data Weather Station Dénia (Comunitat Valenciana, Spain)*. URL: http://www.aemet.es/en/eltiempo/prediccion/municipios/denia-id03063 (visited on 07/05/2019).

[AVAa] AVAMET (Associació valenciana de meteorologia Josep Peinado). *AVAMET weather station "Dénia Platja de Pego"*. URL: https://www.avamet.org/mx-fitxa.php?id=c30m063e10 (visited on 07/04/2019).

[AVAb] AVAMET (Associació valenciana de meteorologia Josep Peinado). *AVAMET weather station "Oliva pople"*. URL: https://www.avamet.org/mx-fitxa.php?id=c25m181e02 (visited on 07/04/2019).

[Cen] Centro de Descargas del Centro Nacional de Información Geográfica (CNIG). *Interface of the Download Center of the National Center of Geografical Information "Centro de Descargas del CNIG (IGN)"*. URL: http://centrodedescargas.cnig.es/CentroDescargas/buscadorCatalogo.do? (visited on 07/04/2019).

[com] Kestrel company. *Kestrel 5500 Fire Weather Meter Pro*. URL: https://es-kestrelmeters.glopalstore.com/products/kestrel-5500-fire-weather-meter-pro?utm%7B%5C_%7Dcampaign=pr%7B%5C_%7Dr%7B%5C&%7Dutm%7B%5C_%7Dsource=https://kestrelmeters.com%7B%5C&%7Dutm%7B%5C_%7Dmedium=wi%7B%5C_%7Dproxy%7B%5C&%7Dutm%7B%5C_%7Dcontent=en%7B%5C_%7DUS%7B%5C&%7Dutm%7B%5C_%7Dterm=a (visited on 07/04/2019).

[Drä] Dräger. *Dräger Polytron 7000*. URL: https://www.draeger.com/en%7B%5C_%7Dseeur/Applications/Products/Stationary-Gas-Detection-Systems/Detection-of-Toxic-Gases-and-Oxygen/Polytron-7000 (visited on 07/04/2019).

[EA] EPA and AERMIC. *AERMOD model on EPA official webpage*. URL: https://www.epa.gov/scram/air-quality-dispersion-modeling-preferred-and-recommended-models%7B%5C#%7Daermod (visited on 07/05/2019).

[EU] EU. *List of radiosonde weather stations in Western Europe*. URL: http://radiosonde.eu/RS00-S/RS02C-S.html (visited on 07/04/2019).

[Glo] Global Omnium S.L. *Global Omnium S.L.* URL: https://www.globalomnium.com/Group/Our-work/Waste/Depuration/ (visited on 07/04/2019).

[Goo] Google Maps Coordinates. *Google Maps - Find GPS coordinates, longitude, latitude, altitude*. URL: https://www.mapcoordinates.net/en (visited on 07/04/2019).

[Nas] Nasal Ranger. *Nasal Ranger - Field Olfactometer - St. Croix Sensory, Inc.* URL: http://www.fivesenses.com/equipment/nasalranger/nasalranger/ (visited on 07/04/2019).

[NOAa] NOAA. *FTP data base of the Integrated Global Radiosonde Archive (IGRA)*. URL: ftp://ftp.ncdc.noaa.gov/pub/data/igra (visited on 07/04/2019).

[NOAb] NOAA. *Integrated Global Radiosonde Archive (IGRA)*. URL: https://www.ncdc.noaa.gov/data-access/weather-balloon/integrated-global-radiosonde-archive (visited on 07/04/2019).

[NOAc] NOAA. *Integrated Surface Database (ISD) - Data Access | National Centers for Environmental Information (NCEI) formerly known as National Climatic Data Center (NCDC)*. URL: https://www.ncdc.noaa.gov/isd/data-access (visited on 07/05/2019).

[OSH] OSHA. *Hydrogensulfide Hazards*. URL: https://www.osha.gov/SLTC/hydrogensulfide/hazards.html (visited on 10/15/2018).

[Pla] Instituto Geográfico Nacional (IGN) Plan Nacional de Ortofotografía Aérea (PNOA). *Satellite Image Products of the National Aerial Orthophotography Plan*. URL: https://pnoa.ign.es/productos (visited on 07/04/2019).

[RD] Agency for Toxic Substances Registry and Disease. *Hydrogen sulfide definition fact sheet*. URL: https://www.atsdr.cdc.gov/toxfaqs/tfacts114.pdf (visited on 08/26/2019).

[Unia] United States Geological Survey (USGS). *EarthExplorer Homepage*. URL: https://earthexplorer.usgs.gov/ (visited on 07/04/2019).

[Unib] United States Geological Survey (USGS). *Land Use Classifications- National Land Cover Data Set 1992 (NLCD)*. URL: https://my.usgs.gov/confluence/display/nawqadatasynth/Land%7B%5C%%7D2BUse%7B%5C%%7D2BClassifications (visited on 07/04/2019).

[Unic] United States Geological Survey (USGS). *Metadata of the Enhanced National Land Cover Data 1992 (NLCDe 92)*. URL: https://water.usgs.gov/GIS/metadata/usgswrd/XML/nlcde92.xml (visited on 07/04/2019).

[Unid] United States Geological Survey (USGS). *USGS EROS Archive - Digital Elevation - Shuttle Radar Topography Mission (SRTM) 1 Arc-Second Global*. URL: https://www.usgs.gov/centers/eros/science/usgs-eros-archive-digital-elevation-shuttle-radar-topography-mission-srtm-1-arc?qt-science%7B%5C_%7Dcenter%7B%5C_%7Dobjects=0%7B%5C#%7Dqt-science%7B%5C_%7Dcenter%7B%5C_%7Dobjects (visited on 07/04/2019).

[Wika] Wikipedia. *Boundary layer thickness*. URL: https://en.wikipedia.org/wiki/Boundary%7B%5C_%7Dlayer%7B%5C_%7Dthickness (visited on 06/10/2018).

[Wikb] Wikipedia. *Bulk Richardson number*. URL: https://en.wikipedia.org/wiki/Bulk%7B%5C_%7DRichardson%7B%5C_%7Dnumber (visited on 06/10/2018).

[Wikc] Wikipedia. *Electronic nose*. URL: https://en.wikipedia.org/wiki/Electronic%7B%5C_%7Dnose (visited on 06/11/2018).

[Wikd] Wikipedia. *European Terrestrial Reference System 1989*. URL: https://en.wikipedia.org/wiki/European%7B%5C_%7DTerrestrial%7B%5C_%7DReference%7B%5C_%7DSystem%7B%5C_%7D1989 (visited on 07/04/2019).

[Wike] Wikipedia. *Inorganic or mineral acid*. URL: https://en.wikipedia.org/wiki/Mineral%7B%5C_%7Dacid (visited on 06/26/2018).

[Wikf] Wikipedia. *Monin-Obukhov length*. URL: https://en.wikipedia.org/wiki/Monin%E2%80%93Obukhov%7B%5C_%7Dlength (visited on 06/10/2018).

[Wikg] Wikipedia. *Outline of air pollution dispersion*. URL: https://en.wikipedia.org/wiki/Outline%7B%5C_%7Dof%7B%5C_%7Dair%7B%5C_%7Dpollution%7B%5C_%7Ddispersion (visited on 06/06/2018).

[Wikh] Wikipedia. *Richardson number*. URL: https://en.wikipedia.org/wiki/Richardson%7B%5C_%7Dnumber (visited on 06/10/2018).

[Wiki] Wikipedia. *Roughness length*. URL: https://en.wikipedia.org/wiki/Roughness%7B%5C_%7Dlength (visited on 06/10/2018).

[Wina] Windguru.cz. *Windguru station - Dunes Kite Piles Club / Platja de Piles, DKPiles Meteo*. URL: https://www.windguru.cz/station/51 (visited on 07/04/2019).

[Winb] Windguru.cz. *Windguru station - Playa de l'Ahuir, Gandia Surf*. URL: https://www.windguru.cz/station/1064 (visited on 07/04/2019).